

SPECIAL ISSUE



TECHNICAL, SCIENTIFIC
AND
RESEARCH REPORTS

Vol. 6 (2014)

KLIMA-IASI
Final Report of Project

Sensitivity analysis and application of
KLIMA algorithm to GOSAT and OCO validation

KLIMA-IASI Final Report of Project *

**Sensitivity analysis and application of
KLIMA algorithm to GOSAT and OCO validation**

Ugo Cortesi⁽¹⁾, Samuele Del Bianco⁽¹⁾, Marco Gai⁽¹⁾,
Lucia Maria Laurenza⁽¹⁾, Simone Ceccherini⁽¹⁾, Bruno Carli⁽¹⁾,
Flavio Barbara⁽¹⁾, Michael Buchwitz⁽²⁾

⁽¹⁾ Istituto Fisica Applicata "Nello Carrara" del CNR (IFAC-CNR)

⁽²⁾ Institute of Environmental Physics (IUP), University of Bremen

* ESA-ESRIN/Contract n. 21612/08/I-OL

1 Introduction

The present document constitutes the final report of the KLIMA-IASI project carried out by IFAC-CNR with the contribution of IUP, University of Bremen and supported by ESA-ESRIN under contract n. 21612/08/I-OL. The report describes the activities conducted by the IFAC-CNR team for the adaptation and optimization of the KLIMA algorithm to the retrieval of carbon dioxide vertical distribution and columnar values from thermal infrared spectral radiances observed by the IASI spectrometer, on-board the MetOp-A satellite, the integration of this retrieval algorithm into the ESA Grid Processing On-Demand (G-POD) operative system for bulk processing of IASI data and the results of inter-comparison of KLIMA Level 2 (L2) products with EUMETSAT L2 operational products, with TANSO-FTS/GOSAT L2 products and with selected TCCON ground stations products. We also report a brief description of the KLIMA-IASI algorithm and conclusions of the sensitivity tests performed during the Phase 1 of this project. The results of the work executed by IUP University of Bremen under WP-5100 (Analysis of SCIAMACHY CO₂ retrieval) are described in details in the Technical Report IUP-TR-SCIAGHG-08-001 (Initial application of WFM-DOAS CO₂ and CH₄ retrieval algorithm to SCIAMACHY Level 1 (L1) version 6) and are reported in summary in Sect. 4.4 of this document.

2 Objectives and rationale of the project

Carbon dioxide is the primary greenhouse gas released into the Earth's atmosphere by human activities. The balance of natural sources and sinks of carbon dioxide, leading to stable values of about 280 ppm for atmospheric CO₂ concentration in pre-industrial times, has been significantly perturbed by anthropogenic forcing - mostly from fossil fuel burning and cementification and from deforestation and other land use change (LUCs) - since the beginning of the industrial era in the late eighteenth century. Current levels of CO₂ in the atmosphere exceed the value of 390 ppm, with a mean annual global growth rate by decade varying from 0.8 ppm yr⁻¹ in 1960-1969, to 1.3 ppm yr⁻¹ in 1970-1979, to 1.6 and 1.5 ppm yr⁻¹ in 1980-1989 and in 1990-1999 respectively and raising to 1.9 ppm yr⁻¹ in 2000-2009, as shown in Fig. 1 [24], [4].

In the 50 years period from 1959 to 2008, the fraction of the total anthropogenic emissions of CO₂ that remained in the atmosphere each year, the so called *Airborne Fraction* (AF), has likely increased from about 40% to 45% [36]. The rest of the emissions, the *Sink Fraction*, was absorbed partly by oceans and partly by the land biosphere. According to the estimates given by the *Global Carbon Project* for the fate of CO₂ anthropogenic emissions (see, for instance, [28], updated from [36] and [4]), in 2000-2009, the AF was 47% and the natural sinks of the ocean and of the biosphere retained respectively 27% and 26% of CO₂ anthropogenic emissions, but their capability for sequestering carbon dioxide is strongly variable in space and in time. Over the last 200 years, the oceanic uptake constituted the only true net sink mechanism for anthropogenic CO₂ with the absorption of 118 ± 19 Pg C, whilst the terrestrial biosphere was a net source of CO₂ to the atmosphere in the same period with the release of 39 ± 28 Pg C [54]. On the other hand, indications exist that the uptake of CO₂ by the ocean has diminished from 28 to 34% to about 26%, with the sink strength of the biosphere remaining constant at the level of about 30%. A crucial task to achieve reliable predictions of future levels of atmospheric CO₂ is, along with monitoring of CO₂ emissions, an accurate determination of the geographic distribution of surface carbon fluxes on a variety of spatial scales, from local and regional to continental and global, and of the partitioning of the total uptake between the ocean and land sinks [35]. An improvement in our understanding of the specific processes responsible for absorption of the CO₂ amounts released into the atmosphere from year to year by natural and anthropogenic sources is strictly needed both for the scientific community, as well as for policy makers. This is, in fact, a key issue when dealing with periodical assessments of the effects of measures applied to mitigate the response of Earth's climate to human perturbation of atmospheric carbon dioxide concentration. A consolidated approach to retrieve quantitative estimates of the strengths and spatial distribution of CO₂ sources and sinks relies on inverse modeling of surface carbon fluxes. This is based on atmospheric transport models, that include advection, convection and eddy mixing processes and simulate the air-ocean and the air-land exchange, being constrained by observed spatial and time gradients of CO₂ concentration and by the associated uncertainties [27], [52].

First applications of inverse modeling to infer net surface fluxes of carbon dioxide were based on best matching in situ measurements from surface flask sampling network, which despite the high precision of the individual products are too sparse to provide the geographical coverage optimally suited for these inversion studies [55]. An alternative source of observations, providing the adequate global coverage to characterize the spatial distribution of CO₂ sources and sinks, is now available with measurements of column averaged CO₂ from space-borne remote-sounders, as originally highlighted by [45]. The potential of satellite-based CO₂ observations to drastically improve the performances of the inverse models clearly derives, at first instance, from their better global coverage compared to surface networks especially over land and from the large amount of data that can be acquired from space platforms.

Passive remote-sounding of atmospheric CO₂ total columns from space can basically be performed by nadir viewing sensors measuring spectra of the reflected sunlight in the near infrared spectral region (CO₂ bands at 1.6 μm and 2.0 μm) using differential absorption optical spectroscopy (DOAS) or observing the radiance emitted by CO₂ bands in the thermal infrared. (4 μm and 15 μm). Each of the two methods has relative advantages and drawbacks, but observations in the NIR certainly offer a better framework, as they are sensitive down to the lowermost layers of the atmosphere, thus being capable to retrieve the CO₂ content in the entire air column, so that are less affected by uncertainties in vertical transport when applied to inversion models of the carbon cycle [3]. Moreover, the NIR is less sensitive to temperature and water vapour and less affected by possible interferences. Major strengths of CO₂ remote-sounding in the thermal infrared, on the other hand, are represented by the better global coverage (TIR measurements can be performed both at day and at night and over land and ocean, whilst NIR observations can only cover the sunlit part of the globe and shall be acquired in the sun-glint mode over the ocean to compensate for the low surface albedo) and by the much stronger absorption bands of carbon dioxide. One of the first attempts to retrieve CO₂ information from space-borne measurements acquired by a nadir-viewing thermal infrared sounder and to use the retrieved concentration to infer CO₂ surface fluxes was made with data from the NOAA TIROS-N Operational Vertical Sounder (TOVS) [6], [7] and demonstrated limited capability to constrain atmospheric transport in the inversion of CO₂ sources and sinks [9].

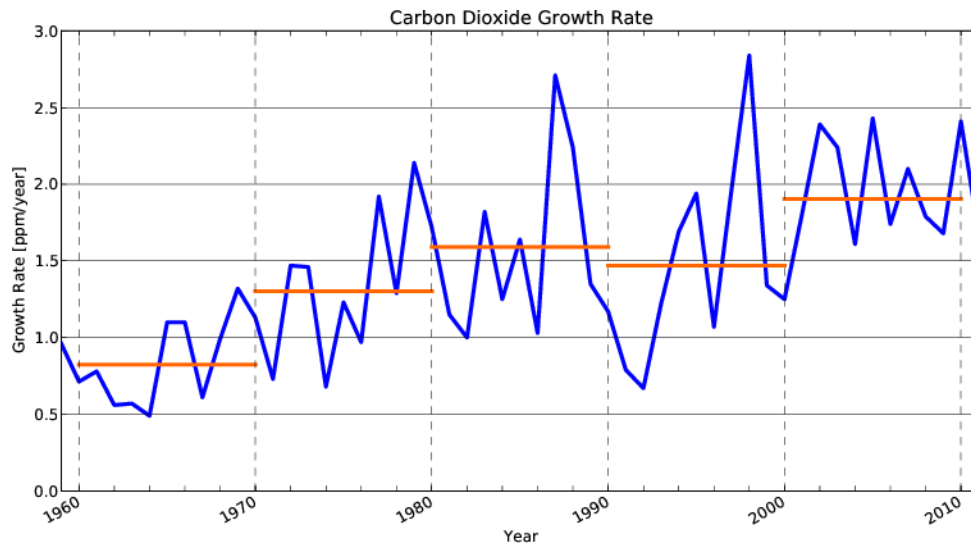


Fig. 1: Annual mean carbon dioxide growth rates based on globally averaged marine surface data, as from values reported by Thomas Conway and Pieter Tans, NOAA/ESRL (www.esrl.noaa.gov/gmd/ccgg/trends/)

Current generation of high resolution hyperspectral infrared sounders, such as the Atmospheric Infrared Sounder (AIRS) and the Infrared Atmospheric Sounder Interferometer (IASI) were shown to provide better results [9], [21], [19], despite their sensitivity to mid upper tropospheric carbon dioxide still representing a limiting factor for potential exploitation of infrared satellite data in carbon dioxide flux inversion. The performances of inverse modeling of the carbon cycle based on near infrared measurements were evaluated by using data from SCIAMACHY [3] and from the Greenhouse gases Observing SATellite (GOSAT) [30], which has been the first mission specifically designed for monitoring atmospheric CO₂ distribution from space. Additional space measurements in the near infrared spectral region will become available soon with the replacement of the OCO mission (OCO-2), that is planned to be launched in July 2014 and will provide more precise data on CO₂ concentration, thus making possible a further reduction of the uncertainties associated to the inferred CO₂ surface flux [39], [10]. A comprehensive study, providing a clear overview of current and emerging capabilities for the global monitoring of CO₂ surface fluxes, was conducted by Hungershofer et al. [29]. They evaluated the potential information content of nine different observing systems, that included the existing network of surface stations for in-situ observation of CO₂ concentration, two extended versions of the current network, the nadir sounding in the thermal infrared of AIRS, the near-infrared measurements of SCIAMACHY, GOSAT and OCO and the active measurements which might be performed by the space-based lidar mission A-SCOPE (Advanced Space Carbon and Climate Observation of Planet Earth) of the European Space Agency [34]. The results of the study confirmed the better performance of space remote-sounding in the NIR with respect to the TIR, and showed a higher information content for the A-SCOPE system in comparison to OCO. Similar performances could be attained by the two extended surface networks, that might be implemented at the same cost of the A-SCOPE satellite mission. Additional insight was gained by testing, along with the nine individual systems mentioned above, different combinations of them. In summary, a crucial issue to further develop our understanding of the processes controlling the balance between sources and sinks of atmospheric carbon dioxide is the assessment and improvement of the quality and spatial and time coverage of observations of CO₂ concentration. This is, in fact, directly linked to the information retrievable from inverse modeling of the carbon cycle on CO₂ surface fluxes associated to natural and anthropogenic emissions and uptake. And it is mandatory to guide corrective and preventive actions for mitigation of climate change towards most effective measures aimed to reduce CO₂ sources from human activities and to protect and enhance natural carbon sinks.

In this context, the KLIMA-IASI project was conceived, arising from the proposal submitted to ESA-ESRIN in response to RFQ/3.12339/08/I-OL (Proposal - Sensitivity Analysis and Application of KLIMA algorithm to GOSAT and OCO validation, May 2008). The general objective of the project can be outlined as follows:

To investigate the ultimate capabilities of the KLIMA-IASI algorithm to retrieve CO₂ total abundance from IASI/MetOp-A observations over a monthly to seasonal time scale and over a spatial scale compatible with the requirements of a comparison with CO₂ operational products of the satellite missions OCO and GOSAT.

The IASI instrument, as briefly reported in some detail hereafter (see Sect. 4), is a Fourier transform spec-

trometer flying on-board the MetOp satellite series and operating in the thermal infrared range for nadir looking observations of Earth's surface and atmospheric emission. The mission concept is primarily driven by measurement requirements for meteorological sounding and global climate monitoring and the operational retrieval targets are: atmospheric temperature and water vapour vertical profiles, O₃, CH₄, N₂O and CO total columns. The broad spectral coverage from 645 to 2760 cm⁻¹ and the high spectral resolution of 0.5 cm⁻¹ after apodization make also possible to extract from IASI spectra the total amount of other atmospheric minor constituents with spectral signatures in the thermal infrared region. In particular, the potential of IASI measurements to provide information on integrated content of carbon dioxide was demonstrated by feasibility studies [7], using simulated IASI data to investigate the sensitivity to CO₂ of the shorter and longer wavelength bands of the TIR, at 4.4 μm and 15 μm respectively, and to evaluate the capability of inverse modeling to disentangle CO₂ from the effects of temperature and other interfering species such as water vapour and ozone. Real data from IASI and from AMSU (Advanced Microwave Sounding Unit), both on-board the MetOp-A mission, have also been used to retrieve the upper tropospheric column of CO₂ in the range 11-15 km, based on fourteen channels of IASI in the ν₂ band of CO₂ at 15 μm and collocated measurements of AMSU, not sensitive to carbon dioxide as independent information on temperature [19]. The capability of advanced high resolution infrared sounders, and specifically of IASI, to retrieve information on CO₂ integrated content in the upper troposphere is definitely relevant both as a direct source of experimental data to constrain inversion models of CO₂ surface fluxes and as an independent measurement for cross-comparison with other existing or planned space-borne sensors such as TANSO-FTS/GOSAT and OCO.

In order to meet the general objective of the project, the KLIMA-IASI study was organized in two phases.

Specific goals of Phase 1 were:

- Adaptation of the KLIMA retrieval algorithm into a non-operational inversion code optimized for fast and accurate retrieval of CO₂ average information from IASI calibrated spectra.
- Sensitivity assessment and evaluation of the performance of the optimized KLIMA-IASI code for retrieval of CO₂ information from single spectra.
- Conclusions about the level of time and spatial averaging required to meet the uncertainty requirements necessary for the comparison with TANSO-FTS/GOSAT CO₂ retrieval products.

Phase 2 included the following objectives:

- Integration of the optimized KLIMA-IASI CO₂ retrieval code into the ESA Grid Processing On-Demand (G-POD) operational environment.
- Inter-comparison of KLIMA-IASI CO₂ total column values with EUMETSAT Polar System (EPS) IASI L2 data.
- Inter-comparison of CO₂ products retrieved from collocated IASI and TANSO-FTS measurements for cross-validation of the two instruments, aimed at identifying possible recommendations for calibration and algorithms improvement.
- Inter-comparison of CO₂ products retrieved from IASI spectra with KLIMA-IASI algorithm with the Total Carbon Column Observing Network (TCCON) ground stations products.

From the MARC code developed for a previous study, during the Phase 1 of this project we developed a prototype software system - indicated as KLIMA-IASI *Reference Retrieval Model (RRM)* - essentially driven by the requirements for optimal accuracy of CO₂ retrieval product. A further step of Phase 1 consisted in introducing some approximations in the radiative transfer model to obtain a version of the retrieval code that could be integrated into the ESA-ESRIN G-POD (GRID Processing On Demand) operative system to have access to the computing resources for processing an adequate amount of IASI data within the time frame of the project. The approximate version of the code represents the best trade-off between accuracy and computing time and it will be referred to, throughout this Final Report, as KLIMA-IASI *Accelerated Retrieval Model (ARM)*.

The main innovation introduced by the KLIMA-IASI ARM is the retrieval of XCO₂ together with most of the relevant interfering parameters so that interferences contribute directly to the retrieval error and do not pose difficult error assessment problems. The performance of the ARM in terms of total retrieval uncertainty are only slightly degraded with respect to the *Reference Retrieval Model (RRM)* and are fully consistent with the requirement of 0.3% accuracy of CO₂ total column at monthly intervals on regional scales for TANSO-FTS/GOSAT validation. The use of KLIMA-IASI ARM introduces a small bias in the retrieved CO₂ total column, when using the full IASI spectral range. This can be however corrected by including the errors due to Forward Model (FM) approximations

in the Variance Covariance Matrix (VCM) of the observations. A brief summary of the consolidated results obtained during the sensitivity tests carried out to evaluate the best trade-off between accuracy and efficiency of the KLIMA-IASI forward and retrieval model are shown in Sect. 3.

A general overview of the main features of the KLIMA-IASI retrieval code and the retrieval strategy used for IASI and TANSO-FTS are presented in Sect. 4. In this section, background information on the characteristics, that the KLIMA-IASI prototype software inherited from existing forward and inverse models, is reported along with full details of the innovative features that have been implemented in the upgraded version of the code. In Sect. 5, we report the options available for the access to IASI and TANSO-FTS operational data, in terms of data dissemination means and measurement products types and format. The rationale for the use of IASI Level 1 B (L1B), 1 C (L1C) and L2 data obtained from the EUMETSAT archive facility (UMARF) in EPS Native format and of TANSO-FTS L2 data downloaded from GOSAT User Interface Gateway (GUIG) is also discussed. In Sect. 6, we describe the integration of an optimized version of the KLIMA-IASI code (KLIMA-IASI version 2.0) on the G-POD for Earth Observation Application System available at ESA-ESRIN. Section 7 illustrates a brief overview of the adopted strategy for data analysis. The results of bulk processing of the IASI measurements, carried out using the G-POD computing resources, are reported in Sect. 8, while in the last sections with report the results of inter-comparison between carbon dioxide retrieved with the integrated version of the KLIMA-IASI algorithm, EUMETSAT L2 operational product (Sect. 9), TANSO-FTS L2 (Sect. 10) and selected TCCON ground stations (Sect. 11). In Sect. 12, final conclusions are presented.

In the appendices, we provide a more detailed description of the software tool developed for pre-processing the IASI input dataset (Appendix A), of the Measurement Space Solution method (Appendix B), and of the calculation of the Jacobians for the target species investigated in the current study (Appendix C). Finally, in Appendix D we report the first inter-comparison between KLIMA and Version 1 (V1) of TANSO-FTS L2 products, that has been updated in the final part of the project to Version 2 (V2).

3 Summary and conclusions of Phase 1 activities: sensitivity tests and performances of the KLIMA-IASI code

In this section, we summarize the main results obtained during Phase 1 of the project. More detailed information is provided in the conference proceedings [20] and [17] as well as in the final report of the Phase 1 [16]. This section contains also the results of some complementary activities such as the validation obtained by means of the comparison of the forward models of KLIMA with the calculations made by the LBLRTM code (see <http://rtweb.aer.com/lblrtm.html>) and the main outcome of the activities conducted by the Institute of Environmental Physics (IUP), University of Bremen, FB1 for the application of WFM-DOAS CO₂ and CH₄ retrieval algorithm to the processing of SCIAMACHY L1v6 data.

The retrieval of atmospheric state parameters from broadband measurements acquired by high spectral resolution sensors such as IASI generally requires dealing with a prohibitively large number of spectral elements (8461 samples in the case of each IASI observation, covering the 645–2760 cm⁻¹ range with a resolution of 0.5 cm⁻¹ and a spectral sampling of 0.25 cm⁻¹). Most inversion algorithms developed for both operational and scientific analysis of IASI spectra perform a reduction of the data - typically based on channel selection, super-channel clustering or Principal Component Analysis (PCA) techniques - in order to handle the high dimensionality of the problem. Accordingly, simultaneous processing of all IASI channels received relatively low attention.

Here, we will show, using the Kyoto protocol Informed Management of the Adaptation (KLIMA) code, the feasibility of a retrieval approach exploiting all spectral channels of IASI, to extract simultaneously information on water vapour, temperature and ozone profiles, as well as on CO₂. This multi target retrieval removes the systematic errors due to interfering parameters and makes the channel selection no longer necessary. The challenging computation is made possible by the use of some approximations in the forward model, that are tuned for an optimum compromise between speed and accuracy.

3.1 KLIMA-IASI forward model

3.1.1 Reference Forward Model

The forward model (FM) used to simulate IASI wide-band measurements was developed at IFAC and is called KLIMA FM. It is a line-by-line radiative transfer model based on the code developed by upgrading the algorithm employed for the analysis of REFIR-PAD measurements [1], adapted in turn from the MARC inversion code for the MARSHALS study [5], with a few added features which make it suitable for the simulation of the wide-band spectral radiances acquired by the IASI instrument. The most recent spectroscopic database (which is HITRAN 2004 in the early test and HITRAN 2008 [26] in the final data processing) is used, the correction of the Planck function [14] to take into account the optical depth of the atmospheric layer at the different frequencies has been included.

A validation of KLIMA FM was conducted, by comparing synthetic IASI measurements generated by the KLIMA FM code with those of the FM of the LBLRTM (Line-By-Line Radiative Transfer Model) code. The simulations were based on the night-time measurement acquired by IASI over the Southern Great Plains in Oklahoma, USA, on 19 April 2007, during the Joint Airborne IASI Validation Experiment (JAIVEx) [56]. The atmospheric scenario for the simulations was set according to the state retrieved by LBLRTM from this observation. Synthetic IASI measurements were calculated using the KLIMA FM code and the LBLRTM FM and the difference between the two simulations was calculated. In Fig. 2, we report the result of the comparison, showing the residual difference between KLIMA simulation and LBLRTM simulation, compared with the nominal values of IASI radiometric noise. Please note that the IASI spectrum considered in this comparison is apodized and, accordingly, its radiometric noise is smaller than that of the unapodized spectra that will be considered in subsequent intercomparisons. Furthermore, please also note that the differences shown in this comparison are smaller than the residuals of preliminary tests reported in [17] because of some further improvements. The current residuals are, with very few exceptions, significantly smaller than the measurement errors.

In Fig. 3, we report the IASI measurement used for the validation activity (top) and the residuals between the observations and the simulations performed with the two FMs (bottom - KLIMA red line and LBLRTM blue line). The two codes have comparable performances and reproduce very well the observation. The comparison with a state of the art forward model and the good agreement with real observations validate the quality of the KLIMA FM. A further and much more stringent validation of this forward model (even if limited to a less extensive spectral range) will be provided by the analysis of the residuals of the IASI data analysis which will be presented in Fig. 34. This validated FM, when used with a fine sampling of the functional parameters and a complete accounting of all contributions, provides a *Reference Forward Model* (RFM) to which we shall refer to as KLIMA RFM.

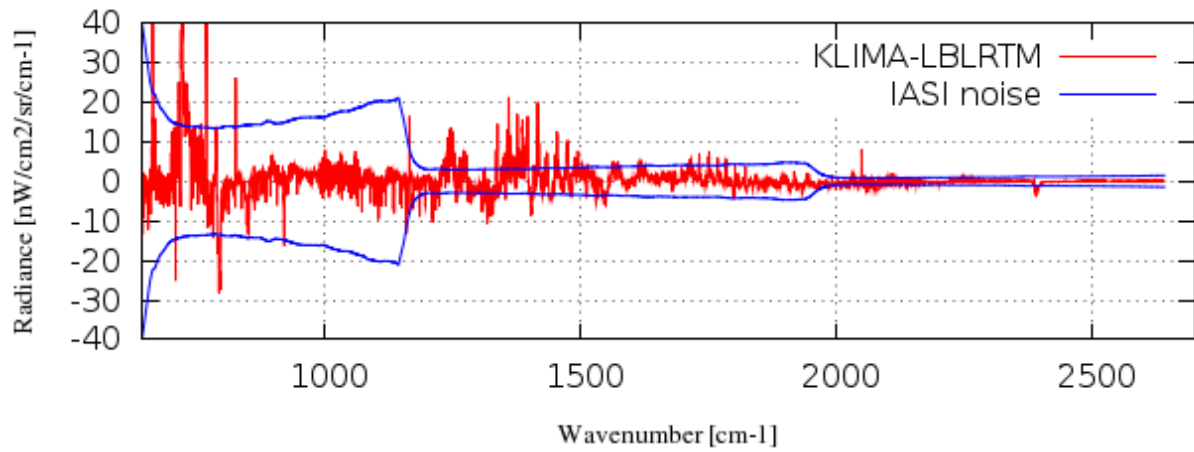


Fig. 2: Residuals between KLIMA simulation and LBLRTM simulation, compared with the nominal values of IASI radiometric noise

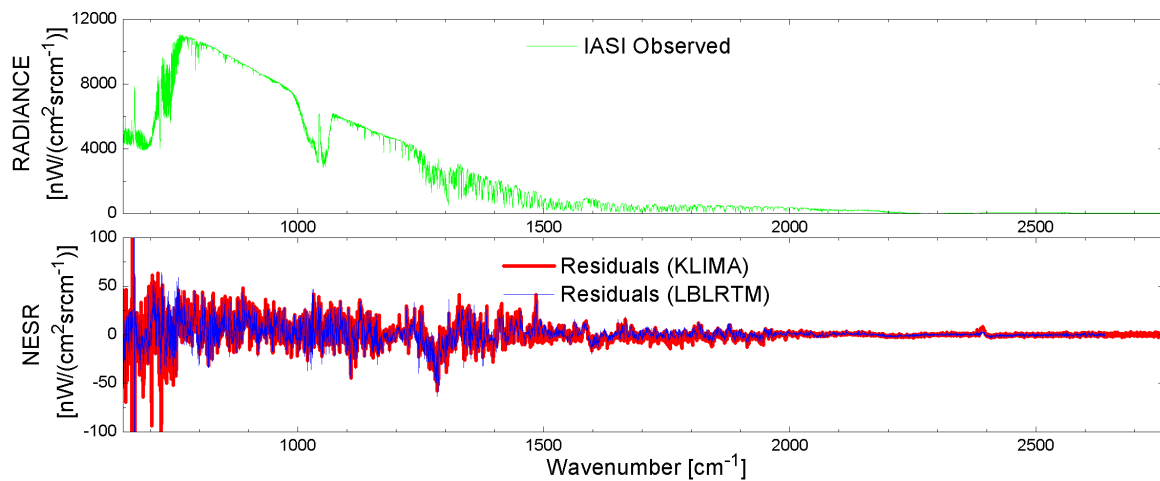


Fig. 3: IASI measurements (top) and residuals wrt KLIMA (red line) and LBLRTM (blue line) simulation (bottom)

Tab. 1: KLIMA-IASI Forward Model approximations tested in the sensitivity study

	KLIMA-IASI RFM	KLIMA-IASI AFM
Fine Frequency Grid	$\approx 0.002 \text{ cm}^{-1}$ (1/128 of IASI spectral sampling)	$\approx 0.004 \text{ cm}^{-1}$ (1/64 of IASI spectral sampling)
CO ₂ Line Mixing	Modelled in the band [645 - 2760] cm^{-1}	Modelled in the bands [650 - 800] and [2000 - 2500] cm^{-1}
Spectroscopic Database	HITRAN 2004 (all lines)	HITRAN 2004 (skipping all lines $< 10^{-5}$ the largest line in the selected band)
Atmospheric Line Shape	All lines modelled up to $\pm 25 \text{ cm}^{-1}$ from the line centre	Target species lines modelled up to $\pm 25 \text{ cm}^{-1}$ from the line centre
Vertical Grid	90 levels from 1050 to 0.005 hPa	44 levels from 1050 to 0.005 hPa
Field Of View	Not modelled	Not modelled

3.1.2 Accelerated Forward Model

In order to make possible the use of the validated KLIMA-FM in operational analyses of IASI observations, some approximations have been implemented in the code aimed at reducing its computing time. This KLIMA-FM configuration, called *Accelerated Forward Model* (AFM) is a trade-off between efficiency (in term of program size and running time) and accuracy taking into account that the goal is the retrieval of the carbon dioxide column in the contest of the 'Sensitivity Analysis and Application of KLIMA algorithms to GOSAT and OCO validation' project [22]. For each approximations several tests were performed in order to identify the entity of the approximation that best satisfies the aimed compromise.

The approximations listed in Tab. 1 are here below briefly summarized:

- *Fine Frequency Grid*: a regular grid with steps equal to 1/128 the spectral sampling of the IASI instrument (0.25 cm^{-1}) is adopted for the RFM. (Tests have shown that the use of a finer frequency grid (i.e. with steps equal to 1/256 of the IASI spectral sampling) is unnecessary because the differences are much smaller than the nominal instrumental noise). A coarser grid, with steps equal to 1/64 the spectral sampling of IASI, was adopted in the AFM. The difference between the spectrum simulated using the downgraded and the reference fine wave number grid was calculated for the full IASI spectral range and is displayed in Fig. 4 (panel a). These difference mainly affect the modelling of the uppermost altitude levels. The largest differences are observed in the CO₂ band between 650 cm^{-1} and 800 cm^{-1} and in the O₃ band close to 1100 cm^{-1} , where the contribution of carbon dioxide and ozone concentration in the uppermost levels is important.
- *CO₂ line mixing*: in the RFM line-mixing effects are taken into account, by adding to the simulated radiances the contribution of CO₂ line mixing calculated according to the model by Niro et al. [41], [42] over the full IASI spectral range. A significant reduction of the computing time is obtained in the AFM by evaluating the contribution of line-mixing in a sub-set of spectral intervals. We calculated the difference between synthetic spectra simulated over the full IASI spectral range, with and without the contribution of CO₂ line-mixing. The residuals are plotted in Fig. 4 (panel b), along with the nominal instrumental noise. They show that modeling of CO₂ line-mixing can be limited to the spectral intervals [645-825] cm^{-1} and [1995-2445] cm^{-1} , where these differences are larger than the nominal instrument noise.
- *Spectroscopic database*: The spectroscopic database adopted for the RFM includes all lines listed in HITRAN 2004. In order to limit the total number of spectral features to be considered in the AFM, we evaluated the impact of skipping for each species, all the lines smaller than 10^{-5} the largest line in the selected band. Fig. 4 (panel c) shows the difference between the spectrum simulated with and without the line skipping. The largest differences are observed around 700 cm^{-1} (CO₂ band) and are due to the approximation introduced by CO₂ lines skipping. Considering that in the AFM the spectroscopic data for CO₂ are taken from the line-mixing database [41], [42] and are not affected by the filtering criteria applied to HITRAN 2004, we can adopt the proposed line skipping for all other species without introducing any major source of systematic error in the forward model.
- *Atmospheric line shape*: In the RFM the atmospheric line shape was modelled up to $\pm 25 \text{ cm}^{-1}$ from the line centre. The impact on computing time and FM accuracy of modelling the atmospheric line shape for non-target species (i.e., all the simulated species except H₂O, CO₂, and O₃) up to $\pm 10 \text{ cm}^{-1}$ from the line centre was evaluated by calculating the difference between the spectrum simulated with and without this approximation. Results are displayed in Fig. 4 (panel d), showing that the largest differences, observed

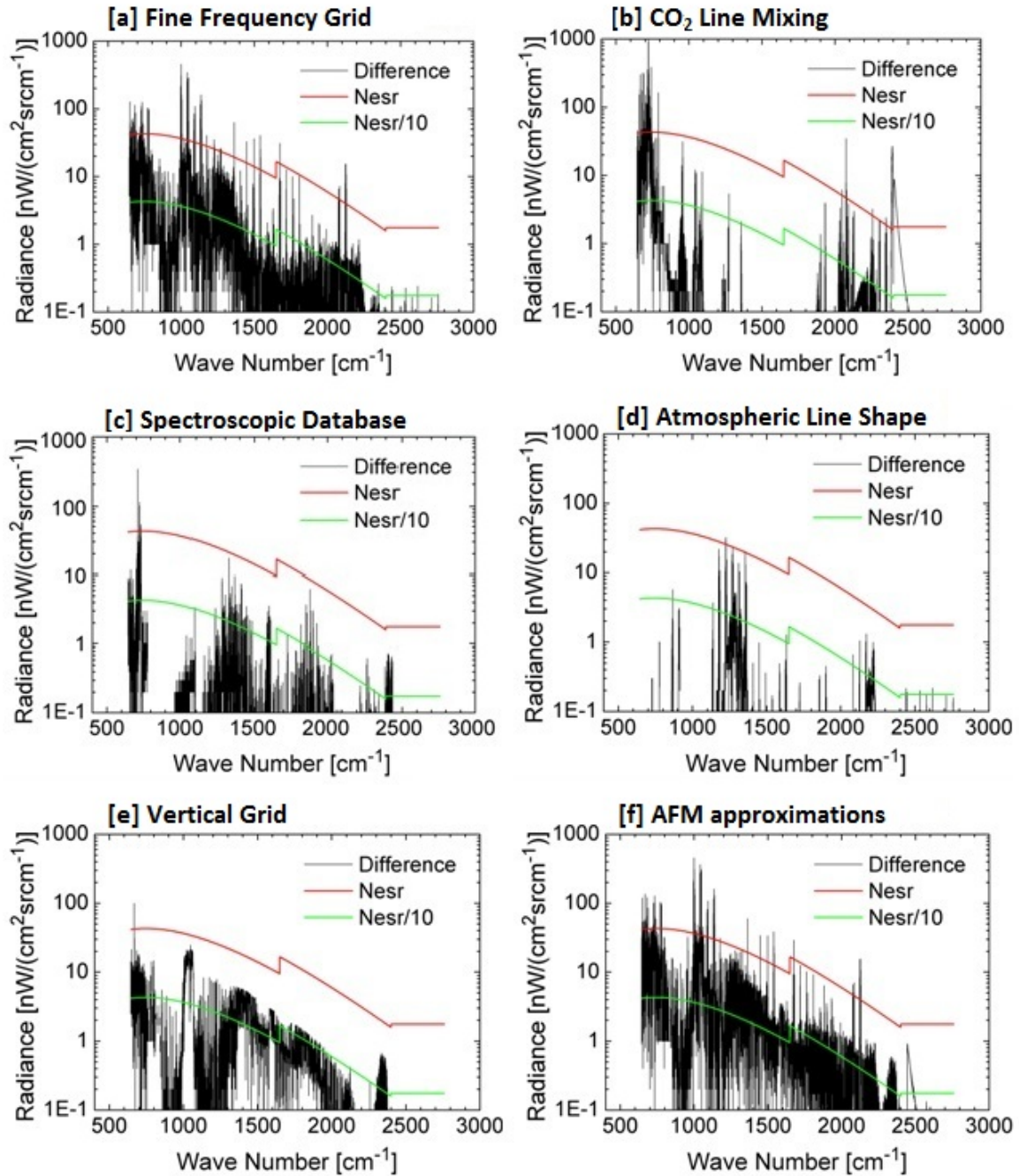


Fig. 4: Absolute values of the error spectra associated to the FM approximations listed in Tab. 1. The red line is the nominal NESR; the green line is the nominal NESR reduced by a factor 10

around 1250 cm^{-1} , never exceed the nominal instrumental noise. We conclude that the error introduced by this approximation does not affect the CO_2 information.

- *Atmospheric vertical grid:* The vertical grid adopted for modelling the stratification of the atmosphere in the RFM is the same that is used to represent IASI L2 operational products for temperature and water vapour, consisting of 90 levels in the pressure range from 1050.0 hPa to 0.005 hPa. In the AFM, the vertical resolution of the pressure grid was degraded: the 21 lowermost levels from 1050.0 hPa to 478.4 hPa (2 km) were the same as in the reference vertical grid. For the levels above, only one every third pressure level was maintained in the new grid. The total number of pressure levels in this approximation is 44. Fig. 4 (panel e) shows the difference between the spectrum simulated with the downgraded and with the reference vertical grid. The largest differences are observed around 670 cm^{-1} in the middle of the CO_2 band, where the CO_2 content in the upper tropospheric and lower stratospheric levels provide a significant contribution to the observed radiance and where a coarser vertical resolution of the atmospheric model at higher altitude may affect the accuracy of the simulation.
- *Field of view:* The effects due to the field of view of the instrument neither in the RFM nor in the AFM are taken into account. We verified that the spectral intensity simulated using KLIMA-IASI RFM in nadir viewing geometry is uniform within the field of view of the instrument. Assuming uniform surface properties for the observed pixel, for different lines of sight within the field of view the spectral intensity varies by less than 1/10 the nominal IASI NESR.

The total spectral difference between the RFM and the AFM, obtained implementing simultaneously all the approximations discussed above, is reported in Fig. 4 (panel f) where it is compared with the nominal Noise Equivalent Spectral Radiance (NESR) of IASI. Please note that in this case NESR specified in the IASI requirements was used. The NESR of the real IASI measurements is often better, but this does not change significantly our conclusions. With the only exception of a few spectral channels the approximations introduce differences that are significantly smaller than the measurement error.

In principle these residuals can be used to build the variance covariance matrix (VCM) of the FM approximations equal to the VCM of the summation of the errors, made of the square of the calculated difference in the diagonal elements and of terms with correlation equal to unit in the off-diagonal elements. This matrix will be added to the VCM of the measurements in some of the sensitivity tests that will be reported in the next section.

3.2 KLIMA-IASI retrieval model

The FM module (either the RFM or the AFM) is used in the retrieval procedure implement for the analysis of IASI measurements. The basic features of this retrieval model are:

- Wide band retrieval;
- Multi-target retrieval;
- Marquardt parameters equal to 0.01 for all targets;
- Marquardt and Gauss dumping factor equal to 3;
- Use of the optimal estimation;
- Possible use of the VCM that accounts for the FM approximations.

The target parameters of the retrieval are:

- The vertical profile of temperature;
- The vertical profile of water vapour;
- The total and partial column of carbon dioxide, and ozone;
- The total column of N_2O , CO and CH_4 ;
- The surface temperature.

The atmospheric scenarios (initial guesses and a priori values) selected for the retrievals are taken from the IG2 climatology developed by University of Leicester for the operational analysis of MIPAS-ENVISAT data [46]. These IG2 profiles were used for the retrieved gases and temperature and pressure profiles. The thermal contrast between the Earth surface and lowest atmospheric layer (defined as the difference between Earth skin temperature and the air temperature at ground level) was taken equal to zero for the true atmospheric state and equal to +10 K for the a priori state. The a priori uncertainties that we have assumed on the retrieval targets are reported in Table 2.

Tab. 2: A priori errors and correlation length used for the retrieval tests

Target Parameter	A Priori Error	Error Correlation Length
Temperature	4 K	3 km
H ₂ O	80%	5 km
CO ₂	10%	N.A.
O ₃ , N ₂ O, CO, CH ₄	100%	N.A.
Surface Temperature	20 K	N.A.

3.2.1 The Reference Retrieval Model and the ultimate IASI performances

When the RFM is used in the retrieval model we have the *Reference Retrieval Model* (RRM), and in this configuration the code can be used to assess the ultimate retrieval capabilities of IASI. We performed a simulated retrieval test in which the IASI measurement was calculated using the RFM, a noise that reproduces the noise of real IASI measurements was added to this synthetic spectrum and the retrieval was performed using the RRM. Results of this retrieval, performed on an unapodized spectrum and exploiting all the spectral channels, are shown in Fig. 5, Fig. 6 and Tab. 3. In Fig. 5, top panel, we report the plot of the simulated IASI measurements: the green curve is the observations, while the red and blue curves are the simulated spectra, respectively, at the first and at the last retrieval iteration. The green curve is almost completely covered by the blue curve. In order to highlight the differences, the residuals of the fit at the last iteration are compared to the variance of the modelled measurement error in bottom panel of Fig. 5. The distribution of the residuals is consistent with the variance confirming the absence of systematic errors (as expected since the same code is used for both the simulation and the retrieval). In Fig. 6 we report the errors of the retrieved profiles for water vapour, in the left panel, and temperature, in the right panel. The points show the difference between the retrieved profile and the true value (which in this case is known because equal to the value used for the calculation of the synthetic spectrum) and the horizontal bars indicate the retrieval errors. This difference indicates the bias of the retrieval. The continuous black line shows the difference between the a priori profile (also used as initial guess) and the true profile. The bias is explained by the statistical fluctuations of the retrieval error and does not show any significant effect that can be attributed to the a priori. In the lower atmosphere we obtain accuracy of 20% for water vapour and of 1 K for temperature. Tab. 3 shows

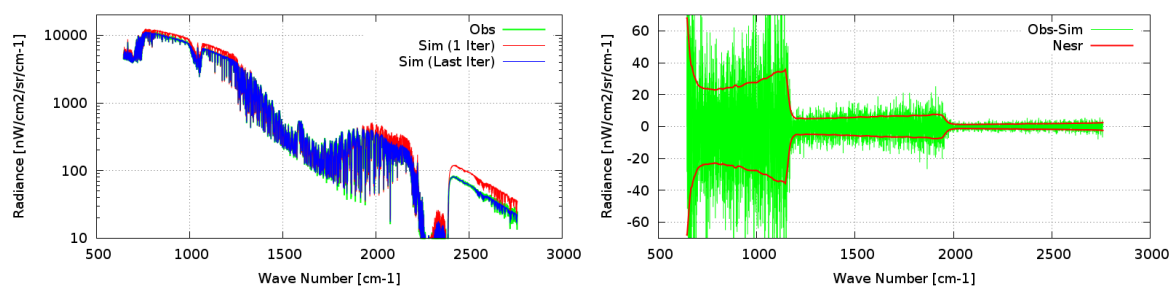


Fig. 5: Fit of the simulated IASI measurements and comparison between the residuals and the IASI variance using the RRM

the accuracy of the other retrieved parameters. In particular, the total and boundary column of CO₂ are retrieved with an accuracy of 1% and 5% respectively. The result of this test demonstrates the capability of the exploiting all the spectral channels of IASI for a multi-target retrieval of the atmospheric state and a very interesting ultimate retrieval capability for CO₂ total column. The accuracy of these retrieved products agrees with the recent work by Clerbaux et al. [13]. For some targets (e.g. O₃, CH₄, and CO), taking into account the mutual interference using the multi target retrieval, RRM provides a better accuracy.

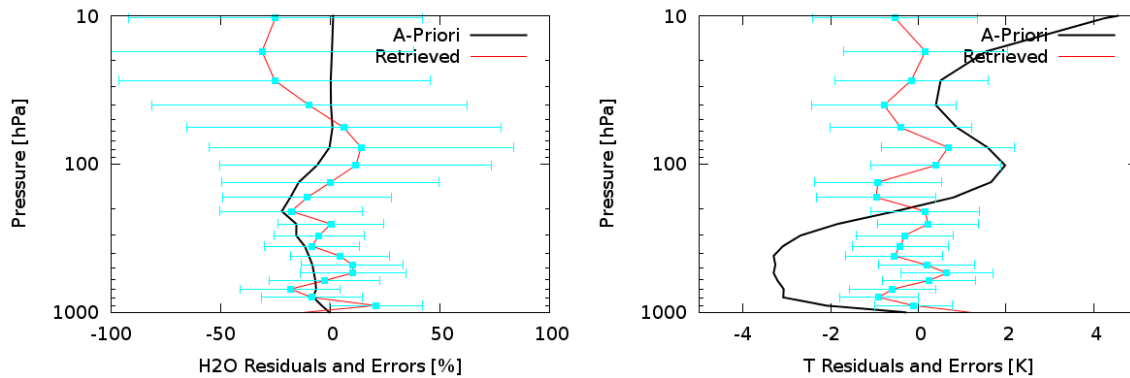


Fig. 6: Temperature and H₂O retrieval performance from IASI simulated data using the RRM

Tab. 3: Retrieved parameters of RM with RFM

Target Parameter	Accuracy
CO ₂ Total Column	1%
CO ₂ Boundary Column	5%
O ₃ Total Column	0.5%
O ₃ Boundary Column	20%
N ₂ O, CO, CH ₄ , and Surface Temperature	better than 1%

3.2.2 The Accelerated Retrieval Model and the sensitivity tests

We recall that, consistently with the requirements of the GOSAT mission, our accuracy requirement for CO₂ total column is better than 0.3% (1 ppm out of 370 ppm) on regional scales (1000 x 1000 km) at monthly intervals. At the same time there are requirements for program size and running time of the retrieval code that are driven by the need to integrate the KLIMA-IASI processor into the ESA Grid Processing On-Demand (G-POD) system for subsequent processing of IASI data. The required maximum program size is 1 Gb and the running time is that of processing 1 orbit of IASI data within 1 day when using one of the G-POD computing resources. A few strategies (use of the AFM for the radiative transfer calculations, reduction of the size of the analyzed band, use of the VCM of the modelling errors) have been considered.

In Fig. 7, Fig. 8 and Tab. 4 we report the results obtained when in the simulated retrieval the AFM is used instead of the RFM. The results, in terms of residuals and errors, are practically equal to those of the ultimate retrieval presented in the previous section. However, a bias larger than the retrieval error is observed in the case of the water vapour profile above the tropopause. This is probably due to the approximations of the line shape modelling adopted in the AFM, because of the use of a coarse frequency grid. A bias in the modelling of the stratosphere is not expected to affect our retrieval of carbon dioxide total column, however careful tests are needed in order to verify that the approximations adopted in order to reduce the size and the computing time of our code do not jeopardize the accuracy of the CO₂ retrieval. Tab. 4 shows the precision on the other retrieved parameters. In particular, as reported Tab. 3 for the RRM test, the total and boundary column of CO₂ are retrieved with an precision of 1% and 5% respectively.

Tab. 4: Retrieved parameters of RM with AFM

Target Parameter	Accuracy
CO ₂ Total Column	1%
CO ₂ Boundary Column	5%
O ₃ Total Column	0.5%
O ₃ Boundary Column	20%
N ₂ O, CO, CH ₄ , and Surface Temperature	better than 1%

On the basis of these considerations, a detailed sensitivity study was conducted on the KLIMA retrieval model in order to obtain a good trade-off between accuracy and computing requirements of the retrieval process. Using as a starting point the IASI RRM and its performances described in the previous section the retrieval tests, listed in Tab. 5, have been performed. The main variables are:

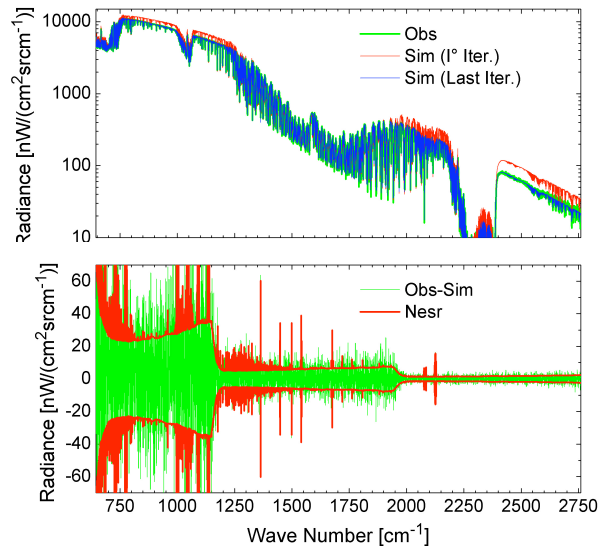


Fig. 7: Fit of the simulated IASI measurements and comparison between the residuals and the IASI variance (containing the FM errors) using the AFM in the FM

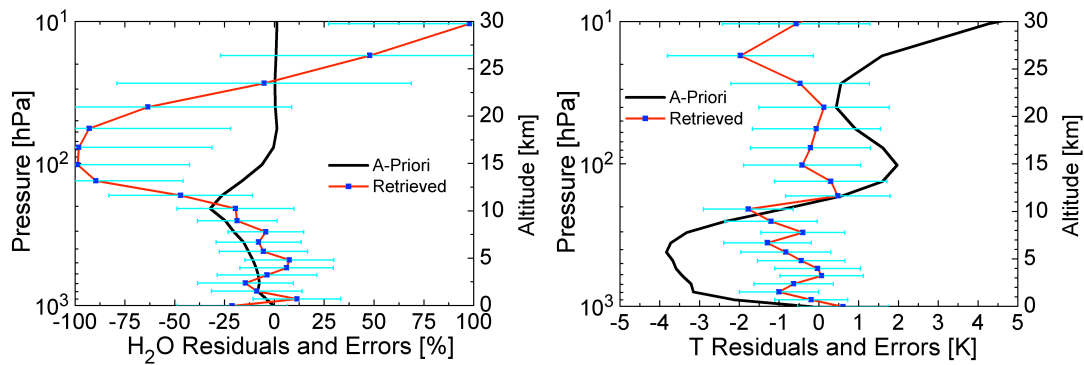


Fig. 8: Temperature and H₂O retrieval performance from IASI simulated data using the AFM in the RM

- The FM used in the retrieval. While the analysed spectrum is in all cases calculated using the RFM, in retrieval model either the RFM or the AFM can be used. When the RFM is used for both the synthetic spectrum and the retrieval process we have the RRM discussed in the previous section.
- The extension of the analyzed spectral range. The trade-off between accuracy and computing time strongly depend on the selected spectral interval and a few different cases have been considered.
- The use of the VCM of the model errors. The retrieval code minimized the difference between the observed and the simulated spectrum. This quantity is best characterized by the VCM of the differences given by the summation of VCM of the observations plus the VCM of the model used for the calculation of the simulated spectrum. This second VCM is usually small and is often neglected in operational retrieval codes.

In order to account for the statistical variability of the retrieval products, N runs of the retrieval simulation, using the same synthetic observations generated by the RFM with different measurement noise, were carried out for each test.

Five runs were considered to be enough for test 1, where the RFM was used for both the forward model and the retrieval process and now further information was going to be provided by a larger statistics. An example of the performances of a run of this test are given in Sect. 3.2.1.

Twentyfive runs have been used for tests from 2 to 5 because this number of observations was found to be necessary for the retrieval of CO₂ total column with the required accuracy. An example of the performances of a run of test 3 are given in this section (Sect. 3.2.2).

In the case of test 4 and 5 the computation was repeated also with $N = 100$ because in the tests with $N = 25$ the average difference between retrieved and true CO₂ column had vales comparable with the retrieval error and it

was necessary to verify the absence of a bias.

In the case of test 1 and $N = 25$ an extrapolated value is reported, all the others are actual test cases.

The results of these tests are summarized in Tab. 6. For each test we report the retrieval error of the average CO₂ total column, the observed offset between the retrieved and the true value and the computing time for one iteration of the retrieval, when made on a reference machine (RAM 28 GB - Xeon 5410 2.33 GHz).

Tab. 5: Setup of the sensitivity tests on KLIMA-IASI inverse model

	FM Synthetic Observations	FM Retrieval Process	VCM including a priori Errors	Spectral Range
TEST 1	RFM	RFM	NO	[645 - 2760] cm ⁻¹
TEST 2	RFM	AFM	NO	[645 - 2760] cm ⁻¹
TEST 3	RFM	AFM	YES	[645 - 2760] cm ⁻¹
TEST 4	RFM	AFM	NO	[650 - 800] and [2000 - 2500] cm ⁻¹
TEST 5	RFM	AFM	YES	[650 - 800] and [2000 - 2500] cm ⁻¹

Tab. 6: Retrieval error of the average and difference between retrieved and true CO₂ total column values for N runs.

	N	Retrieval Error [%]	(Retrieved - True) [%]	Computing Time [min]
TEST 1	5	0.43	-0.09	800
TEST 1 (bis)	25	0.19		800
TEST 2	25	0.19	-0.40	200
TEST 3	25	0.19	-0.22	200
TEST 4	25	0.27	-0.19	150
TEST 4 (bis)	100	0.14	<0.04	150
TEST 5	25	0.27	-0.25	150
TEST 5 (bis)	100	0.14	<0.04	150

From the analysis of the results reported in Tab. 6 the following conclusions can be drawn. Using the AFM in the retrieval code (tests from 2 to 5) a significant reduction of the computing time is obtained with respect to the use of the RFM (test 1) and no significant loss of accuracy (tests 2 and 3 versus test 1) is observed. The use of the full IASI spectral band (tests 2 and 3) makes the code too large and a reduction of the selected spectra range (tests 4 and 5) is necessary. This choice has to be made despite the fact that from the point of view of the best compromise between accuracy and computing time a slightly better result is obtained in tests 2 and 3. Concerning the use of the VCM of the forward model errors no significant difference is observed between test 4 and test 5. In principle test 5 should provide better results, but our knowledge of the FM error is based on simulated calculations which could lead to rather arbitrary corrections. It was decided not to implement the VCM of the FM and postpone its use to when an experimental understanding of the residuals is obtained (such as it was subsequently obtained with the data analysis, see e.g. Fig. 34). On the basis of these considerations the code used in test 4, that we shall call KLIMA-IASI *Accelerated Retrieval Model* (ARM), is the one chosen for integration into the ESA Grid Processing On-Demand (G-POD) system.

The tests show that with this ARM, that satisfies the requirements of program size and computing time described in Sect. 3.2, it is possible to meet the requirement of 0.3% precision and accuracy by averaging 25 IASI observations (0,27% retrieval error in Tab. 6). In order to make sure that the retrieval error not only measures the precision of the retrieval, but also its accuracy, the offset must be smaller than what observed in the test with 25 runs. The test performed with 100 runs confirms that the offset observed in test with 25 runs is a statistical fluctuation and that the observed 0.3% precision also corresponds to 0.3% accuracy.

3.3 Application of WFM-DOAS CO₂ and CH₄ retrieval algorithm to the processing of SCIAMACHY L1 version 6 data

At the beginning of this project University of Bremen has conducted some (unfunded) activities relevant for this project. At that point in time the latest version of WFM-DOAS (WFMD) algorithm, for the retrieval of column-averaged mixing ratios of the two greenhouse gases (GHG) CO₂ and CH₄ denoted XCO₂ (in ppm) and XCH₄ (in ppb), from the SCIAMACHY spectra, was version 1.0 (WFMDv1.0). WFMDv1.0 has been applied to L1 version 5 nadir spectra to retrieve XCO₂ and XCH₄ for the years 2003-2005 ([58]). A study was performed to assess the feasibility of extending the analysis to observation made after 2005, when IASI observations start to be available.

In order to process data after 2005 L1 version 6 has to be used, because this is the latest version and most of the SCIAMACHY data after 2005 are only available as L1v6. The following tasks have been undertaken:

- *Task 1: Processor adjustments* - Adjustments of the WFMD processor to process L1v6.
- *Task 2: Orbit selection* - Selection of orbits covering the time period 2003-2008.
- *Task 3: Consistency assessment* - Processing of selected orbits during 2003-2005 and comparison with the (published) WFMDv1.0 data products (obtained using L1v5). This step is a pre-requisite for processing data after 2005 using L1v6. The main goal of this task was to find out if the retrieved GHGs obtained by applying WFMDv1.0 to L1v6 are similar as the WFMDv1.0 GHG data products obtained from L1v5.
- *Task 4: Stability assessment* - Processing of the selected orbits during 2006-2008 to find out if the instrument is stable after 2005.

The following results were found.

Consistency: Significant differences have been found between L1v5 and L1v6 when processing the orbits with the same WFMD retrieval algorithm. The spectral fits are typically worse for L1v6 and also the vertical columns and column averaged-mixing ratios are different. This is true for all three gases: CO₂, CH₄, and O₂. Especially O₂ (which is needed for the computation of XCO₂) shows a significant (few percent) low bias. As a consequence, the number of retrievals classified good is nearly zero if the (strict) WFMDv1.0 quality-filtering scheme is used.

Stability: From the analysis of the CO₂ and O₂ column retrievals it can be concluded that the SCIAMACHY instrument behaves quite stable during the entire time period investigated, i.e., 2003 to at least Oct 2008 (for the CO₂ fit detector pixels located in channel 6+ ($\lambda > 1590nm$) have been excluded due to larger fit residuals after 2005). This seems not to be the case for CH₄ retrieval, which exhibits increasingly lower quality of the spectral fits and retrieved columns after 2005 most likely due to degradation of channel 6+.

The cause(s) of the lower quality of the retrievals based on L1v6 compared to L1v5 needs to be investigated and solutions have to be developed to ensure similar (or better) quality for L1v6 retrievals compared to L1v5 based retrievals. This is a pre-requisite for processing data after 2005. For methane it needs to be investigated what causes the observed low quality retrievals after 2005 and to assess to what extent the SCIAMACHY CH₄ is useful after 2005.

These difficulties have prevented the generation of SCIAMACHY products at a time when also IASI is observing and a comparison exercise between the two instrument has not been possible.

4 An overview of the observations: instruments and retrieval codes

A brief overview is given here, to describe the instrument characterization and the retrieval algorithms applied to the measurement data to obtain information on atmospheric CO₂ columnar amount from IASI on the MetOp-A platform, from TANSO-FTS (Thermal And Near infrared Sensor for carbon Observation-Fourier Transform Spectrometer) on the GOSAT satellite, and from TCCON (Total Carbon Column Observing Network).

4.1 IASI/MetOp-A: instrument description and CO₂ operational retrieval code

The Infrared Atmospheric Sounding Interferometer (IASI) consists of a high resolution nadir-viewing Fourier transform spectrometer, associated with an imaging instrument. It is designed to measure the spectrum emitted by the Earth-atmosphere system in the Thermal InfraRed (TIR), with full coverage of the spectral range from 645 cm⁻¹ to 2760 cm⁻¹ (from 15.5 μm to 3.62 μm). Each spectrum is sampled every 0.25 cm⁻¹, with an apodized spectral resolution of 0.5 cm⁻¹, providing a total of 8461 radiance channels [2].

The sensor is flying on board the Meteorological Operational Satellite (MetOp) platform, launched in 19 October 2006 [11], [12]. The satellite flies in a sun-synchronous polar orbit at an altitude of around 817 km and crosses the equator at two fixed local solar times: 09:30 a.m. (descending) and 09:30 p.m. (ascending). The time to complete one orbit is about 101 min with a total of 14 orbits a day and a repeat cycle of 29 days.

The instrument scans the Earth's surface perpendicularly to the satellite's flight track with 15 individual views on each side of the track. Each Instantaneous Field Of View (IFOV) has a size of 50x50 km and consists of 2x2 circular pixels with a diameter of 12 km each (at the nadir point). The maximum scan angle is 48.3° from nadir with a total swath width of 2200 km. A swath (120 views) is achieved in 8 s, allowing global coverage twice a day. In Fig. 9 the IASI observation mode is described.

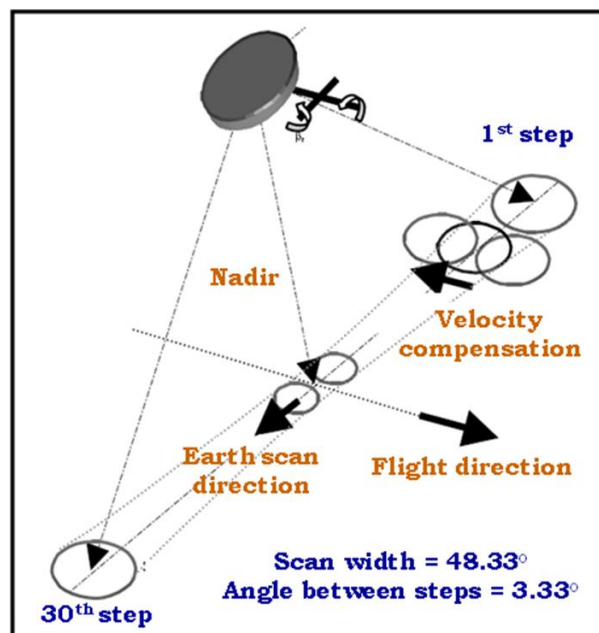


Fig. 9: IASI Viewing Geometry (Simeoni et al., 2004 [57])

In IASI the retrieval of the columnar amount of CO₂ is still experimental, but is delivered together with the other operational products, even if without an associated retrieval error. In this report we refer to IASI L2 data as an operational product.

The retrieval method, described by Crevoisier et al. [19], is a non-linear inference method, based on the multilayer perceptron neural network, and it is applied on selected 14 channels of the IASI spectrum, which have the highest sensitivity to CO₂ and minimum interference with the other species.

4.2 TANSO-FTS/GOSAT: instrument description and CO₂ operational retrieval code

The Greenhouse gases Observing SATellite (GOSAT) is an Earth observation satellite and was the first satellite designed for the study of the greenhouse gases from space. Primary mission goals are: short wave infrared observation, retrieval of CO₂ and CH₄ column density (during the orbital day time). Secondary mission goals are: thermal IR observation, retrieval of CO₂ and CH₄ altitude profile and column density (during orbital night time), other

trace gases (O_3 etc.) and other products, such as temperature profile and Earth radiation. GOSAT is a joint project of JAXA (Japan Aerospace Exploration Agency) and NIES (National Institute of Environmental Studies). JAXA is responsible for the development of the instruments, the launch and operations of the spacecraft while NIES develops algorithms for data analysis. The satellite was launched on January 23, 2009 to the sun-synchronous sub-recurrent orbit (local sun time at crossing the descending node at 13:00) having an approximate altitude of 666 km with an inclination of 98.06° to the equator. The orbital period of GOSAT is approximately 98.1 minutes, corresponding to approximately 14.6 revolutions per day and a revisiting time of 3 days.

GOSAT is equipped with two instruments: the Thermal And Near infrared Sensor for carbon Observation-Fourier Transform Spectrometer (TANSO-FTS) and the Cloud and Aerosol Imager (TANSO-CAI) [30]. TANSO-FTS has three narrow bands in the Short Wave InfraRed (SWIR) region (band 1 at $0.76 \mu\text{m}$, band 2 at $1.6 \mu\text{m}$ and band 3 at $2.0 \mu\text{m}$) and a wide TIR band (band 4 from $5.5 \mu\text{m}$ to $14.3 \mu\text{m}$) with a spectral resolution of about 0.2 cm^{-1} . The sensor IFOV is a nadir circular footprint of about 10.5 km in diameter. The maximum scan angle is 35° from nadir with a total swath width of 790 km.

TANSO-FTS observes solar light reflected from the Earth surface only during the daytime, as well as the thermal radiance emitted from the atmosphere and the surface during both the daytime and night-time. The sensor observes scattered sunlight over land using a nadir-viewing observation mode and over ocean using a sun glint observation mode. The SWIR region is observed in bands 1 to 3 in the daytime only and TIR region is captured in band 4 during both the day and the night. The spectral bands of TANSO-FTS and the associated target products are summarized in Tab. 7.

Tab. 7: TANSO-FTS Spectral bands

Spectral band n°	1	2	3	4
Spectral range	VIS	SWIR	SWIR	MWIR/TIR
Coverage (μm)	0.75-0.78	1.56-1.72	1.92-2.08	5.5-14.3
Target of the measurement	O_2 , air pressure, cirrus	CO_2 , CH_4 , H_2O	CO_2 , CH_4 , H_2O cirrus	CO_2 , CH_4 , H_2O
Calibration	Solar irradiance, deep space, moon, diode laser			Black body, deep space
Spectral resolution	0.2 cm^{-1} both sides (maximum optical path difference 2.5 cm)			

The TANSO-FTS viewing geometry is illustrated in Fig. 10.

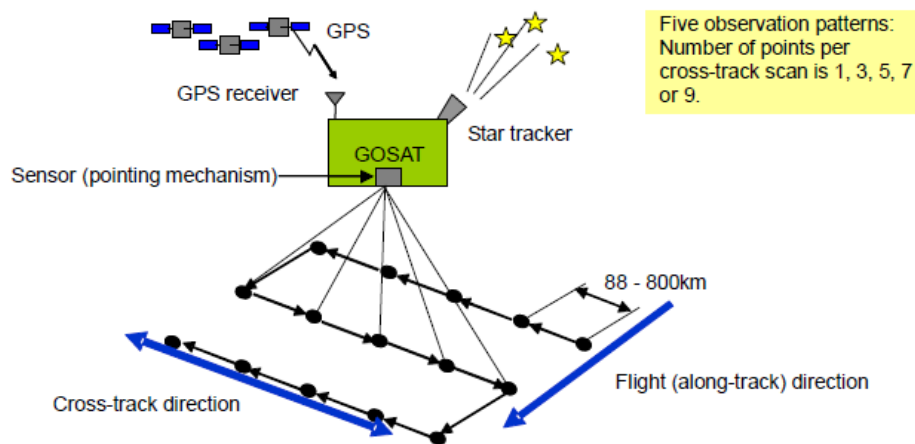


Fig. 10: TANSO-FTS Viewing Geometry http://www.jaxa.jp/press/2009/02/20090209_ibuki_e.html

In the normal operations, one interferogram is acquired every four seconds. Orientating mechanism about the along track axis and cross track axis allow the sensor to scan in the cross direction, to point to the sunlight spot and/or predetermined locations, and to keep pointing a place during one whole interferogram capturing. In routine observation, sensor observes a predetermined number of points scanning 1, 3, 5, 7 or 9 points along the cross track direction and the scan is repeated at an interval along the along track direction, so that the observed points form a grid-like pattern on the Earth's surface. The instrument keeps pointing in the same place during the whole capture of an interferogram. In order to improve Signal to Noise Ratio (SNR), TANSO may observe a same place repeatedly to sum the observed data up (3 times of repetition, or only once with no repetition).

Currently, the column-averaged dry air mole fraction of atmospheric carbon dioxide (XCO_2) derived from the TANSO-FTS SWIR channels has been largely validated, against ground-based TCCON observation and models (as reported in [40] or [15]). On the contrary, we have not found publications on measurement campaigns carried out to validate the profiles of CO_2 obtained from the TIR band or comparison using ground-based stations. On the dedicated page GOSAT related references (<http://www.gosat.nies.go.jp/eng/technology/references.htm>) are present few publications of preliminary retrieval of CO_2 profiles within the upper troposphere. As reported for example in [33], some systematic biases exist in the TIR spectrum, because of the opacity of the mirrors of SWIR bands that obstruct the field of view of band 4 in the TIR. Due to the non-global coverage in the range of time selected and the fact that the L2 products of the TIR band have not yet been validated, we decided to focus mainly on the total columnar content obtained from SWIR bands.

The SWIR TANSO-FTS L2 data (see Sect. 5.2) contain the retrieval results of the total columnar amount of CO_2 and the CO_2 in dry air mixing ratio (indicated in this document as XCO_2) along with the vertical profile of CO_2 in dry air mixing ratio (indicated in this document as XCO_2 profile). In the L2 data also the error budget (in terms of retrieval, smoothing, interferences and external errors) are provided. The retrieval method (described by Yoshida et al. [59]) is based on the optimal estimation approach and on a pre-data screening suitable for the retrieval analyses and a post-quality checking of the retrieved results.

4.3 TCCON and CO_2 retrieval code

The Total Carbon Column Observing Network (TCCON) is a network of ground-based Fourier transform spectrometers recording direct solar spectra in the near-infrared spectral region. The TCCON site map is shown in Fig. 11. The TCCON data are calibrated using the method described in [62], [38], [25]. From these spectra, accurate



Fig. 11: TCCON site map

and precise column-averaged abundance of CO_2 , CH_4 , N_2O , HF, CO, H_2O , and HDO are retrieved. TCCON provides an essential validation resource for the Orbiting Carbon Observatory (OCO), SCIAMACHY (Scanning Imaging Absorption Spectrometer for Atmospheric Cartography/Chemistry), and GOSAT.

TCCON database (see Sect. 5.3) contains the retrieval results of the CO_2 in dry air mixing ratio (XCO_2) along with its associated error.

4.4 KLIMA CO_2 retrieval code

KLIMA-IASI (hereafter referred to as KLIMA) is the inverse model developed to process IASI/MetOp-A L1 data and to retrieve CO_2 information, for comparison and cross-validation with TANSO-FTS CO_2 products. The KLIMA algorithm consists of two distinct modules, the Forward Model (FM) and the Retrieval Model (RM). The retrieval approach used for the processing of IASI measurements, exploits the wide-band of IASI spectra, to extract information on CO_2 , taking into account the systematic errors due to interfering parameters so that the channel selection is no longer necessary. This goal has been achieved using a multi-target approach: the RM algorithm retrieves the atmospheric CO_2 along with the interfering atmospheric parameters and interference errors are included in the retrieval error [20], [17].

The FM used to simulate IASI wide-band measurements has been developed by upgrading the algorithm employed for the analysis of REFIR-PAD measurements [1], adapted in turn from the MARC inversion code [5]. The FM is a line-by-line radiative transfer model, with capability to simulate wide-band spectral radiances acquired by the IASI instrument based on the following key features: radiative transfer calculations performed using Curtis-Godson approximation; atmospheric line-shapes modeled with Voigt profile; atmospheric continuum model takes into account the main contributions from N_2 , O_2 , O_3 , H_2O , and CO_2 ; scattering and Non Local Thermodynamic

Equilibrium (NLTE) effects have not yet been implemented because usually not necessary the first in clear sky conditions and not significant the second in the tropopause (these are, however, issues that deserve attention in our analysis). With respect to the FM used during Phase 1 of the project, described in Sect. 3.1, the spectroscopic database adopted for data processing is HITRAN 2008 [26]. Dedicated spectroscopic database and line shape are adopted for CO₂, to take into account the line-mixing effect [41], [42]. The fine frequency grid sampling used to simulate the IASI spectra before the convolution with the instrumental function has been fixed to 0.004 cm⁻¹. Moreover, the correction of the Planck function [14] to take into account the optical depth of the atmospheric layer at the different frequencies has been included. The new spectroscopic data base [56] adopted in the Phase 2 of the project implied an update of the code and required a new validation iteration.

The RM uses a constrained Non-linear Least Square Fit (NLSF) approach and the cost function to be minimized takes into account the a priori information (Optimal Estimation Method - OEM) and the Marquardt parameter. The a priori is used to maintain the retrieved values within physically justified boundaries and only introduces a very weak constraint with negligible bias. On the other hand, the a priori is necessary because we want to model the vertical structure of the profiles (CO₂, temperature and water vapour) and to account for its induced errors. The measurements alone do not allow the retrieval of all the degrees of freedom that we are modelling and some a priori is needed. This use of the OEM is quite different from what usually done in most operational codes. There OEM is used to retrieve more parameters, here OEM is used to model more variables and make a more careful error estimate. Exploitation of broadband measurements is made possible by implementing a procedure, that reduces the impact of systematic uncertainties. The code implements the multi-target retrieval: more than one species is simultaneously retrieved and systematic errors due to interfering parameters are removed. A complete Variance-Covariance Matrix (VCM) can be used, including both the measurement errors and the errors in the estimate of FM parameters [5].

The state vector used in the IASI measurements data analysis includes: the profile of temperature; the profiles of H₂O; the total column of CO₂, O₃, N₂O, CO, and CH₄; the surface temperature and emissivity. The profiles are retrieved on a vertical grid of 30 levels from 1050 to 0.005 hPa. For temperature and H₂O a priori profiles we used the operational L2 data provided by UMARF archive (see Sect. 5.1). The a priori errors have been incremented by a factor equal to $\sqrt{2}$, in order to reduce its constraint. The columnar a priori information has been obtained using the IG2 database [46] with a priori errors of 10% for CO₂, and 100% for the others. The used a priori surface temperature and emissivity is provided by UMARF archive with a priori error of 5 K and of 0.01 respectively.

From the retrieved values of the total column amount of CO₂ and from H₂O profile, we obtain the XCO₂ as:

$$XCO_2 = \frac{Column_{CO_2}}{(Column_{Air} - Column_{H_2O})} * 10^6 \quad (1)$$

where the $Column_{Air}$ is computed using the L2 IASI value of the surface pressure and supposing the hydrostatic equilibrium in the atmosphere. Equation 1 is also used to obtain the XCO₂ value from the L2 IASI results.

A screening of the IASI L1 data was performed using a pre-processing filtering. The adopted selection criteria allow to exclude the IASI data when a bad quality flag is reported on L1 data (due to the validation the L1 product) and L2 data (due to the convergence of the L2 iterative retrieval and to the validation the L2 product) and to exclude the observation in cloudy sky conditions (see Sect. 5.1). No selection criteria have been included in IASI data pre-processing, in order to exclude latitude ranges, as performed in [19] due to the atmospheric temperature profile interferences, because the multi-target approach adopted by KLIMA reduce the interferences effects.

Main requirements established for the inter-comparison with TANSO-FTS products and for the integration on G-POD environment are a target accuracy of 0.3% (1 ppm out of 370 ppm) on regional scales (1000x1000 km) at monthly intervals (consistent with the requirement of TANSO-FTS CO₂ products and on the required precision established by Rayner and O'Brien [45]); a program size not exceeding 1 Gbyte and a running time aimed at processing the IASI central pixels with respect to nadir of one orbit in one day using the G-POD computing resources. Cortesi et al. [17] demonstrated that the optimization of KLIMA needs to analyse a wide-band of IASI spectrum containing the CO₂ bands (near 15 and 4.3 μm) on G-POD environment met the requirements established averaging 25 retrieval products of the IASI observations. The results reported in this work have been produced analysing the IASI spectrum between 645 and 800 cm⁻¹ (see Sect. 4.4.2), providing a CO₂ precision between 1 and 3% from the retrieval of a single observation, and increasing between 25 and 100 the average of the retrieval products of IASI observations. This retrieval configuration allowed analysing 20 000 observations in a week on G-POD environment, corresponding to the central pixels of all the orbits of a week, increasing the performance of a factor 10 with respect to the time requirement.

4.4.1 Comparison between IASI L1B and L1C datasets

The original version of the KLIMA code can process either L1B or L1C IASI data. A series of tests was conducted to verify that the retrieval products (XCO_2) obtained by applying the KLIMA inversion model to L1B and L1C data have negligible differences and the decision was taken to focus on the use of L1C dataset, which consist of geolocated and apodised spectra.

Figure 12 reports an example of the processing of IASI data carried out to test the capability of the KLIMA algorithm to retrieve XCO_2 from IASI L1B and L1C data. The KLIMA code was used to retrieve XCO_2 in a

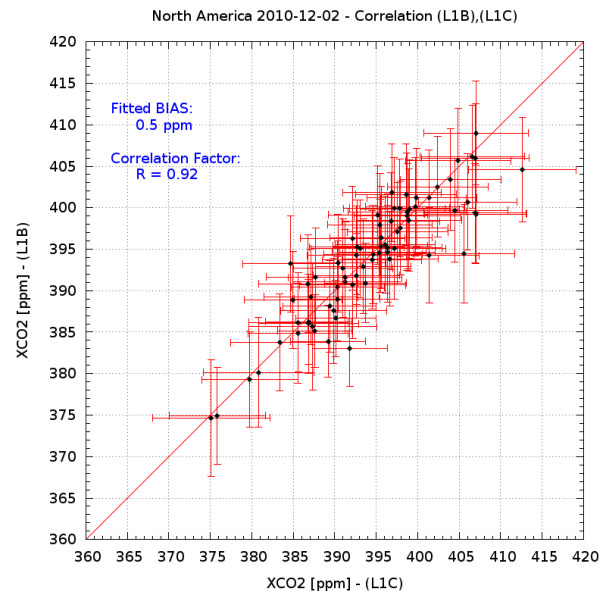


Fig. 12: Scatter plot (and errors) of the two dataset of XCO_2 retrieved using KLIMA code from IASI L1B and L1C data

selected area over North America on 2 December 2010. Consistent results were obtained from the two datasets and IASI L1C has been selected to perform the KLIMA/G-POD data analysis.

4.4.2 IASI spectral band selection

The channels sensitive to carbon dioxide features are located in two spectral bands: around 700 cm^{-1} and 2300 cm^{-1} respectively. The multi-target retrieved strategy implemented by the KLIMA code would have suggested the fitting of the entire spectrum, but the constraints imposed by the integration and operation on the G-POD system made necessary a selection of the spectral bands for the inversion data processing. For the analysis of the CO_2 we considered three bands (see Sect. 3.2.2 where the ARM to be implemented in G-POD system has been defined) within the IASI spectral coverage, where CO_2 features are present:

- band1 = $645\text{-}800\text{ cm}^{-1}$;
- band2 = $2000\text{-}2380\text{ cm}^{-1}$;
- band3 = $2400\text{-}2500\text{ cm}^{-1}$.

In order to perform a bulk processing of the IASI measurements, a further reduction of the IASI spectrum has been taken into account, and an new evaluation of the performances has been done. The band3 contains less information with respect to band1 and band2 so it was discarded. We performed several tests to assess the information content that is possible to obtain from a combination of band1 + band2 and from band1 only. Two geographical areas were selected over North America (between 15° , 40° latitude and -115° , -105° longitude) and Asia (between 25° , 50° latitude and 115° , 125° longitude), where a comparison was performed between XCO_2 retrieved with the KLIMA algorithm (in the following referred as KLIMA L2) using band1 and using the combination band1 + band2. The results of bands comparison, performed on about 600 observations both for North America and Asia, are shown in Fig. 13. Figure 14 shows, both for North America and Asia areas, the distribution of the differences between XCO_2 retrieved using only band1 and band1+band2. A bias of about -1.5 ppm has been found when only band1 is used in the retrieval; the width of the distribution (about 6 ppm) is in agreement with the XCO_2 retrieval error reported in Tab. 8.

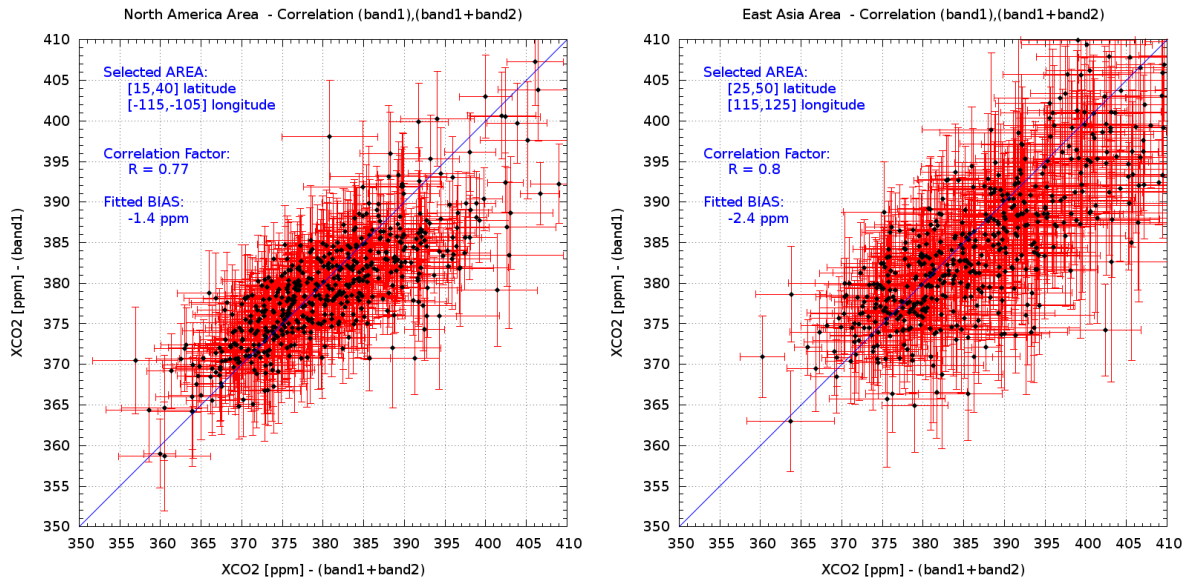


Fig. 13: Scatter plot (and errors) of the XCO₂ retrieved from band1 and band1+band2 over North America (on left panel) and Asia (on the right panel)

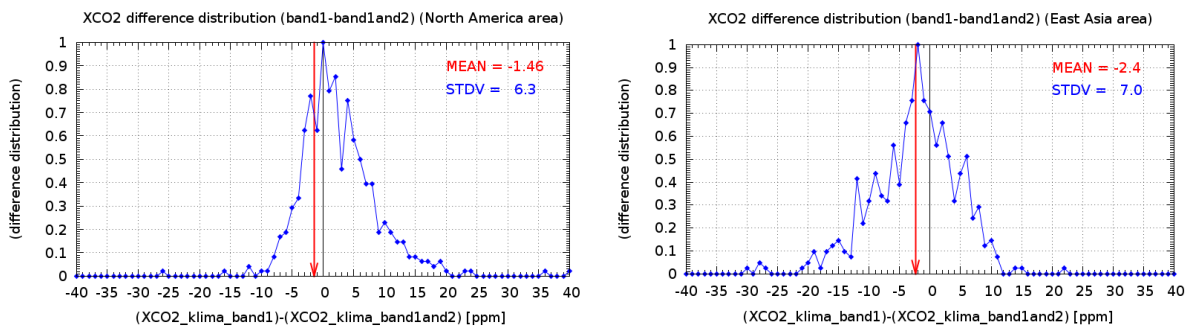


Fig. 14: Distribution of the differences between XCO₂ retrieved using only band1 and using band1+band2: case North America (on left panel) and Asia (on the right panel)

The comparison shows that retrieval performed using band1 and the combination of band1 + band2 give comparable results, even if the use of band1 only increases the XCO₂ error, as reported in Tab. 8.

Tab. 8: XCO₂ errors using using band1 and the combination of band1 + band2

Geographical area	band1	band1 + band2
North America	5.4 [ppm]	3.9 [ppm]
Asia	6.7 [ppm]	5.2 [ppm]

With respect to the performances of the ARM reported in Sect. 3.2.2, the smaller information content due to the reduction of the analysed IASI band increases the retrieval error obtained from ARM of about 30 % (from 5.2 ppm to 6.7 ppm on Asia and from 3.9 ppm to 5.4 ppm on North America), but the scatter plots shown in Fig. 13 give consistent results using a computation time reduced of about 60-70 %. On the basis of these tests, taking into account the reduction of the computation time and the increase of the retrieval error (always within the accuracy requirement of the project), band1 has been selected for the current analysis to perform the retrieval of carbon dioxide and the comparison with TANSO-FTS products.

The average accuracy on the retrieved XCO₂ column can be estimated in 1.1%, as reported in Tab. 9. This value has been computed by averaging the retrieval error extracted from a dataset composed of 519 observations selected in concurrence with TANSO-FTS ones (see par. 10.3.1). The dataset consists of observations having a uniform distribution in space (all the Earth surface, both land and water) and in time (from Mar-2010 to Feb-2011) and can be considered adequate to represent the average case. However, concurrently with the XCO₂, KLIMA code retrieves a set of parameters having some spectral information on this band: the O₃ and N₂O column, the

surface temperature, the vertical profile of temperature and water vapour. The accuracies obtained for the scalar parameters are summarized in Tab. 9, while the accuracies for temperature and water vapour profiles are reported in Fig. 15, as a function of the vertical pressure.

Tab. 9: Parameters of ARM using IASI band1

Target Parameter	Accuracy
CO ₂ Total Column	1.1%
O ₃ Total Column	3%
N ₂ O Total Column	100%
Surface Temperature	better than 1%

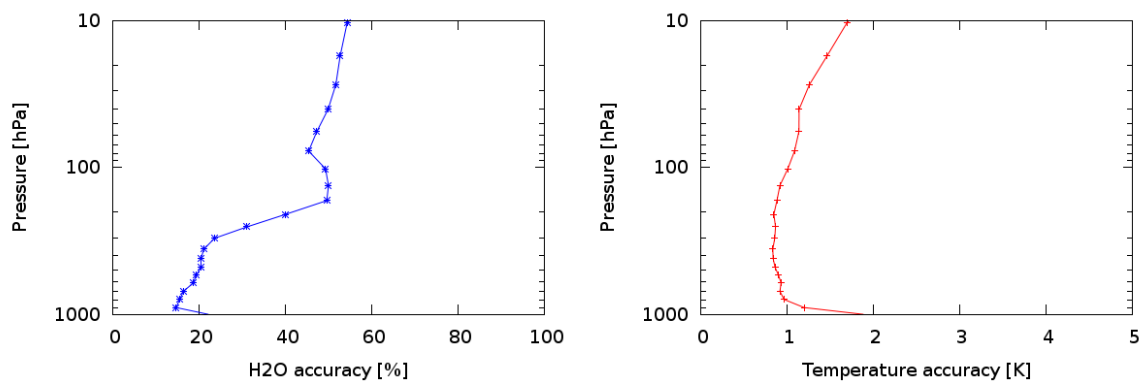


Fig. 15: Temperature and H₂O retrieval accuracy from IASI ARM data processing using band 1 only

5 Identification and acquisition of IASI, TANSO-FTS and TCCON datasets

In this section, we summarize the available options for the access to IASI, TANSO-FTS and TCCON operational data and describe the solutions adopted for the KLIMA-IASI project, in order to obtain a statistically significant dataset on which to perform our analysis.

5.1 IASI data

5.1.1 IASI data dissemination means

Different dissemination means are available for accessing the IASI operational products.

- EUMETCast - Data in near real time can be received via the EUMETSAT's Data Distribution System (EUMETCast) that utilizes the services of a satellite operator and telecommunications provider to distribute data files using Digital Video Broadcast (DVB). A standard EUMETCast reception station must be set up and an Agreement for the License of use of Meteosat Second Generation (MSG) data must be signed with the Italian Air Force on behalf of EUMETSAT.
- GTS - A subset of IASI products is distributed via the Global Telecommunication System (GTS) (WMO integrated network of point-to-point circuits and multi-point circuits which interconnect meteorological telecommunication centres).
- UMARF - Archived IASI data are made available to users from the EUMETSAT Unified Meteorological Archive and Retrieval Facility (UMARF). The UMARF archive can be accessed through a web interface (<http://archive.eumetsat.int/umarf>), which permits on-line ordering and delivery of the operational products in a variety of formats.

5.1.2 IASI data products

The processing of IASI measurements using KLIMA retrieval code requires an input dataset that includes both L1 data (spectral radiance data, etc.) and L2 operational products (atmospheric and surface data, etc.). The following products are foreseen by the IASI spectral data processing and distribution chain:

- Level 0 - Raw IASI measurement data, after on-ground de-multiplexing, include pre-calibrated spectra, the corresponding non calibrated images, calibration images, verification data and auxiliary data necessary for further processing.
- Level 1 A - Non apodized calibrated spectra and corresponding images; this step of processing comprises data decoding, radiometric post-calibration, spectral calibration, IASI/AVHRR co-registration via IASI images, geo-location and dating.
- Level 1 B - Level 1 A data re-sampled.
- Level 1 C - Level 1 B apodized to obtain a nominal Instrument Spectral Response Function (ISRF).
- Level 2 - Geophysical products derived after co-processing of data from IASI and the METOP meteorological instruments (profiles of temperature, humidity, surface temperature, trace gas distribution, cloud parameters, etc.).

The use of non apodized calibrated spectra in combination with diagonal variance covariance matrix and reading of L1B IASI data files was implemented as our baseline for Phase 1. The possibility of using L1C data was also implemented. We have tested the CO₂ retrieval from IASI measurements using either L1B or L1C data and results are reported in Sec. 4.4.1.

5.1.3 IASI data formats

The following formats are used for the dissemination of IASI L1 and L2 products:

- BUFR (Binary Universal Form for the Representation of Meteorological data) is a standard binary format created by the World Meteorological Organization for the exchange and storage of any meteorological data. L1C and L2 IASI data are disseminated in BUFR format via EumetCast and via GTS.

- EPS Native (EUMETSAT Polar System format) is a generic EPS format (not IASI specific). It is a binary data format organized in sections containing header section providing general data, global data and measurement data (L1a, L1B, L1C) or retrieved data (L2).
- HDF5 (Hierarchical Data Format) Products in HDF5 format are the same as for the EPS Native with a different organization of the data. They can be read using standard HDF libraries. IASI L1C and L2 data are available in HDF5 format.
- EPS format readers (Fortran 90 and IDL) are available on-line on the EUMETSAT web site and have been implemented in the KLIMA-IASI pre-processor to read the IASI EPS Native data files.

For the purposes of the KLIMA project, the UMARF distribution mean was selected as the only option available to access archived IASI data. In the current version of the pre-processor for the acquisition of IASI operational products L1B, L1C and L2, in EPS Native format has been implemented.

5.2 GOSAT data

5.2.1 GOSAT data products

Several types of the GOSAT data products are provided for the users. Data users can search and order the L1 data (FTS L1B, CAI L1B, and CAI L1B+ data) and the higher level data products (FTS L2, CAI L2, FTS Level 3, CAI Level 3, Level 4A, and Level 4B data products) by accessing GOSAT DHF through GUIG.

The following products are available by the GOSAT spectral data processing and distribution chain:

- The FTS L1B data are radiance spectra that are obtained by performing the Fourier transformation on the signals detected by FTS. The degrees to which the targeted gas species absorb the reflected and emitted light in each of the spectral bands can be seen. A single data file of the FTS L1B data contains the radiance spectra obtained during 1/60 of an orbital revolution (defined as "one scene").
- The CAI L1B data are pixel-by-pixel radiances obtained by multiplying the digital image data of CAI by conversion factors.
- The CAI L1B+ data carry the same L1B radiance data, but the geographical locations of the image pixels are corrected for the skewness caused by the topographical roughness of the ground surface and are projected onto a map of the earth via interpolation. A single data file of the CAI L1B and L1B+ data contains the radiance data obtained during 1/60 of an orbital revolution (defined as "one frame").
- The FTS SWIR L2 data products store column abundances of CO₂ and CH₄ retrieved from the radiance spectra in the bands 1 through 3 of FTS. When ordering the L2 data products at GUIG, users can specify the observation areas and periods of their interests. The ordered data are provided to the users in a single data file.
- The FTS TIR L2 data products are vertical concentration profiles of CO₂ and CH₄ derived from the radiance spectra in band 4 of FTS.

With the scope of performing an inter-comparison of the CO₂ total column retrieved from KLIMA and TANSO-FTS L2, we downloaded from the GUIG, the following data products:

- FTS SWIR L2 V1.20
- FTS SWIR L2 V1.30
- FTS SWIR L2 V1.40

The different versions of the L2 products correspond to different versions of the input TANSO-FTS L1B product (measured spectrum) [59]. Our analysis and comparison was performed using the latest version of FTS SWIR data. After the first results of the validation team, a new version of FTS SWIR data (V2) was released, a few months before the end of the project, which have much better quality compared to the initial V1 data set. So it was decided to download also the latest version and repeat our analysis with the new data set:

- FTS SWIR L2 V2.00 (March 2010 - August 2010)
- FTS SWIR L2 V2.10 (September 2010 - December 2010)
- FTS SWIR L2 V2.11 (January 2011 - February 2011)

Only the V2 of the TANSO-FTS products are here used for the cross-comparison activity. Access to different releases of this version of TANSO-FTS L2 data (V2.00, V2.10 and V2.11) was necessary, as from the list of FTS SWIR datasets displayed above, in order to cover the entire period of one year identified for the comparison with IASI measurements. The results of the analysis performed using the original V1 dataset are summarized in Appendix D in order to provide a complete report of the activity but have not been used for the comparison.

5.2.2 Data processing and data products distribution

The GOSAT observational data are routinely processed at the GOSAT Data Handling Facility, and the data products are distributed to general users through the GOSAT data product distribution website (<http://data.gosat.nies.go.jp/GosatUserInterfaceGateway/guig/GuigPage/open.do>). The FTS and CAI data that the satellite has collected are received and processed at JAXA Tsukuba Space Center first. Then, these data are transferred to GOSAT Data Handling Facility (GOSAT DHF) via Tsukuba WAN, a high-speed wide area network in Tsukuba. GOSAT DHF gathers reference data, such as meteorological data necessary for the higher-level data processing, from cooperating institutions on a regular basis. Using these reference data, the observational data from JAXA are processed into column abundances of CO₂ and CH₄, CO₂ sources and sinks, and CO₂ three-dimensional distributions. The data processing is performed in conjunction with other external computing resources. Reference data used for validating the data products are also stored in this facility. All together, the amount of the data to be archived during the satellite's five-year operation period is about 400 terabytes.

The GOSAT data products are distributed through the GOSAT User Interface Gateway (GUIG), a website for GOSAT data distribution. Prior user registration is required for accessing the data products and can be done on "user authentication" page reached from "product & service" page on GUIG.

5.2.3 Validation of GOSAT data products

Validation of the GOSAT data products acquired through the routine processing of the GOSAT observational data is necessary, in order for the data products to be used meaningfully in the science community. The precision and bias of the data products must be clarified. To this end, the GOSAT data validation team used high-precision reference data obtained with ground-based and airborne measurements. For validating the L2 column abundances of CO₂ and CH₄, the team uses data from ground-based high-resolution Fourier transform spectrometers and in-situ observation instruments installed on aircrafts. Properties of clouds and aerosols calculated in the routine data processing are checked against the data obtained with remote sensing instruments, such as ground-based sky radiometers and lidars.

The data validation team has carried out a series of initial data validation activities and compared the L2 data products to the ground-based and airborne reference data. Data obtained in Japan, Europe, Oceania, and North America were used in these validation activities. Also, data collected by the aircrafts of Japan Airlines that participate in CONTRAIL (Comprehensive Observation Network for Trace gases by Airliner) project and the US National Oceanic and Atmospheric Administration's airborne measurement program were employed. The first results of the comparison indicated that the TANSO-FTS SWIR XCO₂ (V1) are biased low by $2.3 \pm 1.2\%$ than the reference values [40]. The latitudinal pattern of the L2 zonal means, however, were broadly consistent with those of the reference values.

5.3 TCCON data

TCCON data can be downloaded from the TCCON database (link: <http://tcccon.ipac.caltech.edu/>).

5.3.1 TCCON Database

A defined dataset of gases (CO₂, CH₄, N₂O, HF, CO, H₂O, O₂ and HDO) and supporting data sufficient to allow the calculation of the tropospheric average mixing ratio (e.g. Averaging Kernels (AKs), a priori profiles) are archived in a central TCCON database. All co-Is have access to all data in the TCCON archive. Use of these data is contingent upon reciprocity; all PI's agree to make their own data available to the TCCON community.

Archived data includes flags to identify which data are deemed of sufficient quality for specific purposes. Data, which pass all defined Quality Control (QC) tests, i.e. data which remain unflagged (flag = 0) at the end of the QC procedure, are deemed suitable for public release. Quality control criteria may evolve in time as our characterisation of measurement errors improves. The QC criteria applied are documented for each public release. PI's are encouraged to release their data to the public as soon as possible, but no later than one year after acquisition.

Each TCCON site PI is responsible for archiving sufficient raw data and ancillary information at their own site to allow the data to be reprocessed when necessary.

5.3.2 TCCON Data Processing

Individual TCCON sites are responsible for processing their collected interferograms in a standardized procedure to ensure consistency across the network. Standard processing should use the current release versions of the relevant software packages and requires:

- Transformation of interferograms to spectra using the Interferogram Processing Program (IPP), which reads OPUS- and slice-format interferograms, computes spectra using standardized phase correction, Fourier transformation and DC correction algorithms, and writes OPUS-format spectra;
- Fitting of spectra using GGG to retrieve total column amounts and derived output data. TCCON standards (spectral windows, levels, correction factors, vmrs, etc.) are documented on the wiki. The results are delivered in a *.eof.csv file in which specifies the site, date, and current version of the software is indicated in a standardized manner.

Following release of new software versions, each site shall reprocess and deliver their data to the TCCON archive within 4 months.

5.3.3 TCCON Calibration

Calibration of the TCCON facilities follows the description identified by Wunch et al. [62].

6 KLIMA-IASI software suite: integration on G-POD

The KLIMA-IASI software suite installed on G-POD, devoted to the analysis of the IASI observations, consists of two independent modules:

- *The KLIMA pre-processor module*

The pre-processor is the interface between the IASI operational products (both L1 and L2 data provided by EUMETSAT) and the Retrieval module. It is devoted to the selection of specific observations from the data orbit files according to a set of filtering criteria provided by the user. From the selected observations the pre-processor extracts relevant information required by the retrieval (spectral data from L1 file, auxiliary data from L2 files) and arranges them in an input data set for the analysis using KLIMA retrieval module.

- *The KLIMA retrieval module*

This module includes the Forward Model and the Retrieval Model that can be independently operated to produce simulated observations or be combined for inverse processing of real or synthetic data from the IASI instrument. The retrieval module reads the input data set arranged by the pre-processor and performs the retrieval according to the settings provided by the users. The retrieved quantities and the auxiliary products are exported by the module at the end of the retrieval process and saved in an output data set (data files in ASCII format).

Both modules do not allow a direct interface with the user during the execution: all parameters used to trigger the applications are provided by the user through two setting files (in ASCII format): the setting file of the pre-processor module and the setting file of the retrieval module.

The input and output files for pre-processor and retrieval are described in sections from 6.1.1 to 6.1.6. A template for input/output products of the pre-processor and of the retrieval is provided in Appendix E.

6.1 *The logic flow of the analysis*

The flow chart of the KLIMA software is shown in Fig. 16. The analysis starts with the pre-processor that reads the IASI L1 and L2 data files; extracts data related to the observations selected according to the filtering criteria set by the users and generates the input data sets for the retrieval. When the pre-processing phase is terminated, the retrieval module is started for each input data set provided by the pre-processor. The results of the retrieval are provided in output in ASCII format. All the retrieval options and the triggering parameters are specified in the setting file, an ASCII file editable by the user. Furthermore, the retrieval procedure requires some auxiliary data (e.g. spectroscopy data, climatological data, etc.). During the execution of the retrieval procedure, some output data are generated and updated. The results of the retrieval procedure are stored in the output products files (retrieval results and retrieval diagnostic).

6.1.1 *The input of the pre-processor*

The pre-processor requires as input:

- a IASI L1B or L1C and a IASI L2 data file; both L1 and L2 have to be in EPS format (downloaded from UMARF database).
- a settings file containing all input parameters necessary to trigger the pre-processor procedure. This file is in ASCII format and can be directly edited by the user.

6.1.2 *The Auxiliary data for pre-processor module*

The measurement errors associated with the observed spectrum are extracted from the file IASI_NCM_xx.M02_*.nat, provided by the UMARF database.

6.1.3 *The output of the pre-processor: the KLIMA Input Dataset*

The pre-processor module produces as output a series of files related to the selected observations that constitute the input dataset for the retrieval module.

Each file is classified by using the orbit ID (date and time), the scan ID and the observation ID.

The file generated by the pre-processor are listed in the following:

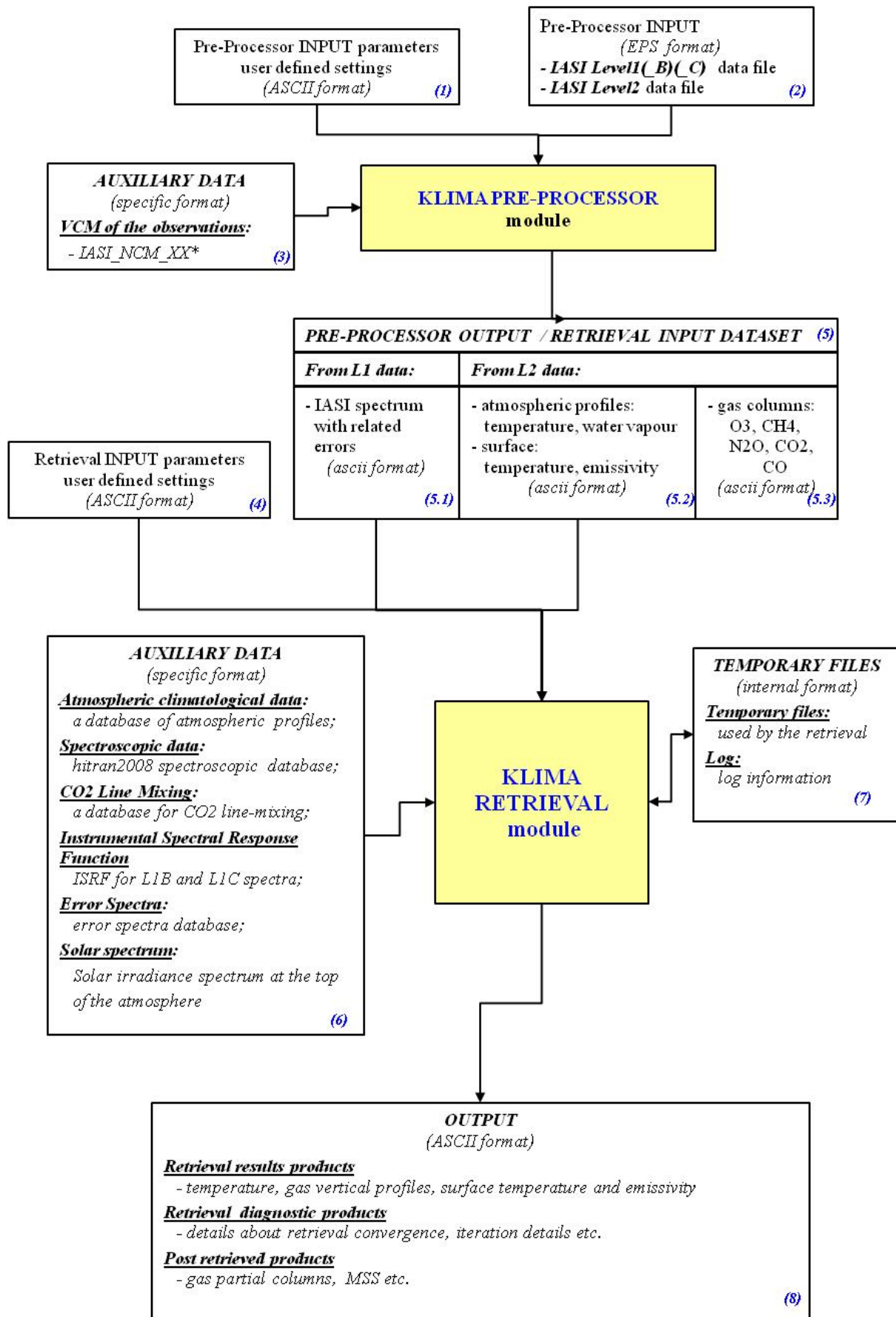


Fig. 16: Flow chart identifying the main blocks of KLIMA software

- `orbitID_scanID_obsID_observ.dat`
Containing the observation measurements, the observation errors and the non-zero elements of the VCM of the observations;
- `orbitID_scanID_obsID_temperature.dat`
Containing the L2 operational retrieved profiles of atmospheric temperature;
- `orbitID_scanID_obsID_vmr_h2o.dat`
Containing the L2 operational retrieved profiles of the water vapour;
- `orbitID_scanID_obsID_surface.dat`
Containing the L2 operational retrieved values of the surface temperature;
- `orbitID_scanID_obsID_col_[species].dat`
Containing the L2 operational retrieved values of the total columnar amount of the species indicated in the file name;
- `orbitID_scanID_obsID_partial_col_O3.dat`
Containing the L2 operational retrieved values of the partial columnar amount of Ozone.

6.1.4 The input of the retrieval module

The retrieval module requires in input:

- The observation measurements file, generated by the pre-processor module and containing the observed spectrum, the observation errors and the non-zero elements of the VCM of the observations, and some temporal, spatial, geometrical and spectral information;
- The settings file (the name of the file is user defined) containing all input parameters necessary to trigger the retrieval as well as all the retrieval options. This file is in ASCII format and can be directly edited by the user.

6.1.5 The auxiliary data of the retrieval module

The auxiliary data used by the retrieval procedure are listed here below:

- Atmospheric Climatological Data: a climatological database containing information on the vertical distribution of atmospheric pressure, temperature and minor constituents concentration; data are classified by year and latitude [47].
- Spectroscopic Data: the HITRAN 2008 spectroscopic database [50] .
- CO₂ Line Mixing: a spectroscopic database used in CO₂ line-mixing computation [41],[42].
- Instrumental Spectral Response Function: the ISRF of the IASI instrument provided by the UMARF data archive.
- Error Spectra: the error spectra database that models the forward model errors.
- Solar Spectrum: the irradiance of the solar source at the top of the atmosphere, used to model the surface reflection [23].

Note that each set of auxiliary data comes from different sources and, as consequence, data are organized in different formats. The specific format is not reported here. For the format description please refer to the documentation reported in the references ([32]).

6.1.6 The output of the retrieval module

The set of the retrieval product files generated by the procedure changes according to the input parameters: the user is allowed to enable/disable the retrieval of the atmospheric temperature profile, of the atmospheric gases profiles and of the surface temperature and emissivity. As a consequence, only the files related to the selected retrieved parameters are generated.

- `temperature.dat`

The file contains the retrieved profile of the temperature and some auxiliary information. Data are arranged in columns and contains in details (key-word `[Temperature]`):

- the value of the atmospheric pressure [mBar]; for each pressure
 - * the logical flag to identify the retrieved (T) or interpolated (F) level;
 - * the related pressure [mBar];
 - * the related altitude [km];
 - * the temperature value used as initial guess of the retrieval [K];
 - * the temperature retrieved values [K];
 - * the retrieval unbiased error [K];
 - * the retrieval biased error [K];
 - * the a priori error related to the initial temperature [K].

- `[species].dat`

The file contains the retrieved profile of the gas specified by the string `[species]` and some auxiliary information. Data are arranged in columns and contain in details (key-word `[[species]]`):

- the value of the atmospheric pressure [mBar]; for each pressure
 - * the logical flag to identify the retrieved level;
 - * the related pressure [mBar];
 - * the related altitude [km];
 - * the VMR used as initial guess of the retrieval [ppm];
 - * the VMR retrieved values [ppm];
 - * the retrieval unbiased error [ppm];
 - * the retrieval biased error [ppm];
 - * the a priori error related to the initial guess VMR [ppm].

The last row contains some information about the columnar amount: the total air column [mol/cm^2], the `[species]` total column amount and the related biased error [mol/cm^2].

- `surface_temperature.dat`

The file contains the retrieved surface temperature and some auxiliary information. In details (key-word `[Surface_Temperature]`):

- the initial guess of the surface temperature used in the retrieval [K];
- the retrieved value of the surface temperature [K];
- the retrieval unbiased error [K];
- the retrieval biased error [K];
- the a priori error of the initial guess surface temperature [K].

- `surface_emissivity.dat`

The file contains the retrieved surface emissivity as a function of the wavenumber. Data are arranged in columns and contain in details (key-word `[Surface_Emissivity]`):

- the wavenumber [cm^{-1}]; for each wavenumber
 - * the initial guess value for the surface emissivity;
 - * the retrieved emissivity;
 - * the unbiased error;
 - * the biased error;
 - * the a priori error of the initial guess surface emissivity.

6.1.7 The retrieval diagnostics

The set of retrieval diagnostics output files contains essential information to characterize the performance of the retrieval process.

- `iterationdetails.dat`

The file contains some quantifier about the performance of the retrieval procedure relative to each iteration as well as the retrieval convergence information. In the file are reported the total number of retrieved parameters (key-word `[N_TARGET]`) and the kind of parameters (key-word `[TARGET]`).

The file is updated after each iteration with a row containing (key-word `[ITERATIONS]`):

- the number of Gauss iteration;
- the number of Marquardt iteration;
- the reduced χ^2 ;
- the linear reduced χ^2 computed at iteration;
- the trace of the AK matrix;
- the information content from the AK matrix for each retrieved parameter;
- the Marquardts lambda parameter.

The final section of the file contains information about the retrieval convergence and a row showing the above quantifier computed at the end of the retrieval (key-word `[LAST_ITERATION]`).

- `spectrum.dat`

The `spectrum.dat` file contains the simulated spectrum related to the retrieved profiles, the simulated spectrum computed using the adopted initial guess values for atmosphere and surface, and the original observed spectrum as extracted from IASI L1 data. Data related to spectrum and error are reported both in radiance and in brightness temperature (key-word `[SPECTRA]`). Data are arranged in columns and contain:

- the progressive number;
- the band index (the index refers to the spectral bands defined in the retrieval input);
- the wavenumber [cm^{-1}];
- the observed spectrum [$\text{nW}/(\text{cm}^2 \text{ sr cm}^{-1})$];
- the spectrum computed using the initial guess atmosphere [$\text{nW}/(\text{cm}^2 \text{ sr cm}^{-1})$];
- the spectrum computed at the last successful iteration [$\text{nW}/(\text{cm}^2 \text{ sr cm}^{-1})$];
- the observed spectrum error (diagonal of the VCM of observations) [$\text{nW}/(\text{cm}^2 \text{ sr cm}^{-1})$];
- the observed spectrum [K];
- the spectrum computed using the initial guess atmosphere [K];
- the spectrum computed at the last successful iteration [K];
- the observed spectrum error (diagonal of the VCM of observations) [K].

- `MSS_temperature.dat`

The file contains the MSS data related to the retrieval of the temperature profile. Data are arranged in columns and contain:

- key-word `[SPECTRAL_POINT]`: number of spectral points used in the retrieval;
- key-word `[RETRIVED_POINT]`: number of retrieved temperature levels;
- key-word `[Temperature_MSS_Data]`: data are arranged in columns according to the following fields:
 - * the observed spectrum [$\text{nW}/(\text{cm}^2 \text{ sr cm}^{-1})$];
 - * the simulated spectrum [$\text{nW}/(\text{cm}^2 \text{ sr cm}^{-1})$];
 - * the $\text{VCM}^{-\frac{1}{2}}$ times the residual;
 - * the $\text{VCM}^{-\frac{1}{2}}$ times the Jacobian matrix.

- `MSS_[species].dat`

These files contain the MSS data related to the retrieval of the [species] profile. Data are arranged in columns and contain:

- key-word `[SPECTRAL_POINT]`: number of spectral points used in the retrieval;
- key-word `[RETRIVED_POINT]`: number of retrieved [species] level;
- key-word `[[species]_MSS_Data]`: data are arranged in columns according to the following fields:
 - * the observed spectrum [$nW/(cm^2 \text{ sr cm}^{-1})$];
 - * the simulated spectrum [$nW/(cm^2 \text{ sr cm}^{-1})$];
 - * the $VCM^{-\frac{1}{2}}$ time the residual;
 - * the $VCM^{-\frac{1}{2}}$ time the Jacobian matrix.

- `[species]_column.dat`

Note that the KLIMA retrieval code does not retrieve directly the total column of a specific gas in the atmosphere. These files contain:

- key-word `[N_LAYERS]`: number of layers in column profile;
- key-word `[[species]_column]`: data are arranged in columns according to the following fields:
 - * the highest altitude [km];
 - * the lowest altitude [km];
 - * the air column [n°/cm^2];
 - * the column retrieved values [n°/cm^2];
 - * the VCM.

6.2 *The integration of the KLIMA code on ESA G-POD for Earth Observation Application system*

The run of the pre-processor and retrieval code, the making of directories and the interactions between pre-processor and retrieval code are managed by a dedicated task-manager developed by the G-POD team.

The G-POD environment is accessible using a dedicated Web portal (<http://gpod.eo.esa.int/>) allowing the user to select a region of interest, in terms of geographical coordinates and observation time, by using a graphical tool. Selected observations are grouped in a Task and sent in execution on the computer grid. At the end of the retrieval process, the output data set containing the retrieval results and auxiliary outputs are exported to a selected user machine.

The workspace is composed of some Graphical User Interfaces (GUI) that have been developed by the G-POD team for the management of the analysis.

- *Configuration Panel*

A panel dedicated to selection of the orbit to be process configures the task to submit to the system and start the analysis. In particular, the Configuration Panel (see Fig. 17) is composed of:

- a graphical interface dedicated to time and spatial selection;
- a graphical interface for task configuration;
- a section dedicated to execute query on orbit database and to the selection of the orbit for data processing;
- a text interface that allows the user to create or modify the setting files for pre-processor and retrieval.

- *Task Monitor Panel*

A panel dedicated to monitor the state of the execution of tasks.

- *Log Panel*

A panel dedicated to display the log of the execution of each task

An example of the graphical user interface provided by the G-POD system is shown in Fig. 17: the panel dedicated to the query of the orbit database and to the selection of the orbits for data processing.

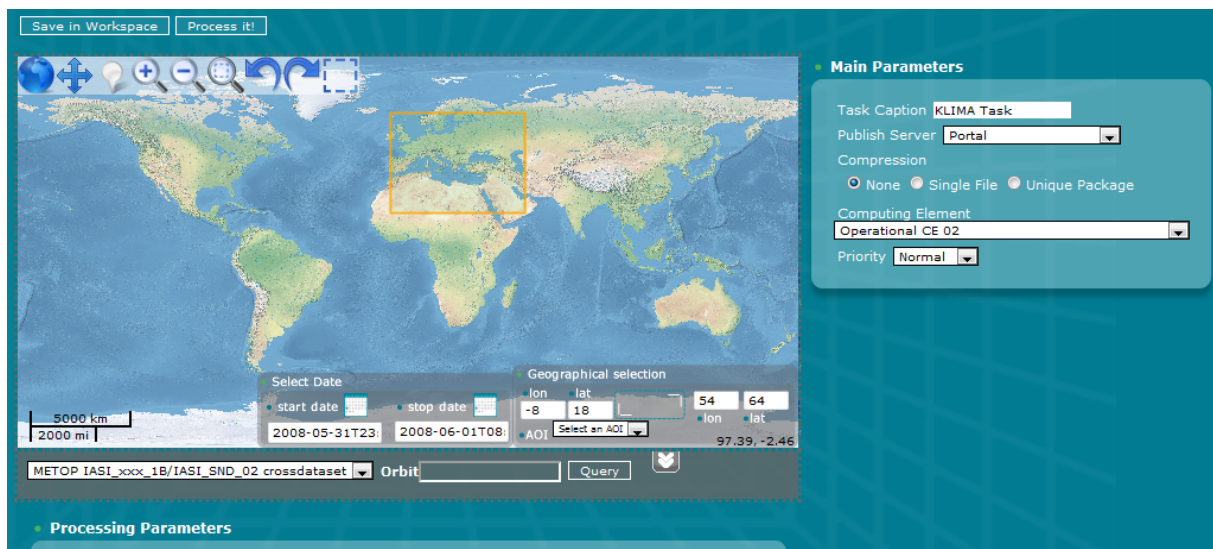


Fig. 17: The G-POD Configuration Panel

7 IASI data processing using KLIMA retrieval code and inter-comparison strategies

The main goal of this project is the processing of IASI data and the comparison of its retrieved L2 products by KLIMA-IASI code with EUMETSAT L2 operational products, with TANSO-FTS/GOSAT L2 products and with the TCCON ground station products.

This objective has been achieved by processing one week per month of IASI data in the selected period of one year (from March 1, 2010 to February 28, 2011) on a global geographical coverage. For each month a complete week has been processed, retrieving the XCO₂ both on land and on water and both during day and night. Only clear sky IASI observations have been analysed, up to a maximum number of 20000 for each week. On water, because of the moderate CO₂ variability, a limited number of observations has been selected by only using the central pixels of the IASI scan. On land some off-axis azimuth scans are considered, up to the maximum number of 20000 (this is a small number when compared with the about 2 millions observations made each week by IASI).

As described in Sect. 4.4, the analysis was preceded by a pre-processing to screening of the IASI L1 data. The adopted selected criteria allowed to exclude the IASI data when a bad quality flag is reported on L1 operational data (due to the validation the L1 product) and L2 operational data (due to the convergence of the L2 iterative retrieval and to the validation the L2 product) and to exclude the observation in cloudy sky conditions. The retrieval settings have been described in Sect. 4.4 and have been used for the whole data analysis.

The KLIMA-IASI processing campaign was performed on the ESA G-POD facilities in 4 months, starting from June 2012 until the end of September 2012. A large amount of data was processed as summarised by the following Tab. 10.

Tab. 10: Data processed on G-POD

Processing Time	4 Months
Annual number of orbits	≈ 5110 Orbits
Processed Orbits (Water and Land)	≈ 2300 Orbits (≈ the half for the macro areas analysis)
Processed Data Volume	≈ 5 TB
Retrieved L2 products	≈ 240000 Observations

To achieve this results multiple computing resources were dedicated to this objective:

- ESRIN Cluster - 80 cores
- UK-PAC Cluster - 96 cores
- External Cloud Cluster - 24 cores (August and September 2012)

About 200 parallel processes of KLIMA-IASI, equivalent to the number of cores, were run simultaneously for the whole processing period. The G-POD Team also carried out multiple activities which span to different fields:

- Data Ordering and Ingestion in the G-POD stores
- KLIMA-IASI service tuning to be suitable for a bulk processing
- Processing setup and monitoring (both for Water and Land) for each week of data after IFAC-CNR pre-processing analysis
- Output data organization and uploading to IFAC-CNR FTP
- External cloud cluster (2 machines) setup and configuration
- Internal clusters (ESRIN and UK-PAC) configuration to dedicate the necessary resources for a specific processing (when before they were shared for all G-POD users)

As described in Sect. 4.4, (Equation 1), after the bulk processing, the retrieved value of the total column amount of CO₂ is used to compute the XCO₂ from the total column amount of H₂O and the atmospheric pressure at the surface imposing the hydrostatic equilibrium.

To perform the comparison of the L2 data obtained from KLIMA code with EUMETSAT L2 operational products, with TANSO-FTS/GOSAT L2 products and with the TCCON ground stations products different strategies and representations have been adopted. The KLIMA L2 product is described in Sect. 8. In this section we report the maps of mean XCO₂ total column [ppm] and other auxiliary information, averaged on weekly scale (the analysed week per each month) on a 2° x 2° pixel grid. This representation of the XCO₂ is consistent with the requirements established for by Rayner and O'Brien [45]. The other auxiliary information shown is the mean retrieval error

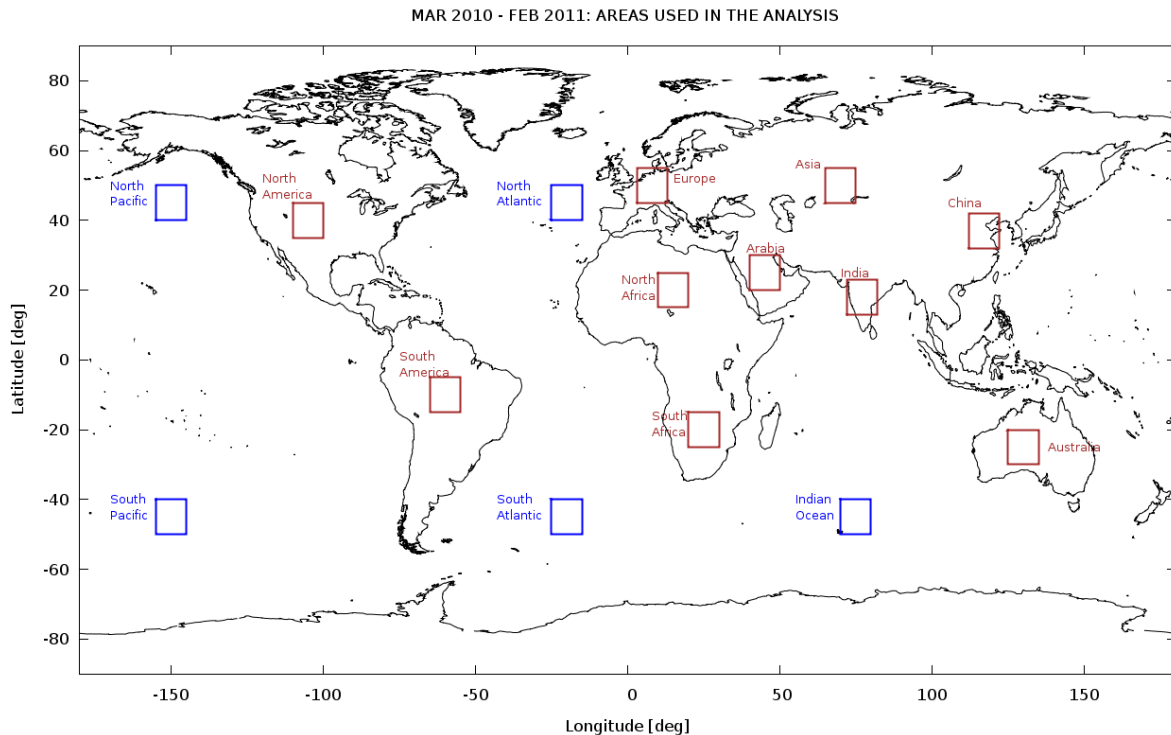


Fig. 18: Macro areas selected for the annual XCO₂ mean values comparisons between KLIMA L2 products, EUMETSAT L2 products and TANSO-FTS L2 products

[ppm], the retrieval error associated to the XCO₂ mean values [ppm] and the geographical and time variability expressed as the ratio between the standard deviation of the retrieved values and the XCO₂ mean retrieval error. Also these quantities refer to the same representation.

The comparison with EUMETSAT L2 operational products present the better condition of coincidence, because the products refer at the same measurements, but are obtained from different algorithms. For this reason it was possible to make a direct comparison of each XCO₂ value. The comparison has been shown on global scale, evaluating the averaged XCO₂ differences on weekly scale and on 2° x 2° pixel grid. From this representation we obtain the maps related to each analyzed months and to the whole year respectively. The seasonal cycle plots and plots of XCO₂ annual mean values over a set of selected geographical macro areas are also included. The selected macro areas are shown in Fig. 18. Results have been reported in Sect. 9.

The comparison between KLIMA L2 results with TANSO-FTS operational products has been performed with a dual representation. The first representation has been done using only the coincident observations. The coincidence criteria adopted in this comparison (see Sect. 10), in term of time and distance between the footprint of the observations, have been fixed in order to verify the reliability of the comparison and to increase the statistical sample. For this reason the selection criterion has been chosen as an acceptable compromise between the need to compare quantities retrieved from measurements observing the same scene and a number of samples suitable for an annual statistics. In this case the correlation plots are shown. The second representation is on global scale, comparing the averaged XCO₂ on weekly scale and on 2° x 2° pixel grid (on the same base used for the KLIMA L2 product) and on 9° x 9° pixel grid (corresponding to a 1000x1000 km² pixel dimension at the equator). For this representation we obtain the correlation plots related to the whole year. Also for this case the seasonal cycle and annual mean values over macro areas plots are included. Results have been reported in Sect. 10.3.

Due to the very reduced coverage, the comparison between KLIMA L2 results with TCCON products was represented using only the coincident observations. These observations have been averaged in order to obtain a single value for each day in which the coincidences has been found to evaluate the correlations with KLIMA L2 products. Also in this case, the comparison results (shown in Sect. 11) have been reported for different coincidence criteria.

7.1 Method to compare retrieval products with different AKs and a priori

To properly compare the XCO₂ results properly, we have to take into account the effect of the different a priori profile used in the retrieval analysis and the effect of the different smoothing described by the AKs matrix [51].

For the comparison with the TANSO-FTS data we applied the a priori profile used in the KLIMA data analysis to the retrieved TANSO-FTS SWIR XCO₂ profile, applying equation 10 reported in [51]. The profile is then smoothed by using the IASI AK matrix, using equation 25 reported in [51] and successively converted in columnar CO₂ by means of the operator pressure weighting function, defined as the ratio between the partial dry air column and the total dry air column. The IASI AKs depend on latitude and on season, for this reason the a priori and the IASI AKs, used to modify the TANSO-FTS data, have been evaluated on five latitude ranges (Northern Polar, Northern Mid Latitude, Equatorial, Southern Mid Latitude and Southern Polar) and on four climatological atmospheres (Winter, Spring, Summer and Autumn). The major effect is due to the different smoothing represented by the AKs. In fact, the IASI AKs present a maximum close to 200 hPa and generally reach low values above 900 hPa and below 100 hPa, while the TANSO-FTS AKs are quite constant on the same altitude range.

As shown in many recent works (for example [60], [40], [48], [64] and [15]), also the TCCON data used as a reference in a validation procedure need to take into account the a priori adjustment and the AKs smoothing. In some cases, these effects can be neglected, because the smoothing error is less than the retrieval error (random and systematic); for example, to validate XCO₂ products obtained from TANSO-FTS SWIR measurements on GOSAT satellite, Cogan et al. [15] and Wunch et al. [64] estimated the smoothing error due to the TANSO-FTS SWIR AK in few tenths of ppm, while the retrieval error was about 2-3 ppm. For the comparison of XCO₂ obtained from IASI measurements using KLIMA code with the TCCON data the effect of the a priori along with the smoothing error, evaluated using Eq. A12 reported in [64] have been estimated of about 5 ppm. In this case, the AK smoothing can not be neglected. However, to perform the AK smoothing, the retrieved XCO₂ profile from TCCON is needed, but it is not directly available from the standard products of the network. For this reason, the comparison between TCCON and KLIMA-L2 products can not be considered as a validation test. On the basis of the previous statements the inter-comparison between KLIMA-L2 and TANSO-FTS products adjusted for the a priori profile and smoothed for the AK matrix can be considered a more reliable step in the validation issue of the XCO₂ measurement from satellite observations.

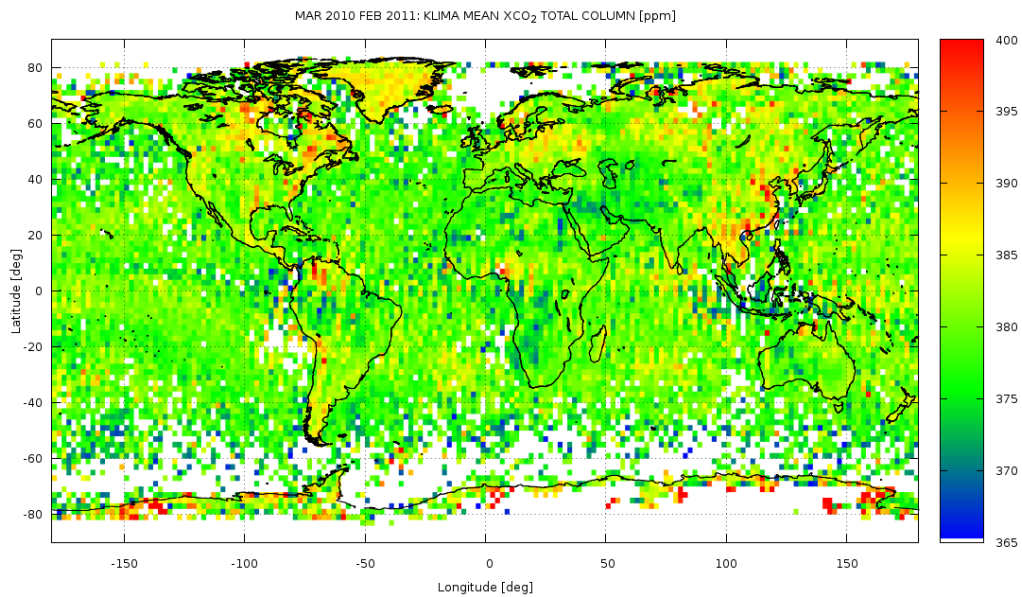


Fig. 19: MARCH 2010-FEBRUARY 2011: KLIMA-IASI L2 XCO₂ total column [ppm] over a grid of 2° x 2°, averaged for one year

8 Global distribution of KLIMA XCO₂ monthly averaged products

8.1 KLIMA products overview

IASI L1C spectra are analysed using the version of KLIMA-IASI algorithm integrated in the G-POD system. The data selection was performed according to the criteria discussed in Sect. 7. The results here presented refer to the retrieved values of XCO₂ total column. An example of the IASI L2 product provided by KLIMA-IASI and used to evaluate the XCO₂ is reported in Fig. 19: the map shows the XCO₂ values [ppm] averaged for the year from March 2010 to February 2011 for a global geographical coverage over a grid of 2° x 2°.

Panels from Fig. 20 to Fig. 31 show for each month the map of the global geographical coverage, as a function of latitude and longitude, of the following quantities:

- the KLIMA L2 mean XCO₂ total columns [ppm];
- the XCO₂ mean retrieval errors [ppm];
- the retrieval errors associated with the XCO₂ mean value [ppm] (i.e., the mean error divided the square root on the number of measurements on every grid pixel);
- the ratio between the standard deviation of the retrieved values and the XCO₂ mean retrieval error;
- the number of observations per pixel.

For the calculation of these means we considered the arithmetic averages, because the retrieval errors associated with individual products do not present a large monthly variability within the single pixel.

The mean XCO₂ total columns retrieved by KLIMA (top map from Fig. 20 to Fig. 31) show a good geographical coverage; data distribution spans from the Polar regions through the Tropics. With the use TIR IASI spectral channels, measurements are available both during day and night, even if no significant diurnal variability has been observed in the limited data set observed so far. Accordingly, no distinction is made in the plotted results between day and night observations. It is possible to see from the global distribution maps that the longitudinal variations in XCO₂ over the oceans are smaller than those over land. Higher concentration values over oceans are found from October to February, in both Hemispheres. Over land, the seasonal variation of XCO₂ is controlled mainly by photosynthesis in the terrestrial ecosystem. The XCO₂ concentrations are generally higher in the Northern

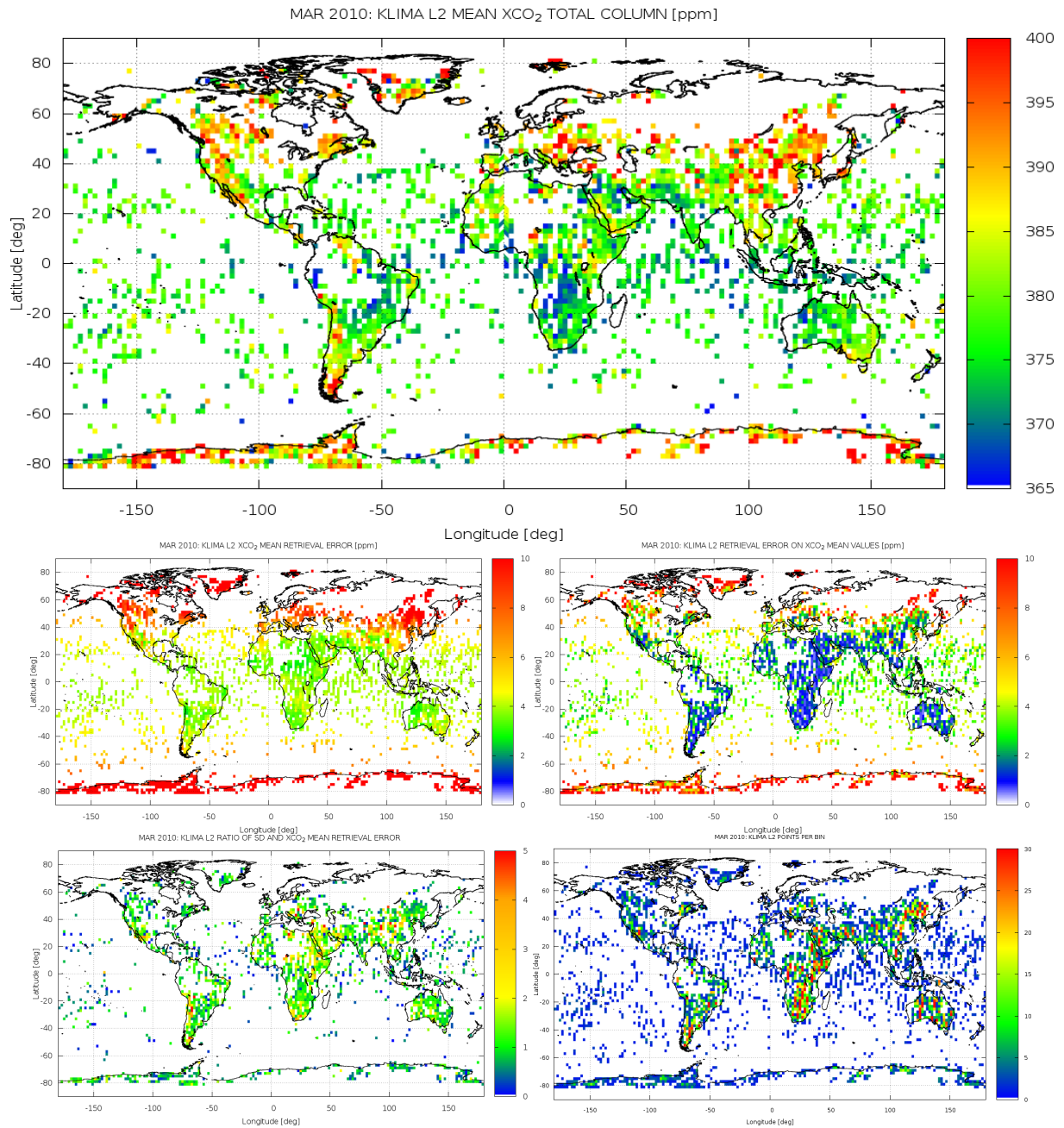


Fig. 20: 8-14 MARCH 2010: Global distribution of KLIMA L2 XCO₂ monthly mean; averaged monthly retrieval errors; errors on XCO₂ mean values; geographical and time variability expressed as the ratio between standard deviation and mean error and number of observations per pixel

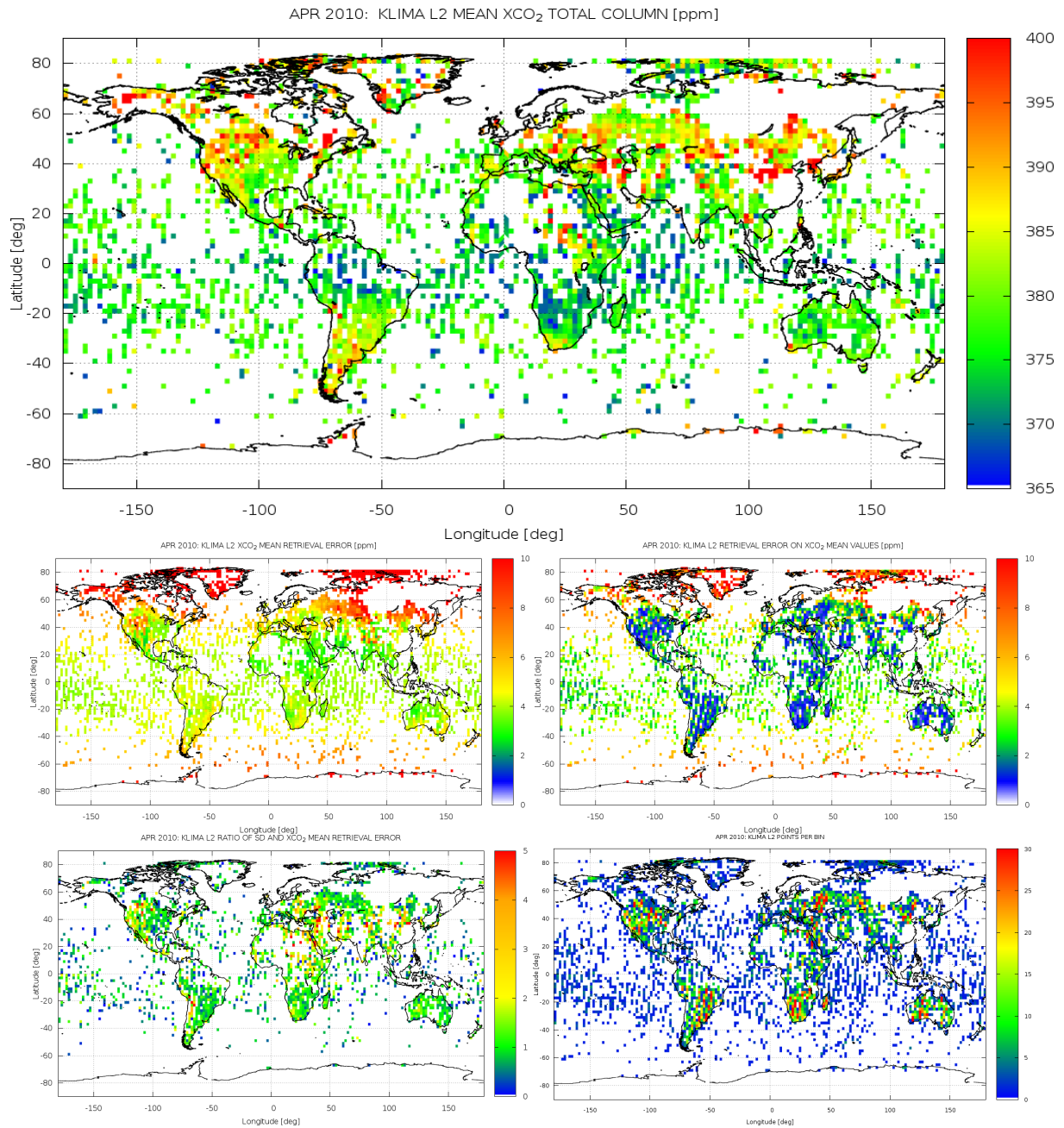


Fig. 21: 5-11 APRIL 2010: Global distribution of KLIMA L2 XCO₂ monthly mean; averaged monthly retrieval errors; errors on XCO₂ mean values; geographical and time variability expressed as the ratio between standard deviation and mean error and number of observations per pixel

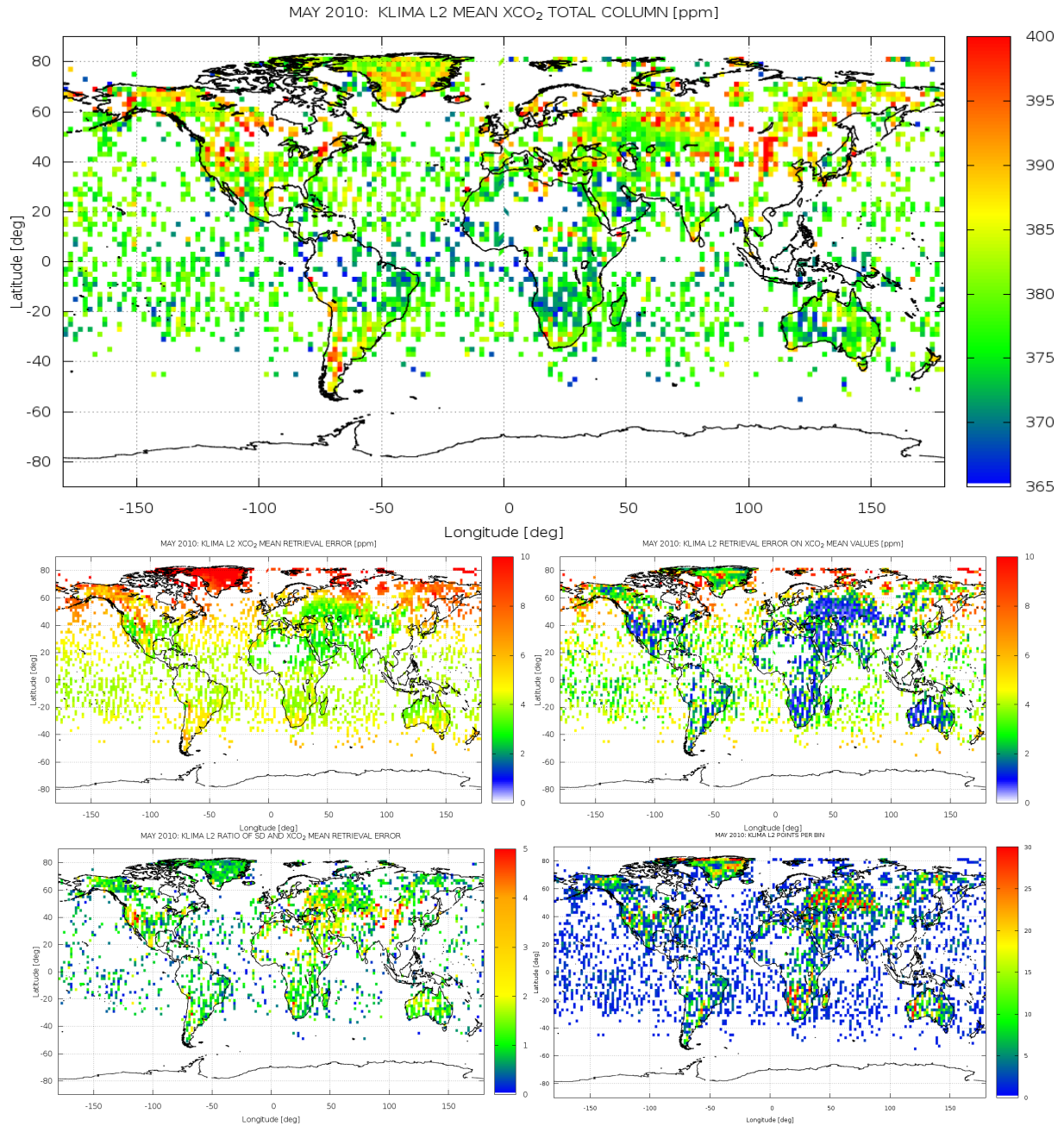


Fig. 22: 3-9 MAY 2010: Global distribution of KLIMA L2 XCO₂ monthly mean; averaged monthly retrieval errors; errors on XCO₂ mean values; geographical and time variability expressed as the ratio between standard deviation and mean error and number of observations per pixel

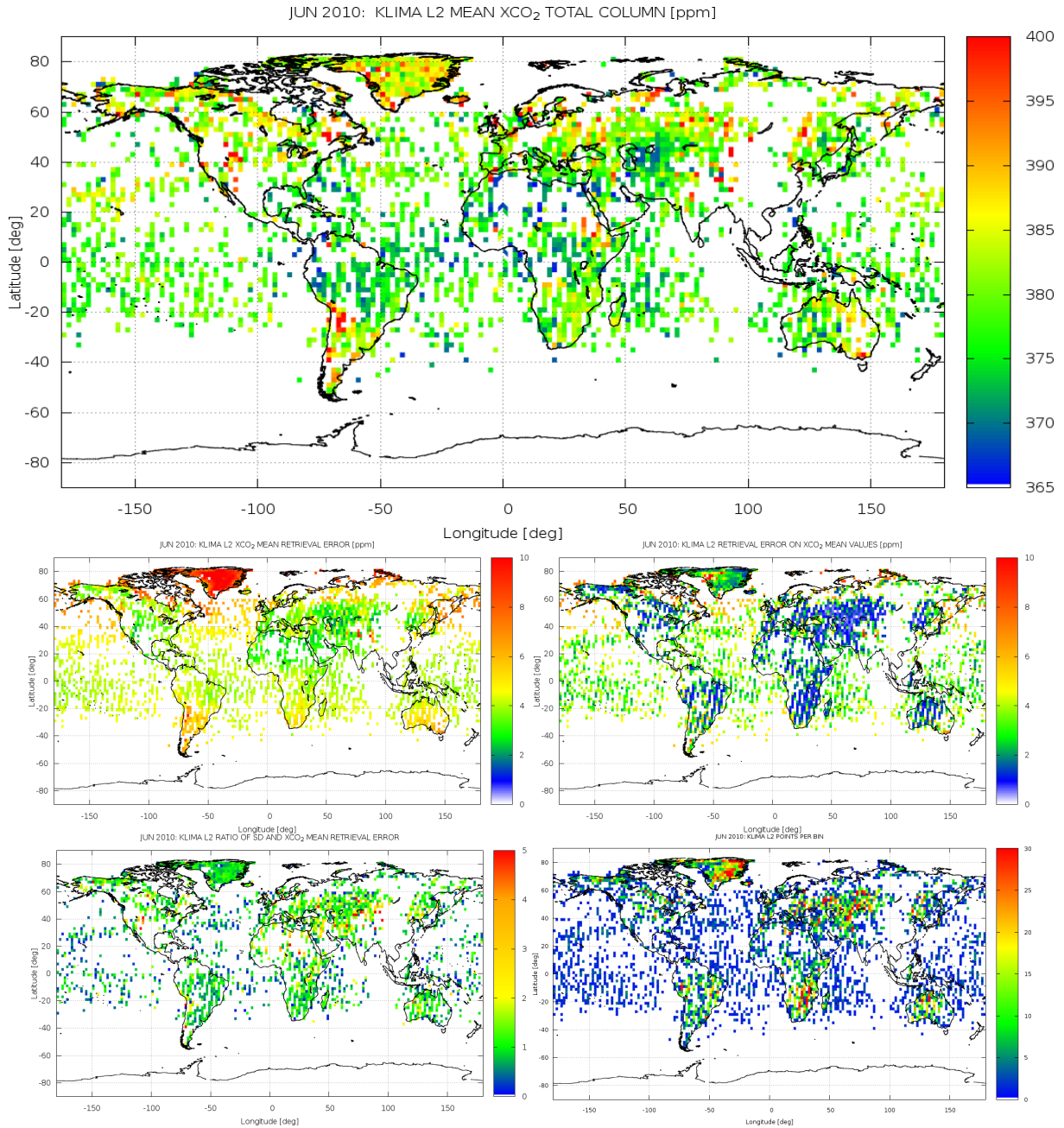


Fig. 23: 3-9 JUNE 2010: Global distribution of KLIMA L2 XCO₂ monthly mean; averaged monthly retrieval errors; errors on XCO₂ mean values; geographical and time variability expressed as the ratio between standard deviation and mean error and number of observations per pixel

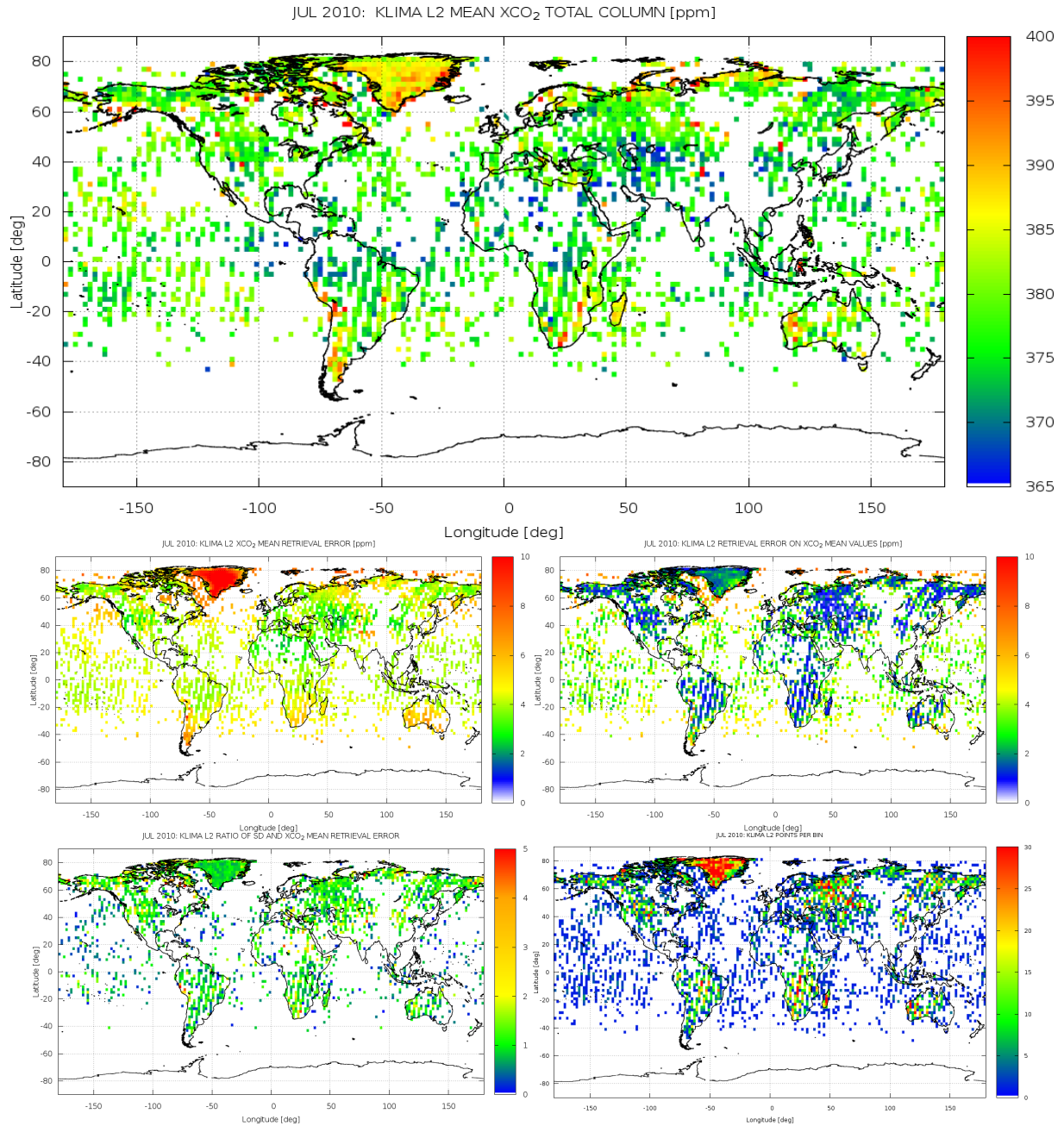


Fig. 24: 5-11 JULY 2010: Global distribution of KLIMA L2 XCO₂ monthly mean; averaged monthly retrieval errors; errors on XCO₂ mean values; geographical and time variability expressed as the ratio between standard deviation and mean error and number of observations per pixel

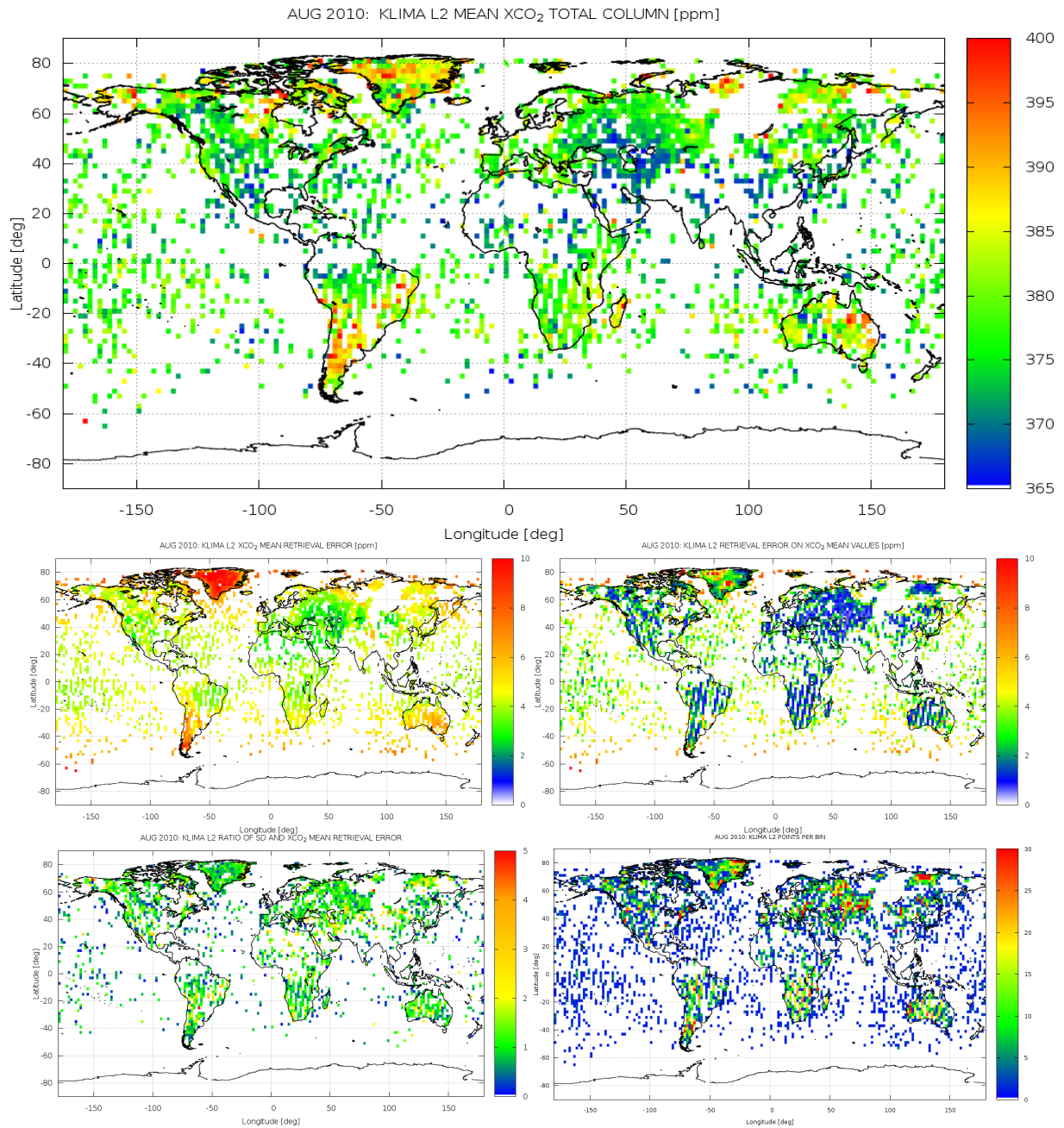


Fig. 25: 2-8 AUGUST 2010: Global distribution of KLIMA L2 XCO₂ monthly mean; averaged monthly retrieval errors; errors on XCO₂ mean values; geographical and time variability expressed as the ratio between standard deviation and mean error and number of observations per pixel

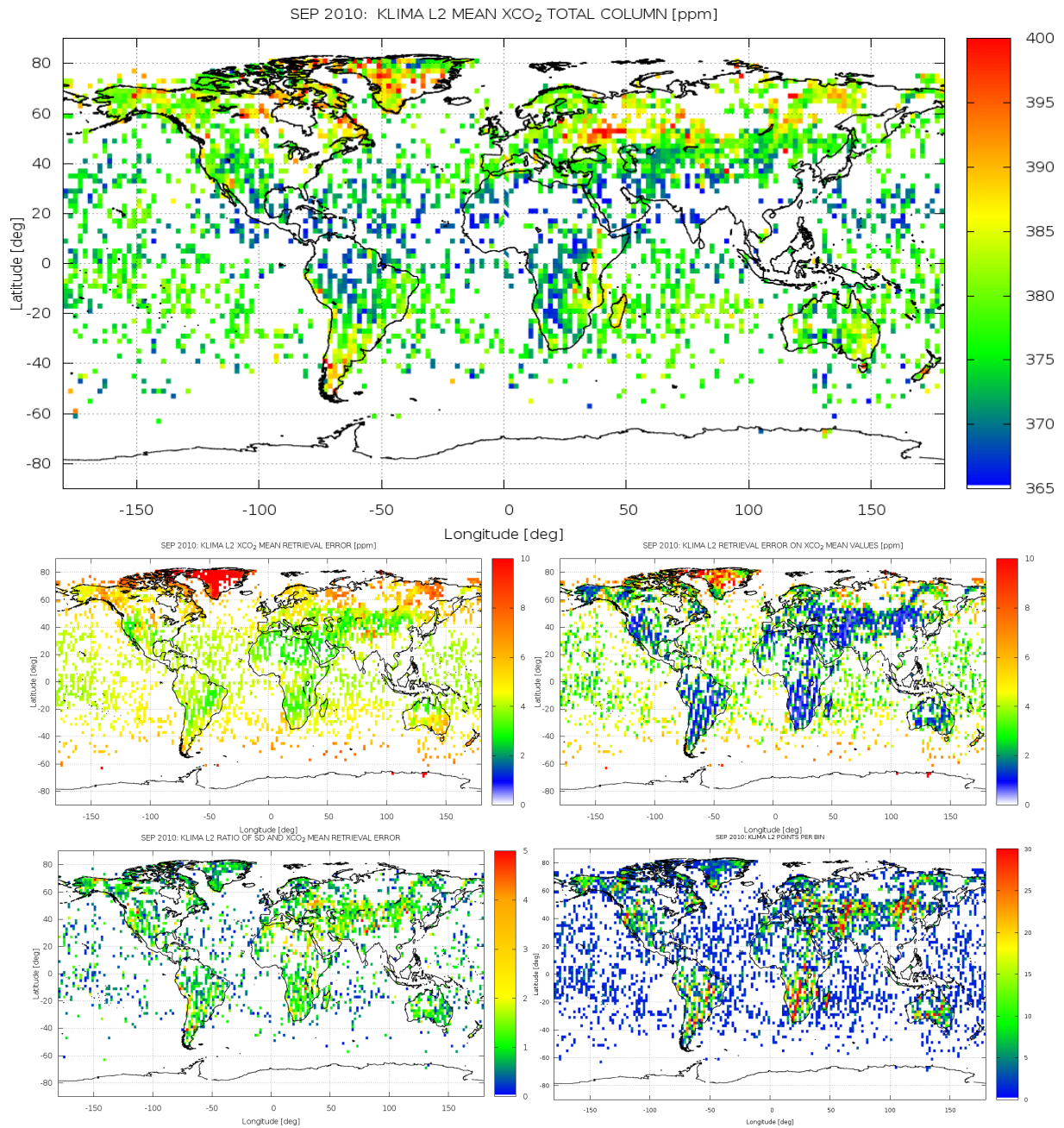


Fig. 26: 6-12 SEPTEMBER 2010: Global distribution of KLIMA L2 XCO₂ monthly mean; averaged monthly retrieval errors; errors on XCO₂ mean values; geographical and time variability expressed as the ratio between standard deviation and mean error and number of observations per pixel

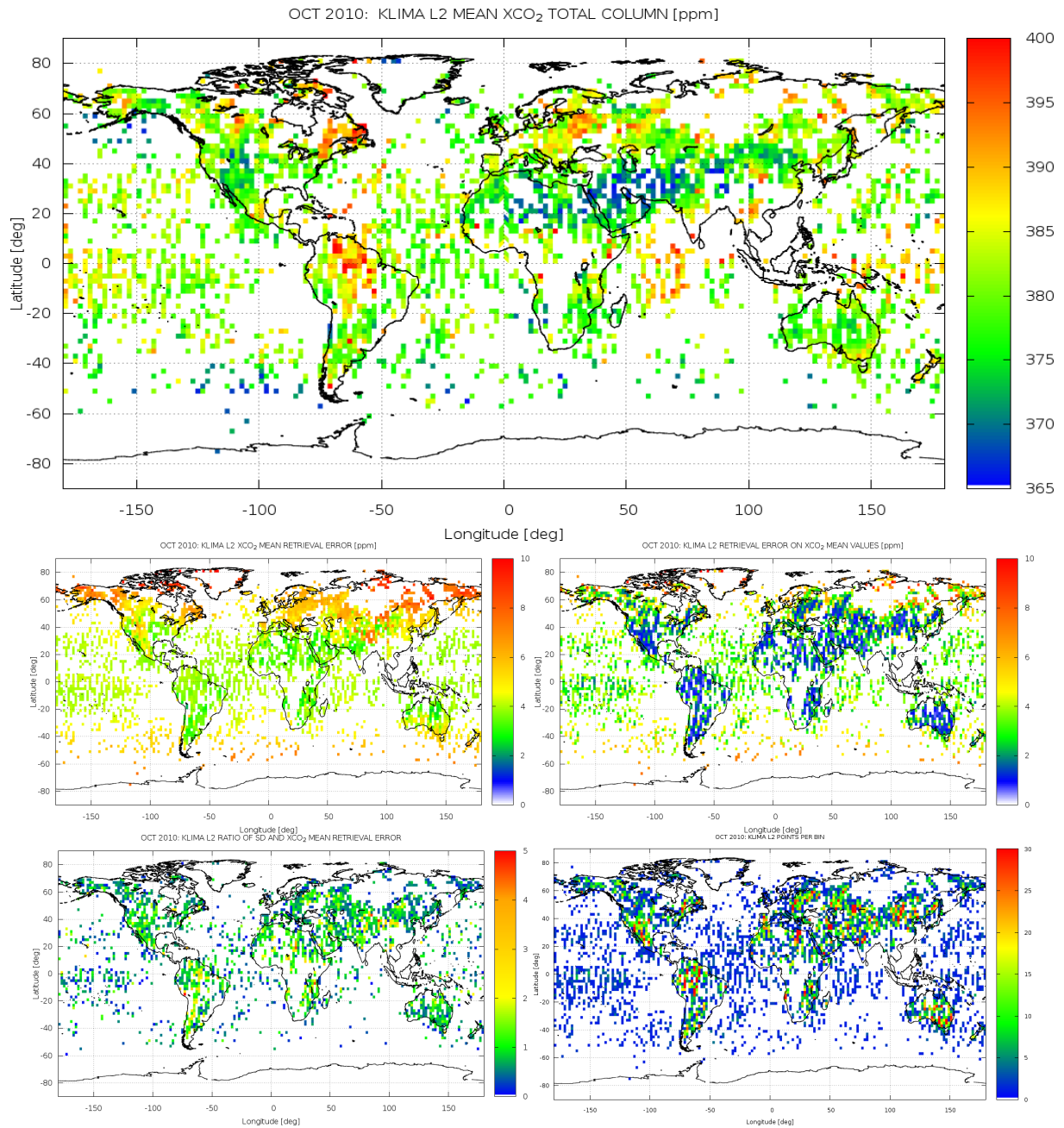


Fig. 27: 4-10 OCTOBER 2010: Global distribution of KLIMA L2 XCO₂ monthly mean; averaged monthly retrieval errors; errors on XCO₂ mean values; geographical and time variability expressed as the ratio between standard deviation and mean error and number of observations per pixel

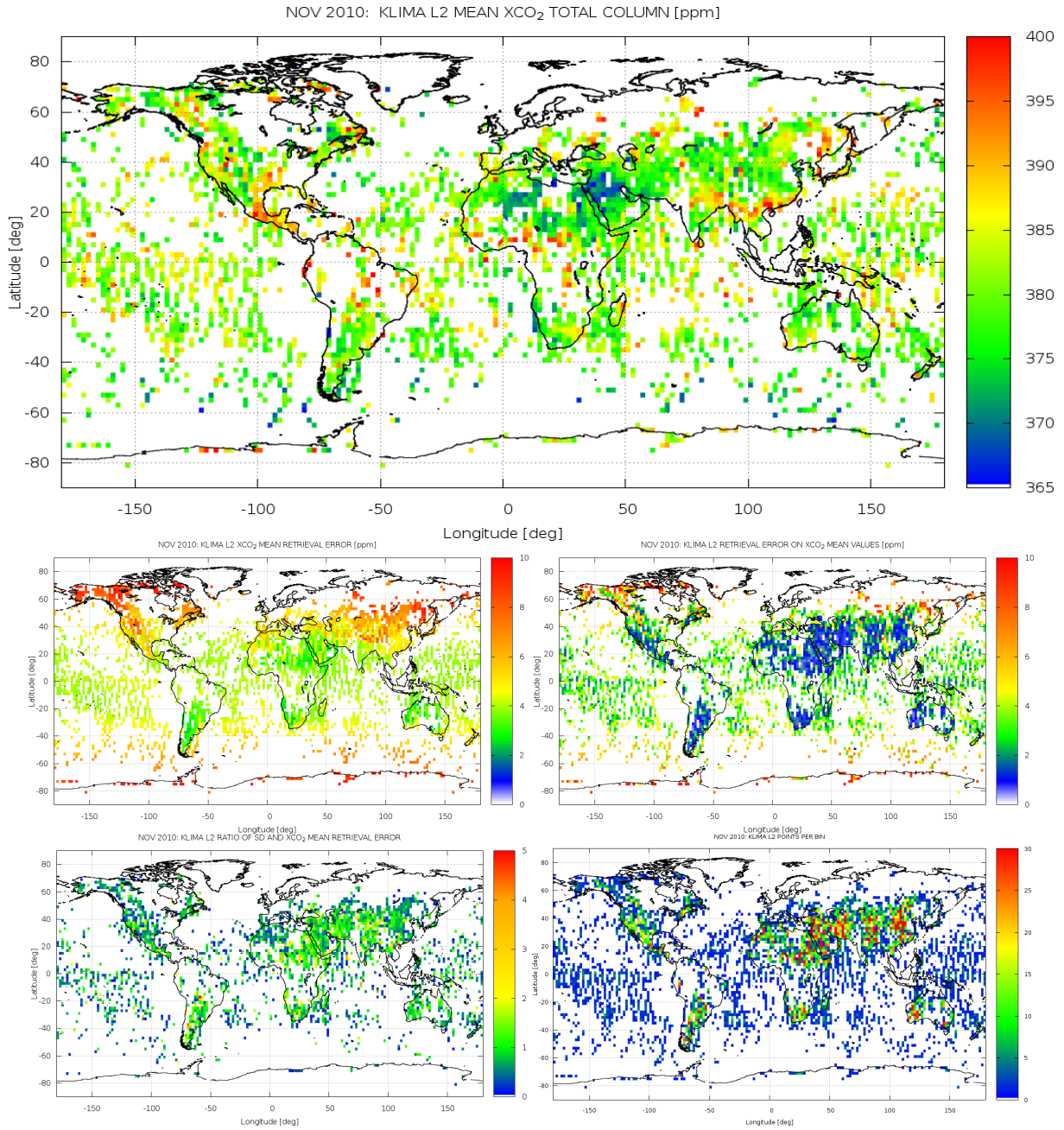


Fig. 28: 8-14 NOVEMBER 2010: Global distribution of KLIMA L2 XCO₂ monthly mean; averaged monthly retrieval errors; errors on XCO₂ mean values; geographical and time variability expressed as the ratio between standard deviation and mean error and number of observations per pixel

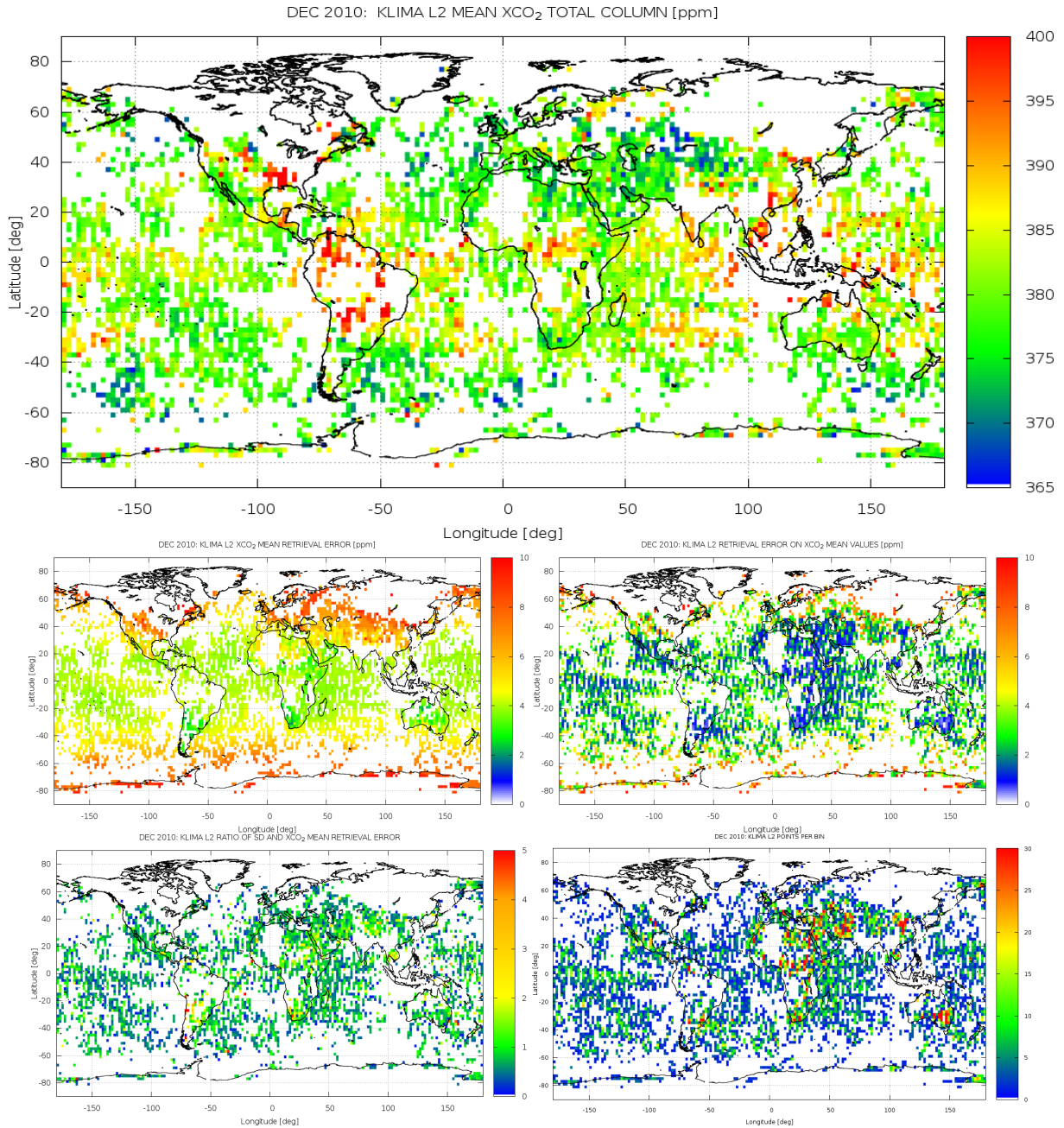


Fig. 29: 8-14 DECEMBER: Global distribution of KLIMA L2 XCO₂ monthly mean; averaged monthly retrieval errors; errors on XCO₂ mean values; geographical and time variability expressed as the ratio between standard deviation and mean error and number of observations per pixel

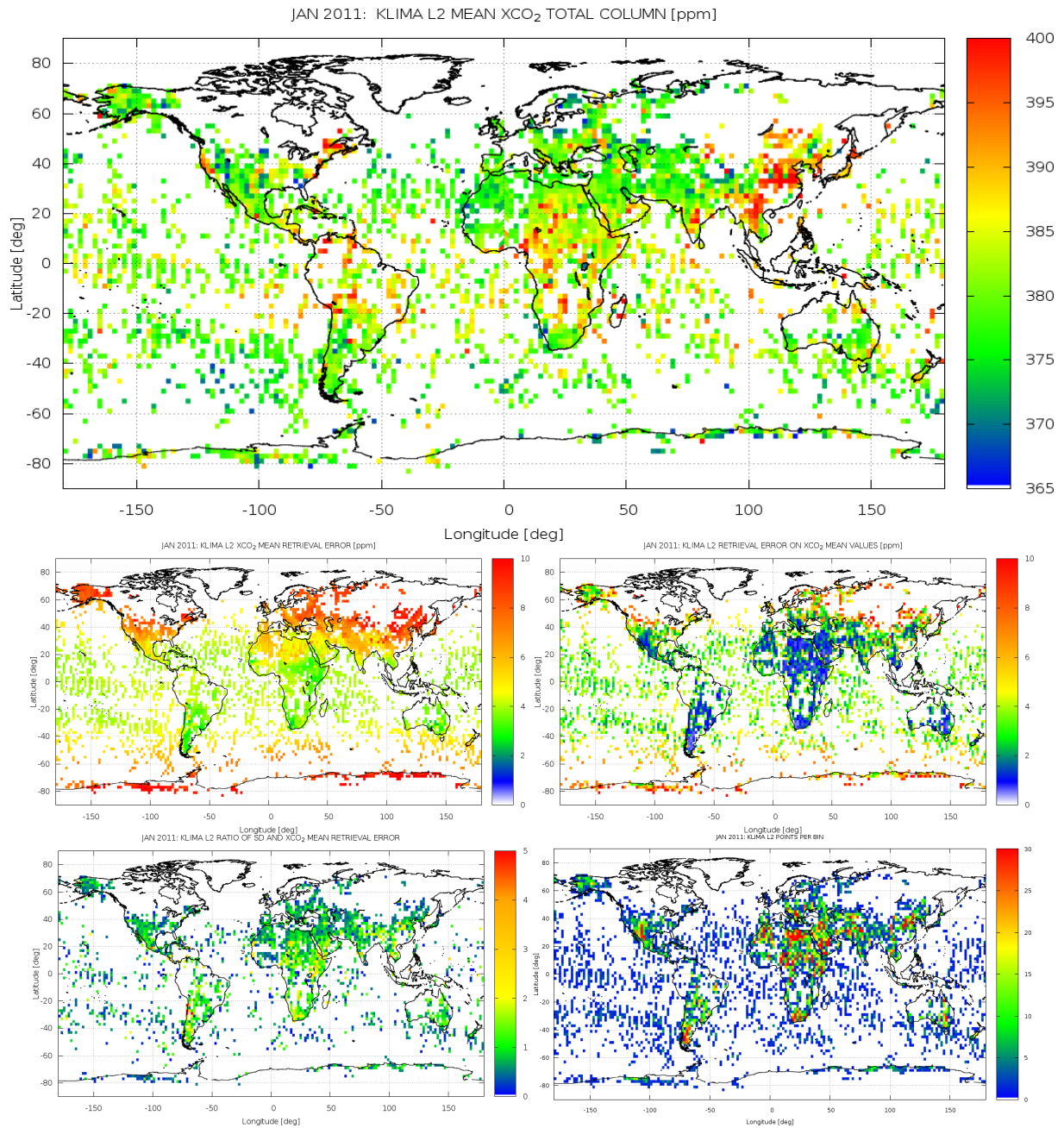


Fig. 30: 3-9 JANUARY 2011: Global distribution of KLIMA L2 XCO₂ monthly mean; averaged monthly retrieval errors; errors on XCO₂ mean values; geographical and time variability expressed as the ratio between standard deviation and mean error and number of observations per bins

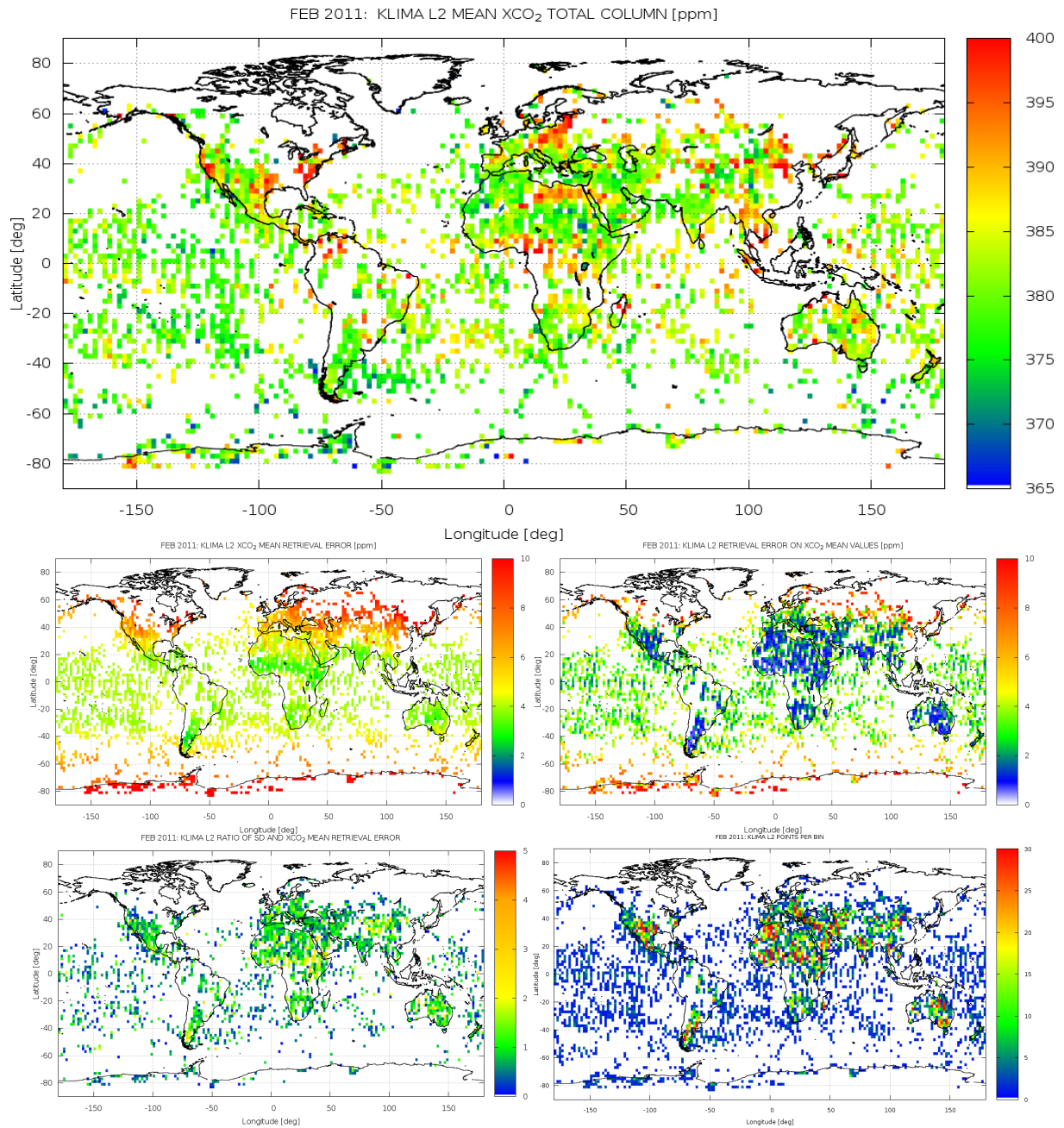


Fig. 31: 7-13 FEBRUARY 2011: Global distribution of KLIMA L2 XCO₂ monthly mean; averaged monthly retrieval errors; errors on XCO₂ mean values; geographical and time variability expressed as the ratio between standard deviation and mean error and number of observations per pixel

Hemisphere during spring months (April, May and June) than in the Southern Hemisphere, while these higher values decrease during summer months (July, August and September). This behaviour could be explained in terms of plant photosynthesis that, for the Northern Hemisphere, is not yet competitive with respiration (primarily due to uptake and release of CO_2). Similar results are also reported in [40] and [19]. During winter months we observe a similar behaviour of XCO_2 concentration in both Hemispheres. High values of XCO_2 concentration are observed over South America and Central Africa (in winter months), possibly due to the occurrence of atmospheric dust or smoke-like phenomena likely correlated with biomass burning (as reported, for example, in [8]), even if the cores of these events are filtered out by our selection criteria of clear-sky pixels. High values of XCO_2 are also observed in continental China and North America (especially in winter and spring months, from October to May), possibly due to pollution phenomena. When present, data over Greenland and over the South Pole (in the Polar summer period) show considerable values of CO_2 concentration, even if these are the regions affected by the highest averaged error values.

In the second map (middle-left) of the figure, from Fig. 20 to Fig. 31, we show the geographical distribution of the mean retrieval error on XCO_2 total column values. This is generally in the range 2–4 ppm in the Tropical and Mid Latitude regions, while larger error values are found above 50° (N and S) of latitude. Retrieval errors are larger in winter than in summer in the two Hemispheres and over sea the retrieval error is either larger or smaller than the retrieval error over land depending on the season. These effects are explained by Fig. 32, where we report the scatter plot of the XCO_2 retrieval error with respect to surface temperature. In this plot, the whole IASI observations dataset has been used, including results obtained over both land and sea and for both day and night time. The 5 ppm retrieval error that was observed in the test case discussed in Sect. 3.2.2, and increased to 6.5 ppm due the further band selection, as described in Sect. 4.4.2, well represents the average behaviour of the retrieval, but real data show a large variability around this value. The retrieval error monotonically decreases with the increase of the surface temperature. This variation can be explained by the higher intensity of the measured spectrum, when the temperature of the surface is larger. Larger values of the observed radiance correspond to larger Jacobians and to a better precision of the retrieved quantity. Therefore, the observed seasonal and latitude variations of the retrieval error as well as the differences between sea and land mainly depend on the surface temperature conditions. This parameter can be effectively used to determine the cases in which TIR observations provide the best results.

In the third map (middle-right) of the figure, from Fig. 20 to Fig. 31, we show the error on the mean XCO_2 which is the quantifier of the theoretical performances of KLIMA. We recall that the requirement on the KLIMA products were 0.3% (1 ppm out of 370 ppm) on regional scales (1000x1000 km) at monthly intervals. The results reported in these maps refer to a pixel $2^\circ \times 2^\circ$ at weekly intervals. The blue pixels in the maps meet the requirements even if referring to smaller spatial (the selected pixels are more than one order of magnitude smaller than the require resolution, even if the coverage is not continuous) and time (only one week of observations has been analysed for each month) ranges. The reduced performances observed over the oceans are due to a smaller number of analysed observations (as discussed in Sect. 7), even if further IASI observations were available. The worst performances are observed in the Polar region because the precision of KLIMA product depends on the temperature of the surface (see Fig. 32).

In the fourth map (bottom-left) of the figure, from Fig. 20 to Fig. 31, we show the ratio between the standard deviation of the retrieved values and their mean retrieval error. These maps contain fewer points than the previous error maps, because the standard deviation was only calculated when more than two observations are present within the pixel. The plotted ratio, when close to unity, shows the consistency between the estimated retrieval error, determined with error propagation calculations, and the experimental statistical distribution of the values. Values larger than unity are due to either unaccounted errors or geographical and time variability. Most of the pixels are characterized by values of the order of unity and often significantly smaller than unity. Values smaller than unity suggest suggests that a conservative estimate of the retrieval error is made. This is due to our choice of retrieving the vertical profiles of water vapour and temperature at high vertical resolution in order to model the influence of the variability of these profiles on the retrieved value of XCO_2 . This choice causes a larger retrieval error for water vapour and temperature and through the simultaneous retrieval this error enhancement propagates into the XCO_2 retrieval error. Probably it is possible to make a less conservative choice, but for this preliminary analysis the adopted strategy appears to be adequate. In particular very small values are observed over all the oceans, in Australia, Northern Asia and Europe. Interesting are also the low values observed over Greenland, probably facilitated by the relatively large retrieval errors present in this area. The frequent and homogeneous distribution of values close to unity provide a strong indication about the correctness of our error assessment and characterizes the corresponding regions as areas of low variability. On the other hand a high variability is observed in some locations over land, and in particular over the Pacific coast of Southern and Northern America, over Southern Africa and over continental Asia and this cases the doubt remains whether we are observing either systematic errors induced by the land background or variability due to the different ecosystems.

In the fifth map (bottom-right) of the figure, from Fig. 20 to Fig. 31, we show the number of observations per

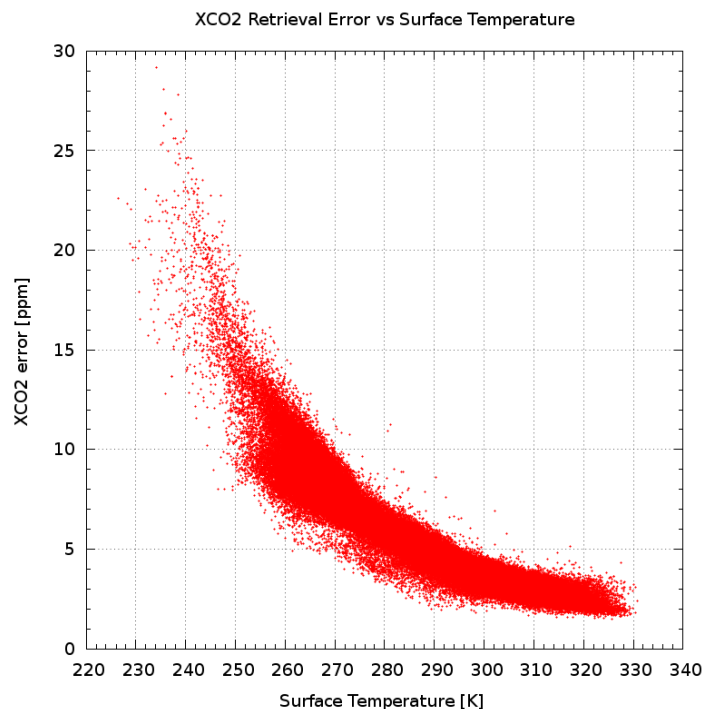


Fig. 32: Scatter plot of the XCO₂ retrieval error wrt the temperature of the surface

each pixel (bin).

8.2 Errors of KLIMA retrievals

The monthly maps discussed in the previous section have already provided some useful information about the quality of the XCO₂ values retrieved with the KLIMA code from IASI. However, some further considerations can be made on the errors of this product.

In Fig. 33 the scatter plot is shown of the χ^2 of the retrieval with respect to surface temperature. This figure indicates that, while the retrieval error is lower for larger surface temperatures (see Fig. 32), the primary retrieval quality flag (the χ -test) show that increasing residuals are observed for larger surface temperatures. A χ^2 greater than unity is usually a sign of unaccounted errors and an indication that the retrieval error must probably be multiplied by the square root of the χ^2 value. The observed increase of χ^2 can be explained by the fact that the residuals increase when the measured radiance is larger. We have averaged the residuals of 1000 retrievals, in order to reduce their random components by a factor 30 and highlight the systematic effects: The results are shown in Fig. 34 and Fig. 35.

In both figures the blue line refers to the residuals obtained in the case of cold observations (average value of surface temperature equal to 264.98 K) while the red line refers to the case of warm observations (average value of surface temperature equal to 300.65 K). A larger residual is observed in the case of observations with larger surface temperature confirming the presence of a contribution due to systematic errors that increases with the spectral radiance. In Fig. 34 these average residuals are compared with the error spectra due to the approximations introduced in the AFM (see Sect. 3.1). The expected correlation between the residuals and the AFM errors due to model approximations is masked by the fit performed by the retrieval process and by the presence of some other effects. Accordingly, in the wide band shown in the top panel of the figure no clear evidence can be observed about which may be the causes of the systematic component. However, in the bottom panel, where a blow up is shown of the region between 700 and 740 cm⁻¹, some correlation can be observed in limited spectral intervals. At any rate, the amplitude of this component is comparable to the model approximations and, as these approximation, much smaller than the measurement error. This demonstrates that our retrieval is based on an accurate forward model that can well reproduce the features of the atmospheric spectrum in a broad spectral interval. In Fig. 35 the average residuals are compared with the residuals between KLIMA FM and LBLRTM FM (see Sect. 3.1.1). Correlations are present between 700 and 740 cm⁻¹ and close to 760 cm⁻¹.

The errors that can contribute to the observed residuals are: FM errors, such as spectroscopic errors, or to missing model implementations, such as the scattering contribution due to aerosols, but also systematic errors in

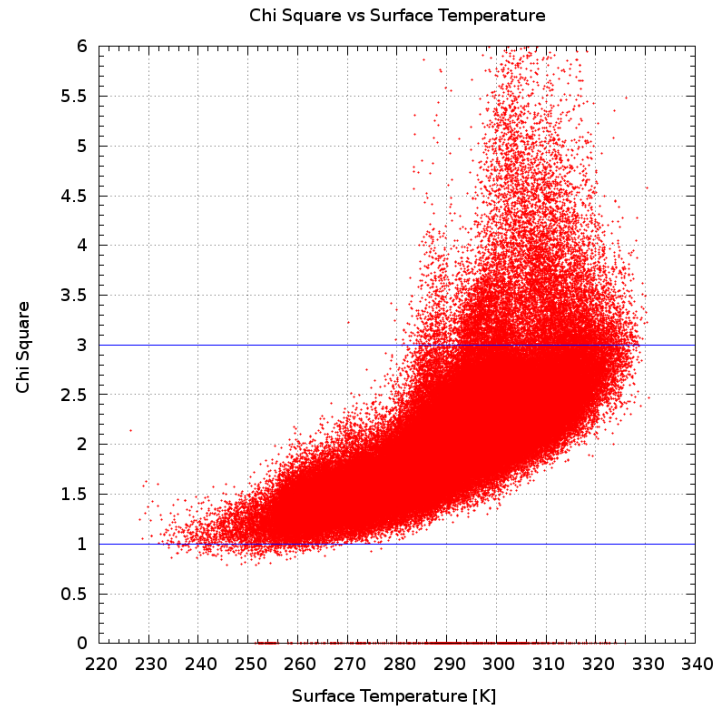


Fig. 33: Scatter plot of the χ^2 retrieval error wrt the temperature of the surface. Blue lines indicate the χ^2 range accepted for the comparison

the IASI measurements (e.g. introduced in the calibration). These errors that manifest themselves in the residuals can also affect the retrieval products increasing the random error of the retrieved product and causing systematic differences (biases) between retrieved and real value. The first effect implies that the precision of the measurements is not fully characterized by the error propagation and by theoretical retrieval error, shown in the third maps of Figs from 20 to 31. However, this error enhancement is expected to be very small because in most cases, as shown by the fourth maps of Figs from 20 to 31, the statistical spread of the observations is consistent with the calculated retrieval error. The variability of the atmosphere (either in time or in space), when present, is the largest cause of precision abatement. The second effect can be contained by reducing the residuals as much as possible, and the result of systematic residual smaller than the IASI noise show that important progresses have been made in this direction, but the actual entity of the biases can only be assessed with intercomparison and validation exercises.

Some other interesting features can be observed in the scatter plot of Fig. 33. The events of the scatter plot are contained within a well defined envelope, suggesting that a reproducible law is governing the observed increase of χ^2 with the surface brightness temperature. Indeed a similar behaviour was also observed in the case of retrieval error and surface brightness temperature shown in Fig. 32. In Fig. 33, however, next to the main envelope we observe one or two clouds of events which do not seem to obey to the general rule. These are the events that have high values of χ^2 corresponding to surface temperature of about 287 K and the events that have high values of χ^2 corresponding to surface temperatures between about 300 and 320 K. Fig. 38 shows the geolocation of the first group of events by selecting retrievals with a χ^2 greater than 3 and a surface temperature less than 292 K. These events only occur in areas where deserts are present. This suggests that the exceptionally large values of χ^2 may be caused by some typical event that can happen in the desert, such as the sand storms. A similar result is obtained by selecting the second group of events. In Fig. 37 the events with a χ^2 greater than 4,5 have been selected and also in this case areas are identified where sand storms are possible. Given the high surface temperature of the events shown in Fig. 37, it is not surprising to observe here mainly desert areas, but to be limited to these areas in the case of the events shown in Fig. 38 strongly suggests that the cause of the high χ^2 is not the desert, but an event occurring in the desert. It will be interesting to investigate the spectral features with which the sand-storms manifest themselves, meanwhile in order to limit the errors that these non-modelled effects may introduce we decided that in all the maps that show the IASI retrieved XCO₂ all the events that have a χ^2 greater than 3 (see the blue lines in Fig. 33) will not be considered. The geolocation of the IASI observations excluded because the χ^2 is larger than 3 is shown in Fig. 36. Also in this selection most of the events are in desertic areas.

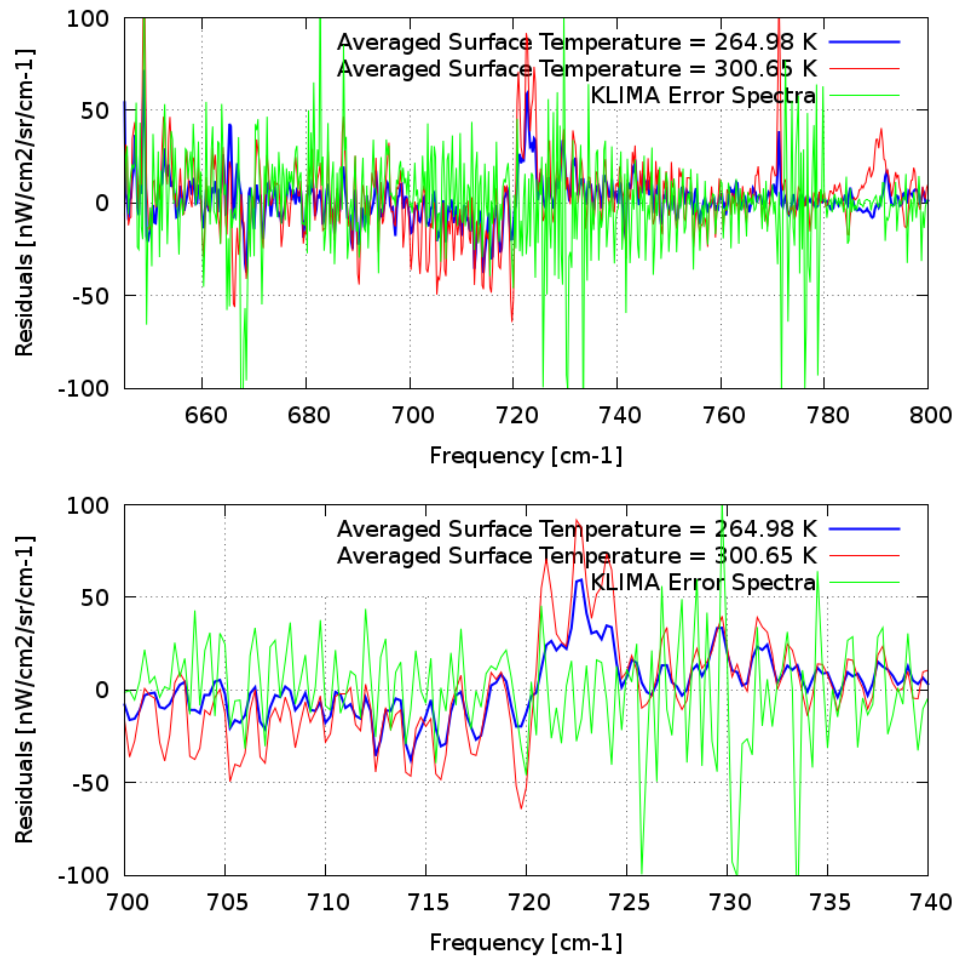


Fig. 34: Top: Comparison between the error spectra (AFM-RFM) due to the approximations introduced in the AFM (green line) (see Sect. 3.1) and the mean residuals (Simulation - Observation) evaluated at lower surface temperature (blue line) and higher surface temperature (red line). Bottom: zoom between 700 and 740 cm^{-1}

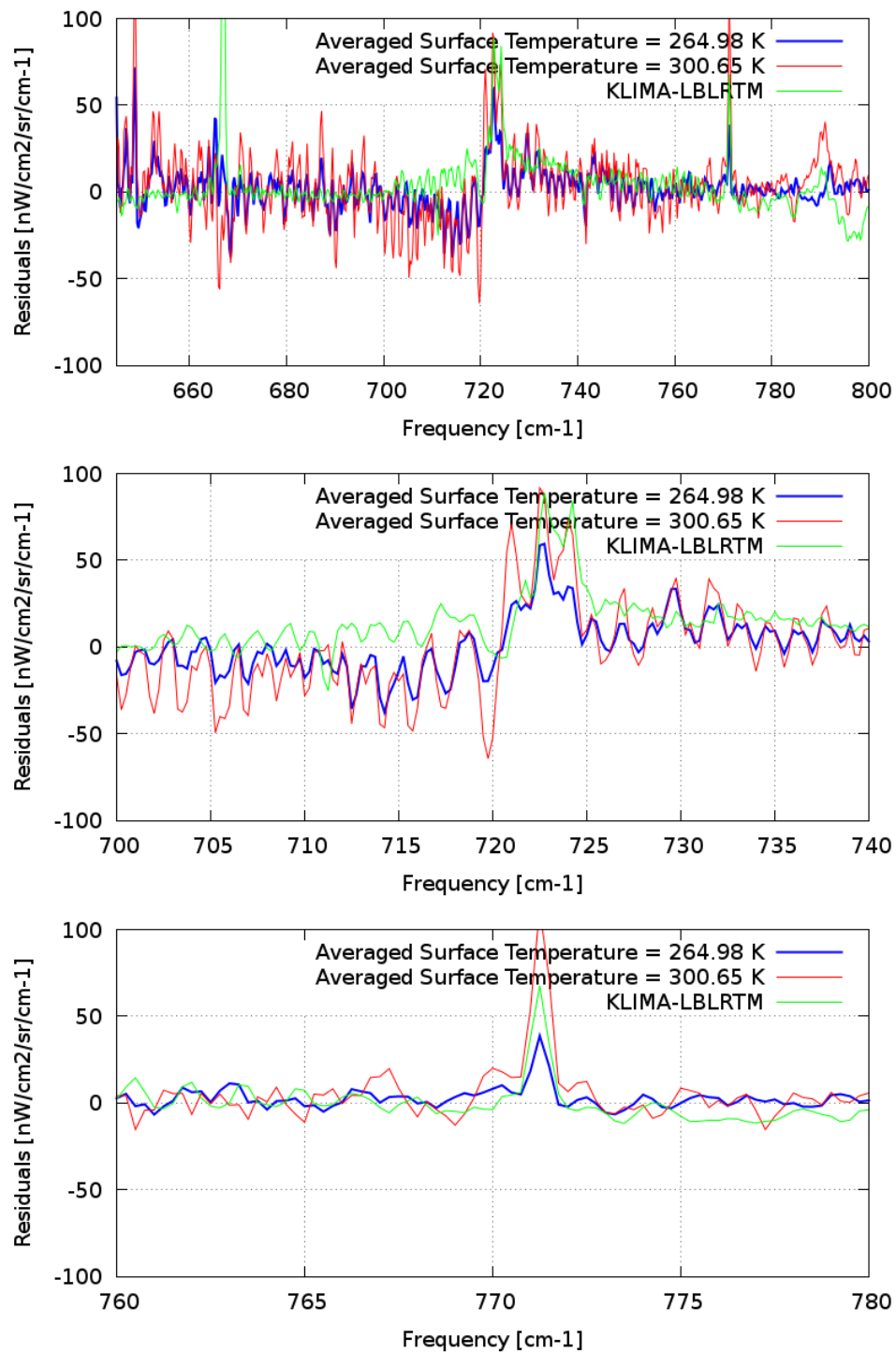


Fig. 35: Top: Comparison between the residuals between KLIMA FM and LBLRTM FM (green line) (see Sect. 3.1.1) and the mean residuals (Simulation - Observation) evaluated at lower surface temperature (blue line) and higher surface temperature (red line). Bottom: zoom between 700 and 740 cm^{-1} and between 760 and 780 cm^{-1}

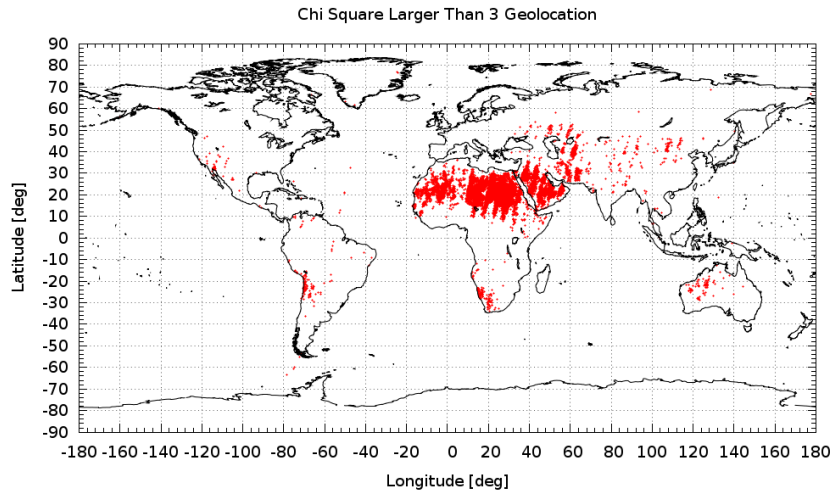


Fig. 36: Geolocation of the analysed KLIMA observations with a χ^2 larger than 3

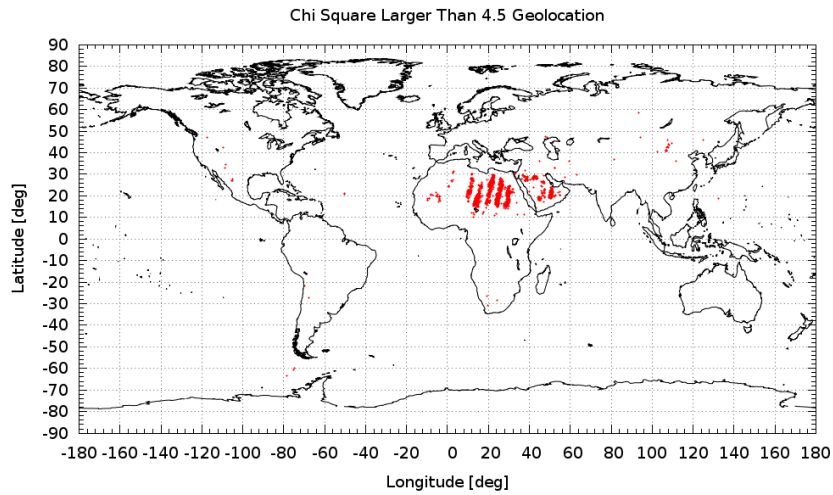


Fig. 37: Geolocation of the analysed KLIMA observations with a χ^2 larger than 4.5

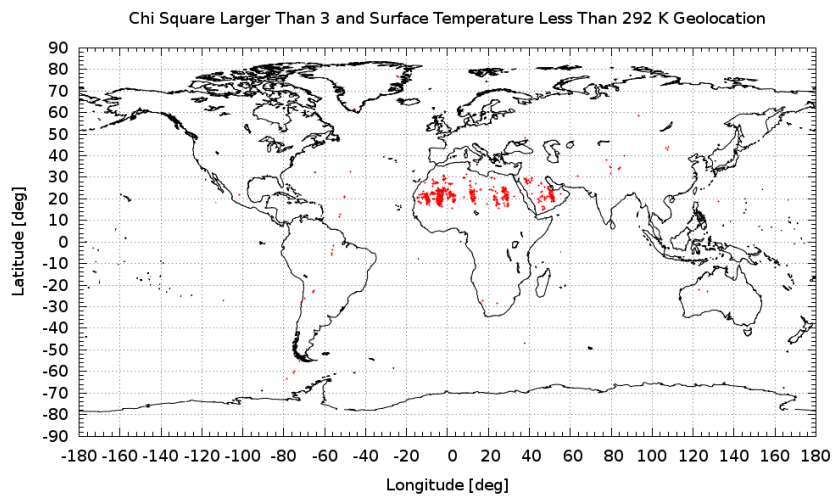


Fig. 38: Geolocation of the analysed KLIMA observations with a χ^2 larger than 3 and the surface temperature less than 292 K

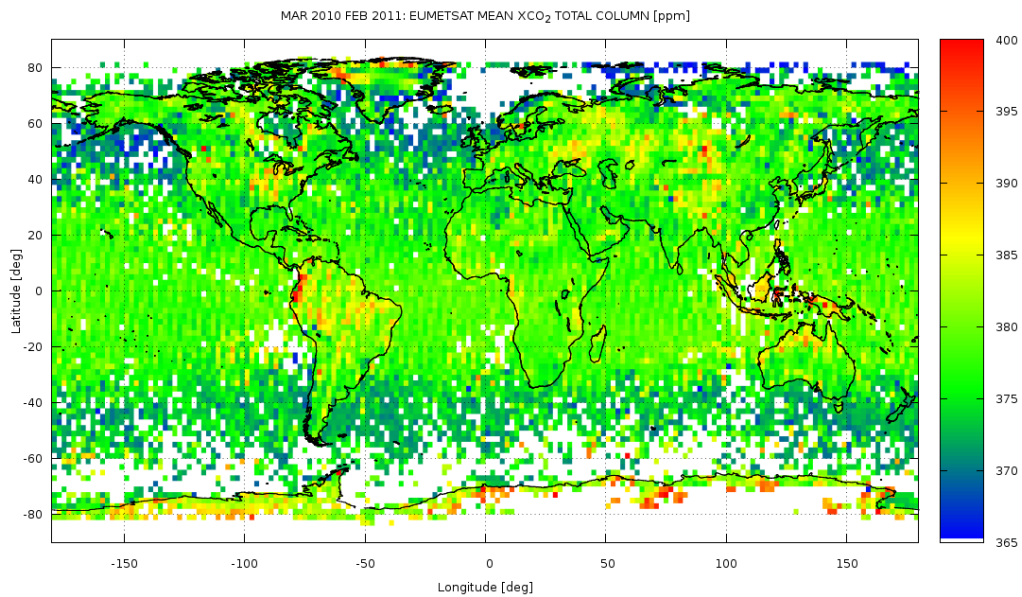


Fig. 39: MARCH 2010-FEBRUARY 2011: EUMETSAT L2 XCO₂ total column [ppm] over a grid of 2° x 2°, averaged for one year

9 Comparison between KLIMA-IASI and EUMETSAT-IASI operational products

9.1 EUMETSAT products overview

The objectives of the IASI L2 ground processing is the derivation of geophysical parameters from the radiance measurements: temperature and humidity profiles, surface temperature and emissivity, cloud properties, total column of CO, CH₄, N₂O, CO₂ and quality flags. The IASI L2 products are disseminated to users in near real-time: with a timeliness of 3 h or 9 h from sensing (timeliness refers to the elapsed time between sensing and dissemination), depending on the data format and dissemination means. The CO₂ product has not yet been validated therefore its dissemination status is still experimental [32].

An example of the IASI L2 product provided by EUMETSAT and used to evaluate the XCO₂ is reported in Fig. 39: the map shows the XCO₂ values [ppm] averaged for the year from March 2010 to February 2011 for a global geographical coverage over a grid of 2° x 2°. This yearly map is directly comparable with the KLIMA-L2 map presented in Fig. 19 and it is clear that EUMETSAT observes in one year a smaller variability than KLIMA. Moreover, this figure highlights larger differences between pixels over land and over ocean compared to KLIMA at latitudes higher than ±45° in the Northern Hemisphere and in the Southern Hemisphere, respectively. In the equatorial belt (at latitudes between -15° and 15°), higher values of XCO₂ (above 385 ppm) are found by KLIMA, whilst EUMETSAT map mostly shows an homogeneous distribution below that threshold in this latitude region, especially over Africa. Similar behaviors are evident over China and Eastern coast of the North America where EUMETSAT values are lower than about 20 - 30 ppm wrt KLIMA ones.

9.2 Objectives of comparison

Despite the experimental status of IASI L2 CO₂ product, however some advantages to perform this comparison exist:

- spatial and time coincident measurements;
- selected spectral bands are the same for KLIMA and IASI L2 (even if KLIMA algorithm uses a number of channels significantly higher than ANN);
- is not necessary to use any type of data correction;

- same observation geometry and IFOV;

The comparison between KLIMA and EUMETSAT data set is difficult because straightforward correlations do not emerge and the absence of an error estimate for one of the two results prevents a clear conclusions. Several comparisons were made and the most instructive are shown in the next section.

9.3 Results of the comparison

In the figures from Fig. 40 to Fig. 51 we report, for each month, the map of the percentage difference between XCO₂ values retrieved with the KLIMA/G-POD code and the L2 products delivered by EUMETSAT. The differences are calculated between average values calculated in the 2° x 2° grids used for the presentation of KLIMA results in the previous section. The error associated with these differences is the error of KLIMA retrievals (third map from Fig. 20 to Fig. 31) plus the unknown errors of EUMETSAT. From March to September it is possible to see that in Tropical latitudes, both over land and water, EUMETSAT L2 XCO₂ values are higher than KLIMA L2, with a difference of approximately 4-5%; while in Northern and Southern mid and high latitude situation reversed: KLIMA XCO₂ values are higher than EUMETSAT. From October, with the exception of North Africa, Arabia and a small part of continental China, KLIMA values are higher than EUMETSAT, for a maximum difference of 5%. These percent differences, that correspond to about 15-20 ppm, are much larger than the retrieval errors of KLIMA, which typically are of the order of 2 ppm over land, 4 ppm over water and 8 ppm at high latitudes. With these large differences, no significant validation is possible and we are left with doubt of whether KLIMA makes errors larger than the estimated values or too large constrains are preventing the EUMETSAT analysis from observing the real variability of the XCO₂ quantity. It is a fact that the global yearly map shows that KLIMA results have a larger dispersion, but EUMETSAT results are likely to have a larger error because based on a subset of spectral points. More significant considerations can be made with large scale comparisons.

In the Fig. 52, we report the seasonal cycle of XCO₂ from March 2010 to February 2011 for Northern Hemisphere and Southern Hemisphere. In the figures the red line shows the values retrieved with KLIMA and the green line the values given by EUMETSAT. KLIMA is observing a seasonal periodic variation in the Northern Hemisphere and a small positive trend in the Southern Hemisphere. Quite a different result is observed in the EUMETSAT data where an unrealistic negative trend is present in both the Northern and Southern Hemisphere seasonal cycles.

Figure 53 shows the annual average related to the macro areas shown in Fig. 18, as obtained from KLIMA-IASI (red) and EUMETSAT (green). The standard deviation of the mean is also shown: the spread of EUMETSAT data is usually smaller than that of KLIMA results. In the bottom of the figure we added the number of observations for each macro area. This plot shows the capability to KLIMA to highlight the presence of sources and sinks. The macro area of 10° x 10° met the spatial requirement of the project, while the annual average refers to a longer period so as to reduce seasonal fluctuations that have already been shown and discussed in the previous figures. KLIMA results highlight many of the expected geographical features such as the higher values over countries characterized by high CO₂ emission and the reduction of XCO₂ in the Southern Hemisphere oceans, while EUMETSAT results provides nearly constant values that differ from KLIMA averages by variable quantities. A large difference is observed by KLIMA between North and South America and equal values are obtained by EUMETSAT. Over China, a large value is measured by KLIMA, while EUMETSAT here provides an averaged value that is smaller than the one found over Australia.

We can conclude that there is no evident correlation between KLIMA and EUMETSAT results, even if obtained from the same data set. In absence of reliable information on the real atmosphere it is difficult to decide which are the causes of this inconsistency. However, the larger variability of KLIMA results is often in the direction of the expected differences and seems to be more realistic than the uniform EUMETSAT results.

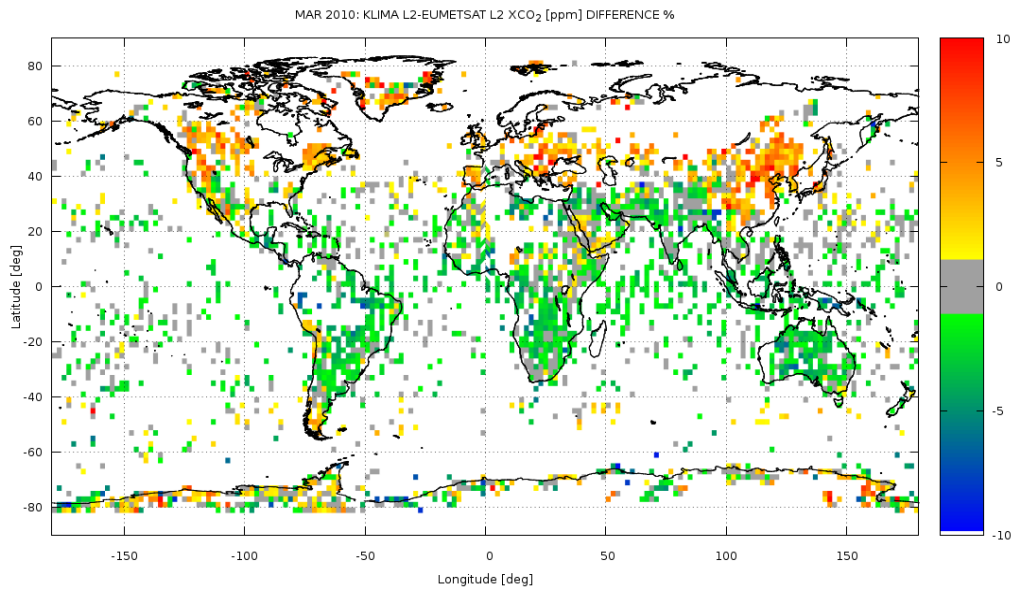


Fig. 40: 8-14 MARCH 2010: KLIMA-EUMETSAT XCO₂ comparison: map of % difference

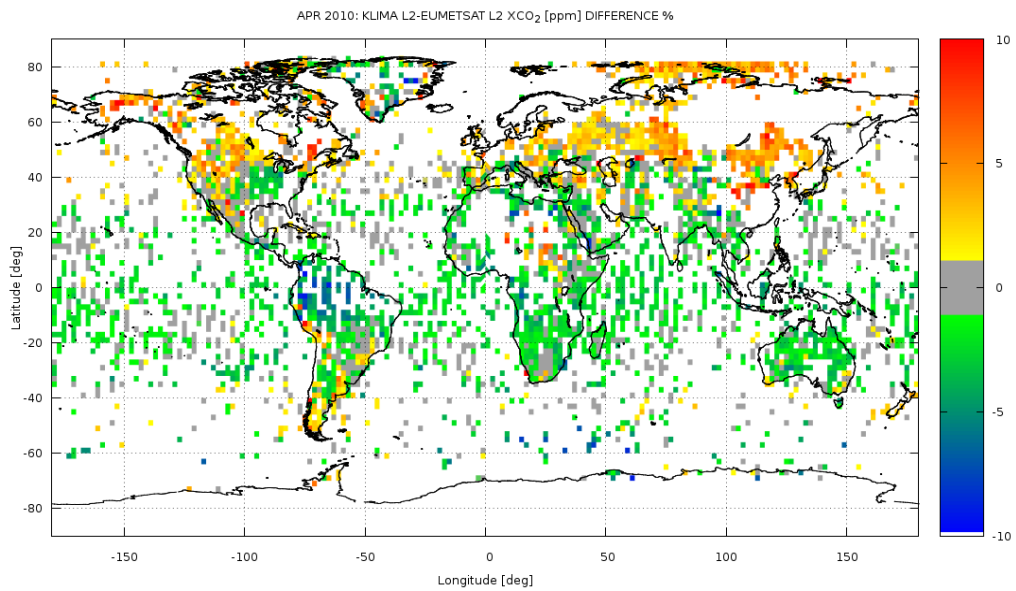


Fig. 41: 5-11 APRIL 2010: KLIMA-EUMETSAT XCO₂ comparison: map of % difference

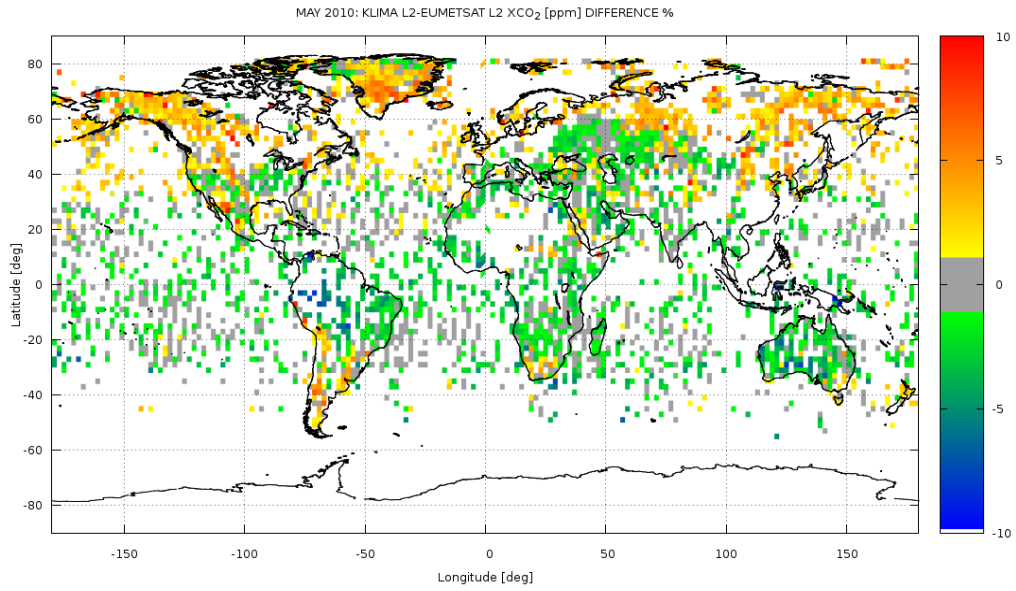


Fig. 42: 3-9 MAY 2010: KLIMA-EUMETSAT XCO₂ comparison: map of % difference

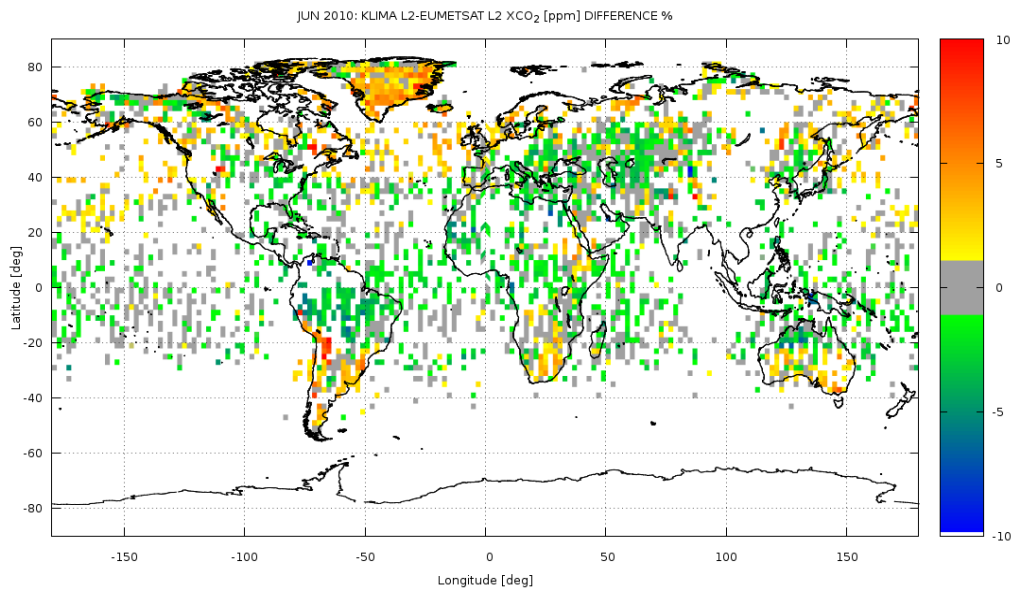


Fig. 43: 3-9 JUNE 2010: KLIMA-EUMETSAT XCO₂ comparison: map of % difference

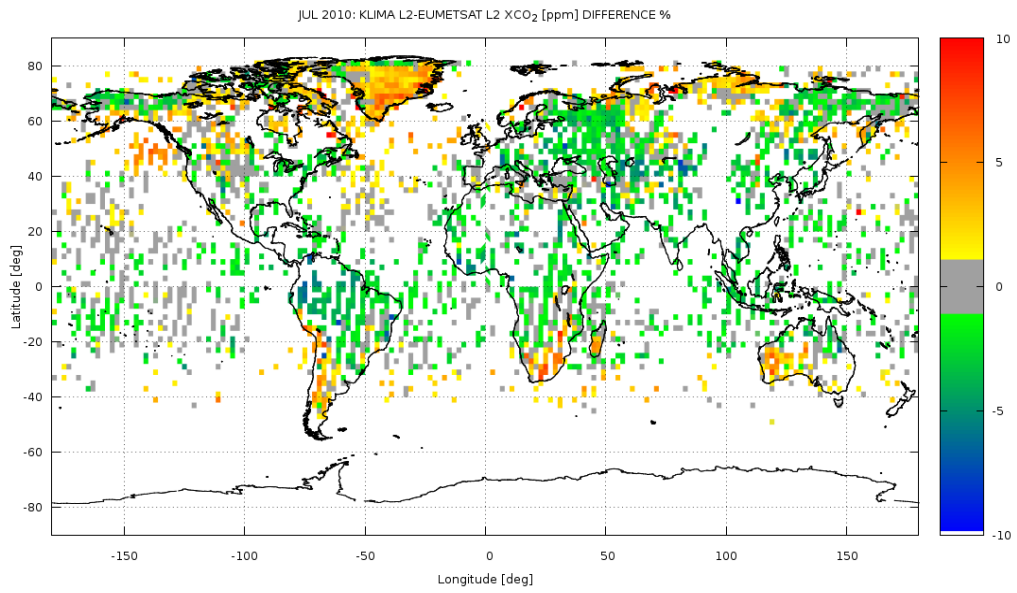


Fig. 44: 5-11 JULY 2010: KLIMA-EUMETSAT XCO₂ comparison: map of % difference

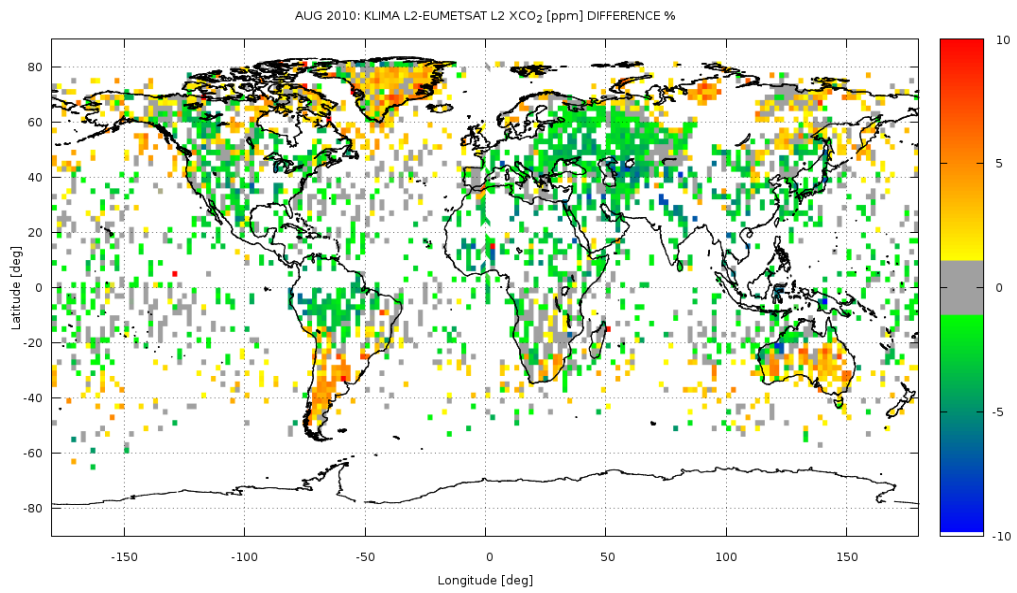


Fig. 45: 2-8 AUGUST 2010: KLIMA-EUMETSAT XCO₂ comparison: map of % difference

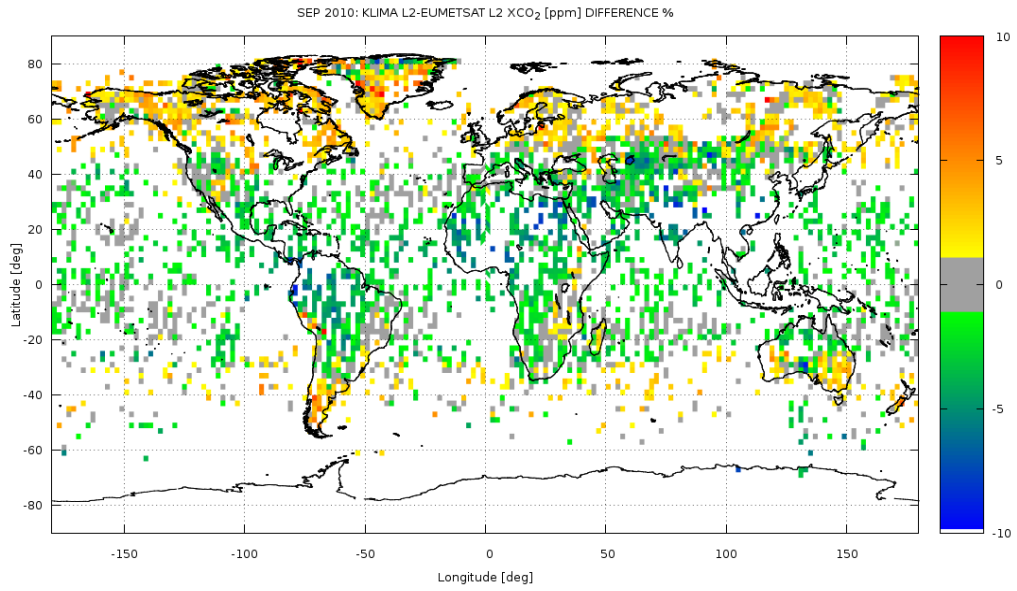


Fig. 46: 6-12 SEPTEMBER 2010: KLIMA-EUMETSAT XCO₂ comparison: map of % difference

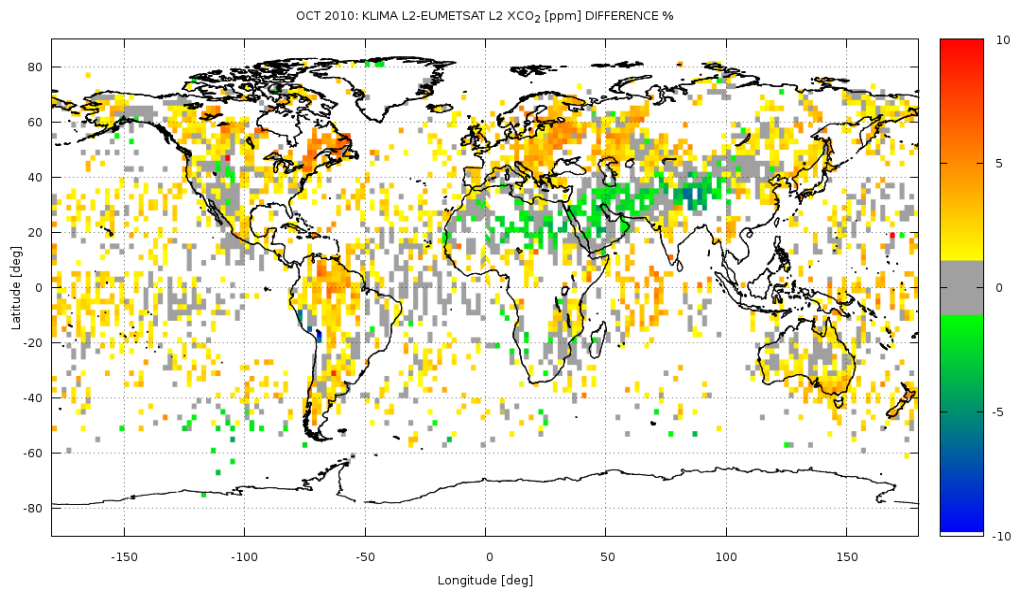


Fig. 47: 4-10 OCTOBER 2010: KLIMA-EUMETSAT XCO₂ comparison: map of % difference

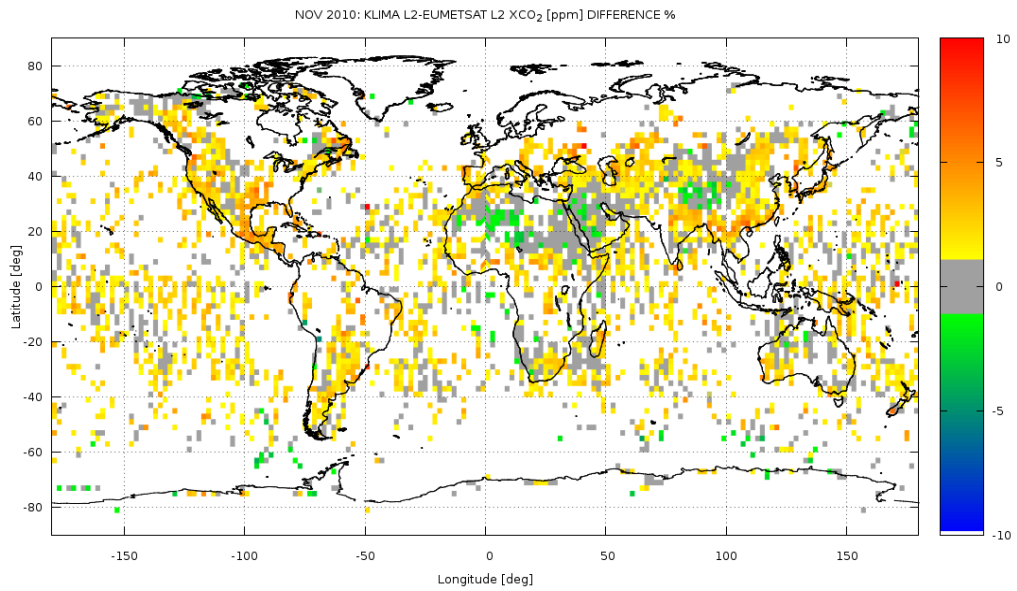


Fig. 48: 8-14 NOVEMBER 2010: KLIMA-EUMETSAT XCO₂ comparison: map of % difference

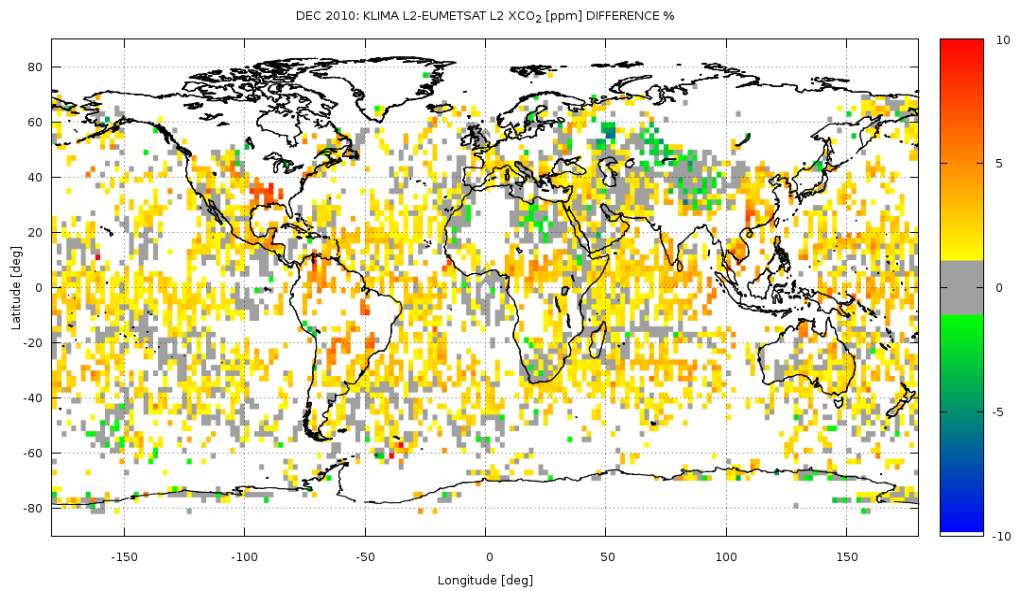


Fig. 49: 8-14 DECEMBER 2010: KLIMA-EUMETSAT XCO₂ comparison: map of % difference

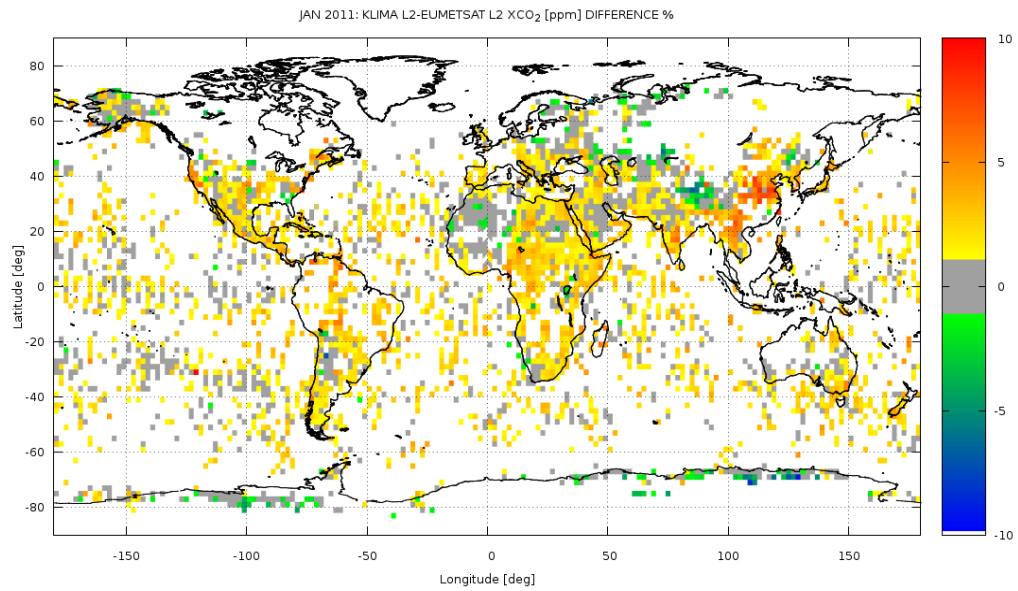


Fig. 50: 3-9 JANUARY 2011: KLIMA-EUMETSAT XCO₂ comparison: map of % difference

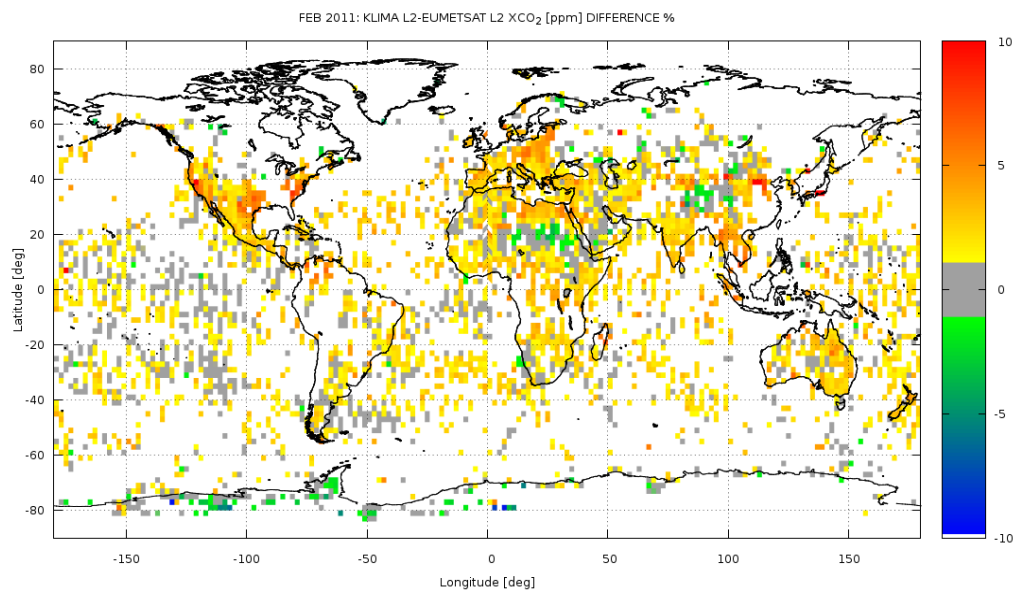


Fig. 51: 7-13 FEBRUARY 2011: KLIMA-EUMETSAT XCO₂ comparison: map of % difference

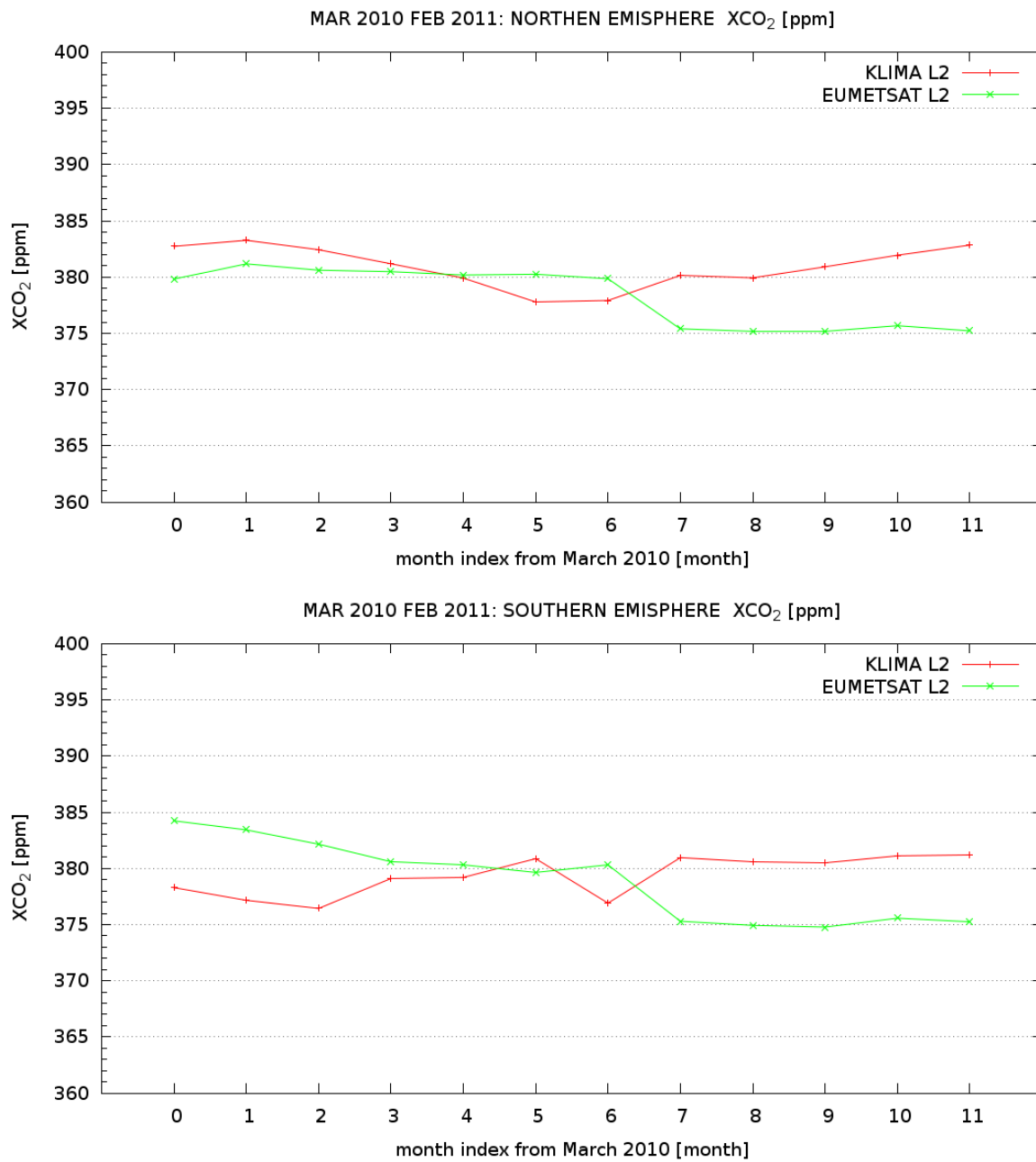


Fig. 52: Northern Hemisphere (top) and Souther Hemisphere (bottom): seasonal variation of the XCO₂ from March 2010 to February 2011. The average on the Hemispheres of the XCO₂ retrieved by KLIMA-IASI (red) is compared with operational L2 products provided by EUMETSAT (green)

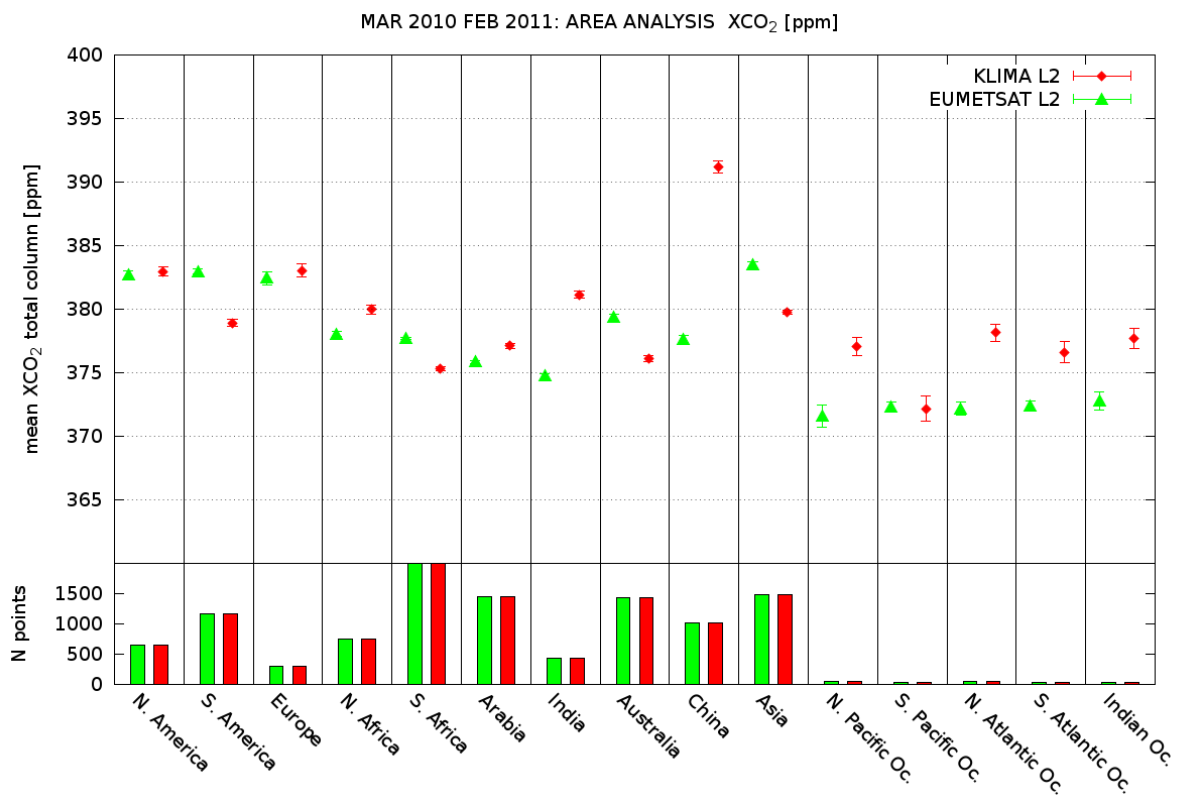


Fig. 53: Top: Average XCO₂ for each macro area reported in Fig. 18. Red points are KLIMA-IASI average XCO₂ green points are EUMETSAT products Bottom: Number of observations for each macro area

10 Comparison between KLIMA and TANSO-FTS/GOSAT

The inter-comparison of the XCO₂ total column retrieved from KLIMA/IASI with TANSO-FTS/GOSAT L2 SWIR product is a major goal of the project. The comparison activity has been performed in the annual range from March 2010 to February 2011 both for land and water observations; however the period of the analysis is restricted to only a week per month since only one week per month of IASI observations has been processed by means of KLIMA processor, as described in Sect. 7. TANSO-FTS L2 operational products have been obtained from for the same period (from March 2010 to February 2011) and for the same weeks. The data set of the KLIMA and TANSO-FTS comparison has a global coverage, but is limited to day observations due to the fact that TANSO-FTS doesn't make observations during night.

In Sect. 10 we provide a short overview of the TANSO-FTS XCO₂ products; in Sect. 10.2 we discuss the objectives and the strategy of the comparison and in Sect. 10.3 we present the results. In particular: Sect. 10.3.1 is dedicated to the comparison of *co-located* observations; the Sect. 10.3.2 reports the results of the *averaged* comparison and Sect. 10.3.3 illustrates the comparison of the seasonal variations for Northern/Southern Hemisphere and for some restricted latitude bands.

10.1 TANSO-FTS/GOSAT XCO₂ Product Overview

An example of the TANSO-FTS/GOSAT product is reported in Fig. 54; the map shows the XCO₂ total column for the year from March 2010 to February 2011 limited to the weeks also considered by KLIMA averaged over a grid of 2° x 2°.

Figure 55 shows, for the same coverage considered in the previous figure, the number of TANSO-FTS XCO₂ measurements that have been averaged. This map is directly comparable with the map obtained by KLIMA and shown in Fig. 19. TANSO-FTS has very few measurements at high latitudes (where also the sensitivity of IASI measurements is reduced) and makes less frequent measurements than IASI.

As in the case of EUMETSAT, for TANSO-FTS too we observe a variability that is smaller than the one observed by KLIMA. Furthermore, the values strongly highlights that on average TANSO-FTS measures higher values of XCO₂ than KLIMA. As described in Sect. 10.1, KLIMA-L2 products show high values of XCO₂ in the equatorial belt. This feature is particularly enhanced in TANSO-FTS retrieval products, with XCO₂ annual mean values in the selected period exceeding 390 ppm around the equator. Large values of XCO₂ are also found by TANSO-FTS in South-East Asia and Central America and are consistent with the average distribution obtained from KLIMA.

10.2 Objectives and strategy of the comparison

As shown in Sect. 10.1 TANSO-FTP products have a good global geographical coverage in the period of analysis (12 weeks in the period from March 2010 to February 2011) but a low coverage in terms of number of observations. The reduced dataset for TANSO-FTS with respect to KLIMA one (after applied selection criteria, KLIMA provides about 240000 XCO₂ values from March 2010 to February 2011 while from TANSO-FTS only the retrieval of about 3000 observations are available in the same period) requires the definition of a strategy in order to compare the two products. Three different strategies have been used for this purpose: the first strategy (or *co-located* comparison) consists in the comparison of the XCO₂ total column retrieved from observations of IASI and TANSO-FTS made in contiguous locations in time and space; the second strategy (or *averaged* comparison) consists in the comparison of the XCO₂ total column averaged on a suitable spatial and time interval (see Sect. 7); the third strategy (or *seasonal-variation* comparison) consists in the comparison of the seasonal variations on macro-areas (Northern/Southern Hemispheres, Pacific Area, some latitude bands).

Furthermore, IASI and TANSO-FTS measurements have different sensitivity as a function of the vertical profile of the atmosphere. A quantitative comparison of the two XCO₂ products must take into account the different AKs of the two instruments. For this reason the results presented in the following sections, further than with the direct comparison of IASI and TANSO-FTS retrieved products, report also a cross-comparison after introducing, on TANSO-FTS XCO₂ values, the smoothing effect described in Sect. 7.1.

10.3 Results of the comparison

10.3.1 Co-located comparison

The *co-located* strategy consists in the comparison of the XCO₂ total column retrieved from single measurements of TANSO-FTS and IASI acquired in the same day and observing the same scene. In details, the IASI observation has been assumed as *co-located* with the TANSO-FTS when measured in the same day and if the centre of the IASI ground pixel is located at a distance of less than 20 km from TANSO-FTS one (see Fig. 56).

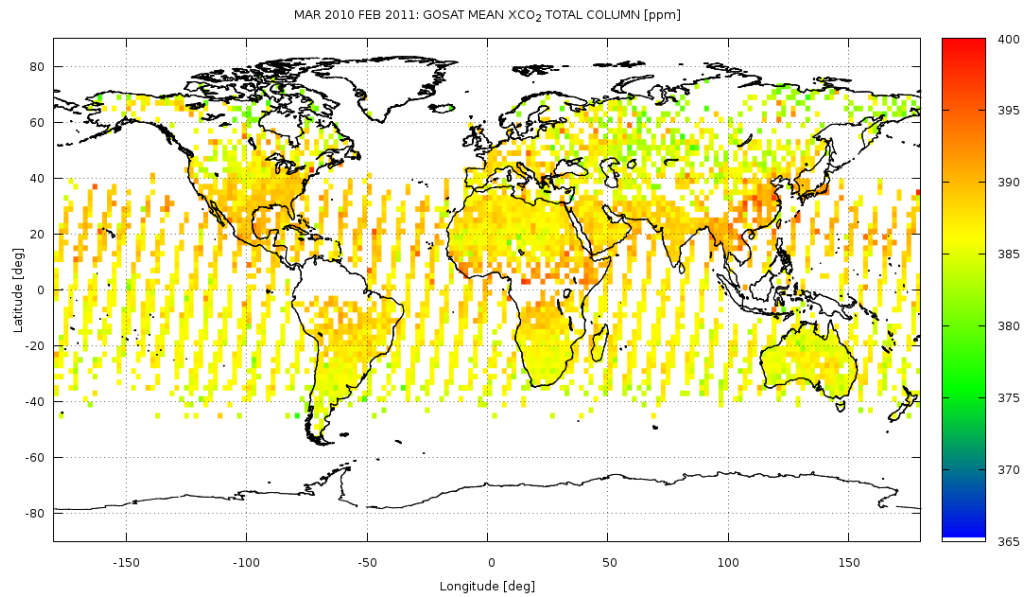


Fig. 54: Map of the TANSO-FTS XCO₂ for the year from March 2010 to February 2011 and a global geographical coverage over a grid of 2° x 2°. TANSO-FTS products are here limited to one week per month that is the same period of KLIMA-IASI products availability

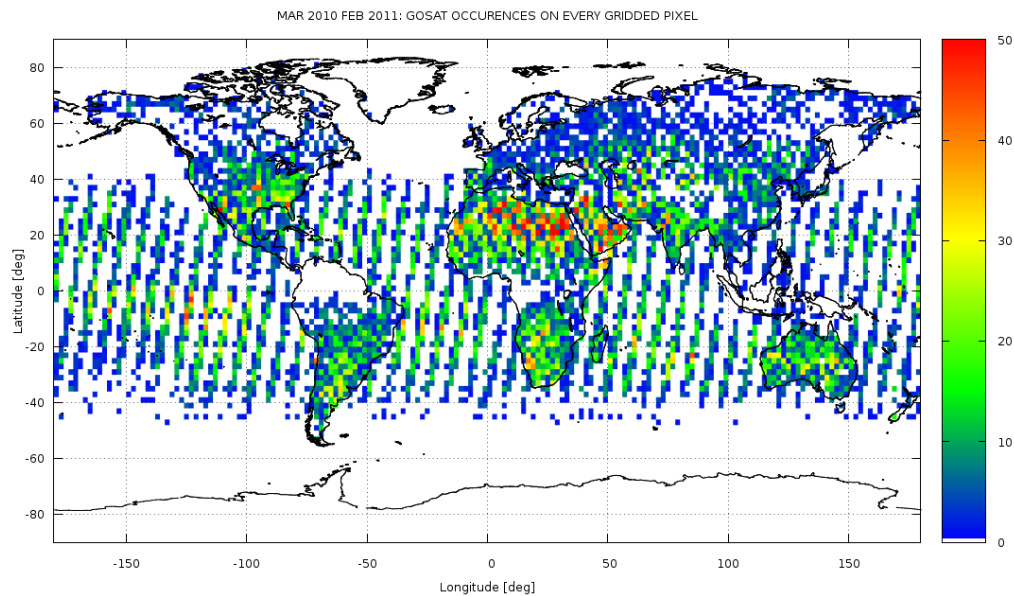


Fig. 55: Map of the TANSO-FTS coverage (in term of number of observations per pixel) for the year from March 2010 to February 2011 and a global geographical coverage over a grid of 2° x 2°. TANSO-FTS products are here limited to one week per month that is the same period of KLIMA-IASI products availability

GOSAT TANSO-FTS and IASI coincidences

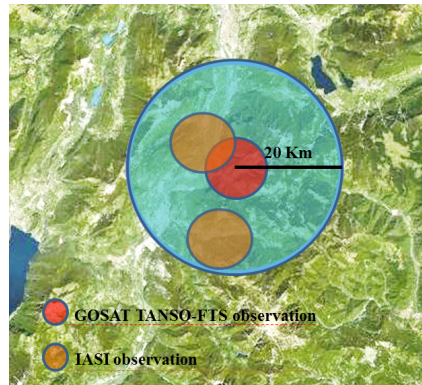


Fig. 56: IASI and TANSO-FTS observations have been assumed as *co-located* if the centre of the IASI ground pixel is located in a 20 Km circular interval from TANSO-FTS one

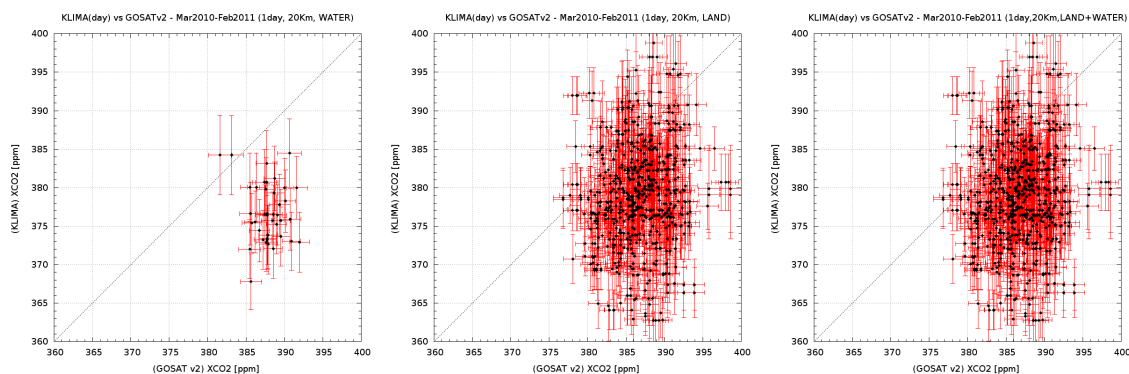


Fig. 57: XCO₂ over water (left), over land (center), and over water+land (right) for the year from March 2010 to February 2011: correlation between KLIMA/IASI retrieved values and TANSO-FTS/GOSAT V2 products. The correlation factor of the distribution is $R=0.15$ for water, $R=0.13$ for land and $R=0.12$ for water+land case

The data selection criterion has been chosen as an acceptable compromise between the need to compare quantities retrieved from measurements observing the same scene and the need to have a significant number of samples, suitable for an annual statistics. As a matter of fact, measurements executed in the same day (for the same location) corresponds to the minimum time distance between IASI and TANSO-FTS observations while the spatial interval of 20 Km from the TANSO-FTS centre of pixel can be considered small enough to neglect horizontal XCO₂ variability. The result of the selection is a subset of 519 pairs of XCO₂ total column values for the year from March 2010 to February 2011.

Figure 57 shows the correlation between the XCO₂ total column retrieved using KLIMA algorithm during the period from March 2010 to February 2011 and the corresponding value provided by TANSO-FTS V2 operational XCO₂ product. Two different cases are considered: observations over water (displayed in Fig. 57 (left)) and observations over land (displayed in Fig. 57 (center)); the correlation of all co-located observations (land+water) is also shown in Fig. 57 (right).

These comparisons provide a cloud of points (scatter-plot) which in the case of correlated measurements should be distributed along the central dotted line at 45°. The XCO₂ total columns retrieved by KLIMA are, both over land and water, smaller than the corresponding TANSO-FTS values, with larger differences in the case of measurements over water (even if fewer events are analyzed in this case). The range of variability of the observations is comparable with the relative dispersion of the two observations leading to an almost uniform distribution of the cloud of points. The gathering of the points along a preferred direction cannot be observed and the numerical fit of the points with a straight line does not provide any useful indication because the result of the fit strongly depend on the assumed errors and, therefore, on the correctness of their assessment. It is possible, however, to make some considerations about the observed distribution in the case of the uniform and highly populated case of Fig. 57 (center). The KLIMA retrieval error varies from 2 to 7 ppm. The TANSO-FTS measurements have an error of about 1.5 ppm. The cloud of points has a peak-to-peak spread (mainly caused by the dispersion of the IASI values) which seems to be rather large relative to the values of the retrieval errors. In order to assess the desirable contribution of

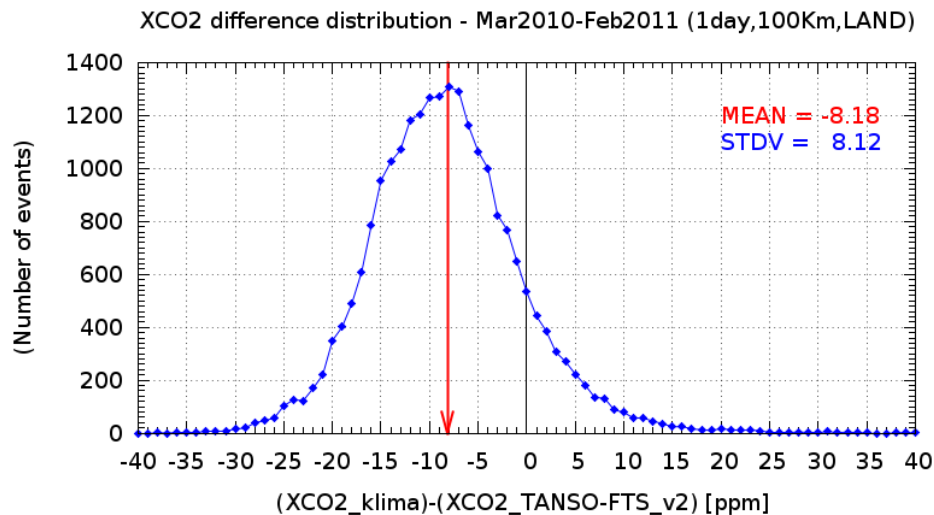


Fig. 58: Distribution of the differences between KLIMA and TANSO-FTS XCO₂ V2 products evaluated with a coincidence criterium equal to 100 km: case observation on land for the period from March 2010 to February 2011

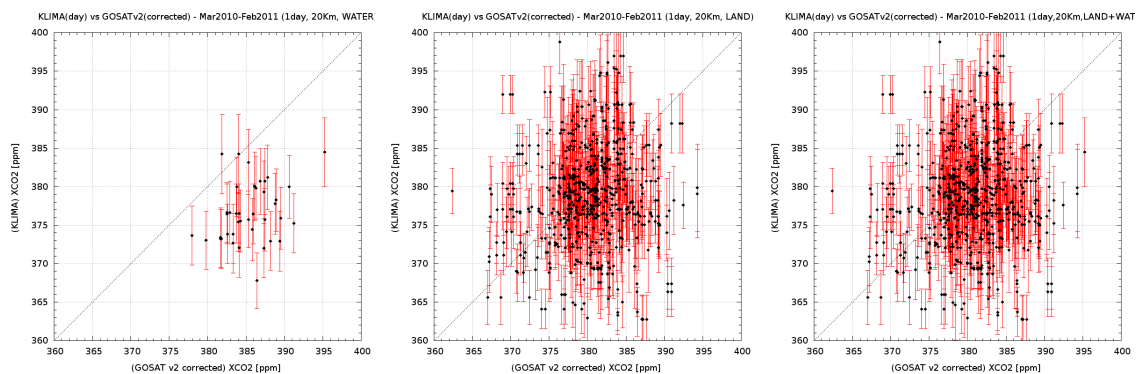


Fig. 59: Distribution of the differences between KLIMA and TANSO-FTS XCO₂ V2 smoothed products: case observation on water (left), on land (center), and on land+water (right) for the period from March 2010 to February 2011 The correlation factor of the distribution is $R=0.30$ for water, $R=0.12$ for land and $R=0.10$ for water+land case

the atmospheric variability to this dispersion of the scatter plot, the differences between KLIMA and TANSO-FTS XCO₂ has been calculated and the histogram of the differences plotted in a figure. In order to increase the statistics and to better evaluate the data dispersion, this histogram has been build using a larger coincidence criterium equal to 100 km. This new coincidence criterium increases the sample from about 950 to about 20 K pairs.

Fig. 58 shows the histogram of the differences of the coincident events over land. The bias of IASI relative to TANSO-FTS is of -8 ppm and the standard deviation of the distribution is 8.2 ppm. As suggested by the spread of the scatter plot, this standard deviation is larger than expected, preventing the observation of that correlation which is the objective of the comparison. Some other sources of error must be present. Indeed a difference can be caused by the assumption of different vertical distribution of CO₂ in the two retrieval codes.

In order to correct for this possible error the comparison above described has been repeated after applying the smoothing to the TANSO-FTS XCO₂ products as described in Sect. 7.1. The results of the correlations are showed in Fig. 59 while the distribution of the differences, evaluated with a coincidence criterium equal to 100 km, is reported in Fig. 60. Note that when the XCO₂ value is smoothed, also its associated error have to be evaluated accordingly. However in this work the smoothing has been applied only to the XCO₂ values but not to its associated error. As a result, in the correlation graphics the error on TANSO-FTS smoothed values has not been displayed.

The application of the KLIMA-IASI a priori and AKs to the TANSO-FTS retrieved product have two main effects: the negative biases observed using the original product of TANSO-FTS is significantly reduced demonstrating a better agreement between KLIMA and smoothed TANSO-FTS products, but the spread of TANSO-FTS XCO₂ increases reaching an entity similar to that of KLIMA. These effects are quantified comparing Fig. 58 (TANSO-FTS) and Fig. 60 (TANSO-FTS smoothed) where the bias is reduced from -8 to -2 ppm, and the standard

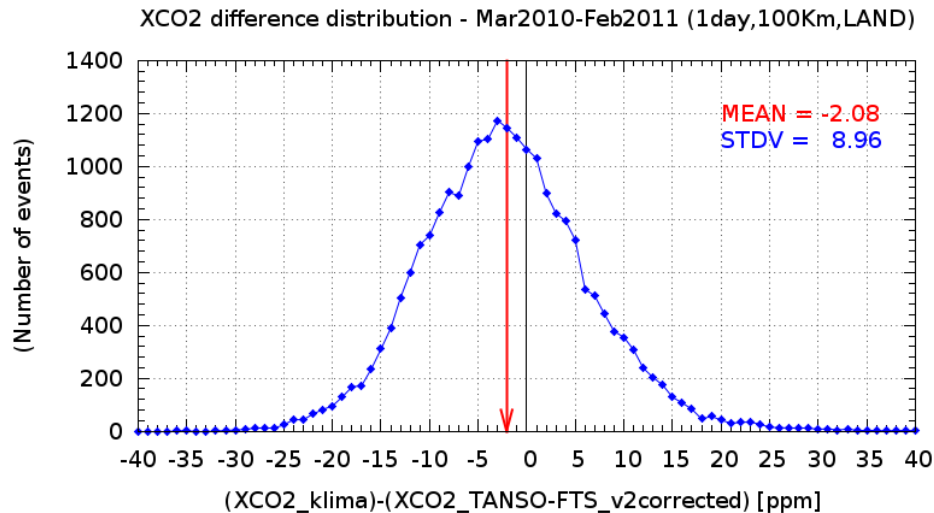


Fig. 60: Distribution of the differences between KLIMA and TANSO-FTS XCO₂ V2 smoothed products evaluated with a coincidence criterium equal to 100 km: case observation on land for the period from March 2010 to February 2011

deviation of the distribution increases from 8.2 to 9.0 ppm.

10.3.2 Comparison of XCO₂ average values

The averaging strategy consists in the comparison of the XCO₂ values, averaged for each month, on the 2° x 2° pixel grid already used in Fig. 54 and on 9° x 9° pixel grid (corresponding to a 1000x1000 km² pixel dimension at the equator) related to the whole year. In order to increase the statistics, for GOSAT data, the complete month has been used. Fig. 61 and Fig. 62 show, for the whole year, the comparison of the two XCO₂ averaged measurements for 2° x 2° and 9° x 9° pixel grid. The left panel of each figure is the scatter plot KLIMA vs TANSO-FTS while the right panel shows the related distribution of the differences. The points with the ratio between the standard deviation of the retrieved values and their mean retrieval error larger than 2 are not included in order to skip in the comparison the pixels where a geographical and/or a time variability was observed. The use of a larger pixel dimension doesn't get a significant improvement in the quality of the comparison: the width of the distribution of the differences is only reduced from 7.3 ppm, computed for 2° x 2°, to 6.0 ppm in case of 9° x 9° pixel grid.

10.3.3 Seasonal variations and mean values over macro areas comparison

This section reports the results of a comparison of the seasonal variations performed on selected macro-areas in the period from March 2010 to February 2011 (with datasets limited to only one week per month). Figure 63 shows the seasonal variation of XCO₂ in the Northern and the Southern Hemispheres (top and bottom panel, respectively) calculated for the monthly averages of KLIMA-IASI and TANSO-FTS. The red line indicates the KLIMA measurements while the TANSO-FTS measurement are indicated by a green line when no correction is applied and by a blue line when the smoothing process is applied. In Fig. 66 the analysis is limited to the Tropical region from -30° latitude to 30° while Fig. 65 and 67 reports the results for Mid Latitude both for latitude band from 30° to 60° and from -30° to -60°; Fig. 64 and 68 refer to Polar regions North (latitude from 60° to 90°) and South (latitude from -60° to -90°) respectively. The XCO₂ products obtained from KLIMA-IASI and TANSO-FTS V2 are considerably different when no correction is applied; however, when the TANSO-FTS products are smoothed taking into account KLIMA AK and KLIMA a priori CO₂ as indicated in Sect. 7.1, a good agreement is achieved both in terms of XCO₂ values and in terms of seasonal variations, especially in the Northern Hemisphere. For Southern Hemisphere the agreement is good for the summer period (from June to October) and degrades in winter (see Fig. 63-bottom). From the analysis per latitude bands a better agreement is found for Northern Mid Latitude and Polar regions (Fig. 65 and 64) and significant differences remain for Tropical regions (see Fig. 66). Missing data for TANSO-FTS V2 in the Southern Polar regions are found (see Fig. 68).

The typical seasonal variation of the Northern Hemisphere is also observed in a 20° x 20° area around the Hawaii island as shown in Fig. 69. The same color code as in Fig. 70 are used for the satellite observations. In this case the measurements of the Mauna Kea station is also reported. Unfortunately, in this geographic area the TANSO-FTS does not have a coverage that lasts for the full year. The three instruments observe a similar seasonal variability, however some offsets exist among them. IASI measurements have a large negative bias relative

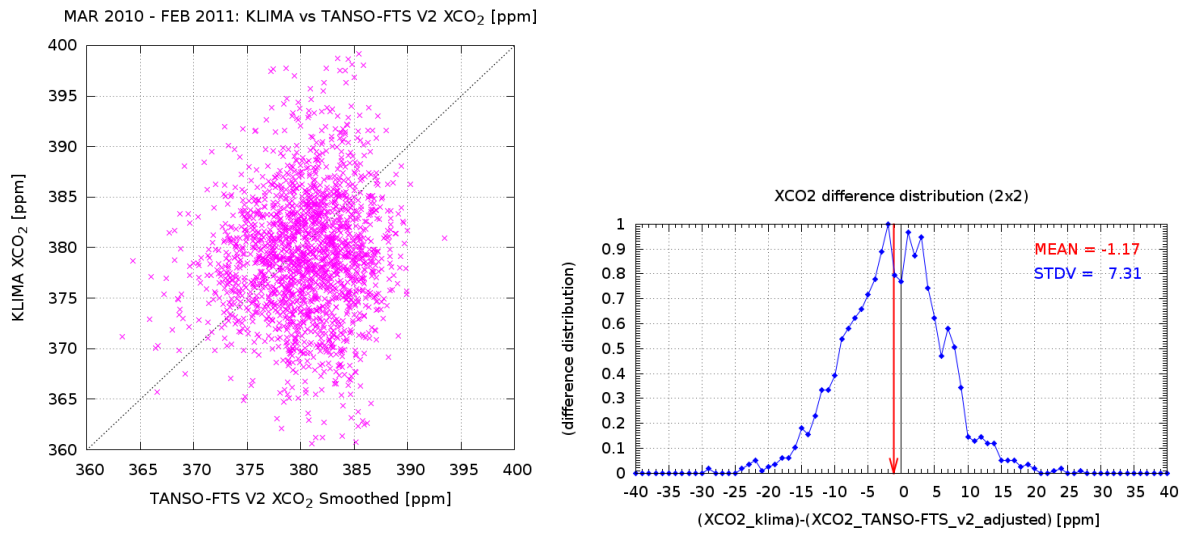


Fig. 61: Scatter diagrams of the XCO₂ KLIMA L2 - TANSO-FTS V2 comparison on a 2° x 2° pixel grid related to the whole year (left) and the distribution of the differences (right)

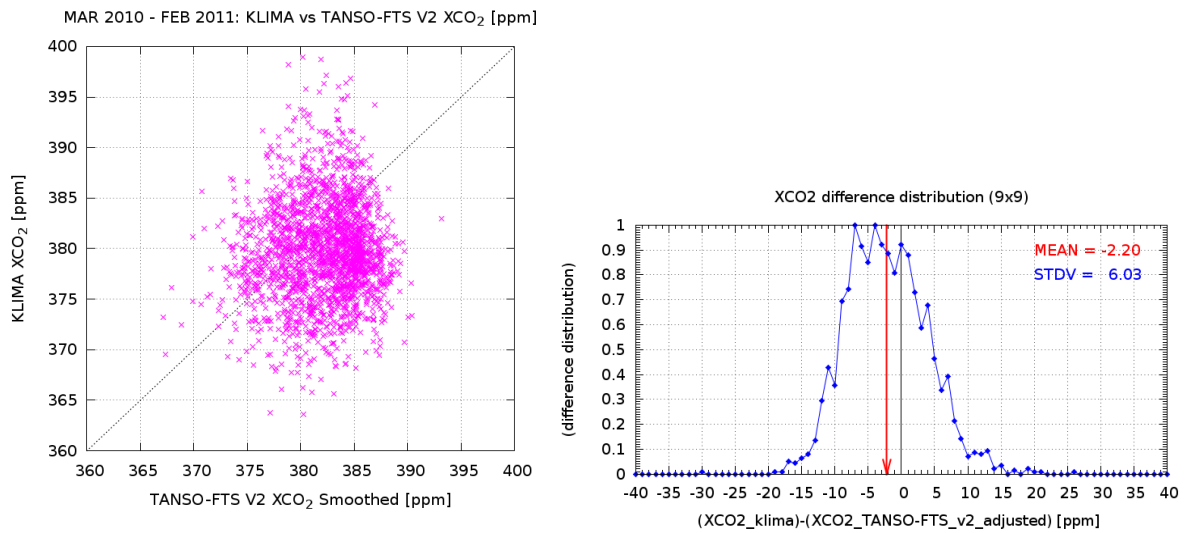


Fig. 62: Scatter diagrams of the XCO₂ KLIMA L2 - TANSO-FTS V2 comparison on a 9° x 9° pixel grid related to the whole year (left) and the distribution of the differences (right)

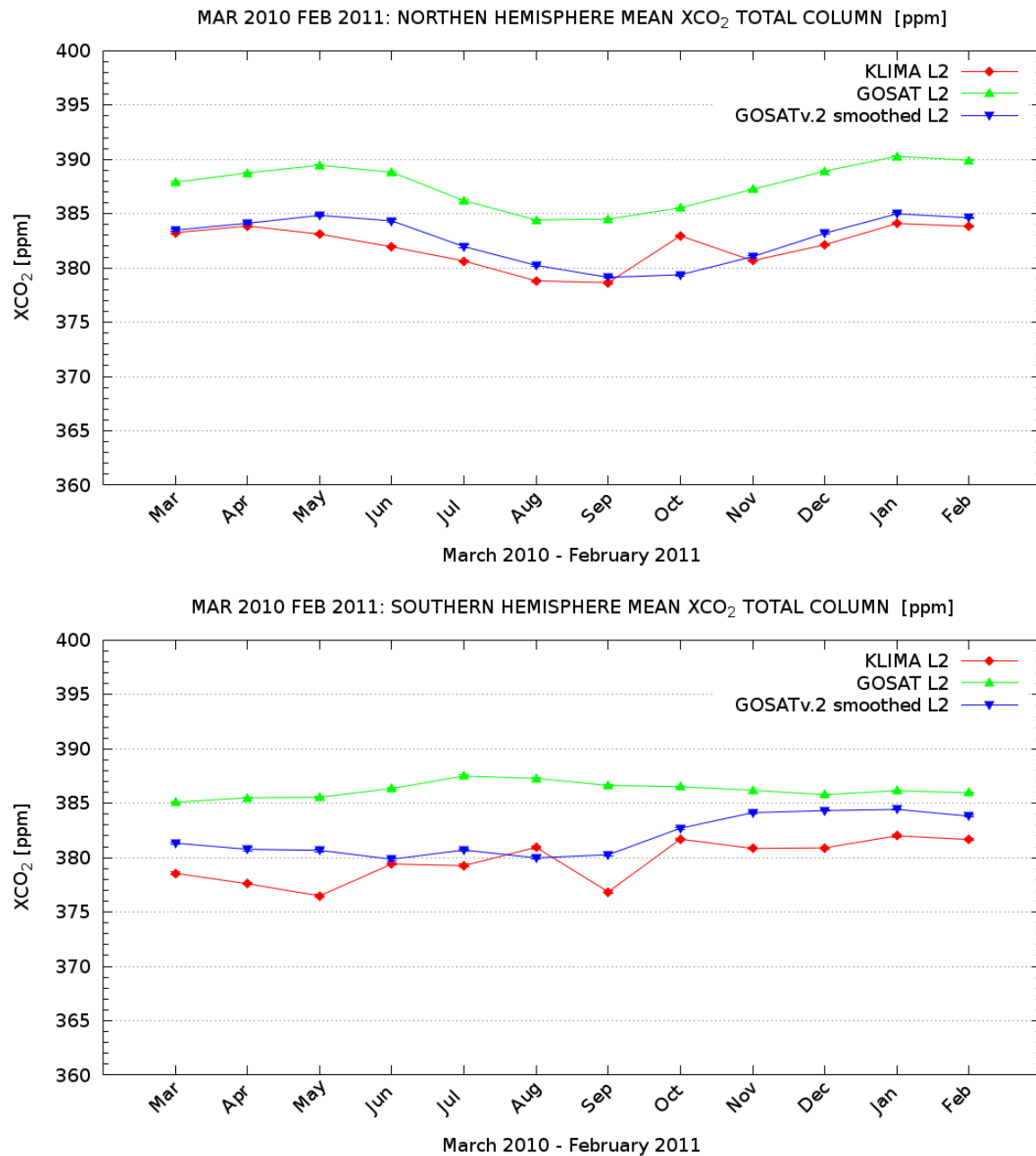


Fig. 63: Northern Hemisphere (top) and Souther Hemisphere (bottom): seasonal variation of the XCO₂ from March 2010 to February 2011. The average on the Hemispheres of the XCO₂ retrieved by KLIMA-IASI (RED connected-points) is compared with the Hemisphere average of TANSO-FTS SWIR XCO₂ products; GREEN marks refer to L2 TANSO-FTS V2 original products while BLUE marks refer to V2 smoothed using the method described in 7.1

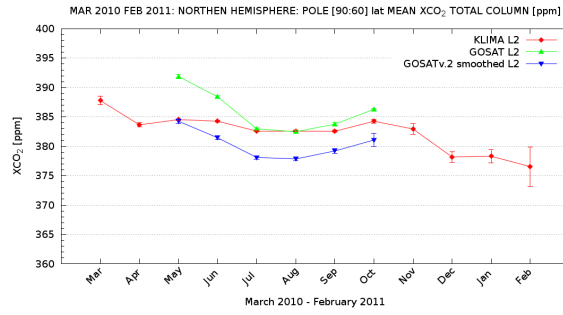


Fig. 64: As Fig. 63 for Northern Hemisphere, Polar regions

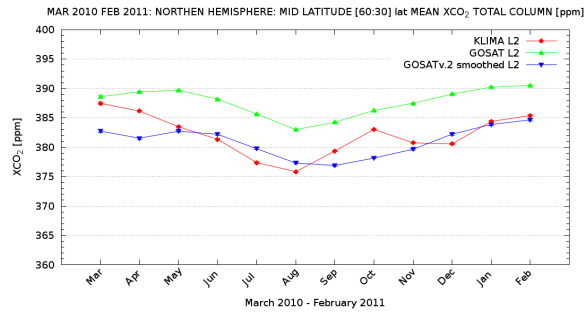


Fig. 65: As Fig. 63 for Northern Hemisphere, Mid Latitude regions

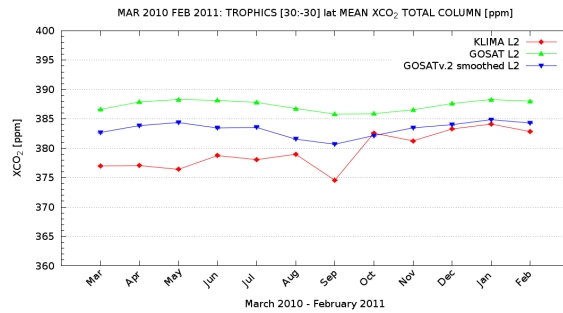


Fig. 66: As Fig. 63 for Tropical regions

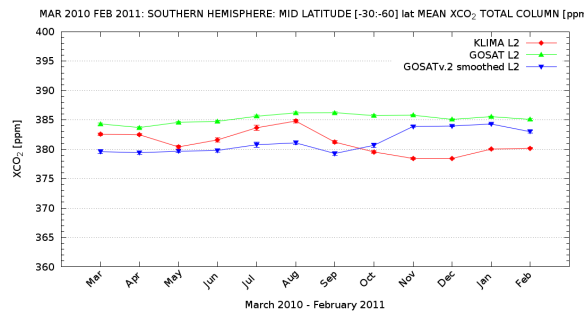


Fig. 67: As Fig. 63 for Southern Hemisphere, Mid Latitude regions

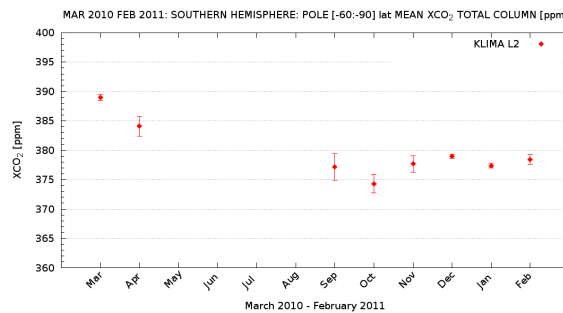


Fig. 68: As Fig. 63 for Southern Hemisphere, Polar regions

to Mauna Kea measurements (about 12 ppm), while TANSO-FTS measurements are in between the other two measurements with values close to those of the Mauna Kea station when not correction is applied and close to IASI when the correction is applied.

Figure 71 shows the annual average related to the macro areas reported in Fig. 18 obtained from KLIMA-IASI (red), TANSO-FTS (green) and TANSO-FTS smoothed (blue). The standard deviation on the mean is also shown. In the bottom of the figure we added the number of observations for each macro area.

Over land TANSO-FTS XCO_2 values are in general reduced after the smoothing and the values are closer to the KLIMA ones, but we note an increase of the dispersion of TANSO-FTS results. Over water the observations are statistically poorer, especially in the case of TANSO-FTS (in some cases the average values are obtained from a few samples and no TANSO-FTS observations are available in two areas). Despite the small number of samples the behaviour over water is consistent with what has been observed for co-located analysis: KLIMA values are significantly lower than TANSO-FTS ones: moreover in this case the effect of the smoothing is very small. For this reasons, and, as said in Sect. 9.3 to show the capability of KLIMA to highlight the presence of sources and sinks, it is better to compare KLIMA XCO_2 values with the TANSO-FTS ones without the application of the smoothing. Apart the South America and over the oceans, the geographical variations agree with TANSO-FTS. The observed bias is greater over the regions where systematic errors that affect KLIMA FM are larger (see Fig. 36).

In conclusion, KLIMA-IASI and TANSO-FTS products are general in a good agreement for land observations as emerged from the comparison in Northern Hemisphere dominated by land measurements. Differences between the two products are more evident for measurement on sea, as also confirmed by the colocated comparison (see Sect. 10.3); in this measurement scenario the application of KLIMA AKs and a priori produces a small smoothing of the TANSO-FTS products. The reduced performances of KLIMA-IASI retrieval found in case of higher surface temperature discussed in Sect. 8 are here confirmed by the significant differences found especially in Tropical area and in the winter period for the Southern Hemisphere.

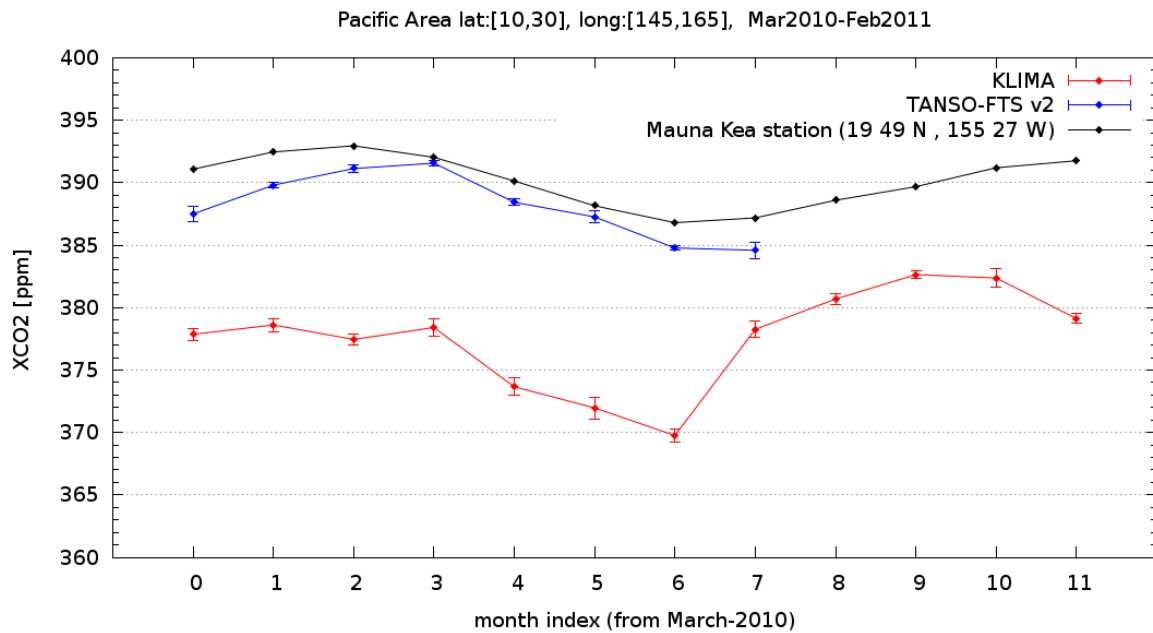


Fig. 69: Average XCO₂ for each month on a Pacific Ocean area; latitude from 10° to 30°, longitude from -145° to -165°. Blue points are TANSO-FTS SWIR (L2 V2) average XCO₂ and red points are KLIMA-IASI average XCO₂. TANSO-FTS observations are available only from March 2010 to October 2010

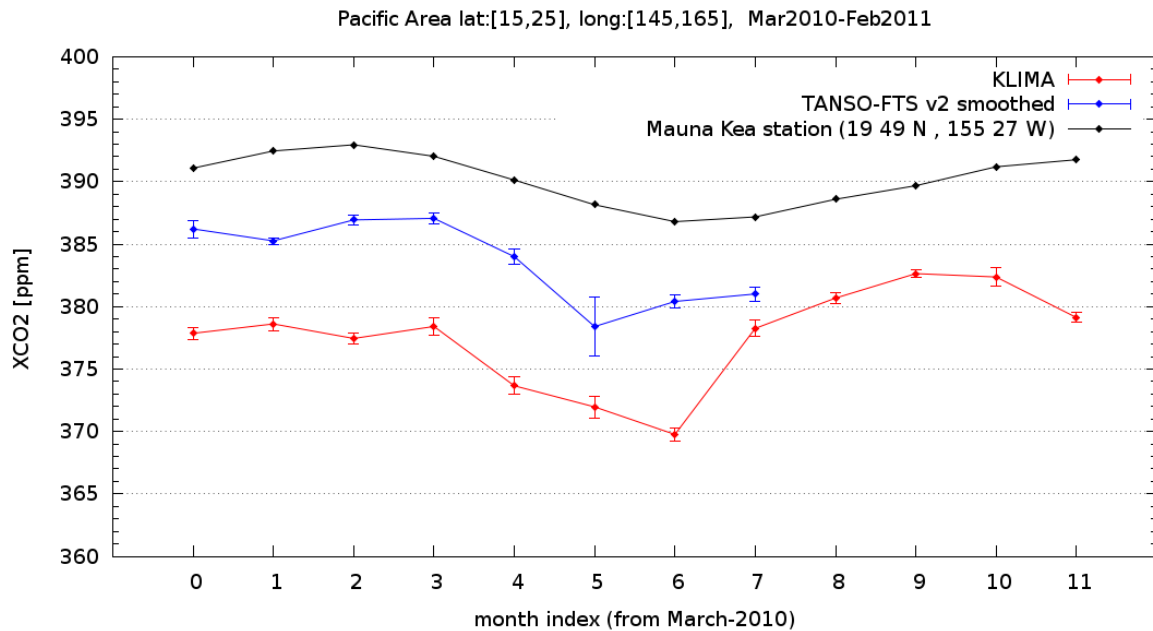


Fig. 70: Average XCO₂ for each month on a Pacific Ocean area; latitude from 10° to 30°, longitude from -145° to -165°. Blue points are TANSO-FTS SWIR (L2 V2 smoothed) average XCO₂ and red points are KLIMA-IASI average XCO₂. TANSO-FTS observations are available only from March 2010 to October 2010

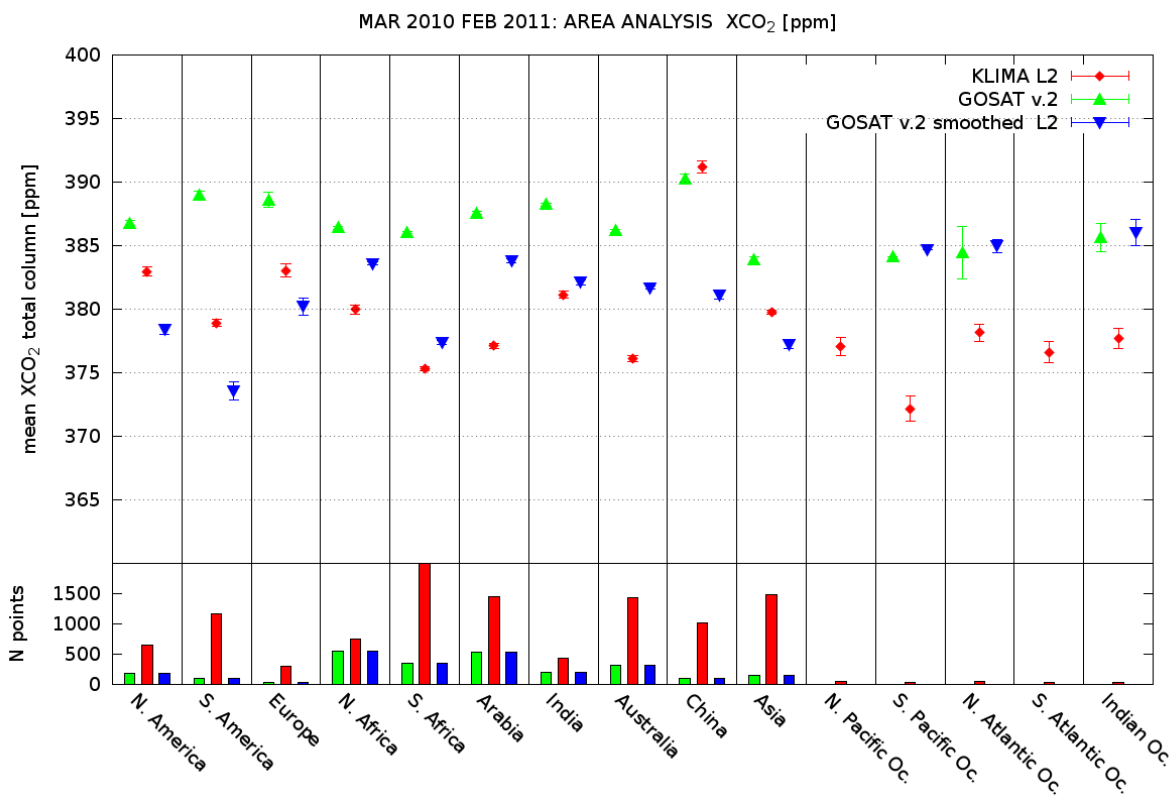


Fig. 71: Top: Average XCO₂ for each macro area reported in Fig. 18. Red points are KLIMA-IASI average XCO₂, green points are EUMETSAT products and blue points are TANSO-FTS ones. Bottom: Number of observations for each macro area

11 Comparison between KLIMA-L2 and TCCON PRODUCTS

In this section we report the comparison of the XCO₂ retrieval products (from the analysis of IASI L1C) obtained using KLIMA code and the TCCON data (see Sect. 4.3 and 5.3) related to 9 sites.

11.1 TCCON products overview

The TCCON sites (see Fig. 11) used for the comparison are reported in Tab. 11. These stations were chosen for

Tab. 11: Ground-based TCCON sites used for KLIMA L2 product comparison

Site	Country	Coordinates [Lat., Long.]
Bialystok	Poland	53.23° N, 23.03° E
Garmisch	Germany	47.48° N, 11.06° E
Lamont	USA	36.60° N, 97.49° W
Lauder	New Zealand	45.04° S, 169.68° E
Ny Alesund	Island	78.92° N, 11.90° E
Orleans	France	47.97° N, 2.11° E
Park Falls	USA	45.94° N, 90.27° W
Sodankyla	Finland	67.37° N, 26.63° E
Wollongong	Australia	34.48° S, 150.79° E

the comparison in order to cover different latitude and longitude range, along with for the availability of data on the same year. The entire dataset has been downloaded from the web server <http://tcccon.ipac.caltech.edu/>. The TCCON dataset related to the stations used in the comparison in the annual range of time selected (March 1, 2010 to February 28, 2011) is reported in Fig. 72, 73, and 74 (red symbols).

11.2 Objectives of the comparison

TCCON provides accurate and precise column-averaged abundances of XCO₂. For this reason the TCCON products usually are used for validation of the products obtained from satellite platform measurements. In this case, to perform the validation, the different AKs, that is the quantification of the sensitivity of the observation to vertical distribution of the target, have to be taken into account. As mentioned in Sect. 7.1 this smoothing can not be applied because the TCCON vertical profiles are not known. Therefore, as observed in the case of the TANSO-FTS comparison, without this correction a bias may be observed. Nevertheless, some complementary indication about consistency and stability of KLIMA-L2 retrieved values can be obtained also from the comparison with TCCON results without smoothing.

11.3 Results of the comparison

The comparison with TCCON data has been performed using the following coincidence criteria:

- Distance from TCCON site less than 200 km, and measurements acquired within 1 hour.
- Distance from TCCON site less than 20 km, and measurements acquired within 1 day.
- Distance from TCCON site less than 50 km, and measurements acquired within 1 day.

The first one imposes a very strong constrain in the time distance between the measurements of IASI and TCCON station. The last two criteria are not so strong in time, but impose a strong constrain in term of distance between the footprint of the observations.

As described in Sect. 7, both the IASI and TCCON measurements that meet the coincidence criteria have been averaged in order to obtain a single value for each day in which the coincidences has been found. The time series relative to each TCCON site have been reported in Fig. 72, 73, and 74 for each of the different coincident criteria respectively. In these plots the complete time series measurements of TCCON is compared with the average IASI coincident measurements.

TCCON measurements show a small daily variability with respect to the KLIMA error on XCO₂ products. In our analysis we first adopted for coincidences the time constraint of 1 hour and the spatial constraints of 200 Km, even if the time constraint is not so critical to establish a coincident criterium and the cases of 1 day coincidences have also been investigated. The spatial constraint is critical in this analysis because the statistics is significantly reduced when the pixel dimensions used for the comparison decreases (see from Fig. 72 to 74).

For some TCCON stations, a dedicated analysis has been performed using the G-POD resources. In particular for Lamont, Lauder, Park Falls, Sodankyla, and Wollongong, a completed analysis on the whole year has been done, while for the other stations we plot the results related to the week for each analysed month. KLIMA measurements are on average lower than the reference data of the TCCON stations. However, as we can see from the most populated comparison with Wollongong station, within the retrieval error, the available KLIMA observations, when corrected for an offset, seem to reproduce well the reference curve.

These differences, as seen in Sect. 7.1, can be explained by means of the effect of the a priori and of the AK related to the different analysis. We performed an assessment of the error due to these effects on a single case related to the Lamont station where some large differences have been observed between TCCON and KLIMA. In a specific case, in which the difference was equal to 7 ppm, the smoothing error, evaluated using Eq. A12 reported in [64] have been estimated of about 5 ppm.

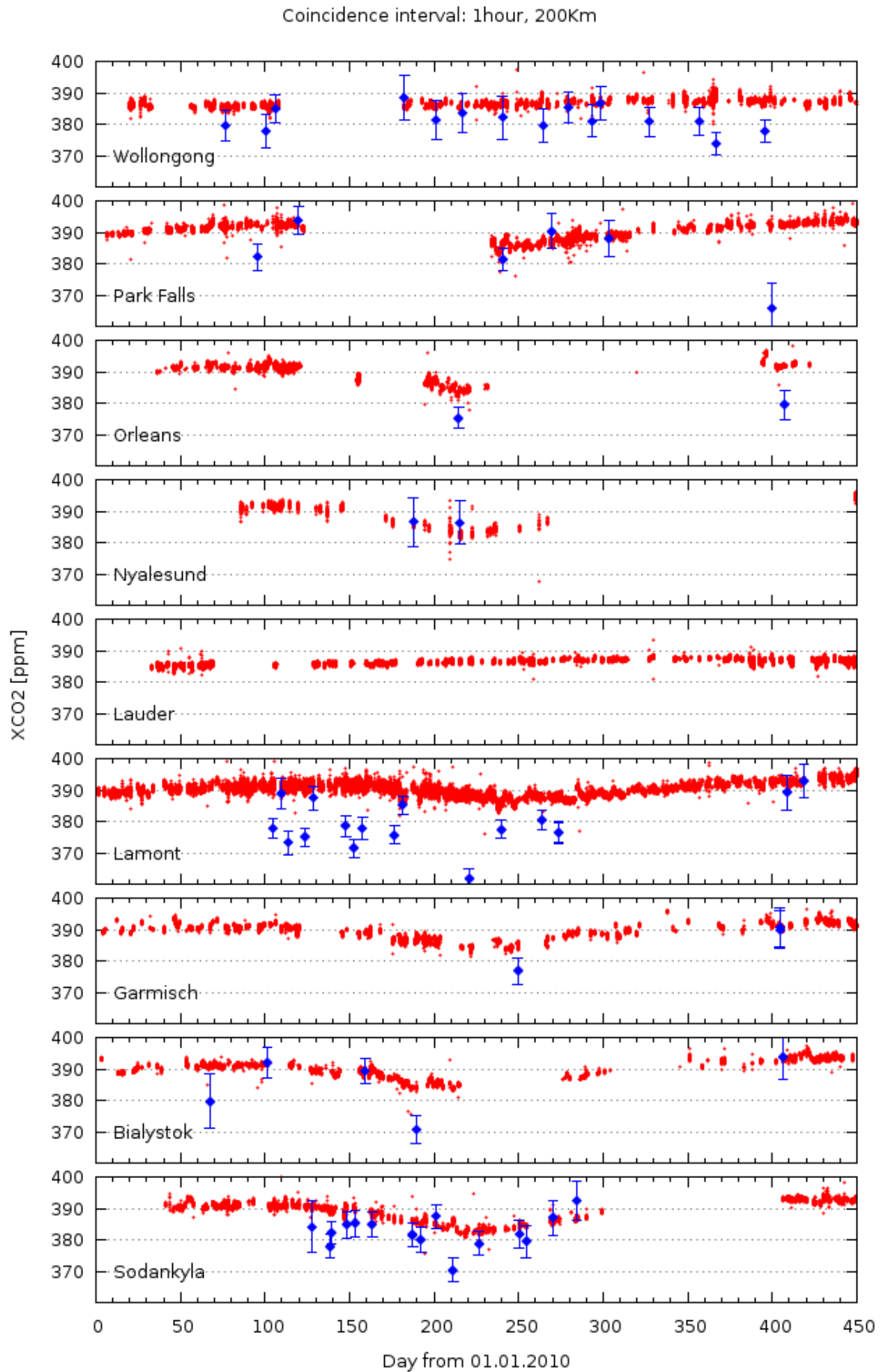


Fig. 72: Time series of TCCON (red) and averaged KLIMA L2 (blue) XCO₂ data within 200 km and 1 hour

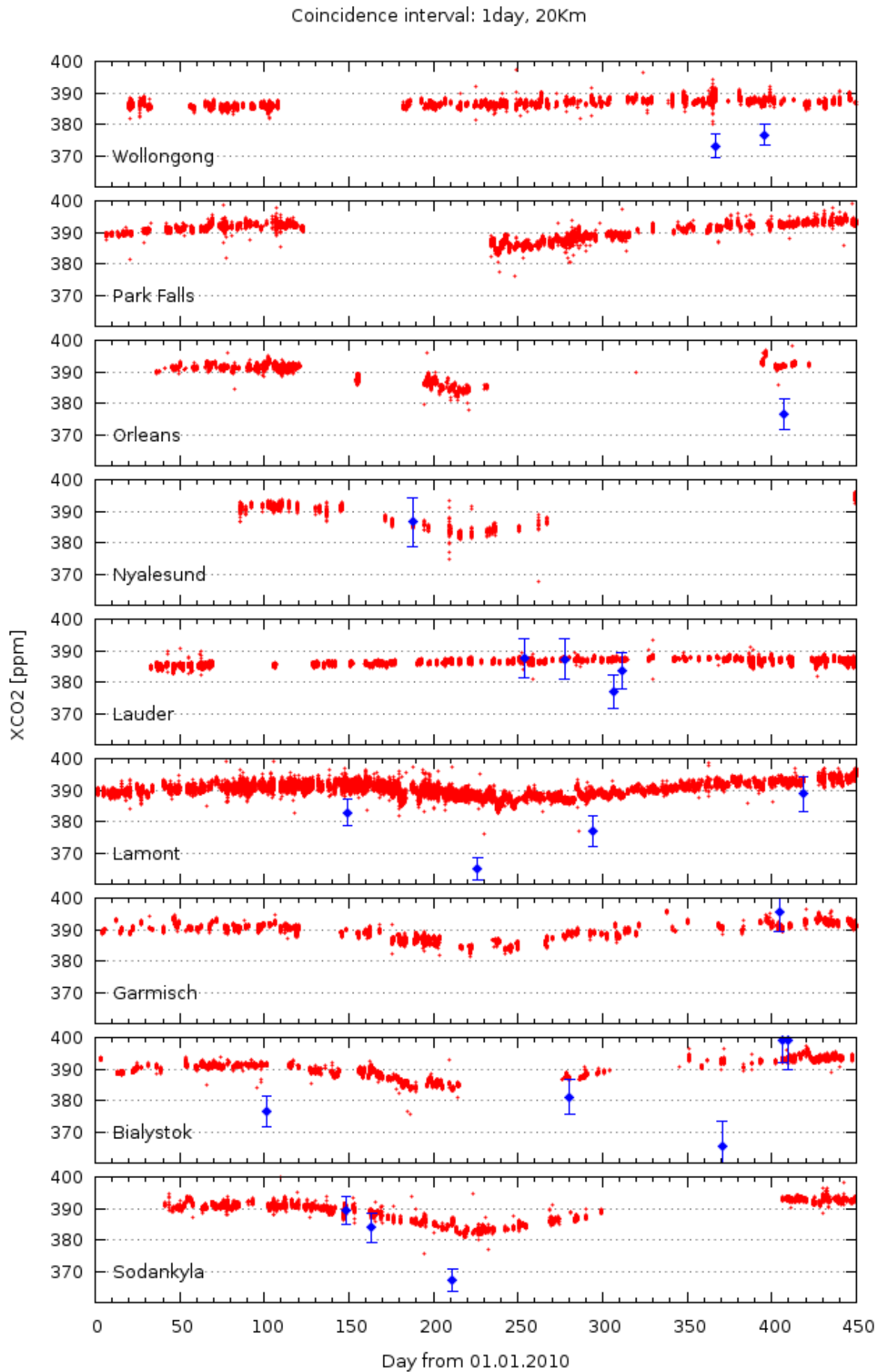


Fig. 73: Time series of TCCON (red) and averaged KLIMA L2 (blue) XCO₂ data within 20 km and 1 day

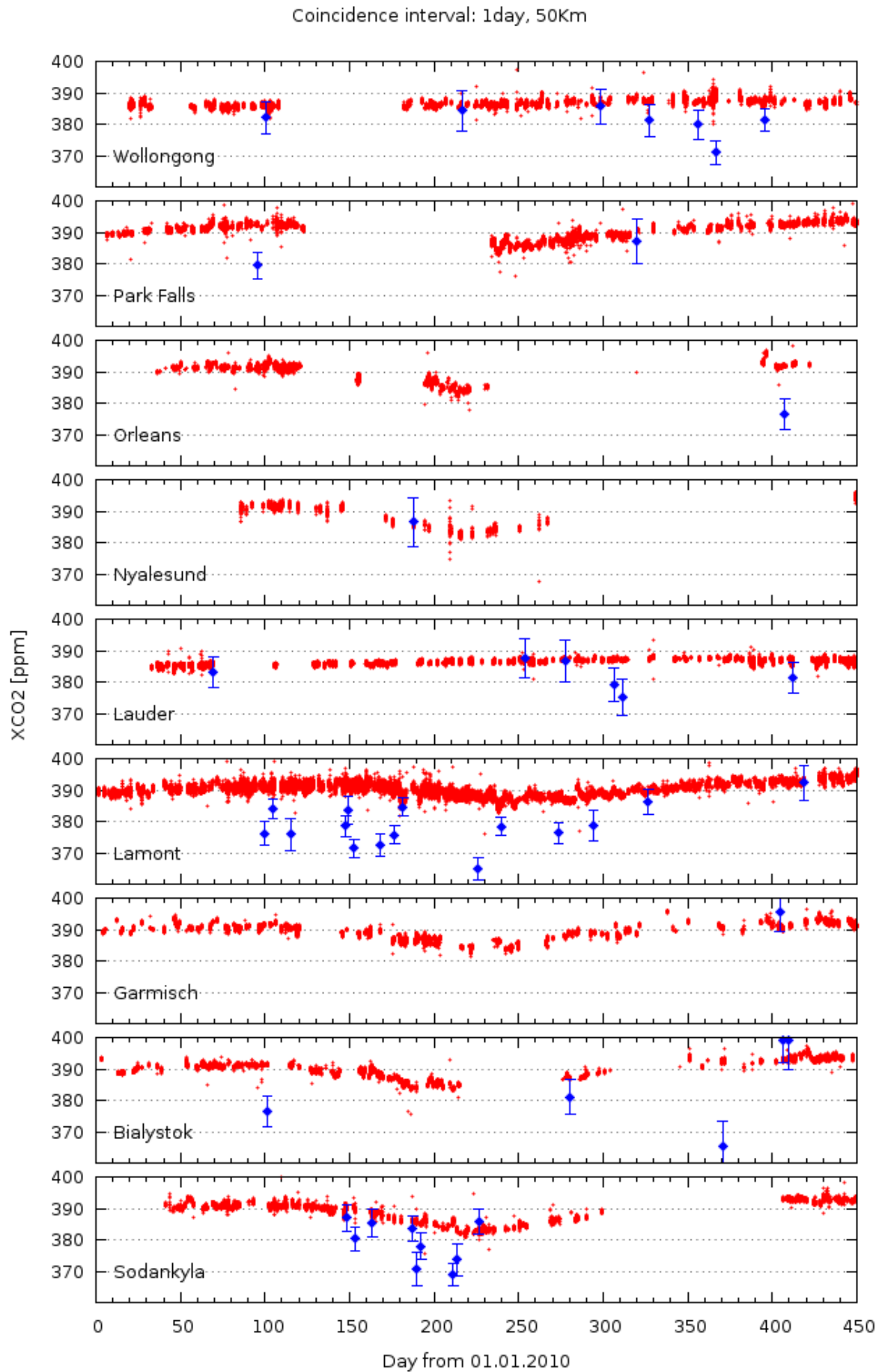


Fig. 74: Time series of TCCON (red) and averaged KLIMA L2 (blue) XCO₂ data within 50 km and 1 day

12 Conclusions

The objective of the KLIMA-IASI study was that of gaining a greater insight in the capabilities of thermal infrared passive remote sounding from space to retrieve accurate information on atmospheric carbon dioxide. The observations of IASI satellite instrument in this spectral region can provide an important contribution to the increase of coverage and quality of the data necessary to constrain the inverse modelling of surface carbon fluxes and to determine the natural and anthropogenic sources and sinks of CO₂. To this purpose the potential was analysed of measurements acquired by the IASI high resolution infrared sounder on-board the MetOp-A satellite to provide CO₂ total column values with precision and accuracy comparable to those of GOSAT/TANSO-FTS, which is the first satellite-based sensor dedicated to the measurement of carbon dioxide. The KLIMA retrieval process, which performs an innovative wide band and multi-target analysis, was used in this study. The combination of these two features makes it possible to exploit for the retrieval all the measured spectral channels and to calculate, in a rigorous way, a retrieval error that also accounts for the errors of interfering parameters.

The results of the first phase of the project, which was focused on the investigation of the sensitivity of IASI spectra and on the demonstration of the possibility to meet with their analysis the requirements for the comparison with GOSAT CO₂ measurements, have been:

- Development of a *Reference Forward Model* (RFM), which has been validated by comparison with both the LBLRTM code and one fully characterized IASI spectrum. The residuals of these comparisons are always smaller than the standard deviation of IASI measurements. Subsequently, the quality of this reference model was also confirmed by the absence of significant biases in the average residuals of a large number of retrievals performed on real measurements.
- Development of the KLIMA retrieval code which when implemented with the RFM provides the *Reference Retrieval Model* (RRM) that can be used to assess the ultimate retrieval performances of IASI. The RRM is capable to retrieve CO₂ total column from a single IASI spectrum with a total error of about $\sim 1.0\%$. This error includes the contributions of the interfering species. Considering that the requirements for the cross-validation with TANSO-FTS products is an accuracy better than 0.3% (1 ppm out of 370 ppm) on regional scales (1000x1000 km²) at monthly intervals (consistent with the required precision established by Rayner and O'Brien [45]), theoretically, about 10 IASI measurements are sufficient for a useful intercomparison.
- Adjustment of the KLIMA retrieval code in order to meet the requirements of the G-POD (Grid Processing On-Demand system) computing resources. These were a program size not exceeding 1 Gbyte and a running time aimed at processing with one processor the IASI central pixels of one orbit in less than one day. Using in the retrieval code an *Accelerated Forward Model* a significant reduction of the computing time is attained with no deterioration of the retrieval error, however the G-POD requirements are not met. A reduction of the analysed spectral range, which causes an increase by a factor 1.4 of the retrieval error of the CO₂ column from a single IASI spectrum, is also needed to meet these preliminary computing requirements. In this case about 25 IASI measurements are desirable for a useful intercomparison. It was also verified that these approximations caused a retrieval bias smaller less than 0.04%. The *Accelerated Retrieval Model* (ARM) that implements these speeding modifications was integrated into the ESA G-POD system, leading to the identification of a further constraint concerning the maximum time of a single processing unit in order to perform a bulk processing of the IASI measurements. This required a further reduction of the analysed spectral range and caused a further increase by a factor 1.2 of the retrieval error which is about 6 ppm for a single retrieval. In the analysis performed with G-POD about 36 IASI measurements are needed for a useful comparison. Therefore, considering the very large number of IASI measurements, the information that has been extracted from IASI using the new code on G-POD is a significant contribution to CO₂ studies, but remains a fraction (about one half in accuracy) of what can be provided by IASI.
- Bulk processing of IASI measurements on G-POD with the adapted KLIMA-IASI retrieval code. A total of 240000 IASI spectra have been analysed covering the period from March 2010 to February 2011. Selection criteria were adopted that limited the analysis to one week each month and reduced the number of selected measurements over the oceans. The number of useful spectra is about two order of magnitude larger than that of the analysed ones. This analysis provides many products and several monitoring parameters, however our subsequent investigation was focused on the retrieved values of XCO₂ column.

In the second phase of the study the processing of IASI observation and the analysis of the results were made. The G-POD analysis made possible the acquisition of a large amount of data with good geographical and time distributions. The global map of XCO₂ column averaged in the full year over 2° x 2° pixels shows a geographical

variability with a structure that (even if not yet validated) is difficult to explain with systematic errors and can reasonably be ascribed to the dynamic of the carbon cycle. The monthly averages, made with the same pixels, show rather uniform fields over the oceans and a large variability with time and location over land, even if some observed differences at high latitudes are caused by the relatively larger errors.

In agreement with 6 ppm retrieval error estimated in the simulations, the experimental retrieval error of a single observation varies from 2 to 20 ppm as a function of the amplitude of the observed spectral radiance and therefore of the surface temperature. This implies that the best precision of IASI observations is obtained in warm seasons and at low latitudes and the worst precision is obtained in the cold seasons and at high latitudes. The dispersion of the retrieved values in each pixel is sometimes smaller than the average retrieval errors, suggesting that a conservative estimate of the retrieval error is made. Pixels with a dispersion larger than the estimated error, which indicate either unaccounted errors or variability of the observed atmosphere, are rather uncommon and occur mainly in specific locations over land.

The average residuals of the retrieval fit are in most spectral channels significantly smaller than the spectral measurement error. However, the χ^2 test shows a correlation with the surface brightness temperature with values close to unity at low temperatures and values that monotonically increase up to 3 at the highest temperatures. Values greater than 3 have been discovered to occur occasionally in desert areas and are most probably due to sand storms. These events are filtered out in all the considered maps. Values of χ^2 greater than unity are a sign of unaccounted errors, which can be:

- (i) Errors due to missing processes in the forward model, such as the scattering contribution due to particles and aerosols (i.e. the observed desert-storm effect) and non-LTE diurnal variations (which are expected to be negligible in the troposphere);
- (ii) Errors due to external constraints such as the surface emissivity in some areas of the globe that are difficult to characterize (e.g. desert and snow-covered regions);
- (iii) Systematic spectroscopic errors;
- (iv) Systematic errors in the IASI measurements (e.g. calibration errors);

The systematic increase of the χ^2 test with the brightness temperature suggests the possible contribution of errors of type iii) and iv) which may depend on this parameter and a negligible effect of the other two which don't. Because of these errors an offset relative to the real atmosphere is possible, but a dispersion of the values is unlikely. In conclusion the diagnostics of the KLIMA-IASI measurement indicate that the measurements have a good coverage and precision and their internal consistency tests do not highlight any anomalous behaviour.

A first comparison was made with the EUMETSAT L2 analysis of IASI observations which provides an extensive set of XCO₂ data that can be directly compared with KLIMA results. These data have not yet been validated and for this product no retrieval errors are given. KLIMA results have a larger dispersion, even if the EUMETSAT results are likely to have a larger error because based on a subset of spectral points. The comparison of these two data sets does not show any straightforward correlations and, since neither of the two has yet been validated, the doubt exists of whether they are observing the same quantity. The two analyses provide different results even when the seasonal variations, in which the monthly averages made in some geographical areas, are compared.

The second comparison was made with the measurements of XCO₂ performed by the TANSO-FTS instrument flying on the GOSAT satellite. TANSO-FTS makes less frequent measurements than IASI and its precision is comparable with the theoretical one of IASI, but better than that obtained in this accelerated analysis. By averaging all its available observations IASI has the potential of providing better measurements than TANSO-FTS. TANSO-FTS has very few measurements at high latitudes (where also the sensitivity of IASI measurements is reduced) and over the oceans (where IASI has instead a very good coverage). The averaging kernels of the two instruments are quite different and this makes the comparison of the measurements more difficult. Therefore, not only IASI has the potential of providing more information than TANSO-FTS, but it is complementary to this instrument because of important contributions such as the ocean coverage and the different averaging kernel. In general KLIMA-IASI results have a value smaller than those of TANSO-FTS. The difference is reduced when the comparison is made with TANSO-FTS measurements smoothed for the effect of the different AKs and a priori profiles. We observe a variability that is smaller than the one observed by KLIMA. No correlation was found between TANSO-FTS and KLIMA-IASI measurements, when either coincident measurements (about 1000 events in the analysed data set), or monthly averages made in 2° x 2° pixels are considered.

However, the two instruments observe similar behaviours when the seasonal variability of XCO₂ is calculated in some latitudinal bands and in the area around Mauna Kea. The agreement is also confirmed by similarities found when comparing the yearly averages of XCO₂ in selected geographical areas of 10° x 10°.

Finally the comparison of KLIMA measurements with ground based observations, such as the in-situ measurements of Mauna Kea and the occultation measurements of the TCCON stations, confirms that KLIMA retrievals are low by about 2-3%. The amplitude of this bias is compatible with existing spectroscopic uncertainties. If corrected for this offset, the KLIMA observations reproduce well the variations observed by the ground stations.

Therefore, even if only a fraction of the available information has been extracted by the analysis on the G-POD, the study demonstrates that IASI can provide very extensive and accurate information on XCO₂ total column which is complementary, in terms of altitude coverage and geographical coverage, to what is currently provided by the GOSAT instrument. The KLIMA code can retrieve from IASI stable and internally consistent XCO₂ data which, apart a negative bias most probably due to spectroscopic errors, do not seem to be affected by unaccounted errors. However, these cannot be excluded because the comparisons, while showing some encouraging agreement in the case of large averages, were not able to constrain the measurements with a stringent validation.

13 Open issues and possible future work

The encouraging results recommend further refinements of the study and its extension to further data. These are here listed without an order of priority.

- Sensitivity tests in order to verify the consistence of the observed negative bias with possible spectroscopic errors.
- Sensitivity tests aimed at quantifying the influence of the assumed profile and of its possible contribution to the spread of the observed differences between KLIMA-IASI and TANSO-FTS.
- Investigation of the possible dependence of the chi-square on other parameters of the retrieval.
- Analysis of the residuals for the identification of the main modelling errors and for the implementation of the VCM of the forward model.
- Improve the comparison with some in-situ (e.g. Wollongong, Mauna Kea and others) with further data processing limited to the coincident measurement that can extend either the time coverage (now limited to one week every month) or the time duration.
- Use of the existing auxiliary data of the retrieval for the calculation of the retrieval error in the case of regularized profiles of water and temperature. The dispersion of the retrieved values in each pixel is sometimes smaller than the average retrieval errors, suggesting that a conservative estimate of the retrieval error is made. This is due to our choice of retrieving the vertical profiles of water vapour and temperature at high vertical resolution in order to model the influence of the variability of these profiles on the retrieved value of XCO₂. This choice causes a larger retrieval error for water vapour and temperature and through the simultaneous retrieval this error enhancement propagates into the XCO₂ retrieval error. It is interesting to assess if a less conservative choice can be made.
- *Improvements of the performance of the KLIMA-IASI retrieval code* - The performance of the KLIMA inversion model applied to the analysis of the IASI data, although optimised according to the results of the sensitivity study, are still affected by a series of limitations and uncertainties. These include the attainment of model capability to process IASI measurements over the full range of azimuth angles (the current analysis was limited to $\pm 30^\circ$ with respect to the full scan of $\pm 48^\circ$) and to extend the coverage of the retrieval products to include the observations of partly cloudy pixels by means of a suitable cloud clearing algorithm (the current analysis only includes clear sky observations); the retrieval code can be further enhanced by appropriate modeling of the contribution of aerosol to the observed radiance.
- *Adaptation of the KLIMA-IASI code for processing IASI/MetOp-B data* - The KLIMA-IASI code has been developed for processing Level-1 data acquired by the IASI instrument onboard the MetOp-A mission launched on 19 October 2006 and currently still in operation. On 17 September 2012, a second mission of the MetOp series was launched (MetOp-B), embarking an upgraded version of the IASI instrument. The KLIMA algorithm could be adapted and optimised for the analysis of the IASI/MetOp-B, to retrieve CO₂ products of improved quality due to the lower noise and better coverage of the new data with respect to IASI/METOP-A observation.
- *Adaptation of the KLIMA-IASI code for the retrieval of CH₄ from IASI/MetOp observations* - The KLIMA-IASI code could be adapted to the retrieval of CH₄ total and partial columns and CH₄ vertical profiles. CH₄ is a target species and total column values of atmospheric methane can be obtained from the validated operational products provided by EUMETSAT for cross-comparison and validation.

- *Application of the KLIMA-IASI code to cross-comparison and validation of CO₂ the operational products of the OCO-2 mission* - The launch date of the OCO-2 mission is currently being planned for July 2014 and potential upgrades of the KLIMA algorithm for the analysis of future IASI measurements and retrieval of carbon dioxide could be used in the framework of cross-comparison and validation activities of OCO-2 products, as originally proposed by the KLIMA-IASI project.
- *Synergistic retrieval of CO₂ total column from satellite-based SWIR and TIR measurements* - The potential synergy of space-borne observations in the SWIR and TIR spectral regions for the retrieval of CO₂ information could be investigated by combining data from the four bands of the TANSO-FTS instrument on GOSAT and by applying the data fusion approach based on the MSS (Measurement Space Solution) algorithm (see Appendix B for more details) or a nearly equivalent procedure. This procedure exploits the same principle of the MSS approach but does not require a reprocessing of the observations that generates the MSS product. Indeed this procedure uses as inputs the averaging kernels and the covariance matrix of the retrieved profiles, usually accessible from the operational products of most satellite missions.
- *Collaboration with the GOSAT team* - As part of the research activities conducted by the IFAC-CNR team in parallel to the workpackages of the KLIMA-IASI project, a collaboration was established with the Japan Aerospace Exploration Agency (JAXA), the National Institute for Environment Studies (NIES) and the Ministry of the Environment (MoE) in response to the Second Research Announcement (RA) aimed to "open to public an opportunity for researching on the data processing algorithms, calibration, validation, carbon balance estimation/atmospheric transport models and scientific use of GOSAT data" (see <http://www.gosat.nies.go.jp/eng/proposal/advertise.htm> for more details). In this context, a direct contact was guaranteed with the GOSAT teams for exchange of information and presentation and check of preliminary results from the retrieval of CO₂ total columns from IASI spectra e comparison with TANSO-FTS SWIR products (e.g. during the GOSAT RA Principal Investigators Meetings held in Kyoto, Japan, 2010; Edinburgh, UK, 2011; Pasadena, USA, 2012; Yokohama, Japan, 2013) organized in close connection with the 6th, 7th and 8th edition of the International Workshop on Greenhouse Gas Measurements from Space).
- *Collaboration with the G-POD team* - The integration of the KLIMA Accelerated Retrieval Model into the G-POD operating system and the access to G-POD computing resources played a key role in project activity. The CAT-1 procedure followed for implementation of the KLIMA/G-POD retrieval code and for its application to bulk processing of IASI Level 1c data is described in details in Section 6 of this report. As a conclusive remark, we can state that the exploitation of G-POD computing resources made it possible to increase the number of cores accessible for IASI data processing by an order of magnitude in terms of parallel processing (i.e. from approximately 20 cores available when using the IFAC system to about 200 cores of the G-POD system). The computing time for single process is comparable for the two systems. G-POD has made available 5 TB of disk space, that corresponds to 100% of the storage resources available at the IFAC system. We underline the fact that the outcome of the analysis of 240.000 IASI spectra was achieved within the timeframe of the project also thanks to a relatively smooth and effective interaction process between the KLIMA-IASI project and G-POD teams that finalised the integration of KLIMA ARM code into the G-POD environment. Moreover, an important feature of this interaction was the capability to establish a reasonable trade-off between the formal process for major upgrading of the KLIMA prototype on G-POD and the flexibility for implementation of minor changes and improvements. An open issue, to consider in case we envisage future uses and modifications of the KLIMA code, is the possibility to allocate further computing resources of the G-POD system to this purpose.
- *Spectroscopic data issue* - The work conducted in the two phases of the project confirmed the high quality of IASI measurements, already highlighted by previous studies and validation activities (e.g., Shephard et al., [56]). The high spectral stability and radiometric accuracy demonstrated by the IASI instrument on board the MetOp-A platform represented a key feature of the mission capable to tease existing spectroscopic uncertainties out of the measurement noise level. Our first analysis, using HITRAN 2004 spectroscopic database (Rothman et al., [49]), identified the need for further refinement of water vapour spectroscopy in the spectral interval [800 - 1750] cm⁻¹, which we implemented by adopting the new line intensities and position values recommended by Coudert [18]. Coudert line parameters were subsequently included in the HITRAN starting from the 2008 version (Rothman et al., [50]), which replaced HITRAN 2004 as the reference spectroscopic data archive of the KLIMA inversion code. Large residuals that persist in KLIMA-IASI data processing are found in the spectral interval between 2380 and 2400 cm⁻¹. Similar differences between simulated data and observation in this spectral region result from the analysis of IASI measurements acquired in the frame of the JAIVEX validation campaign and processed using the LBLRTM code. The

source of these residuals, although most probably associated to spectroscopic uncertainties, needs to be further investigated. Consequently, in current IASI data analysis based on the use of the KLIMA algorithm, we discard the interval [2380-2400] cm^{-1} . Shephard et al., [56] showed negative radiance residuals in the low frequency side of the ν_3 region, from 2170 to 2270 cm^{-1} , associated with N_2O and CO_2 radiation from the surface to the tropopause. They suggested that the Perevalov and Tashkun [43] line parameters might significantly reduce the residuals in this important region. Our tests, performed on this band with the KLIMA code, using the new CO_2 line parameters (Courtesy of Matthew J. Alvarado, Ph.D. Staff Scientist Radiation and Climate Atmospheric and Environmental Research, Inc. (2011)), confirmed this hypothesis. A better insight is also needed in the quality of spectroscopic data around 667 cm^{-1} (15 micron), to identify the source of the relatively large residuals that emerge at the centre of the CO_2 fundamental Q-branch in the analysis of IASI spectra processed by a number of inverse models (Masiello et al., [37] and references therein). We believe that the results of the extensive testing we have performed on the inversion of IASI radiances in Band 1 and in Band 1 + Band 2 might contain pieces of information that might give a clue on this issue. In fact, we observed a different behaviour of the average residuals when we apply the KLIMA inverse model to the retrieval of carbon dioxide from IASI measurements, either by retrieving the vertical profile of atmospheric temperature or by assuming the temperature values given by the operational products. In the first case, the mean value of the residuals from inverse processing of about 500 IASI spectra in Band 1 around 667 cm^{-1} is less than the IASI noise, while in the second case it is comparable with the mean residual obtained from LBLRTM analysis of the same dataset. We repeated this test by fitting the IASI radiances over the extended spectral coverage of Band 1 + Band 2 and obtained in both cases (with and without retrieval of the atmospheric temperature profile) a larger mean value of the residuals very close to the mean value of LBLRTM residuals. This might suggest that the difference between observed and simulated radiances in the 667 cm^{-1} region is reduced by using the temperature profile retrieved by KLIMA when fitting Band 1 only, whilst a larger mean value of the residuals emerges from inversion of Band 1 + Band 2 or from retrieval processing based on other inverse models. Further testing is necessary to investigate whether the discrepancy reported in the literature at 667 cm^{-1} and not found by processing IASI spectra in Band 1 with KLIMA is related to incorrect values of atmospheric temperature at given altitude (e.g., in the stratopause region, as postulated by Masiello et al., [37] and by Shephard et al., [56]) or due to spectroscopic uncertainties. Further refinement of the KLIMA-IASI radiative transfer model and full validation of the inversion code are required, in order to achieve a level of performances that is adequate to dedicated studies for improvement of spectroscopic data.

A The KLIMA-IASI Pre-Processor

Introduction

The KLIMA Pre Processor is intended as a module that, in the logic flow chart of IASI data analysis, can be located between the input data provided by an external source (EUMETSAT operational products and auxiliary data) and the retrieval code (Fig. 75).

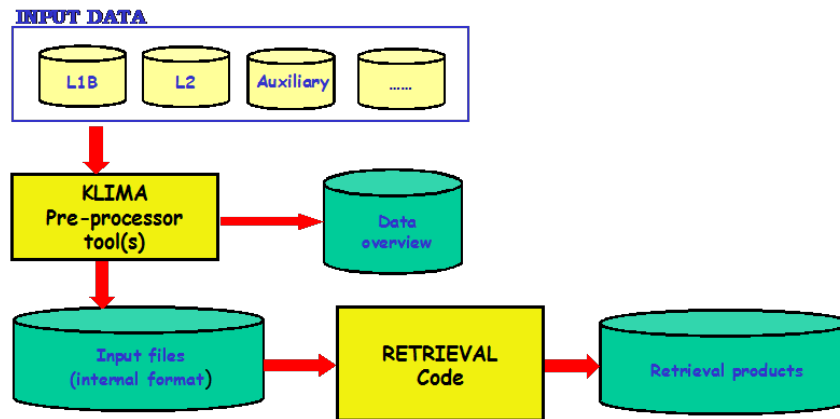


Fig. 75: The flow-chart of KLIMA-IASI data analysis

The primary objectives of the pre-processor are to make the retrieval code independent from the format of the input data provided by external sources (L1B, L2) as well as to provide the user with an overview of the IASI observation dataset in order to plan the activity of data analysis.

The KLIMA processor requires only a small subset of the data contained in IASI L1 files to perform the retrieval. For this reason, we considered the use of pre-processed input data organized according to an internal format more effective than a direct link to operational L1 products. The pre-processor tool was therefore developed to read the spectral radiance data and associated information from IASI L1B files and convert that in the internal data format that could be accessed by the retrieval code. This approach make possible to use the retrieval code with different sets of data, by changing only the pre-processor tool without any modification in the validated retrieval routines.

The second task performed by the pre-processor consists in the preparation of the overview file, containing information about the geo-location and time of individual IASI scans, as well as a subset of measurement and retrieval quality flags extracted from the L2 products. By using this information, the user can set up specific filtering criteria, identify the matching scans and select the dataset to be processed without the need of accessing all individual L1 and L2 IASI operational products.

The strategy of data analysis

The strategy adopted by the pre-processor tool for the preparation of KLIMA-IASI input dataset can be described as a three step procedure:

- **FIRST STEP:** The first step consists in the creation of the KLIMA Look-Up-Table (KLUT) built upon information extracted from IASI L2 operational products and reporting a limited subset of the L2 data. The Look-Up-Table is, basically, a binary file containing information about date, time, geo-location and measurement and retrieval quality flags of all IASI observations in the L2 products files. The idea is to generate one KLUT for each month and use it for the operations of data selection and data analysis planning that would otherwise require repeated and time-consuming access to the original IASI L2 products. The main advantage of the proposed approach derives from the reduced dimension of the KLUT data that allows a much faster pre-processing. The KLUT-builder is the tool of the Pre-Processor suite dedicated to the LUT building
- **SECOND STEP:** In the second step, a dedicated tool provides an overview of the data contained in the KLUTs. The overview can be selected using some filtering criteria about date/time of the observations, geo-location, viewing angle, solar zenith angle and retrieval quality flags. The overview is exported in an ASCII file in order to allow a direct reading and can be used for the selection of the specific observations to be processed by the retrieval code. KLUT-reader is the tool of the Pre-Processor suite dedicated to the KLUT reading and overview creation.

- **THIRD STEP:** In the third step the data required for the retrieval are extracted from IASI L1 and L2 products using a dedicated tool. This tool prepares a retrieval input data set consisting in the L1B spectrum as well as all the input data required by the retrieval code. Kprepro is the tool of the Pre-Processor suite dedicated to the generate the input data set for the retrieval code.

The KLIMA-IASI Look-Up Table

Look-Up Tables (KLUT) represent a summary of IASI measurement and contain, basically, only the data needed for measurement selection. Data are arranged in an internal format and stored in binary files, grouped in one directory for each month. All information contained in the LUTs are extracted from the IASI Level2 data files provided by UMARF. A dedicated software tool (KLUT_builder, see description in section The pre-processor software suite) has been developed in order to read the L2 data provided by the UMARF archive and generate the LUTs Tab. 12 summarises the information contained in the KLIMA-IASI Look-Up-Tables.

Tab. 12: Information contained in the KLIMA-IASI Look-Up Tables

GEOLOCATION and OBSERVATION GEOMETRY	
LATITUDE	Earth Location: latitude of the surface footprint
LONGITUDE	Earth Location: longitude of the surface footprint
VIEWING_ANGLE	angle of observation
SOLAR_ZENITH_ANGLE	solar zenith angle
OBSERVATION_TIME	UTC time of the observation
PIXEL SURFACE INFORMATION	
SURFACE_PRESSURE	Value of the pressure at the earth surface
SURFACE_TEMPERATURE	Value of the temperature at the earth surface
SURFACE_EMISSIVITY	Emissivity of the surface (max 12 values for 12 different wavelengths)
L2 QUALITY FLAGS	
FLG.LANSEA	Specifies the surface type (land, sea, land+sea)
FLG.DAYNIT	Discrimination between day and night
FLG.IASIBAD	Validation flag for IASI L1 product
FLG.IASICLR	IASI IFOV clear, partly cloudy or cloudy
FLG.ITCONV	Convergence of the iterative retrieval
FLG.VARCLR	Cloud clearing by variational analysis
FLG.RETCHC	Choice of combined or IASI stand alone retrieval
FLG.FINCHC	Final choice of retrieval
QUALITY OF MEASUREMENT AND PROCESSING	
DEGRADED_INST_MDR	Quality of MDR has been degraded from nominal due to an instrument degradation
DEGRADED_PROC_MDR	Quality of MDR has been degraded from nominal due to a processing degradation

The pre-processor software suite

The pre-processor software suite consists of 3 main tools dedicated to data management: KLUT-builder, KLUT-reader and Kprepro. The first one reads the IASI L2 datafiles and builds the KLUTs; the second one is used for IASI measurements selection and the third one reads the L1 and L2 data files and generates the input dataset for the retrieval code. In the following the three tools are presented in more details.

The KLUT builder

The KLUT_builder allows generating the KLIMA-IASI LookUp Tables starting from IASI L2 data produced by the operational retrieval. The tool receives as input the IASI data files in EPS native format provided by the UMARF archive and extracts the relevant information (Fig. 76). Data are arranged in a data structure and stored in a binary file (one file for each month).

The KLUT reader

The KLUT_reader allows a selection of the IASI observations starting from the KLIMA-IASI LookUp Tables. The user can select a set of observations using as selection criteria: the date and time of the measurement, the measurement geo-location, the viewing angle, the presence of clouds in the field of view, the day or night measurement

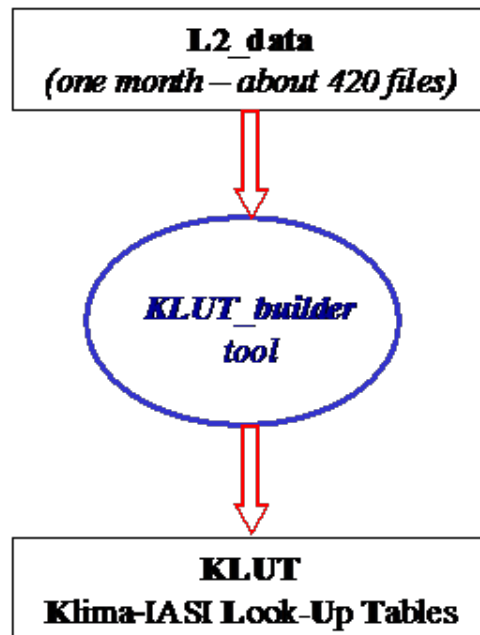


Fig. 76: KLUT_builder Input and Output

ad some quality flags from measurement and operational retrieval. The tool receives as input the Klima LookUp Tables, generated by the KLUT_builder tool, and produces as output an ASCII file containing an overview of the measurements matching the selection criteria (Fig. 77).

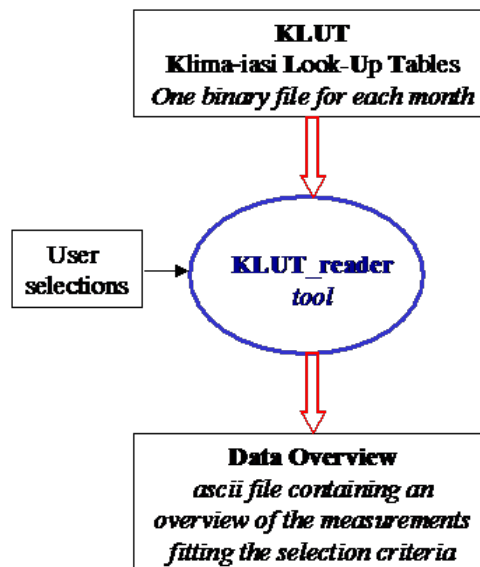


Fig. 77: KLUT_reader Input and Output

The selection criteria are defined by modifying the settings of an ASCII file that can be edited by the user. In the setting file each parameter is preceded by a specific key-word (inserted in square brackets) that make the parameter definition easier.

The KLUT_prepro

The K_prepro is the tool dedicated to the generation of the input dataset for the retrieval code, starting from IASI L1 and L2 data. Using the information contained in the overview of the measurements, the user can select the specific observation to be processed. For a selected orbit, the tool receives as input the L1B and L2 data file in EPS native format and produces as output the data set required as input of the retrieval code.

The data set contains all relevant information required for the retrieval code:

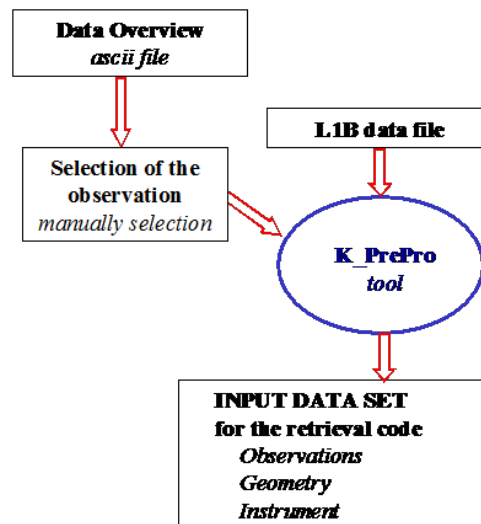


Fig. 78: K_prepro Input and Output

- a file containing the observation date and time, geometry, geo-location and the L1B observed spectrum;
- a file containing the profile of temperature and the related error, retrieved from operational retrieval and extracted from IASI L2 file;
- a file containing the profile of water vapour and the related error, retrieved from operational retrieval and extracted from IASI L2 file;
- a file containing the partial column of ozone retrieved for three different value of pressure and the total ozone column, retrieved by the operational retrieval and extracted from IASI L2 file;
- a file containing the total column of CO₂, CH₄ and CO retrieved by the operational retrieval and extracted from IASI L2 file;
- a file containing the surface emissivity provided by IASI L2 data file.

B The Measurement Space Solution method

In this appendix we recall the basic concepts of the solution of the retrieval problem referred to as Measurement Space Solution (MSS). The problem that we face is that to retrieve the vertical distribution of an atmospheric constituent from remote sensing observations. Since the observations do not provide enough information to retrieve the continuous function of the vertical profile, the problem arises of how to represent, in terms of which and how many parameters, the finite number of independent pieces of information provided by the observations. The first choice is that of the vertical grid on which to represent the profile. This vertical grid should be as fine as possible in order both to make sure that all the information included in the observations is adequately represented by the profile and to limit the need for interpolation in the subsequent applications of the data. Indeed, operations of interpolation do introduce a loss of information. However, whenever the information obtained from the observations is not sufficient to determine as many parameters as the grid points, a too fine grid makes the inversion problem ill-posed or ill-conditioned. This problem is generally overcome using some external information that is referred to as a priori information.

A priori information makes it possible to obtain a vertical profile on a fine grid, but generates other types of problems in utilizing the data. In validation activities, when the compared profiles use different a priori information, it is necessary to assess the error due to this difference. The estimation of the error component due to the use of different a priori information is a difficult task because it requires a reliable knowledge of the climatological variability of the quantity to be compared, which often is not available. Also in data assimilation, which is the combining of diverse data sampled at different times and different locations into atmospheric models, the measurements containing a priori information pose some problems. Profiles in different geo-locations obtained using the same a priori information are correlated among themselves as well as profiles obtained using nearby retrieved profiles as a priori. If not taken into account, these correlations can produce a bias in the products of the assimilation. Also in the case of data fusion, which consists in the synergetic use of more than one measurement of the same atmospheric state obtained with different instruments, the presence of a priori information in the original measurements can produce a bias in the final product.

In order to overcome the problems posed by the a priori information the MSS can be used. The MSS allows to represent the solution without the use of any a priori information and on a vertical grid as fine as needed both for its exhaustive description and for the prevention of subsequent interpolation approximations. In the following the basic equations of the MSS are recalled.

We represent the observations (radiances) with a vector \mathbf{y} of m elements and the vertical profile of the unknown atmospheric parameter with a vector \mathbf{x} of n elements corresponding to a predefined altitude grid. The forward model is a function $\mathbf{F}(\mathbf{x})$ that provides the value of the observations when the profile \mathbf{x} is known. Therefore, the relationship between the vectors \mathbf{x} and \mathbf{y} is:

$$\mathbf{y} = \mathbf{F}(\mathbf{x}) + \epsilon, \quad (2)$$

where ϵ is the vector containing the experimental errors of the observations, characterized by a VCM \mathbf{S}_y given by the mean value of the product of ϵ times its transposed.

We shall consider the case of a nearly linear relationship between \mathbf{y} and \mathbf{x} . In this case $\mathbf{F}(\mathbf{x})$ can be expanded up to the first order around a specific value of \mathbf{x} , identified by \mathbf{x}_0 and referred to as the linearization point, and Eq. 2 becomes equal to:

$$\mathbf{y} = \mathbf{F}(\mathbf{x}_0) + \mathbf{K}(\mathbf{x} - \mathbf{x}_0) + \epsilon, \quad (3)$$

where \mathbf{K} is the Jacobian matrix (that is the partial derivatives of $\mathbf{F}(\mathbf{x})$ with respect to the elements of \mathbf{x}) calculated at \mathbf{x}_0 .

Equation 3 implies that the components of $\mathbf{y} - \mathbf{F}(\mathbf{x}_0)$ are the scalar products between $\mathbf{x} - \mathbf{x}_0$ and the rows of \mathbf{K} plus the error components. It follows that the knowledge of $\mathbf{y} - \mathbf{F}(\mathbf{x}_0)$ determines the knowledge of the component of $\mathbf{x} - \mathbf{x}_0$ that lies in the space generated by the rows of \mathbf{K} . On the basis of the conventions that \mathbf{y} are the observations and \mathbf{x} are the aimed measurements, we shall refer to this space as the measurement space. With the inversion of Eq. 3 one obtains the correction $\mathbf{x} - \mathbf{x}_0$ that has to be applied to \mathbf{x}_0 in order to determine \mathbf{x} . Since the correction is made in the measurement space and no information is acquired about the components of $\mathbf{x} - \mathbf{x}_0$ in the orthogonal space that is complementary to the measurement space, also the determination of \mathbf{x} is to be considered as only made in the measurement space. However, this statement requires some further explanation. In fact, if \mathbf{x}_0 has a component in the orthogonal space, when \mathbf{x}_0 is combined with $\mathbf{x} - \mathbf{x}_0$ to give \mathbf{x} also \mathbf{x} acquires this component. However such a component cannot be considered to be a result of the retrieval process because it is a contingent quantity that depends on the procedure rather than on the observations. On the basis of these considerations it is correct to say that since $\mathbf{x} - \mathbf{x}_0$ is determined in the measurement space, also \mathbf{x} is determined in this space. The orthogonal complement space to the measurement space is referred to as the null space.

In order to weigh the observations with their errors and to avoid the complication of correlated errors it is useful to consider the quantities $\mathbf{S}_y^{-\frac{1}{2}}\mathbf{y}$ instead of the observations \mathbf{y} . Multiplying both terms of Eq. 3 on the left by $\mathbf{S}_y^{-\frac{1}{2}}$ we obtain:

$$\mathbf{S}_y^{-\frac{1}{2}}\mathbf{y} = \mathbf{S}_y^{-\frac{1}{2}}\mathbf{F}(\mathbf{x}_0) + \mathbf{S}_y^{-\frac{1}{2}}\mathbf{K}(\mathbf{x} - \mathbf{x}_0) + \mathbf{S}_y^{-\frac{1}{2}}\epsilon. \quad (4)$$

It is easy to verify that $\mathbf{S}_y^{-\frac{1}{2}}\mathbf{y}$ is characterized by a VCM that is the unity matrix.

The unknown profile \mathbf{x} is a vector of n elements and belongs, therefore, to the space n which can be decomposed in the direct sum of the measurement space and of the null space. If we indicate with p the dimension of the measurement space then the dimension of the null space is $n-p$. Since each vector of n can be decomposed as the sum of a vector belonging to the measurement space and a vector belonging to the null space, we can write:

$$\mathbf{x} = \mathbf{x}_a + \mathbf{x}_b, \quad (5)$$

where \mathbf{x}_a and \mathbf{x}_b , respectively, belong to the measurement space and to the null space. They can be expressed as:

$$\mathbf{x}_a = \mathbf{V}_a, \quad (6)$$

$$\mathbf{x}_b = \mathbf{W}_b, \quad (7)$$

where \mathbf{V} is a matrix whose columns are an orthonormal basis of the measurement space, \mathbf{W} is a matrix whose columns are an orthonormal basis of the null space and \mathbf{a} and \mathbf{b} are the projections of \mathbf{x} on these orthonormal bases:

$$\mathbf{a} = \mathbf{V}^T\mathbf{x}, \quad (8)$$

$$\mathbf{b} = \mathbf{W}^T\mathbf{x}, \quad (9)$$

where the superscript T denotes transposed matrices.

The component of \mathbf{x} in the measurement space is the only quantity that can be derived from the observations. In order to find \mathbf{x}_a from Eq. 6 we need to identify \mathbf{V} and \mathbf{a} . To this purpose we perform the singular value decomposition of $\mathbf{S}_y^{-\frac{1}{2}}\mathbf{K}$:

$$\mathbf{S}_y^{-\frac{1}{2}}\mathbf{K} = \mathbf{U}\mathbf{\Lambda}\mathbf{V}^T, \quad (10)$$

where \mathbf{U} is a matrix of dimension $m \times p$ whose columns (referred to as left singular vectors) are an orthonormal basis of the space generated by the columns of $\mathbf{S}_y^{-\frac{1}{2}}\mathbf{K}$, $\mathbf{\Lambda}$ is a nonsingular diagonal matrix of dimension $p \times p$ and \mathbf{V} is a matrix of dimension $n \times p$ whose columns (referred to as right singular vectors) are an orthonormal basis of the space generated by the rows of $\mathbf{S}_y^{-\frac{1}{2}}\mathbf{K}$. Since $\mathbf{S}_y^{-\frac{1}{2}}$ is a nonsingular matrix the space generated by the rows of $\mathbf{S}_y^{-\frac{1}{2}}\mathbf{K}$ coincides with the space generated by the rows of \mathbf{K} , therefore the columns of \mathbf{V} are an orthonormal basis of the measurement space and, among all the possible orthonormal bases of the measurement space, it can be chosen for representing \mathbf{x}_a with Eq. 6. We can now determine the components of \mathbf{x}_a relative to this orthonormal basis. Substituting Eq. 10 in Eq. 4, multiplying both terms on the left by $\mathbf{\Lambda}^{-1}\mathbf{U}^T$ and using Eq. 8, after some rearrangements, we obtain that \mathbf{a} , i.e. the estimation of \mathbf{a} deduced from the observations, is given by:

$$\hat{\mathbf{a}} = \mathbf{a} + \epsilon_a = \mathbf{V}^T\mathbf{x}_0 + \mathbf{\Lambda}^{-1}\mathbf{U}^T\mathbf{S}_y^{-\frac{1}{2}}(\mathbf{y} - \mathbf{F}(\mathbf{x}_0)), \quad (11)$$

where

$$\epsilon_a = \mathbf{\Lambda}^{-1}\mathbf{U}^T\mathbf{S}_y^{-\frac{1}{2}}\epsilon \quad (12)$$

is the error that we make taking $\hat{\mathbf{a}}$ as the estimation of \mathbf{a} and is characterized by the diagonal VCM:

$$\mathbf{S}_a = \mathbf{\Lambda}^{-2}. \quad (13)$$

From Eq. 13 we see that the components of the vector \mathbf{a} are independent of each other and are characterized by variances given by the inverse of the squared singular values of $\mathbf{S}_y^{-\frac{1}{2}}\mathbf{K}$. Therefore, components corresponding to large singular values are well determined while components corresponding to small singular values are poorly determined.

The definition of \mathbf{x}_a in terms of \mathbf{V} and \mathbf{a} , determined respectively by Eq. 10 and by Eq. 11, is referred to as the MSS. This solution is obtained exploiting all the information coming from the observations without any a priori information. It is, therefore, the optimal quantity to be used for further post-retrieval processing.

The MSS, while optimal for further processing because comprehensive, unbiased and with a diagonal VCM, is not suitable for a representation of the retrieved profile in the form of a graph. Indeed, if the dimension n is chosen with the desirable redundancy, components of the MSS that correspond to small singular values are poorly determined and make this solution ill-conditioned. On the other hand, if the poorly determined components are removed, the size of the null space grows at the expenses of the measurement space and the retrieved profile acquires a rather unphysical shape. This unphysical shape is frequently observed in retrieval techniques and is due to the fact that in a graphical representation the result is presented in a complete space. In a complete space the representation of the profile with only the MSS component corresponds to the selection of the value zero for the null-space component. This is a particular choice among the infinitive possible ones, which does not necessarily provide the best graphical representation.

The above considerations underline the importance of choosing an adequate null-space component when a graphical representation is made. This component can be estimated using several methods. One of this is the Null Space Regularization (NSR) method which provides the smoothest profile compatible with the observations. This is a regularization and is different from the other regularizations since it does not affect the measured component and only determines the one that has not been measured. The fact that two components (the MSS and the NSR) are determined respectively in the measurement space and in the null space provides a clear and easily traceable distinction between the measurement and the constraint. The MSS plus NSR, that is referred to as the Regularized Measurement Space Solution (RMSS), provides a good graphical representation of the retrieved profile.

C Jacobian maps wrt IASI target parameters

Jacobian matrices with respect to the retrieval parameters considered in the sensitivity study have been computed and used to generate maps of the sensitivity of IASI measurements to perturbations of temperature, H₂O, O₃, CO₂ and N₂O vertical distribution (w.r.t. reference climatological values) as a function of altitude and wave number in the spectral range [650 - 2700] cm⁻¹. In this appendix, we report for each species the maps of the product between the columns of the Jacobian matrix and the vertical VMR profile, normalized to the thickness of the layers in the altitude grid used by the FM. This quantity represent the perturbation of the spectral radiance observed by the IASI instrument due to a 100% increment of the VMR at each level and it is expressed in the maps in units of nW/(cm² sterad cm⁻¹)).

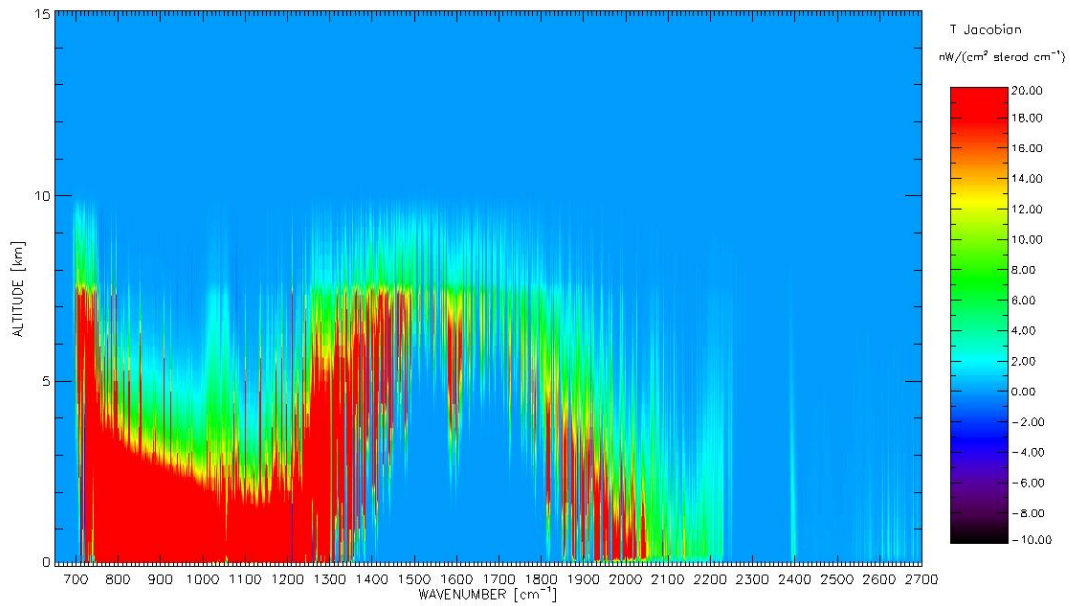


Fig. 79: Temperature Jacobian in the spectral range [650-2700] cm⁻¹

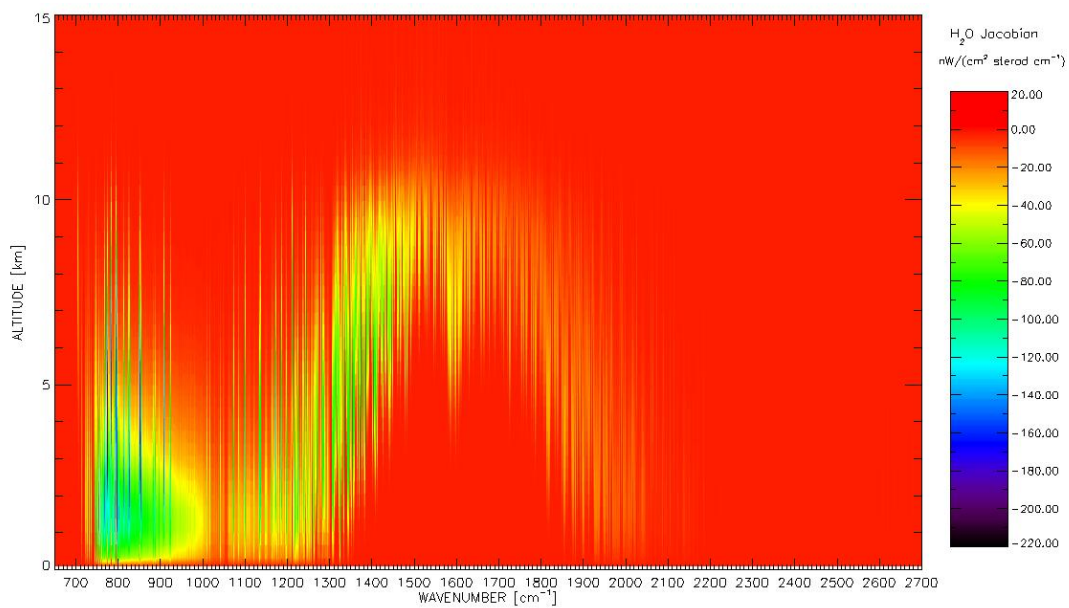


Fig. 80: Water Vapor Jacobian in the spectral range [650-2700] cm⁻¹

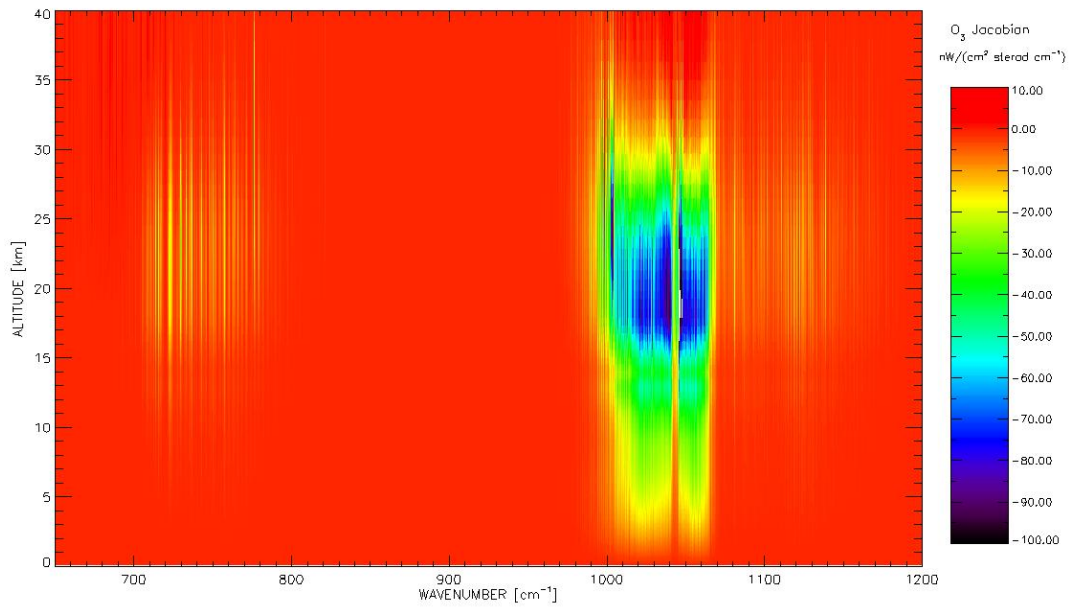


Fig. 81: O₃ Jacobian in the spectral range [650-2700] cm⁻¹

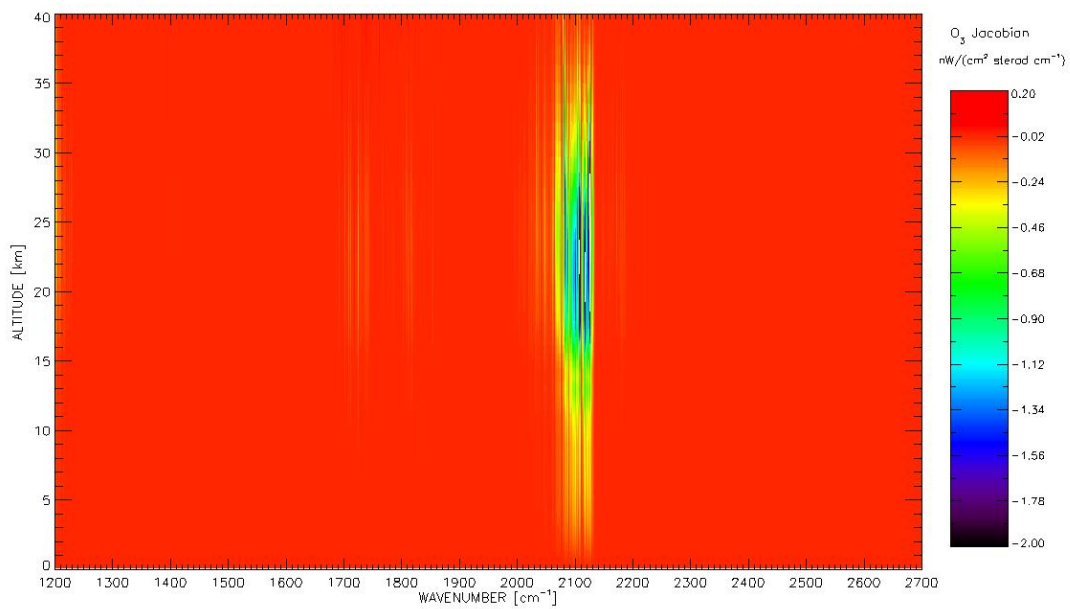


Fig. 82: O₃ Jacobian in the spectral range [1200-2700] cm⁻¹

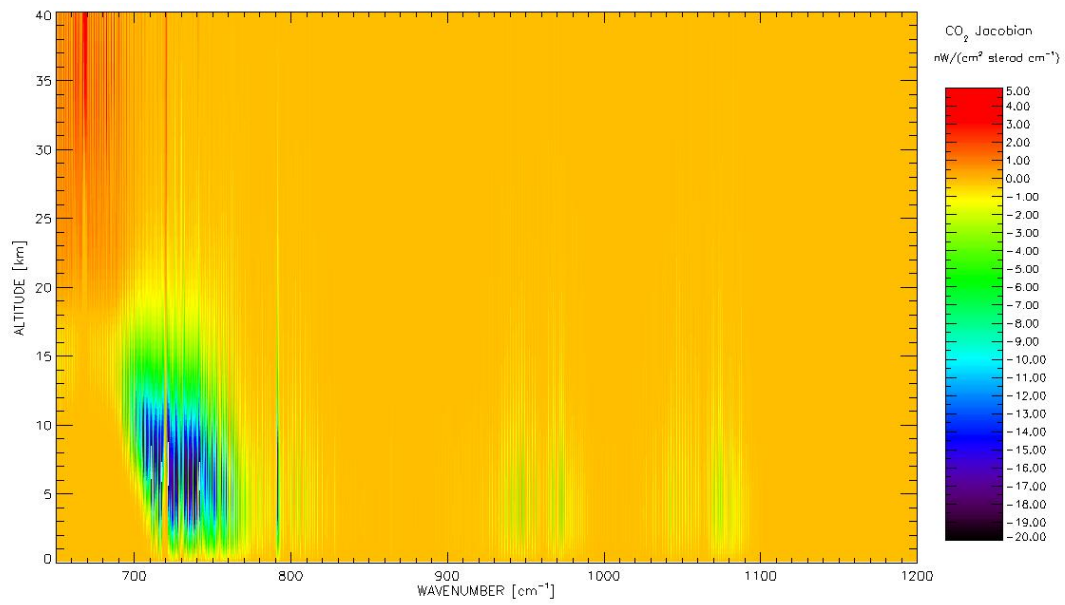


Fig. 83: CO₂ Jacobian in the spectral range [650-2700] cm⁻¹

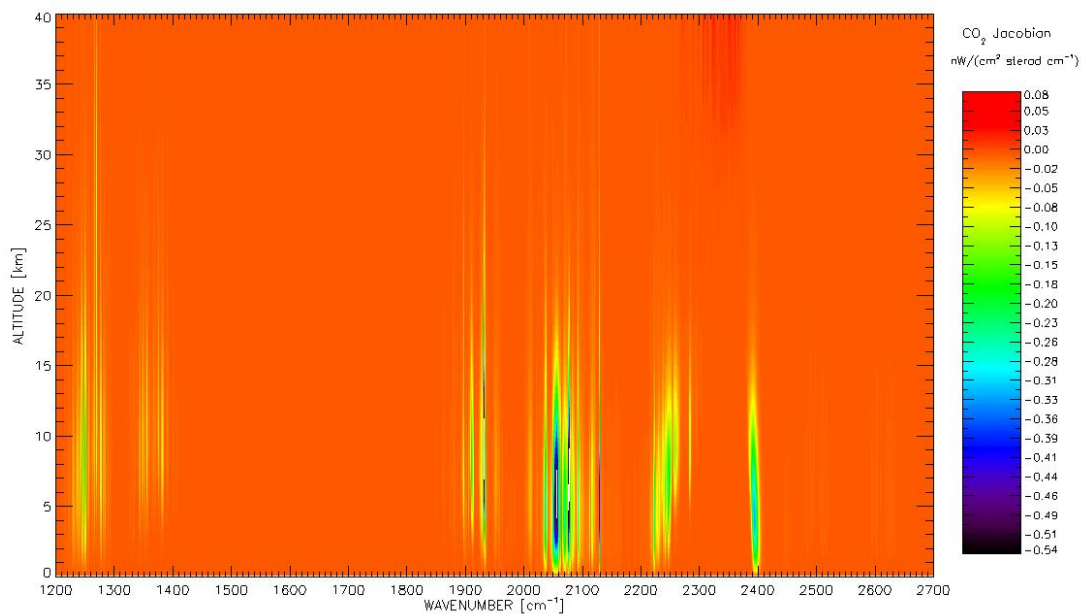


Fig. 84: CO₂ Jacobian in the spectral range [1200-2700] cm⁻¹

D Comparison between KLIMA and TANSO-FTS/GOSAT V1

With the purpose of performing an inter-comparison of the XCO₂ retrieved from KLIMA-IASI and TANSO-FTS L2 SWIR in the selected annual range of time (March 1, 2010 to February 28, 2011), we downloaded from the GUIG the following data products:

- FTS SWIR L2 XCO₂ Column amount V1.20
- FTS SWIR L2 XCO₂ Column amount V1.30
- FTS SWIR L2 XCO₂ Column amount V1.40

Our analysis and comparison was performed using the latest version of FTS SWIR data. After the first results of the validation team, a new version of FTS SWIR data (V2) was released, a few months before the end of the project, which have much better quality compared to the initial V1 data set. So it was decided to download also the latest version and repeat our analysis with the new data set:

- FTS SWIR L2 V2.00 (March 2010 - August 2010)
- FTS SWIR L2 V2.10 (September 2010 - December 2010)
- FTS SWIR L2 V2.11 (January 2011 - February 2011)

The different versions of the L2 products correspond to different versions of the input TANSO-FTS L1B product (measured spectrum) [59]. The TANSO-FTS XCO₂ values were compared with the XCO₂ retrieved with the KLIMA-IASI code from IASI L1C. The comparison between TANSO-FTS and KLIMA was performed using the TANSO-FTS L2 data and the KLIMA L2 retrieved values obtained from the bulk processing of one week per month in the annual range of time selected for a global geographical coverage. For each month a complete week has been processed, in order to retrieve the XCO₂ both on land and on water and both during day and night. For each week the number of IASI analysed observations has been fixed to 20000. On the water, due to the moderate CO₂ variability, a very reduced azimuth coverage has been taken into account (only the central pixel of the IASI scan), while on land a week-dependent number of pixels has been imposed, in order to reach the fixed total amount of 20000 analysis per month.

In the following figures we report the comparison of the two datasets, as a scatter diagram of mean XCO₂ values, obtained for the global geographical coverage over a grid of 2° x 2°. The points with the ratio between the standard deviation of the retrieved values and their mean retrieval error larger than 2 are not included in order to skip in the comparison the pixels where a geographical and/or a time variability was observed. Fig. 85 reports, a scatter plot for each month, the correlation of KLIMA L2 XCO₂ versus the XCO₂ of TANSO-FTS L2 SWIR V1 (green dots), the TANSO-FTS L2 adjusted for the KLIMA a priori (blue dots) and the TANSO-FTS L2 smoothed for KLIMA AKs; similarly Fig. 86 shows the scatter plot of KLIMA L2 versus TANSO-FTS (red dots), the TANSO-FTS L2 adjusted for the KLIMA a priori (green dots) and the scatter plot of KLIMA versus TANSO-FTS L2 smoothed (blue dots).

In general, when smoothed values are used the cloud of points of the scatter plot is better centered relative to 45° line, but the tendency to obtain from KLIMA smaller XCO₂ columns and a much broader spread of values is observed also in this comparison.

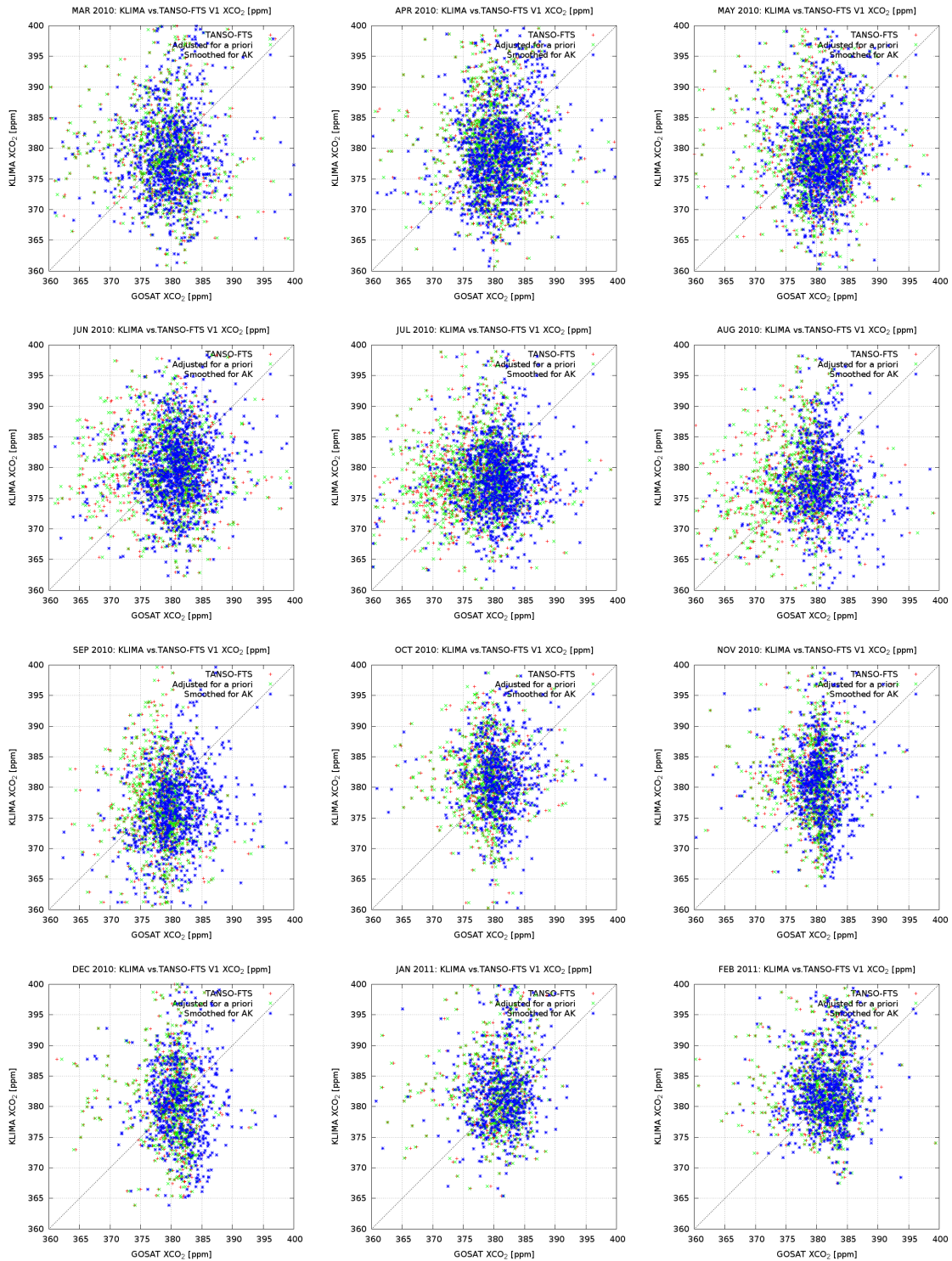


Fig. 85: Scatter diagrams of KLIMA L2 - TANSO-FTS V1 comparison for each month. Green points are TANSO-FTS SWIR XCO₂ V1, blue points are TANSO-FTS SWIR adjusted for KLIMA a priori, purple points are TANSO-FTS SWIR smoothed with KLIMA AKs

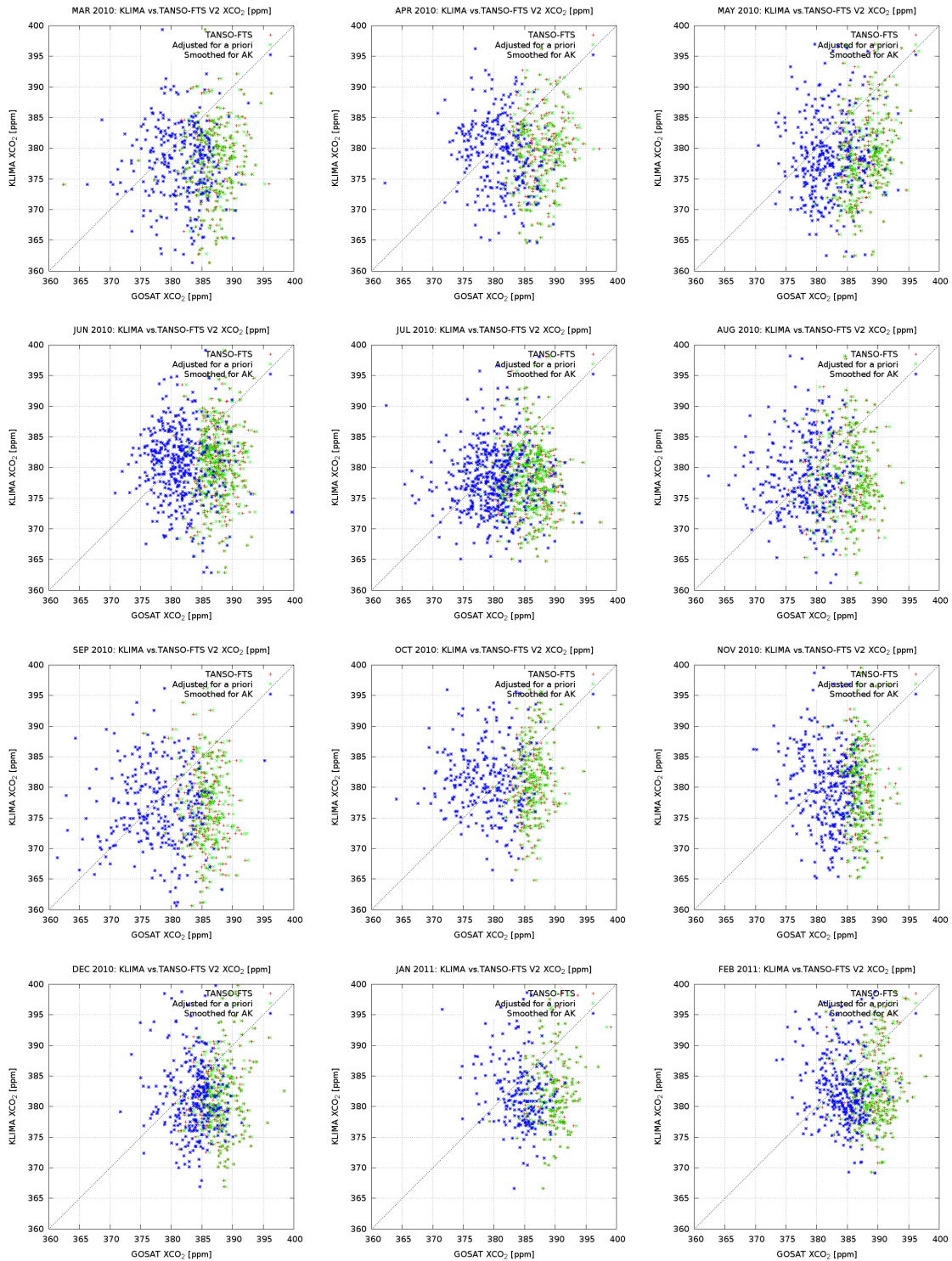


Fig. 86: Scatter diagrams of KLIMA L2 - TANSO-FTS V2 comparison on a $2^\circ \times 2^\circ$ pixel grid for each month. Red crosses represent the TANSO-FTS SWIR XCO₂ V2, green marks are TANSO-FTS SWIR adjusted for KLIMA a priori while blue marks are TANSO-FTS SWIR smoothed with KLIMA AKs

E INPUT and OUTPUT file templates**Input data file of the pre-processor**

```
#####
# File with data related to KLIMA PREPRO_2.0 settings parameters
#
# Note:
# - lines beginning with '#' (comments) and blank lines are not used;
# - each control is specified by a keyword (in square brackets);
# - the first line of each control is a logical flag
# used to enable (T) or disable (F) the control itself.
# When the control is disabled (F) NO check is performed
# (all data are extracted)
#
#####
#
# 1. Selection by index
# [SELECTION_BY_INDEXES]
# F
# 12, 59
# -----
#
# 2. Geographical selection
# [GEOGRAPHICAL_SELECTION]
# T
# Upper right LATITUDE, LONGITUDE
# Lower left LATITUDE, LONGITUDE
# 90, 180
# -90, -180
# -----
#
# 3. Nadir pointing selection
# [ZENITH_POINTING_LIMIT]
# F
# 180
# -----
#
# 4. Observation index range
# [IFOV_INDEX_RANGE]
# T
```

Fig. 87: Template of input data file of the pre-processor

```

55, 76
#-----
#
# 5. Quality of MDR (instrument)
# Quality of MDR has been degraded from nominal due to an
# instrument degradation
#
# when the control is ENABLED (T):
# 0 -> extracts only data having DEGRADED_INST_MDR=0
# 1 -> extracts only data having DEGRADED_INST_MDR=1
#
# when the control is DISABLED (F):
# NO check is performed (all data are extracted)
# [DEGRADED_INST_MDR]
# F
# 0
#-----
#
# 6. Quality of MDR (processing)
# Quality of MDR has been degraded from nominal due to an
# processing degradation
#
# when the control is ENABLED (T):
# 0 -> extracts only data having DEGRADED_PROC_MDR=0
# 1 -> extracts only data having DEGRADED_PROC_MDR=1
#
# when the control is DISABLED (F):
# NO check is performed (all data are extracted)
# [DEGRADED_PROC_MDR]
# F
# 0
#-----
#
# 7. Selection by surface type
# The flag FLG_LANSEA specifies the surface type
#
# 0 -> The IASI IF0V is completely covered by water;
# 1 -> The IASI IF0V is completely covered by land,
# the variability of the surface topography is low;
# 2 -> The IASI IF0V is completely covered by land,

```

Fig. 88: Template of input data file of the pre-processor

```

# the variability of the surface topography is high
# 3 -> The IASI IF0V covers land and water,
# the variability of the surface topography is low
# 4 -> The IASI IF0V covers land and water,
# the variability of the surface topography is high
[FLG_LANSEA]
T
1
#-----

# 8. Selection by day and night
# The flag FLG_DAYNIT is used to discriminate between day and night
#
# 0 -> Day
# 1 -> Night
# 2 -> Twilight
[FLG_DAYNIT]
F
1
#-----

# 9. Selection by clear/cloudy atmosphere
# The flag FLG_IASICLR is used to discriminate clear, partly cloudy or cloudy sky
#
# 0 -> The IASI IF0V is clear
# 1 -> The IASI IF0V is partly cloudy
# 2 -> The IASI IF0V is completely cloudy
[FLG_IASICLR]
T
0
#-----

# 10. Selection by IASI L2 Iterative retrieval convergence
# The flag FLG_ITCONV indicates the convergence of the L2 iterative retrieval
# 0 -> The iteration did not converge, sounding rejected
# 1 -> Iteration did not converge, sounding accepted
# 2 -> Iteration converged, sounding accepted
[FLG_ITCONV]
T
2

```

Fig. 89: Template of input data file of the pre-processor

```

#-----
# 11. Selection by validation L1 product
# The FLAG_IASIBAD flag is used to validate the L1 product
# 0 -> No Problems reported
# >0 -> Some problems are reported
# see the Level 2 Product Guide for more details
[FLAG_IASIBAD]
T
0
#-----

# 12. Product Flags provided by iasi L2
# when the control is ENABLED (T):
# F -> extracts only data with no problems reported
# T -> extracts only data that have been flagged out of range
# when the control is DISABLED (F):
# NO check is performed (all data are extracted)
[IASIL2_CHECKPRODUCTSFLAGS]
T
#Tout h20out o30out co20out ch40out co0out n2o0out surfEout surfTout
F F F F F F
#-----

# 13. Flags on L2 products; flags generated after an internal check on L2 products
# when the control is ENABLED (T):
# F -> extracts only data with no problems reported
# T -> extracts only data that have been flagged out of range
# when the control is DISABLED (F):
# NO check is performed (all data are extracted)
[INTERNAL_L2_PRODUCTSFLAGS]
T
#surfEout surfTout profTout profWout
F F

```

Fig. 90: Template of input data file of the pre-processor

```
#-----  
  
# 14. GPOD Note: The last parameter, full path to the file containing the  
# L1_VCM data, is added at runtime. No need to insert or add it here.  
[L1_ERRORFILE]  
AUX/L1_ERROR/L1_VCM.dat  
  
# FINE  
[end_of_file]
```

Fig. 91: Template of input data file of the pre-processor

Input data file of the retrieval module

```

#####
# KEY-WORDS SYNTAX
#####
#####
##### - GENERAL DEFINITIONS
# Version of the settings file (CHARACTER)
# [version]
# 001
#-----
#####
##### - DEFINITION OF THE BANDS USED FOR THE IASI MEASUREMENT ANALYSIS
# Number of bands (INTEGER) [1,imaxband]
# [nband]
# 3
# A row for each band is provided.
# Each row contains a sequence of the following data:
# String specifying the band name (band_1, band_2, band_3, ... ) (CHARACTER)
# Frequency of the first point of the band (cm-1) (REAL)
# Frequency of the last point of the band (cm-1) (REAL)
# Flag applied to the band (LOGICAL)
# [band]
band_01 645.d0 800.d0 T
band_02 2000.d0 2380.d0 T
band_03 2400.d0 2500.d0 T
##### - RETRIEVED PROFILES
# For there parameters the IG is provided by files
# Retrieval of the Temperature (LOGICAL)
# T -> The Temperature is retrieved
# F -> The Temperature is not retrieved
# [ltempfit]
# T
# Retrieval of the VMR of chemical species (LOGICAL)
# T -> The VMR is retrieved
# F -> The VMR is not retrieved
# [lvmrfit]
# T

```

Fig. 92: Template of input data file of the retrieval module

```

# Number of gases whose VMR is retrieved (INTEGER) [1,imxgfit]
# Note that NfitVMR is only read if lvmrfit = T
[NfitVMR]
6

# VMR code of the chemical species to be retrieved (INTEGER)
# 1 -> h2o
# 2 -> co2
# 3 -> o3
# 4 -> n2o
# 5 -> co
# 6 -> ch4
# Note that NfitVMR is only read if lvmrfit = T
[codefitVMR]
1 2 3 4 5 6

#***** - RETRIEVED SCALAR QUANTITIES
# For there parameters the A-priori error is provided by this settings file

# Retrieval of the Surface Temperature (LOGICAL)
# T -> The Surface Temperature is retrieved
# F -> The Surface Temperature is not retrieved
[learthtemperaturefit]
T

# A-priori error of the Surface Temperature (REAL) [unit = K]
# Note that opt_eathtemperature is only read if learthtemperaturefit = T
[opt_eathtemperature]
5.0d0

# Retrieval of the Surface Emissivity (LOGICAL)
# T -> The Surface Emissivity is retrieved
# F -> The Surface Emissivity is not retrieved
[lemissivity]
T

# A-priori error of the Surface Emissivity (REAL)
# Note that opt_lemissivity is only read if lemmissivity = T
# One value for each degree of the fitted polynomial
#

```

Fig. 93: Template of input data file of the retrieval module


```

# [rMarquardtDumpingFactor]
3
#***** - CONVERGENCE CRITERIA
# Maximum number of allowed Gauss iterations (INTEGER)
# [iMaxIterG]
3
# Maximum number of allowed Marquardt iterations (INTEGER)
# [iMaxIterM]
1
# 1st Convergence Criterion (REAL) (LOGICAL)
# Two parameters are needed to define the Convergence Criterion:
# 1) Percent variation of the chisquare between two subsequent iterations
# 2) Flag for the convergence criterion
# [conv_criterion1]
3.d0 T
# 2nd Convergence Criterion (REAL) (LOGICAL)
# Two parameters are needed to define the Convergence Criterion:
# 1) Maximum percent correction to state vector
# 2) Flag for the convergence criterion
# [conv_criterion2]
5 F
# 3th Convergence Criterion (REAL) (LOGICAL)
# Two parameters are needed to define the Convergence Criterion:
# 1) Maximum percent correction to state vector modified
# 2) Flag for the convergence criterion
# [conv_criterion3]
5 F
# 4th Convergence Criterion (REAL) (LOGICAL)
# Two parameters are needed to define the Convergence Criterion:
# 1) Percent variation between chisquare and linear chisquare
# 2) Flag for the convergence criterion
# [conv_criterion4]

```

Fig. 96: Template of input data file of the retrieval module

```

3.d0 T
# 5th Convergence Criterion (REAL) (LOGICAL)
# Two parameters are needed to define the Convergence Criterion:
# 1) Threshold on marquadt parameter
# 2) Flag for the convergence criterium
#
[conv_criterion5]
0.001 F
# Switch for the convergence criteria (INTEGER)
# 1 = "OR"
# 2 = "AND"
#
[OR_AND]
0
#***** - DEFINITION OF THE PATH OF THE FILES USED FOR THE IASI MEASUREMENT ANALYSIS
# Path of the directory contained (CHARACTER):
# 1) SPECTROSCOPIC FILES
# 2) ATMOSPHERIC CLIMATOLOGICAL FILES
# 3) ERROR SPECTRA FILES
# 4) CO2 LINE-MIXING
# 5) ISFR
# 6) SOLAR SPECTRUM
# 7) CLOUDS REFRACTIVE INDEX
#
[path]
../AUX/HITRAN_2008/
../AUX/IG2_V4.1/
../AUX/ERROR SPECTRA/
../AUX/CO2 LINE_MIXING/
../AUX/ISRF/
../AUX/SUN/
[End_of_File]

```

Fig. 97: Template of input data file of the retrieval module


```

[LONGITUDE]
# Location of the pixel centre in geodetic coordinate (deg)
55.81
#
[LATITUDE]
# Location of the pixel centre in geodetic coordinate (deg)
38.54
#
[EARTH_SATELLITE_DISTANCE]
# distance of satellite from Earth centre (m)
7194594.
#
[NADIR_OBSERVATION]
# nadir pointing angle or measurement zenith measurement angle of the pixel (deg)
6.4000
#
[AZIMUTH_OBSERVATION]
# azimuth measurement angle of the pixel (deg)
262.3900
#
[SOLAR_ZENITH]
# Solar angle at the surface of the pixel (deg)
131.230000
#
[SOLAR_AZIMUTH]
# Solar azimuth at the surface of the pixel (deg)
287.880000
#
[DAY_NIGHT]
# discrimination between day and night (0->day 1->night 2->twilight)
1
#
[LAND_SEA]
# surface type (0->water
1->land_low_variability 2->land_high_variability,
3->land_water_low_variab 4->land_water_high_variab )
1
#####
[Temperature]
#
# data are arranged in column according to the following fields:
# - l_f -> logical flag: 1 indicates a fitted parameter
# - p_mbar -> value of pressure [mbar]
# - H_Km -> Altitude [Km]
# - l_guess_K -> initial guess value [K]
# - Temp_K -> retrieved values [K]
#

```

Fig. 99: Template of temperature.dat file

```

# - U_err_K -> UnBiased error [K]
# - B_err_K -> Biased Error [K]
# - ig_err_K -> A-priori error set for the temperature [K]
#
#l_f p_mBar H_Km iquess_K Temp_K U_err_K B_err_K ig_err_K
F 0.49500000E+02 0.82569E+02 0.18465E+03 0.19052E+03 0.00000E+00 0.00000E+00 0.49745E+01
F 0.50000000E+02 0.82511E+02 0.18465E+03 0.19052E+03 0.31508E+02 0.31508E+02 0.47474E+01
T 0.22300000E-01 0.73794E+02 0.19606E+03 0.19881E+03 0.45984E+02 0.45984E+02 0.42092E+01
T 0.92000000E-01 0.64745E+02 0.22938E+03 0.22938E+03 0.59258E+02 0.59258E+02 0.43958E+01
T 0.22200000E-01 0.58526E+02 0.24964E+03 0.24386E+03 0.75575E+02 0.46318E+01 0.60855E+01
T 0.44730000E+00 0.53393E+02 0.25693E+03 0.24910E+03 0.85292E+02 0.39496E+01 0.55352E+01
T 0.87220000E+00 0.48439E+02 0.25527E+03 0.25014E+03 0.77449E+02 0.32689E+01 0.53595E+01
T 0.16600000E+01 0.43650E+02 0.25303E+03 0.25139E+03 0.59795E+02 0.25148E+01 0.41197E+01
T 0.31095000E+01 0.38973E+02 0.23052E+03 0.25144E+03 0.47308E+02 0.22559E+01 0.42930E+01
T 0.56618000E+01 0.34590E+02 0.24176E+03 0.24290E+03 0.44827E+02 0.15377E+01 0.27492E+01
T 0.10370000E+02 0.30357E+02 0.23016E+03 0.23063E+03 0.51212E+02 0.13047E+01 0.24442E+01
T 0.17381700E+02 0.26889E+02 0.22420E+03 0.22434E+03 0.69998E+02 0.10835E+01 0.19094E+01
T 0.27260000E+02 0.23936E+02 0.22030E+03 0.22054E+03 0.11287E+03 0.97868E+00 0.18995E+01
T 0.40103000E+02 0.21440E+02 0.21792E+03 0.21832E+03 0.17610E+03 0.91031E+00 0.18808E+01
T 0.56730000E+02 0.19218E+02 0.21621E+03 0.21666E+03 0.25254E+03 0.91703E+00 0.19411E+01
T 0.77201300E+02 0.1752E+02 0.21648E+03 0.21693E+03 0.33058E+03 0.92625E+00 0.22247E+01
T 0.10205000E+03 0.15474E+02 0.21602E+03 0.21627E+03 0.38524E+03 0.85469E+00 0.19671E+01
T 0.13249240E+03 0.13819E+02 0.21543E+03 0.21519E+03 0.41773E+03 0.77439E+00 0.16780E+01
T 0.16795000E+03 0.12328E+02 0.21343E+03 0.21252E+03 0.44508E+03 0.79442E+00 0.17659E+01
T 0.20816010E+03 0.10995E+02 0.21149E+03 0.21032E+03 0.48797E+03 0.75686E+00 0.16377E+01
T 0.25371000E+03 0.97617E+01 0.21156E+03 0.21431E+03 0.53801E+03 0.72820E+00 0.14607E+01
T 0.30354890E+03 0.86110E+01 0.22315E+03 0.22293E+03 0.55031E+03 0.66981E+00 0.12357E+01
T 0.35828000E+03 0.75035E+01 0.23225E+03 0.23254E+03 0.54630E+03 0.59717E+00 0.10553E+01
T 0.41639660E+03 0.64585E+01 0.24095E+03 0.24148E+03 0.54375E+03 0.59075E+00 0.12719E+00
T 0.47854000E+03 0.54576E+01 0.24888E+03 0.24931E+03 0.49987E+03 0.57174E+00 0.92709E+00
T 0.54305300E+03 0.45216E+01 0.25540E+03 0.25567E+03 0.36851E+03 0.61533E+00 0.10245E+01
T 0.61060000E+03 0.36345E+01 0.26079E+03 0.26076E+03 0.20886E+03 0.64354E+00 0.11391E+01
T 0.69697020E+03 0.26129E+01 0.26664E+03 0.26639E+03 0.13310E+03 0.64759E+00 0.12831E+01
T 0.79218400E+03 0.16025E+01 0.27268E+03 0.27268E+03 0.73556E+02 0.68515E+00 0.16608E+01
T 0.8968640E+03 0.57852E+00 0.2721E+03 0.2723E+03 0.24185E+02 0.76788E+00 0.21624E+01
F 0.96600000E+03 0.00000E+00 0.27855E+03 0.27855E+03 0.00000E+00 0.00000E+00 0.27039E+03
#
[End_of_File]

```

Fig. 100: Template of temperature.dat file

[specie].dat

```
#####
# # KIMA LEVEL 2 #####
# # #####
# # #####
# # This file contains:
# # retrieved profile of co2 and related data
# #
# # File name : co2.dat
# # Kind of file: retrieval product
# #
# # This file has been created by : KLIMA-1.9
# # Date of creation (dd-mm-yyyy) : 28-03-2013
# # User
# # #####
# # [input key]
# # IASI_XX_IC_M02_20110213155659Z_20110213173859Z_N_0_20110213174109Z.nat|KprePro_2.0|./klima_settings.dat|001
# # [FLIGHT_DATE]
# # Date of the observation (gg-mm-aaaa) - orbit start date
# # 13.02.20
# # [NGEO]
# # Number of observations (IFOV) contained in this file
# # 1
# # #####
# # [IGEO]
# # line_number in L1 data file
# # 1
# # [SCAN]
# # index of the scan
# # 635
# # [OBSERVATION]
# # index of the observation [1,30]
# # 17
# # [IFOV]
# # index of the pixel [1,4]
# # 1
# #
```

Fig. 101: Template of *[specie].dat* file

```

[LONGITUDE]
# Location of the pixel centre in geodetic coordinate (deg)
55.81
#
[LATITUDE]
# Location of the pixel centre in geodetic coordinate (deg)
38.54
#
[EARTH_SATELLITE_DISTANCE]
# distance of satellite from Earth centre (m)
7194594.
#
[NADIR_OBSERVATION]
# nadir pointing angle or measurement zenith measurement angle of the pixel (deg)
6.4000
#
[AZIMUTH_OBSERVATION]
# azimuth measurement angle of the pixel (deg)
262.3900
#
[SOLAR_ZENITH]
# Solar angle at the surface of the pixel (deg)
131.230000
#
[SOLAR_AZIMUTH]
# Solar azimuth at the surface of the pixel (deg)
287.880000
#
[DAY_NIGHT]
# discrimination between day and night (0->day 1->night 2->twilight)
1
#
[LAND_SEA]
# surface type (0->water
1->land_low_variability 2->land_high_variability,
3->land_water_low_variab 4->land_water_high_variab )
1
#####
[co2]
#
# data are arranged in column according to the following fields:
# - l_f -> logical flag: 1 indicates a fitted parameter
# - p_mbar -> value of pressure [mbar]
# - H_Km -> Altitude [Km]
# - igruess_ppm -> initial guess value [ppm]
# - VMR_ppm -> retrieved values [ppm]

```

Fig. 102: Template of [specie].dat file

```

# - U_err_ppm -> UnBiased error [ppm]
# - B_err_ppm -> Biased Error [ppm]
# - Iq_err_ppm -> A-priori error set for the VMR [ppm]
# I f p mBar H Km iquess ppm VMR ppm U_err_ppm B_err_ppm Iq_err_ppm
F 0.49500000E-02 0.82569E+02 0.37080E+03 0.36107E+03 0.00000E+00 0.00000E+00 0.37080E+02
F 0.50000000E-02 0.82531E+02 0.37105E+03 0.36132E+03 0.00000E+00 0.00000E+00 0.37105E+02
F 0.22300000E-01 0.73794E+02 0.37922E+03 0.36927E+03 0.00000E+00 0.00000E+00 0.37922E+02
F 0.92000000E-01 0.64745E+02 0.37922E+03 0.36927E+03 0.00000E+00 0.00000E+00 0.37922E+02
F 0.22220000E+00 0.58526E+02 0.37922E+03 0.36927E+03 0.00000E+00 0.00000E+00 0.37922E+02
F 0.44730000E+00 0.53393E+02 0.37922E+03 0.36927E+03 0.00000E+00 0.00000E+00 0.37922E+02
F 0.87220000E+00 0.48439E+02 0.37922E+03 0.36927E+03 0.00000E+00 0.00000E+00 0.37922E+02
F 0.16600000E+01 0.43650E+02 0.37922E+03 0.36927E+03 0.00000E+00 0.00000E+00 0.37922E+02
F 0.31095000E+01 0.38973E+02 0.37922E+03 0.36927E+03 0.00000E+00 0.00000E+00 0.37922E+02
F 0.56618000E+01 0.34590E+02 0.37922E+03 0.36927E+03 0.00000E+00 0.00000E+00 0.37922E+02
F 0.10370000E+02 0.30357E+02 0.37922E+03 0.36927E+03 0.00000E+00 0.00000E+00 0.37922E+02
F 0.17381700E+02 0.26889E+02 0.37922E+03 0.36927E+03 0.00000E+00 0.00000E+00 0.37922E+02
F 0.27260000E+02 0.23936E+02 0.37957E+03 0.36961E+03 0.00000E+00 0.00000E+00 0.37957E+02
F 0.40103000E+02 0.21440E+02 0.38018E+03 0.37020E+03 0.00000E+00 0.00000E+00 0.38018E+02
F 0.56730000E+02 0.19218E+02 0.38104E+03 0.37105E+03 0.00000E+00 0.00000E+00 0.38104E+02
F 0.77201300E+02 0.17252E+02 0.38222E+03 0.37225E+03 0.00000E+00 0.00000E+00 0.38222E+02
F 0.10205000E+03 0.15474E+02 0.38373E+03 0.37368E+03 0.00000E+00 0.00000E+00 0.38373E+02
F 0.13249240E+03 0.13819E+02 0.38546E+03 0.37534E+03 0.00000E+00 0.00000E+00 0.38546E+02
F 0.16795000E+03 0.12328E+02 0.38673E+03 0.37659E+03 0.00000E+00 0.00000E+00 0.38673E+02
F 0.20816010E+03 0.10995E+02 0.38754E+03 0.37738E+03 0.00000E+00 0.00000E+00 0.38754E+02
T 0.25371000E+03 0.97617E+01 0.38799E+03 0.37781E+03 0.10331E+02 0.63380E+01 0.38799E+02
F 0.30354890E+03 0.86110E+01 0.38799E+03 0.37781E+03 0.00000E+00 0.00000E+00 0.38799E+02
F 0.35828000E+03 0.75035E+01 0.38799E+03 0.37781E+03 0.00000E+00 0.00000E+00 0.38799E+02
F 0.41639660E+03 0.64585E+01 0.38809E+03 0.37791E+03 0.00000E+00 0.00000E+00 0.38809E+02
F 0.47854000E+03 0.54576E+01 0.38844E+03 0.37825E+03 0.00000E+00 0.00000E+00 0.38844E+02
F 0.54305300E+03 0.45216E+01 0.38889E+03 0.37869E+03 0.00000E+00 0.00000E+00 0.38889E+02
F 0.61060000E+03 0.36345E+01 0.38944E+03 0.37923E+03 0.00000E+00 0.00000E+00 0.38944E+02
F 0.69697020E+03 0.26129E+01 0.39067E+03 0.38042E+03 0.00000E+00 0.00000E+00 0.39067E+02
F 0.79218400E+03 0.16025E+01 0.39195E+03 0.38167E+03 0.00000E+00 0.00000E+00 0.39195E+02
F 0.89968640E+03 0.57852E+00 0.39300E+03 0.38269E+03 0.00000E+00 0.00000E+00 0.39300E+02
F 0.96600000E+03 0.00000E+00 0.39355E+03 0.38319E+03 0.00000E+00 0.00000E+00 0.39355E+02
# AIR_column VMR_column VMR_column_err
# 0.20520E+26 0.77640E+22 0.13025E+21
# [End_of_File]

```

Fig. 103: Template of [specie].dat file

surface_temperature.dat

```
#####
# #
# # KIMA LEVEL 2 #
# # #####
# #
# # This file contains:
# # retrieved surface temperature and related data
# #
# # File name : surface_temperature.dat
# # Kind of file: retrieval product
# #
# # This file has been created by : KLIMA-1.9
# # Date of creation (dd-mm-yyyy) : 28-03-2013
# # User
# # #####
# # [input key]
# # IASI_XX_IC_M02_20110213155659Z_20110213173859Z_N_0_20110213174109Z_nat|KprePro_2.0|./klima_settings.dat|001
# # [FLIGHT_DATE]
# # Date of the observation (gg-mm-aaaa) - orbit start date
# # 13.02.20
# # [NGEO]
# # Number of observations (IFOV) contained in this file
# # 1
# # #####
# # [IGEO]
# # line_number in L1 data file
# # 1
# # [SCAN]
# # index of the scan
# # 635
# # [OBSERVATION]
# # index of the observation [1,30]
# # 17
# # [IFOV]
# # index of the pixel [1,4]
# # 1
# #
```

Fig. 104: Template of surface_temperature.dat file

```

[LONGITUDE]
# Location of the pixel centre in geodetic coordinate (deg)
# 55.81
[LATITUDE]
# Location of the pixel centre in geodetic coordinate (deg)
# 38.54
[EARTH_SATELLITE_DISTANCE]
# distance of satellite from Earth centre (m)
# 7194594.
[NADIR_OBSERVATION]
# nadir pointing angle or measurement zenith measurement angle of the pixel (deg)
# 6.4000
[AZIMUTH_OBSERVATION]
# azimuth measurement angle of the pixel (deg)
# 262.3900
[SOLAR_ZENITH]
# Solar angle at the surface of the pixel (deg)
# 131.230000
[SOLAR_AZIMUTH]
# Solar azimuth at the surface of the pixel (deg)
# 287.880000
[DAY_NIGHT]
# discrimination between day and night (0->day 1->night 2->twilight)
# 1
[LAND_SEA]
# surface type (0->water
# 1->land_low_variability 2->land_high_variability,
# 3->land_water_low_variab 4->land_water_high_variab )
# 1
#####
[Surface_Temperature]
#
# data are arranged in column according to the following fields:
# - iguess_K -> initial guess value for surface temperature [K]
# - Sur_T_K -> retrieved surface temperature [K]
# - U_err_K -> UnBiased error [K]
# - B_err_K -> Retrieval Biased Error [K]
# - Ig_err_K -> A-priori error of the surface temperature [K]

```

Fig. 105: Template of surface_temperature.dat file

surface_emissivity.dat

```
#####
# #
# # KIMA LEVEL 2
# #
#####
# #
# # This file contains:
# # retrieved surface emissivity and related data
# #
# # File name : surface_emissivity.dat
# # Kind of file: retrieval product
# #
# # This file has been created by : KLIMA-1.9
# # Date of creation (dd-mm-yyyy) : 28-03-2013
# # User
# #
#####
# #
# # [input key]
# # IASI_XX_IC_M02_20110213155659Z_20110213173859Z_N_0_20110213174109Z.nat|KprePro_2.0|./klima_settings.dat|001
# # [FLIGHT_DATE]
# # Date of the observation (gg-mm-aaaa) - orbit start date
# # 13.02.20
# #
# # [NGEO]
# # Number of observations (IFOV) contained in this file
# # 1
#####
# #
# # [IGEO]
# # line_number in L1 data file
# # 1
# # [SCAN]
# # index of the scan
# # 635
# #
# # [OBSERVATION]
# # index of the observation [1,30]
# # 17
# #
# # [IFOV]
# # index of the pixel [1,4]
# # 1
# #
```

Fig. 106: Template of surface_emissivity.dat file

```

[LONGITUDE]
# Location of the pixel centre in geodetic coordinate (deg)
# 55.81
[LATITUDE]
# Location of the pixel centre in geodetic coordinate (deg)
# 38.54
[EARTH_SATELLITE_DISTANCE]
# distance of satellite from Earth centre (m)
# 7194594.
[NADIR_OBSERVATION]
# nadir pointing angle or measurement zenith measurement angle of the pixel (deg)
# 6.4000
[AZIMUTH_OBSERVATION]
# azimuth measurement angle of the pixel (deg)
# 262.3900
[SOLAR_ZENITH]
# Solar angle at the surface of the pixel (deg)
# 131.230000
[SOLAR_AZIMUTH]
# Solar azimuth at the surface of the pixel (deg)
# 287.880000
[DAY_NIGHT]
# discrimination between day and night (0->day 1->night 2->twilight)
# 1
[LAND_SEA]
# surface type (0->water
# 1->land_low_variability 2->land_high_variability,
# 3->land_water_low_variab 4->land_water_high_variab )
# 1
#####
[Surface_Emissivity]
# data are arranged in column according to the following fields:
# - freq -> frequency [cm-1]
# - iguess -> initial guess value for emissivity
# - emissivity -> retrieved emissivity
# - U_err -> UnBiased error
# - B_err -> Retrieval Biased Error

```

Fig. 107: Template of surface_emissivity.dat file


```

793.750 0.975715 0.974840 0.260528E-01 0.424327E-02 0.100000E-01
794.000 0.975718 0.974843 0.260528E-01 0.424327E-02 0.100000E-01
794.250 0.975721 0.974846 0.260528E-01 0.424327E-02 0.100000E-01
794.500 0.975723 0.974849 0.260528E-01 0.424327E-02 0.100000E-01
794.750 0.975726 0.974852 0.260528E-01 0.424327E-02 0.100000E-01
795.000 0.975729 0.974854 0.260528E-01 0.424327E-02 0.100000E-01
795.250 0.975732 0.974857 0.260528E-01 0.424327E-02 0.100000E-01
795.500 0.975735 0.974860 0.260528E-01 0.424327E-02 0.100000E-01
795.750 0.975737 0.974863 0.260528E-01 0.424327E-02 0.100000E-01
796.000 0.975740 0.974866 0.260528E-01 0.424327E-02 0.100000E-01
796.250 0.975743 0.974868 0.260528E-01 0.424327E-02 0.100000E-01
796.500 0.975746 0.974871 0.260528E-01 0.424327E-02 0.100000E-01
796.750 0.975749 0.974874 0.260528E-01 0.424327E-02 0.100000E-01
797.000 0.975751 0.974877 0.260528E-01 0.424327E-02 0.100000E-01
797.250 0.975754 0.974879 0.260528E-01 0.424327E-02 0.100000E-01
797.500 0.975757 0.974882 0.260528E-01 0.424327E-02 0.100000E-01
797.750 0.975760 0.974885 0.260528E-01 0.424327E-02 0.100000E-01
798.000 0.975762 0.974888 0.260528E-01 0.424327E-02 0.100000E-01
798.250 0.975765 0.974891 0.260528E-01 0.424327E-02 0.100000E-01
798.500 0.975768 0.974893 0.260528E-01 0.424327E-02 0.100000E-01
798.750 0.975771 0.974896 0.260528E-01 0.424327E-02 0.100000E-01
799.000 0.975774 0.974899 0.260528E-01 0.424327E-02 0.100000E-01
799.250 0.975776 0.974902 0.260528E-01 0.424327E-02 0.100000E-01
799.500 0.975779 0.974905 0.260528E-01 0.424327E-02 0.100000E-01
799.750 0.975782 0.974907 0.260528E-01 0.424327E-02 0.100000E-01
800.000 0.975785 0.974910 0.260528E-01 0.424327E-02 0.100000E-01
# [End_of_File]

```

Fig. 109: Template of surface_emissivity.dat file

iterationdetails.dat

```
#####
# #
# # KIMA LEVEL 2
# #
#####
# #
# # This file contains:
# # details about iterations and related data
# #
# # File name : iterationdetails.dat
# # Kind of file: retrieval auxiliary information
# #
# # This file has been created by : KLIMA-1.9
# # Date of creation (dd-mm-yyyy) : 28-03-2013
# # User
# #
#####
# #
# # [input_key]
# # IASI_XX_IC_M02_20110213155659Z_20110213173859Z_N_0_20110213174109Z_nat|KprePro_2.0|./klima_settings.dat|001
# # [FLIGHT_DATE]
# # Date of the observation (gg-mm-aaaa) - orbit start date
# # 13.02.20
# #
# # [NGEO]
# # Number of observations (IFOV) contained in this file
# # 1
#####
# #
# # [IGEO]
# # line_number in L1 data file
# # 1
# # [SCAN]
# # index of the scan
# # 635
# #
# # [OBSERVATION]
# # index of the observation [1,30]
# # 17
# #
# # [IFOV]
# # index of the pixel [1,4]
# # 1
# #
```

Fig. 110: Template of iterationdetails.dat file

```

[LONGITUDE]
# location of the pixel centre in geodetic coordinate (deg)
55.81
#
[LATITUDE]
# location of the pixel centre in geodetic coordinate (deg)
38.54
#
[EARTH_SATELLITE_DISTANCE]
# distance of satellite from Earth centre (m)
7194594.
#
[NADIR_OBSERVATION]
# nadir pointing angle or measurement zenith measurement angle of the pixel (deg)
6.4000
#
[AZIMUTH_OBSERVATION]
# azimuth measurement angle of the pixel (deg)
262.3900
#
[SOLAR_ZENITH]
# Solar angle at the surface of the pixel (deg)
131.230000
#
[SOLAR_AZIMUTH]
# Solar azimuth at the surface of the pixel (deg)
287.880000
#
[DAY_NIGHT]
# discrimination between day and night (0->day 1->night 2->twilight)
1
#
[LAND_SEA]
# surface type (0->water
1->land_low_variability 2->land_high_variability,
3->land_water_low_variab 4->land_water_high_variab )
1
#####
#
[IN_TARGET]
7
#
[TARGET]
Temperature
h2o
co2

```

Fig. 111: Template of iterationdetails.dat file

```

o3
n2o
Surface_Temperature
Surface_Emissivity
#
[ITERATIONS]
#
# data are arranged in column according to the following fields:
# - iG -> index of Gauss iteration
# - iM -> index of Marquardt iteration
# - chisquare -> reduced chisquare
# - chisq_lin -> linear reduced chisquare
# - trace_lin -> trace of AK matrix
# - inf_cont -> information content from AK matrix
# - L_*. .... -> marquardt's lambda relating to retrieved parameters
#
# - start of iterations
# iG iM chisquare chisq_lin chisq_inc inf_cont L_n2o L_Surface_Temperature L_h2o
# L_co2 L_o3 L_n2o L_Surface_Temperature L_Surface_Emissivity
0 0 1.00000000 2.21071 0.00000 0.0000E+00 1.00000000 1.00000000 1.00000000 0.01000000
0 1 0 1.00000000 1.50201 1.40792 0.1683E+02 1.00000000 1.00000000 1.00000000 1.00000000
0 2 0 1.00000000 1.39926 1.36340 0.1690E+02 1.00000000 1.00000000 1.00000000 1.00000000
3 0 0.3333333 1.38478 1.36428 0.1692E+02 0.3333333 0.3333333 0.3333333 0.00333333
1 0 0.1111111 0.1111111 0.1111111 0.1111111 0.1111111 0.1111111 0.1111111 0.00111111
#
[LAST ITERATION]
# - end of iterations
#
# CONVERGENCE REACHED
# Convergence has been reached after GAUSS iteration: 3
#
[!convergence]
#
T
[!last_successfull_iteration]
3 0 1.38478 1.36428 0.1692E+02 55.83188 0.111111 0.111111 0.111111 0.00111111
1 0 0.111111 0.111111 0.111111 0.111111 0.111111 0.111111 0.111111 0.111111
#

```

Fig. 112: Template of iterationdetails.dat file

[End_of_File]

Fig. 113: Template of iterationdetails.dat file

spectrum.dat

```
#####
# #
# # KIMA LEVEL 2 #
# # #####
# #
# # This file contains:
# # observed, initial guess and retrieved spectrum and related data
# #
# # File name : spectrum.dat
# # Kind of file: retrieval auxiliary information
# # This file has been created by : KLIMA-1.9
# # Date of creation (dd-mm-yyyy) : 28-03-2013
# # User
# # #####
# # [input key]
# # IASI_XX_IC_M02_20110213155659Z_20110213173859Z_N_0_20110213174109Z.nat|KprePro_2.0|./klima_settings.dat|001
# # [FLIGHT_DATE]
# # Date of the observation (gg-mm-aaaa) - orbit start date
# # 13.02.20
# # [NGEO]
# # Number of observations (IFOV) contained in this file
# # 1
# # #####
# # [IGEO]
# # line_number in L1 data file
# # 1
# # [SCAN]
# # index of the scan
# # 635
# # [OBSERVATION]
# # index of the observation [1,30]
# # 17
# # [IFOV]
# # index of the pixel [1,4]
# # 1
# #
```

Fig. 114: Template of spectrum.dat file

```

[LONGITUDE]
# location of the pixel centre in geodetic coordinate (deg)
# 55.81
[LATITUDE]
# location of the pixel centre in geodetic coordinate (deg)
# 38.54
[EARTH_SATELLITE_DISTANCE]
# distance of satellite from Earth centre (m)
# 7194594.
[NADIR_OBSERVATION]
# nadir pointing angle or measurement zenith measurement angle of the pixel (deg)
# 6.4000
[AZIMUTH_OBSERVATION]
# azimuth measurement angle of the pixel (deg)
# 262.3900
[SOLAR_ZENITH]
# Solar angle at the surface of the pixel (deg)
# 131.230000
[SOLAR_AZIMUTH]
# Solar azimuth at the surface of the pixel (deg)
# 287.880000
[DAY_NIGHT]
# discrimination between day and night (0->day 1->night 2->twilight)
# 1
[LAND_SEA]
# surface type (0->water
# 1->land_low_variability 2->land_high_variability,
# 3->land_water_low_variab 4->land_water_high_variab )
# 1
#####
[SPECTRA]
# data are arranged in column according to the following fields:
# - pn -> progressive number
# - bn -> band index
# - freq -> frequency [cm-1]
# - observed -> observed spectrum [nW/cm2/sr/cm-1]

```

Fig. 115: Template of spectrum.dat file

```

# - iniguess -> spectrum computed using initial guess atmosphere [nW/cm2/sr/cm-1]
# - lastspect -> spectrum computed at the last succesful iteration [nW/cm2/sr/cm-1]
# - obs_err -> observed spectrum error (diagonal of the VCM of observations) [nW/cm2/sr/cm-1]
# - observed K -> observed spectrum [K]
# - iniguess K -> spectrum computed using initial guess atmosphere [K]
# - lastspect K -> spectrum computed at the last succesful iteration [K]
# - obs_err_K -> observed spectrum error (diagonal of the VCM of observations) [K]
#
# pn bn freq observed iniguess lastspect obs_err observed K iniguess K lastspect K obs_err_K
.217195E+03 0.2176077E+03 0.3251920E+00 0.4474000E+04 0.4567368E+04 0.4557231E+04 0.4816989E+02 0.2166842E+03 0
.2181358E+03 0.2180761E+03 0.3563614E+00 0.4509000E+04 0.4602860E+04 0.4597427E+04 0.5279583E+02 0.2170996E+03 0
.2202972E+03 0.2203544E+03 0.3566897E+00 0.4788000E+04 0.4799691E+04 0.4805027E+04 0.5285335E+02 0.2201717E+03 0
.2244264E+03 0.2244878E+03 0.3566981E+00 0.5250000E+04 0.5190648E+04 0.5196621E+04 0.5286347E+02 0.2250345E+03 0
.2244134E+03 0.2244533E+03 0.3567036E+00 0.5223000E+04 0.5186956E+04 0.5190839E+04 0.5287312E+02 0.2247832E+03 0
.2199299E+03 0.2199266E+03 0.3567087E+00 0.4796000E+04 0.4758398E+04 0.4757721E+04 0.5288269E+02 0.2203341E+03 0
.2175813E+03 0.2174669E+03 0.3567136E+00 0.4565000E+04 0.4540789E+04 0.4530445E+04 0.5289220E+02 0.2178485E+03 0
.2181203E+03 0.2179903E+03 0.3567184E+00 0.4612000E+04 0.4587343E+04 0.4575526E+04 0.5290168E+02 0.2183909E+03 0
.2218874E+03 0.2217463E+03 0.3567231E+00 0.4903000E+04 0.4934794E+04 0.4921438E+04 0.5291113E+02 0.2215511E+03 0
.2268629E+03 0.2266806E+03 0.3567278E+00 0.5300000E+04 0.5415924E+04 0.5397778E+04 0.5292054E+02 0.2266024E+03 0
.2266058E+03 0.2265221E+03 0.3567324E+00 0.5450000E+04 0.5387883E+04 0.5379575E+04 0.5292993E+02 0.2272289E+03 0
.2221596E+03 0.2221255E+03 0.3567371E+00 0.4987000E+04 0.4953406E+04 0.4950169E+04 0.5293930E+02 0.2225127E+03 0
.2194361E+03 0.2193514E+03 0.3567417E+00 0.4653000E+04 0.4696079E+04 0.4688270E+04 0.5294864E+02 0.2189679E+03 0
.2211118E+03 0.2210726E+03 0.3567463E+00 0.4806000E+04 0.4849655E+04 0.4845978E+04 0.5295796E+02 0.2206457E+03 0
.2283169E+03 0.2282922E+03 0.3567509E+00 0.5450000E+04 0.5549482E+04 0.5540626E+04 0.5296724E+02 0.2273274E+03 0
.2344266E+03 0.2341364E+03 0.3567535E+00 0.6070000E+04 0.6182514E+04 0.6151495E+04 0.5297620E+02 0.2333701E+03 0
.235547E+03 0.2332594E+03 0.3565721E+00 0.6021000E+04 0.6087071E+04 0.6055770E+04 0.5295783E+02 0.2329305E+03 0
.2284172E+03 0.2283426E+03 0.3558688E+00 0.5485000E+04 0.5552189E+04 0.5544646E+04 0.5283485E+02 0.2277504E+03 0
.2199299E+03 0.2199266E+03 0.3567087E+00 0.4796000E+04 0.4758398E+04 0.4757721E+04 0.5288269E+02 0.2203341E+03 0

```

Fig. 116: Template of spectrum.dat file

```

2 705249E+03 0.2703412E+03 0.1633177E+00
618 band_01_8 799.25000 0.9082000E+04
.2727215E+03 0.2725585E+03 0.1633389E+00
619 band_01_8 799.50000 0.9175000E+04
.2734298E+03 0.2732466E+03 0.1633702E+00
620 band_01_8 799.75000 0.9139000E+04
.2732062E+03 0.2730249E+03 0.1634003E+00
621 band_01_8 800.00000 0.9080000E+04
.2728104E+03 0.2726391E+03 0.1634534E+00
#
[End_of_File]
0.9104322E+04 0.9081042E+04 0.2478771E+02 0.2725652E+03 0
0.9202163E+04 0.9175846E+04 0.2479056E+02 0.2732407E+03 0
0.9166402E+04 0.9140425E+04 0.2479321E+02 0.2730150E+03 0
0.9106078E+04 0.9081612E+04 0.2479936E+02 0.2726278E+03 0

```

Fig. 117: Template of spectrum.dat file


```

[LONGITUDE]
# Location of the pixel centre in geodetic coordinate (deg)
# 55.81
[LATITUDE]
# Location of the pixel centre in geodetic coordinate (deg)
# 38.54
[EARTH_SATELLITE_DISTANCE]
# distance of satellite from Earth centre (m)
7194594.
[NADIR_OBSERVATION]
# nadir pointing angle or measurement zenith measurement angle of the pixel (deg)
# 6.4000
[AZIMUTH_OBSERVATION]
# azimuth measurement angle of the pixel (deg)
262.3900
[SOLAR_ZENITH]
# Solar angle at the surface of the pixel (deg)
131.230000
[SOLAR_AZIMUTH]
# Solar azimuth at the surface of the pixel (deg)
287.880000
[DAY_NIGHT]
# discrimination between day and night (0->day 1->night 2->twilight)
1
[LAND_SEA]
# surface type (0->water
# 1->land_low_variability 2->land_high_variability,
# 3->land_water_low_variab 4->land_water_high_variab )
1
#####
[SPECTRAL_POINT]
621
[RETRIVED_POINT]
29
# [Temperature_MSS_Data]
#

```

Fig. 119: Template of MSS_temperature.dat file

```

# data are arranged in column according to the following fields:
# - Obs -> Observed spectrum [nW/cm2/sr/cm-1]
# - Sim -> Simulated spectrum [nW/cm2/sr/cm-1]
# # - Sy^-1/2*Res -> VCM^-1/2 time the residual
# # - Sy^-1/2*Jac -> VCM^-1/2 time the Jacobian Matrix
# #
# Obs Sim Sy^-1/2*Res Sy^-1/2*Jac
4474.0000 4557.2309 -1.3978 -0.589477E-003 -0.146046E-003 0.271594E-002 0.578340E-002 0.643532E
-002 0.694265E-002 0.957615E-002 0.153596E-001 0.275867E-001 0.481982E-001 0.747955E-001 0.106
978 0.143558 0.183226 0.220117 0.248939 0.247668 0.206627 0
.146297 0.875935E-001 0.429993E-001 0.161368E-001 0.439969E-002 0.851905E-003 0.110265E-003
0.848525E-005 0.526151E-007 -0.414517E-007 -0.223656E-008 -0.109601E-002 -0.167543E-002 0.860344E
4509.0000 4597.4269 -1.0121 0.112056E-002 0.588689E-003 -0.180231E-001 0.120002E-001 0.659340E-002 0.508
-003 0.529405E-002 0.105928E-001 0.159153E-001 0.430310E-001 0.050122E-001 0.782523E-001 0.755154E-001 0
468E-002 0.937852E-002 0.227581E-001 0.1245136E-001 0.108916E-001 0.352570E-002 0.821461E-003 0.139384E-003
.613463E-001 0.425142E-001 0.202926E-005 0.124067E-006 0.472364E-008
0.191593E-004 4805.0273 -0.8932 -0.210648E-002 -0.102795E-002 0.103076E-002 0.172238E-002 0.993298E
4788.0000 4805.0273 -0.8932 -0.210648E-002 -0.102795E-002 0.204349E-001 0.412358E-001 0.769547E-001 0.124
-004 -0.175962E-002 0.160283E-003 0.798801E-002 0.216497 0.197911 0.146813 0.818157E-001 0
371 0.172107 0.207046 0.216497 0.199406E-002 0.977624E-003 -0.309348E-003 -0.730986E-004
.321825E-001 0.684706E-002 0.134549E-002 0.159406E-002 0.161618E-002 0.170613E-004 0.266753E-002 0.116726E
-0.146275E-004 -0.216536E-005 -0.165581E-006 -0.677573E-008
5250.0000 5196.6208 2.2415 0.773185E-002 0.347184E-002 0.170613E-004 0.266753E-002 0.116726E
-001 0.289265E-001 0.517127E-001 0.789196E-001 0.116544 0.141015 0.147683 0.136
229 0.110048 0.758072E-001 0.405542E-001 0.143746E-001 0.195040E-003 -0.422716E-002 -0
.292674E-002 -0.168014E-003 0.132618E-002 0.127110E-002 0.670380E-003 0.242537E-003 0.664552E-004
0.151138E-004 0.242841E-005 0.193632E-006 0.800750E-008
5223.0000 5190.8391 -1.1331 0.353423E-002 0.161618E-002 0.369064E-002 0.116348E-001 0.183652E
-001 0.296955E-001 0.507866E-001 0.849637E-001 0.136239 0.175859 0.170600E-001 0.529147E-002 0.185
265 0.165726 0.135009 0.849637E-001 0.907151E-001 0.466456E-001 0.170600E-001 0.529147E-002 0
.207142E-002 0.451474E-003 -0.592724E-003 -0.789849E-003 -0.497636E-003 -0.206310E-003 -0.628502E-004
-0.153493E-004 -0.256249E-005 -0.207832E-006 -0.861464E-008
4796.0000 4757.7214 1.6625 -0.191653E-002 0.176325E-003 0.475778E-002 0.669543E-002 0.360117E
-002 -0.843074E-003 -0.423926E-002 -0.477700E-002 0.770587E-003 0.152306E-001 0.381800E-001 0.747
304E-001 0.119640 0.159507 0.159507 0.177131 0.163174 0.117010 0.625168E-001 0
.246645E-001 0.692450E-002 0.148770E-002 0.538995E-003 0.349020E-003 0.172224E-003 0.587250E-004
0.151874E-004 0.259563E-005 0.211933E-006 0.876367E-008
4565.0000 4530.4450 -0.8098 0.971685E-003 -0.824370E-004 0.838237E-004 0.173388E-002 0.365869E
-002 0.557189E-002 0.764667E-002 0.113422E-001 0.191372E-001 0.305491E-001 0.438588E-001 0.548
238E-001 0.658929E-001 0.830666E-001 0.108310 0.139871 0.156919 0.140548 0
.100885 0.578616E-001 0.257151E-001 0.813402E-002 0.162137E-002 0.138044E-003 -0.259852E-004
4612.0000 4575.5258 -1.7647 -0.206188E-006 -0.850461E-008
-002 0.401948E-002 0.685367E-002 0.912533E-002 0.909745E-003 0.143914E-002 0.114320E-002 0.202094E
771E-001 0.500817E-001 0.893328E-001 0.130232 0.159627 0.159739 0.884757E-002 0.225
.869550E-001 0.487909E-001 0.222219E-001 0.776615E-002 0.204493E-002 0.433703E-003 0.829044E-004

```

Fig. 120: Template of MSS_temperature.dat file

```

8084.0000 8115.3670 -1.0891 -0.320554E-002 -0.320535E-002 -0.320279E-002 -0.319507E-002 -0.317723E
-002 -0.313523E-002 -0.303879E-002 -0.289282E-002 -0.278120E-002 -0.276865E-002 -0.282941E-002 -0.288
303E-002 -0.294186E-002 -0.300069E-002 -0.301468E-002 -0.302615E-002 -0.312876E-002 -0.333804E-002 -0
.376379E-002 -0.406135E-002 -0.422139E-002 0.106524E-001 0.554087E-001 0.148279 0.270626
0.448846 0.627613 0.726633 0.590630
8760.0000 8771.3349 -0.0669 -0.912804E-002 -0.912844E-002 -0.912922E-002 -0.912885E-002 -0.912539E
-002 -0.911435E-002 -0.908932E-002 -0.907841E-002 -0.914972E-002 -0.927951E-002 -0.938283E-002 -0.943
203E-002 -0.941945E-002 -0.935046E-002 -0.924751E-002 -0.912642E-002 -0.901616E-002 -0.893342E-002 -0
.893365E-002 -0.936649E-002 -0.112171E-001 -0.155350E-001 -0.203627E-001 -0.148150E-001 0.170429E-001
0.106126 0.300275 0.685356 1.02659
9082.0000 9081.0423 0.1998 -0.359188E-002 -0.359261E-002 -0.359027E-002 -0.357593E-002 -0.353331E
-002 -0.341675E-002 -0.315082E-002 -0.283371E-002 -0.283350E-002 -0.321148E-002 -0.364796E-002 -0.391
351E-002 -0.406506E-002 -0.409886E-002 -0.406832E-002 -0.402841E-002 -0.403122E-002 -0.407695E-002 -0
.411694E-002 -0.404368E-002 -0.349285E-002 -0.124206E-002 0.514105E-002 0.1173089E-001 0.348133E-001
0.638815E-001 0.140017 0.295123 0.515482
9175.0000 9175.8460 -0.1211 -0.817025E-003 -0.816483E-003 -0.814844E-003 -0.810486E-003 -0.794882E
-003 -0.746617E-003 -0.640817E-003 -0.529429E-003 -0.520482E-003 -0.570519E-003 -0.553904E-003 -0.448
106E-003 -0.302618E-003 -0.116932E-003 0.885183E-004 0.346484E-003 0.628141E-003 0.886394E-003 0
.116803E-002 -0.138955E-002 0.125460E-002 0.165378E-003 -0.233701E-002 -0.5182274E-002 -0.583374E-002
-0.177561E-002 0.147586E-001 0.706641E-001 0.191811
9139.0000 9140.4251 -0.0217 -0.160260E-002 -0.160477E-002 -0.160580E-002 -0.159766E-002 -0.157616E
-002 -0.152709E-002 -0.140935E-002 -0.126167E-002 -0.132771E-002 -0.171066E-002 -0.223990E-002 -0.272
046E-002 -0.312011E-002 -0.340964E-002 -0.364058E-002 -0.392887E-002 -0.428387E-002 -0.464409E-002 -0
.497894E-002 -0.508835E-002 -0.443084E-002 -0.294110E-002 0.317389E-002 0.114886E-001 0.222473E-001
0.418925E-001 0.795235E-001 0.163072 0.309470
9080.0000 9081.6116 -0.0650 -0.193274E-002 -0.193652E-002 -0.193844E-002 -0.192523E-002 -0.189157E
-002 -0.181778E-002 -0.164380E-002 -0.142533E-002 -0.152258E-002 -0.209438E-002 -0.289313E-002 -0.363
784E-002 -0.430439E-002 -0.485438E-002 -0.533633E-002 -0.592518E-002 -0.659931E-002 -0.723355E-002 -0
.781835E-002 -0.809597E-002 -0.736728E-002 -0.456409E-002 0.125403E-002 -0.104140E-001 0.228371E-001
0.457164E-001 0.891053E-001 0.162854 0.348173
[Temperature]
# # data are arranged in column according to the following fields:
# - p_mbar -> value of pressure [mbar]
# - H_Km -> Altitude [Km]
# - Temp_K -> retrieved values [K]
# #
#p_mBar H_Km Temp_K
0.500000E-02 82.5111 190.515
0.223000E-01 73.7935 198.809
0.920000E-01 64.7451 229.382
0.272200 58.5262 243.855
0.447300 53.3931 249.102
0.872200 48.4388 250.143
1.66000 43.6495 251.394
3.10950 38.9734 251.441

```

Fig. 121: Template of MSS_temperature.dat file

```

5.66180      242.896
10.3700     230.633
17.3817     224.338
27.2600     220.540
40.1030     218.319
56.7300     216.662
77.2013     216.935
102.050     216.270
132.492     215.191
167.950     212.523
208.160     210.322
253.710     214.307
303.549     8.6110
358.280     7.5035
416.397     6.4585
478.540     5.4576
543.053     4.5216
610.600     3.6345
696.970     2.6129
792.184     1.6025
896.686     0.5785

# [End_of_File]

```

Fig. 122: Template of MSS_temperature.dat file

MSS_[specie].dat

```
#####
# #
# # KIMA LEVEL 2 #
# # #####
# #
# # This file contains:
# # co2 MSS data and related data
# #
# # File name : MSS_co2.dat
# # Kind of file: retrieval auxiliary information
# # This file has been created by : KLIMA-1.9
# # Date of creation (dd-mm-yyyy) : 28-03-2013
# # User
# # #####
# # [input key]
# # IASI_XX_IC_M02_20110213155659Z_20110213173859Z_N_0_20110213174109Z.nat |KprePro_2.0|. /klima_settings.dat|001
# # [FLIGHT_DATE]
# # Date of the observation (gg-mm-aaaa) - orbit start date
# # 13.02.20
# # [NGEO]
# # Number of observations (IFOV) contained in this file
# # 1
# # #####
# # [IGEO]
# # line_number in L1 data file
# # 1
# # [SCAN]
# # index of the scan
# # 635
# # [OBSERVATION]
# # index of the observation [1,30]
# # 17
# # [IFOV]
# # index of the pixel [1,4]
# # 1
# #
```

Fig. 123: Template of MSS_[specie].dat file

```

[LONGITUDE]
# Location of the pixel centre in geodetic coordinate (deg)
55.81
#
[LATITUDE]
# Location of the pixel centre in geodetic coordinate (deg)
38.54
#
[EARTH_SATELLITE_DISTANCE]
# distance of satellite from Earth centre (m)
7194594.
#
[NADIR_OBSERVATION]
# nadir pointing angle or measurement zenith measurement angle of the pixel (deg)
6.4000
#
[AZIMUTH_OBSERVATION]
# azimuth measurement angle of the pixel (deg)
262.3900
#
[SOLAR_ZENITH]
# Solar angle at the surface of the pixel (deg)
131.230000
#
[SOLAR_AZIMUTH]
# Solar azimuth at the surface of the pixel (deg)
287.880000
#
[DAY_NIGHT]
# discrimination between day and night (0->day 1->night 2->twilight)
1
#
[LAND_SEA]
# surface type (0->water
1->land_low_variability 2->land_high_variability,
3->land_water_low_variab 4->land_water_high_variab )
1
#####
[SPECTRAL_POINT]
621
#
[RETRIVED_POINT]
1
#
[co2_MSS_Data]
#

```

Fig. 124: Template of MSS_[specie].dat file

```

# data are arranged in column according to the following fields:
# - Obs      -> Observed spectrum [nW/cm2/sr/cm-1]
# - Sim      -> Simulated spectrum [nW/cm2/sr/cm-1]
# # - Sy^-1/2*Res  -> VCM^-1/2 time the residual
# # - Sy^-1/2*Jac  -> VCM^-1/2 time the Jacobian Matrix
# #
# Obs      Sim      Sy^-1/2*Res  Sy^-1/2*Jac
4474.0000  4557.2309  -1.3978     0.285196E-002
4509.0000  4597.4269  -1.0121     -0.846511E-003
4788.0000  4805.0273  -0.8932     0.930592E-002
5250.0000  5196.6208  2.2415     0.902150E-002
5223.0000  5190.8391  -1.1331     0.122936E-001
4796.0000  4757.7214  1.6625     0.454160E-002
4565.0000  4530.4450  -0.8098     0.203043E-002
4612.0000  4575.5258  1.7647     0.130400E-002
4903.0000  4921.4383  -1.1205     0.819837E-002
5390.0000  5397.7780  -0.5122     0.999581E-002
5450.0000  5379.5748  1.5392     0.126774E-001
4987.0000  4950.1689  0.9618     0.694149E-002
4653.0000  4688.2698  -1.7570     0.639667E-002
4806.0000  4845.9778  0.9500     0.536784E-002
5450.0000  5540.6257  -2.0072     0.109610E-001
6070.0000  6151.4951  -0.9979     0.140487E-001
6021.0000  6055.7697  0.2533     0.131054E-001
5485.0000  5544.6464  -0.7920     0.133330E-001
5044.0000  5110.4950  -1.3410     0.872172E-002
4871.0000  4913.5342  0.5155     0.900294E-002
4915.0000  4962.5337  -1.6608     0.719032E-002
5351.0000  5354.2780  0.7198     0.110300E-001
5492.0000  5483.2220  -0.0682     0.134933E-001
5092.0000  5085.9073  -0.3745     0.918415E-002
4766.0000  4729.2506  0.8862     0.714391E-002
4664.0000  4623.0296  0.2849     0.717370E-002
4795.0000  4747.1763  0.4607     0.621279E-002
5254.0000  5204.9201  1.0325     0.105344E-001
5452.0000  5437.5298  -0.1546     0.141421E-001
5073.0000  5090.4178  0.0202     0.846105E-002
4760.0000  4787.7673  -0.8988     0.877645E-002
4662.0000  4666.4279  0.4079     0.874830E-002
4734.0000  4729.1511  -0.1549     0.609248E-002
5165.0000  5175.4206  0.3469     0.106734E-001
5430.0000  5473.5325  -1.0446     0.149753E-001
5092.0000  5137.5475  -0.4371     0.918757E-002
4788.0000  4812.9837  -0.4616     0.864404E-002
4640.0000  4651.6700  0.2313     0.784474E-002
4680.0000  4682.6545  -0.6438     0.632166E-002

```

Fig. 125: Template of MSS_[specie].dat file

```

9163.0000 9132.0455 1.3558 -0.844988E-002
9190.0000 9200.0120 -0.0535 -0.171268E-002
9191.0000 9226.6565 -2.4199 -0.385308E-002
9198.0000 9198.1229 1.2155 0.367382E-003
9053.0000 9028.0045 -0.2472 -0.783589E-002
9049.0000 9011.7140 2.0396 -0.686021E-003
9181.0000 9179.8177 -0.0619 -0.354784E-002
9210.0000 9249.2608 -1.7437 0.961418E-003
9203.0000 9242.0855 -0.3942 -0.187803E-002
9191.0000 9227.7930 -1.3346 0.164029E-002
9134.0000 9155.7716 -0.3889 -0.731819E-002
8954.0000 8958.4672 -0.0113 -0.376910E-002
8415.0000 8409.0670 0.0643 -0.279442E-003
8343.0000 8328.3091 0.4765 0.299007E-003
8955.0000 8912.7472 0.3360 -0.124269E-002
9196.0000 9176.6778 1.1479 0.116945E-002
9152.0000 9153.6907 -0.7867 -0.553982E-002
9131.0000 9127.2793 0.1541 -0.800576E-002
9178.0000 9159.1087 0.6878 0.607336E-003
9149.0000 9131.3484 0.3783 -0.727665E-003
9157.0000 9146.5018 0.3038 -0.255715E-003
9122.0000 9122.8187 0.0194 0.283979E-004
8670.0000 8686.5485 -0.3701 -0.270014E-002
7934.0000 7965.7162 -0.8410 -0.761562E-002
8084.0000 8115.3670 -1.0891 -0.250627E-003
8760.0000 8771.3349 -0.0669 0.226606E-005
9082.0000 9081.0423 0.1998 -0.150238E-002
9175.0000 9175.8460 -0.1211 0.250346E-002
9139.0000 9140.4251 -0.0217 -0.690093E-002
9080.0000 9081.6116 -0.0650 -0.112071E-001
[co2]
# data are arranged in column according to the following fields:
# - p_mbar -> value of pressure [mbar]
# - H_Km -> Altitude [Km]
# - VMR_ppm -> retrieved values [ppm]
# - iguess_K -> initial guess value [K]
#p_mbar H_Km VMR_ppm
# 0.500000E-02 82.5111 377.812
#[End_of_File]

```

Fig. 126: Template of MSS_[specie].dat file

[specie]_column.dat

```
#####
# #
# # KIMA LEVEL 2 #
# # #####
# #
# # This file contains:
# # retrieved column profile of co2 and related data
# #
# # File name : co2_column.dat
# # Kind of file: retrieval auxiliary information
# # This file has been created by : KLIMA-1.9
# # Date of creation (dd-mm-yyyy) : 28-03-2013
# # User
# # #####
# # [input key]
# # IASI_XX_IC_M02_20110213155659Z_20110213173859Z_N_0_20110213174109Z_nat|KprePro_2.0|./klima_settings.dat|001
# # [FLIGHT_DATE]
# # Date of the observation (gg-mm-aaaa) - orbit start date
# # 13.02.20
# # [NGEO]
# # Number of observations (IFOV) contained in this file
# # 1
# # #####
# # [IGEO]
# # line_number in L1 data file
# # 1
# # [SCAN]
# # index of the scan
# # 635
# # [OBSERVATION]
# # index of the observation [1,30]
# # 17
# # [IFOV]
# # index of the pixel [1,4]
# # 1
# #
```

Fig. 127: Template of [specie]_column.dat file

```

[LONGITUDE]
# Location of the pixel centre in geodetic coordinate (deg)
55.81
#
[LATITUDE]
# Location of the pixel centre in geodetic coordinate (deg)
38.54
#
[EARTH_SATELLITE_DISTANCE]
# distance of satellite from Earth centre (m)
7194594.
#
[NADIR_OBSERVATION]
# nadir pointing angle or measurement zenith measurement angle of the pixel (deg)
6.4000
#
[AZIMUTH_OBSERVATION]
# azimuth measurement angle of the pixel (deg)
262.3900
#
[SOLAR_ZENITH]
# Solar angle at the surface of the pixel (deg)
131.230000
#
[SOLAR_AZIMUTH]
# Solar azimuth at the surface of the pixel (deg)
287.880000
#
[DAY_NIGHT]
# discrimination between day and night (0->day 1->night 2->twilight)
1
#
[LAND_SEA]
# surface type (0->water
1->land_low_variability 2->land_high_variability,
3->land_water_low_variab 4->land_water_high_variab )
1
#####
#
[N_LAYERS]
30
#
[co2_column]
# data are arranged in column according to the following fields:
# - H_Km

```

Fig. 128: Template of [specie].column.dat file

```

# - h_Km -> Lower Altitude [Km]
# - AIR_column -> air column [n°/cm²]
# - VMR_column -> column retrieved values [n°/cm²]
# - VCM -> Variance Covariance Matrix
#
# H_Km AIR_column VMR_column VCM
82.568 82.511 0.36848E+15 0.10755E+19 0.42471E+26 0.15044E+29 0.60261E+29 0.11370E+30 0.19689E+30 0.371
45E+30 0.68766E+30 0.12637E+31 0.22260E+31 0.41045E+31 0.60974E+31 0.85819E+31 0.11160E+32 0.14464E+32 0.1
7842E+32 0.21725E+32 0.26713E+32 0.31224E+32 0.35486E+32 0.40228E+32 0.44012E+32 0.48316E+32 0.51300E+32 0
.54875E+32 0.57015E+32 0.59762E+32 0.62644E+32 0.65644E+32 0.68648E+32 0.71832E+32 0.75230E+32
82.511 73.794 0.13760E+18 0.37574E+21 0.15044E+29 0.53287E+31 0.21345E+32 0.40274E+32 0.69741E+32 0.131
57E+33 0.24358E+33 0.44763E+33 0.78848E+33 0.14539E+34 0.21598E+34 0.30398E+34 0.39528E+34 0.51234E+34 0.6
3200E+34 0.76952E+34 0.94622E+34 0.11960E+35 0.12570E+35 0.14249E+35 0.15590E+35 0.17114E+35 0.18171E+35 0
.19437E+35 0.20196E+35 0.21168E+35 0.22120E+35 0.22983E+35 0.23945E+35 0.24980E+35
73.794 64.745 0.55121E+18 0.14927E+22 0.60261E+29 0.21345E+32 0.85503E+32 0.16133E+33 0.27937E+33 0.527
05E+33 0.97571E+33 0.17931E+34 0.31584E+34 0.58238E+34 0.86515E+34 0.12177E+35 0.15834E+35 0.20523E+35 0.2
5316E+35 0.30825E+35 0.37903E+35 0.44303E+35 0.50351E+35 0.57078E+35 0.62448E+35 0.68555E+35 0.72789E+35 0
.77861E+35 0.80898E+35 0.84795E+35 0.8864E+36 0.12011E+36 0.13597E+36 0.16133E+36 0.84039E+35
64.745 58.526 0.10400E+19 0.28164E+22 0.11370E+30 0.40274E+32 0.16133E+33 0.30439E+33 0.52711E+33 0.994
43E+33 0.18410E+34 0.33832E+34 0.59593E+34 0.10989E+35 0.16324E+35 0.22975E+35 0.29876E+35 0.38723E+35 0.4
7766E+35 0.58160E+35 0.71515E+35 0.83500E+35 0.95002E+35 0.10770E+36 0.11783E+36 0.12935E+36 0.13734E+36 0
.14691E+36 0.15264E+36 0.15999E+36 0.20497E+36 0.22661E+36 0.25655E+36 0.28577E+36 0.3184E+36 0.35184E+36 0.38493E+36 0.42258E+36 0.44868E+36 0
.47994E+36 0.49866E+36 0.52268E+36 0.66964E+36 0.74034E+36 0.83815E+36 0.9443E+36 0.99443E+36 0.10944E+36 0.11879E+36 0.12720E+36 0.1324
48.439 43.650 0.62900E+19 0.17034E+23 0.68766E+30 0.24358E+33 0.97571E+33 0.18410E+34 0.31879E+34 0.601
44E+34 0.11134E+35 0.20462E+35 0.36042E+35 0.66458E+35 0.98726E+35 0.13895E+36 0.18069E+36 0.23420E+36 0.2
8895E+36 0.35175E+36 0.43252E+36 0.50555E+36 0.57457E+36 0.65134E+36 0.71262E+36 0.78230E+36 0.83062E+36 0
.88850E+36 0.92316E+36 0.96762E+36 0.12397E+37 0.13706E+37 0.15516E+37 0.17931E+37 0.1931E+37 0.20988E+37 0.22876E+37 0.24888E+37 0.27129E+37 0.29683E+37 0.32323E+37 0.35175E+37 0.38288E+37 0.41644E+37 0.45396E+37 0.49443E+37 0.53944E+37 0.58238E+37 0.63238E+37 0.68458E+37 0.74303E+37 0.80898E+37 0.88166E+37 0.96458E+37 0.10599E+38 0.11720E+38 0.13062E+38 0.14644E+38 0.16515E+38 0.18644E+38 0.21062E+38 0.23944E+38 0.27238E+38 0.31062E+38 0.35396E+38 0.40396E+38 0.46458E+38 0.53896E+38 0.62396E+38 0.72396E+38 0.84396E+38 0.99443E+38 0.11879E+39 0.14303E+39 0.17205E+39 0.20720E+39 0.24944E+39 0.30062E+39 0.36396E+39 0.44396E+39 0.54396E+39 0.67396E+39 0.84396E+39 0.10662E+40 0.13596E+40 0.17396E+40 0.22396E+40 0.28896E+40 0.37396E+40 0.48896E+40 0.63896E+40 0.83896E+40 0.11062E+41 0.14896E+41 0.19896E+41 0.26896E+41 0.36396E+41 0.48896E+41 0.65396E+41 0.87396E+41 0.11596E+42 0.15896E+42 0.21896E+42 0.29896E+42 0.40396E+42 0.54396E+42 0.73396E+42 0.98396E+42 0.13196E+43 0.17896E+43 0.24396E+43 0.32896E+43 0.44396E+43 0.59396E+43 0.79396E+43 0.10596E+44 0.14396E+44 0.19396E+44 0.25896E+44 0.34896E+44 0.46896E+44 0.63396E+44 0.85396E+44 0.11396E+45 0.15396E+45 0.20396E+45 0.27396E+45 0.36396E+45 0.48396E+45 0.64396E+45 0.86396E+45 0.11496E+46 0.15496E+46 0.20496E+46 0.27496E+46 0.36496E+46 0.48496E+46 0.64496E+46 0.86496E+46 0.11496E+47 0.15496E+47 0.20496E+47 0.27496E+47 0.36496E+47 0.48496E+47 0.64496E+47 0.86496E+47 0.11496E+48 0.15496E+48 0.20496E+48 0.27496E+48 0.36496E+48 0.48496E+48 0.64496E+48 0.86496E+48 0.11496E+49 0.15496E+49 0.20496E+49 0.27496E+49 0.36496E+49 0.48496E+49 0.64496E+49 0.86496E+49 0.11496E+50 0.15496E+50 0.20496E+50 0.27496E+50 0.36496E+50 0.48496E+50 0.64496E+50 0.86496E+50 0.11496E+51 0.15496E+51 0.20496E+51 0.27496E+51 0.36496E+51 0.48496E+51 0.64496E+51 0.86496E+51 0.11496E+52 0.15496E+52 0.20496E+52 0.27496E+52 0.36496E+52 0.48496E+52 0.64496E+52 0.86496E+52 0.11496E+53 0.15496E+53 0.20496E+53 0.27496E+53 0.36496E+53 0.48496E+53 0.64496E+53 0.86496E+53 0.11496E+54 0.15496E+54 0.20496E+54 0.27496E+54 0.36496E+54 0.48496E+54 0.64496E+54 0.86496E+54 0.11496E+55 0.15496E+55 0.20496E+55 0.27496E+55 0.36496E+55 0.48496E+55 0.64496E+55 0.86496E+55 0.11496E+56 0.15496E+56 0.20496E+56 0.27496E+56 0.36496E+56 0.48496E+56 0.64496E+56 0.86496E+56 0.11496E+57 0.15496E+57 0.20496E+57 0.27496E+57 0.36496E+57 0.48496E+57 0.64496E+57 0.86496E+57 0.11496E+58 0.15496E+58 0.20496E+58 0.27496E+58 0.36496E+58 0.48496E+58 0.64496E+58 0.86496E+58 0.11496E+59 0.15496E+59 0.20496E+59 0.27496E+59 0.36496E+59 0.48496E+59 0.64496E+59 0.86496E+59 0.11496E+60 0.15496E+60 0.20496E+60 0.27496E+60 0.36496E+60 0.48496E+60 0.64496E+60 0.86496E+60 0.11496E+61 0.15496E+61 0.20496E+61 0.27496E+61 0.36496E+61 0.48496E+61 0.64496E+61 0.86496E+61 0.11496E+62 0.15496E+62 0.20496E+62 0.27496E+62 0.36496E+62 0.48496E+62 0.64496E+62 0.86496E+62 0.11496E+63 0.15496E+63 0.20496E+63 0.27496E+63 0.36496E+63 0.48496E+63 0.64496E+63 0.86496E+63 0.11496E+64 0.15496E+64 0.20496E+64 0.27496E+64 0.36496E+64 0.48496E+64 0.64496E+64 0.86496E+64 0.11496E+65 0.15496E+65 0.20496E+65 0.27496E+65 0.36496E+65 0.48496E+65 0.64496E+65 0.86496E+65 0.11496E+66 0.15496E+66 0.20496E+66 0.27496E+66 0.36496E+66 0.48496E+66 0.64496E+66 0.86496E+66 0.11496E+67 0.15496E+67 0.20496E+67 0.27496E+67 0.36496E+67 0.48496E+67 0.64496E+67 0.86496E+67 0.11496E+68 0.15496E+68 0.20496E+68 0.27496E+68 0.36496E+68 0.48496E+68 0.64496E+68 0.86496E+68 0.11496E+69 0.15496E+69 0.20496E+69 0.27496E+69 0.36496E+69 0.48496E+69 0.64496E+69 0.86496E+69 0.11496E+70 0.15496E+70 0.20496E+70 0.27496E+70 0.36496E+70 0.48496E+70 0.64496E+70 0.86496E+70 0.11496E+71 0.15496E+71 0.20496E+71 0.27496E+71 0.36496E+71 0.48496E+71 0.64496E+71 0.86496E+71 0.11496E+72 0.15496E+72 0.20496E+72 0.27496E+72 0.36496E+72 0.48496E+72 0.64496E+72 0.86496E+72 0.11496E+73 0.15496E+73 0.20496E+73 0.27496E+73 0.36496E+73 0.48496E+73 0.64496E+73 0.86496E+73 0.11496E+74 0.15496E+74 0.20496E+74 0.27496E+74 0.36496E+74 0.48496E+74 0.64496E+74 0.86496E+74 0.11496E+75 0.15496E+75 0.20496E+75 0.27496E+75 0.36496E+75 0.48496E+75 0.64496E+75 0.86496E+75 0.11496E+76 0.15496E+76 0.20496E+76 0.27496E+76 0.36496E+76 0.48496E+76 0.64496E+76 0.86496E+76 0.11496E+77 0.15496E+77 0.20496E+77 0.27496E+77 0.36496E+77 0.48496E+77 0.64496E+77 0.86496E+77 0.11496E+78 0.15496E+78 0.20496E+78 0.27496E+78 0.36496E+78 0.48496E+78 0.64496E+78 0.86496E+78 0.11496E+79 0.15496E+79 0.20496E+79 0.27496E+79 0.36496E+79 0.48496E+79 0.64496E+79 0.86496E+79 0.11496E+80 0.15496E+80 0.20496E+80 0.27496E+80 0.36496E+80 0.48496E+80 0.64496E+80 0.86496E+80 0.11496E+81 0.15496E+81 0.20496E+81 0.27496E+81 0.36496E+81 0.48496E+81 0.64496E+81 0.86496E+81 0.11496E+82 0.15496E+82 0.20496E+82 0.27496E+82 0.36496E+82 0.48496E+82 0.64496E+82 0.86496E+82 0.11496E+83 0.15496E+83 0.20496E+83 0.27496E+83 0.36496E+83 0.48496E+83 0.64496E+83 0.86496E+83 0.11496E+84 0.15496E+84 0.20496E+84 0.27496E+84 0.36496E+84 0.48496E+84 0.64496E+84 0.86496E+84 0.11496E+85 0.15496E+85 0.20496E+85 0.27496E+85 0.36496E+85 0.48496E+85 0.64496E+85 0.86496E+85 0.11496E+86 0.15496E+86 0.20496E+86 0.27496E+86 0.36496E+86 0.48496E+86 0.64496E+86 0.86496E+86 0.11496E+87 0.15496E+87 0.20496E+87 0.27496E+87 0.36496E+87 0.48496E+87 0.64496E+87 0.86496E+87 0.11496E+88 0.15496E+88 0.20496E+88 0.27496E+88 0.36496E+88 0.48496E+88 0.64496E+88 0.86496E+88 0.11496E+89 0.15496E+89 0.20496E+89 0.27496E+89 0.36496E+89 0.48496E+89 0.64496E+89 0.86496E+89 0.11496E+90 0.15496E+90 0.20496E+90 0.27496E+90 0.36496E+90 0.48496E+90 0.64496E+90 0.86496E+90 0.11496E+91 0.15496E+91 0.20496E+91 0.27496E+91 0.36496E+91 0.48496E+91 0.64496E+91 0.86496E+91 0.11496E+92 0.15496E+92 0.20496E+92 0.27496E+92 0.36496E+92 0.48496E+92 0.64496E+92 0.86496E+92 0.11496E+93 0.15496E+93 0.20496E+93 0.27496E+93 0.36496E+93 0.48496E+93 0.64496E+93 0.86496E+93 0.11496E+94 0.15496E+94 0.20496E+94 0.27496E+94 0.36496E+94 0.48496E+94 0.64496E+94 0.86496E+94 0.11496E+95 0.15496E+95 0.20496E+95 0.27496E+95 0.36496E+95 0.48496E+95 0.64496E+95 0.86496E+95 0.11496E+96 0.15496E+96 0.20496E+96 0.27496E+96 0.36496E+96 0.48496E+96 0.64496E+96 0.86496E+96 0.11496E+97 0.15496E+97 0.20496E+97 0.27496E+97 0.36496E+97 0.48496E+97 0.64496E+97 0.86496E+97 0.11496E+98 0.15496E+98 0.20496E+98 0.27496E+98 0.36496E+98 0.48496E+98 0.64496E+98 0.86496E+98 0.11496E+99 0.15496E+99 0.20496E+99 0.27496E+99 0.36496E+99 0.48496E+99 0.64496E+99 0.86496E+99 0.11496E+100 0.15496E+100 0.20496E+100 0.27496E+100 0.36496E+100 0.48496E+100 0.64496E+100 0.86496E+100 0.11496E+101 0.15496E+101 0.20496E+101 0.27496E+101 0.36496E+101 0.48496E+101 0.64496E+101 0.86496E+101 0.11496E+102 0.15496E+102 0.20496E+102 0.27496E+102 0.36496E+102 0.48496E+102 0.64496E+102 0.86496E+102 0.11496E+103 0.15496E+103 0.20496E+103 0.27496E+103 0.36496E+103 0.48496E+103 0.64496E+103 0.86496E+103 0.11496E+104 0.15496E+104 0.20496E+104 0.27496E+104 0.36496E+104 0.48496E+104 0.64496E+104 0.86496E+104 0.11496E+105 0.15496E+105 0.20496E+105 0.27496E+105 0.36496E+105 0.48496E+105 0.64496E+105 0.86496E+105 0.11496E+106 0.15496E+106 0.20496E+106 0.27496E+106 0.36496E+106 0.48496E+106 0.64496E+106 0.86496E+106 0.11496E+107 0.15496E+107 0.20496E+107 0.27496E+107 0.36496E+107 0.48496E+107 0.64496E+107 0.86496E+107 0.11496E+108 0.15496E+108 0.20496E+108 0.27496E+108 0.36496E+108 0.48496E+108 0.64496E+108 0.86496E+108 0.11496E+109 0.15496E+109 0.20496E+109 0.27496E+109 0.36496E+109 0.48496E+109 0.64496E+109 0.86496E+109 0.11496E+110 0.15496E+110 0.20496E+110 0.27496E+110 0.36496E+110 0.48496E+110 0.64496E+110 0.86496E+110 0.11496E+111 0.15496E+111 0.20496E+111 0.27496E+111 0.36496E+111 0.48496E+111 0.64496E+111 0.86496E+111 0.11496E+112 0.15496E+112 0.20496E+112 0.27496E+112 0.36496E+112 0.48496E+112 0.64496E+112 0.86496E+112 0.11496E+113 0.15496E+113 0.20496E+113 0.27496E+113 0.36496E+113 0.48496E+113 0.64496E+113 0.86496E+113 0.11496E+114 0.15496E+114 0.20496E+114 0.27496E+114 0.36496E+114 0.48496E+114 0.64496E+114 0.86496E+114 0.11496E+115 0.15496E+115 0.20496E+115 0.27496E+115 0.36496E+115 0.48496E+115 0.64496E+115 0.86496E+115 0.11496E+116 0.15496E+116 0.20496E+116 0.27496E+116 0.36496E+116 0.48496E+116 0.64496E+116 0.86496E+116 0.11496E+117 0.15496E+117 0.20496E+117 0.27496E+117 0.36496E+117 0.48496E+117 0.64496E+117 0.86496E+117 0.11496E+118 0.15496E+118 0.20496E+118 0.27496E+118 0.36496E+118 0.48496E+118 0.64496E+118 0.86496E+118 0.11496E+119 0.15496E+119 0.20496E+119 0.27496E+119 0.36496E+119 0.48496E+119 0.64496E+119 0.86496E+119 0.11496E+120 0.15496E+120 0.20496E+120 0.27496E+120 0.36496E+120 0.48496E+120 0.64496E+120 0.86496E+120 0.11496E+121 0.15496E+121 0.20496E+121 0.27496E+121 0.36496E+121 0.48496E+121 0.64496E+121 0.86496E+121 0.11496E+122 0.15496E+122 0.20496E+122 0.27496E+122 0.36496E+122 0.48496E+122 0.64496E+122 0.86496E+122 0.11496E+123 0.15496E+123 0.20496E+123 0.27496E+123 0.36496E+123 0.48496E+123 0.64496E+123 0.86496E+123 0.11496E+124 0.15496E+124 0.20496E+124 0.27496E+124 0.36496E+124 0.48496E+124 0.64496E+124 0.86496E+124 0.11496E+125 0.15496E+125 0.20496E+125 0.27496E+125 0.36496E+125 0.48496E+125 0.64496E+125 0.86496E+125 0.11496E+126 0.15496E+126 0.20496E+126 0.27496E+126 0.36496E+126 0.48496E+126 0.64496E+126 0.86496E+126 0.11496E+127 0.15496E+127 0.20496E+127 0.27496E+127 0.36496E+127 0.48496E+127 0.64496E+127 0.86496E+127 0.11496E+128 0.15496E+128 0.20496E+128 0.27496E+128 0.36496E+128 0.48496E+128 0.64496E+128 0.86496E+128 0.11496E+129 0.15496E+129 0.20496E+129 0.27496E+129 0.36496E+129 0.48496E+129 0.64496E+129 0.86496E+129 0.11496E+130 0.15496E+130 0.20496E+130 0.27496E+130 0.36496E+130 0.48496E+130 0.64496E+130 0.86496E+130 0.11496E+131 0.15496E+131 0.20496E+131 0.27496E+131 0.36496E+131 0.48496E+131 0.64496E+131 0.86496E+131 0.11496E+132 0.15496E+132 0.20496E+132 0.27496E+132 0.36496E+132 0.48496E+132 0.64496E+132 0.86496E+132 0.11496E+133 0.15496E+133 0.20496E+133 0.27496E+133 0.36496E+133 0.48496E+133 0.64496E+133 0.86496E+133 0.11496E+134 0.15496E+134 0.20496E+134 0.27496E+134 0.36496E+134 0.48496E
```

```

2. 98E+38 0.24715E+38 0.30390E+38 0.35521E+38 0.40370E+38 0.45764E+38 0.50069E+38 0.54965E+38 0.58360E+38
0.62427E+38 0.64862E+38 0.67986E+38 0.71010E+38 0.74298E+38 0.77791E+38 0.81633E+38 0.85933E+38 0.90798E+38
7.503 6.459 0.46924E+21 0.12418E+25 0.51300E+32 0.18171E+35 0.72789E+35 0.13734E+36 0.23782E+36 0.448
68E+36 0.83062E+36 0.15265E+37 0.26888E+37 0.49578E+37 0.73650E+37 0.10366E+38 0.13480E+38 0.17471E+38 0.2
1552E+38 0.26241E+38 0.32267E+38 0.37715E+38 0.42864E+38 0.48591E+38 0.53162E+38 0.58360E+38 0.61965E+38 0
.6283E+38 0.68868E+38 0.72186E+38 0.7481E+38 0.77025E+38 0.7876E+38 0.80255E+38 0.81937E+38 0.83633E+38
6.459 5.458 0.50194E+21 0.13276E+25 0.54875E+32 0.19437E+35 0.77861E+35 0.14691E+36 0.25440E+36 0.479
94E+36 0.88850E+36 0.16328E+37 0.28762E+37 0.53033E+37 0.78783E+37 0.11088E+38 0.14419E+38 0.18689E+38 0.2
3054E+38 0.28070E+38 0.34515E+38 0.40343E+38 0.45851E+38 0.51977E+38 0.56867E+38 0.62427E+38 0.66283E+38 0
.70902E+38 0.73668E+38 0.77216E+38 0.80926E+38 0.84833E+38 0.88937E+38 0.93233E+38 0.97823E+38 0.10270E+39
5.458 4.522 0.52152E+21 0.13780E+25 0.57015E+32 0.20196E+35 0.80898E+35 0.15264E+36 0.26432E+36 0.498
66E+36 0.92316E+36 0.16965E+37 0.29883E+37 0.55101E+37 0.81855E+37 0.11521E+38 0.14981E+38 0.19418E+38 0.2
3953E+38 0.29165E+38 0.35861E+38 0.41917E+38 0.47639E+38 0.54004E+38 0.59084E+38 0.64862E+38 0.68868E+38 0
.73668E+38 0.78541E+38 0.80220E+38 0.10278E+39 0.11364E+39 0.12865E+39 0.14937E+39 0.17951E+39 0.21691E+39
4.522 3.635 0.54664E+21 0.14425E+25 0.59762E+32 0.21168E+35 0.84793E+35 0.15999E+36 0.27705E+36 0.522
68E+36 0.96762E+36 0.17782E+37 0.31323E+37 0.57755E+37 0.85798E+37 0.12076E+38 0.15703E+38 0.20353E+38 0.2
5106E+38 0.30569E+38 0.37589E+38 0.43936E+38 0.49934E+38 0.56605E+38 0.61930E+38 0.67986E+38 0.72186E+38 0
.77216E+38 0.80228E+38 0.84092E+38 0.10774E+39 0.11911E+39 0.13485E+39 0.15264E+36 0.20497E+36 0.2669
3.635 2.613 0.70033E+21 0.18438E+25 0.76564E+32 0.27120E+35 0.10864E+36 0.20497E+36 0.35495E+36 0.669
64E+36 0.12397E+37 0.22782E+37 0.40129E+37 0.73994E+37 0.10902E+38 0.15471E+38 0.20118E+38 0.26075E+38 0.3
2165E+38 0.39164E+38 0.48157E+38 0.56288E+38 0.63973E+38 0.72521E+38 0.79343E+38 0.87101E+38 0.92481E+38 0
.98926E+38 0.10278E+39 0.10774E+39 0.13803E+39 0.15260E+39 0.17276E+39 0.19343E+39 0.21691E+39 0.24270E+39
2.613 1.603 0.77428E+21 0.20319E+25 0.84648E+32 0.29883E+35 0.12011E+36 0.22661E+36 0.39242E+36 0.740
34E+36 0.13706E+37 0.25187E+37 0.44366E+37 0.81807E+37 0.12153E+38 0.17104E+38 0.22242E+38 0.28829E+38 0.3
5562E+38 0.43300E+38 0.53242E+38 0.62232E+38 0.70728E+38 0.80178E+38 0.87720E+38 0.96298E+38 0.10225E+39 0
.10937E+39 0.11364E+39 0.11911E+39 0.15260E+39 0.16871E+39 0.19100E+39 0.11805E+39
1.603 0.579 0.87657E+21 0.22935E+25 0.95832E+32 0.33945E+35 0.13597E+36 0.25655E+36 0.44427E+36 0.838
15E+36 0.15516E+37 0.28515E+37 0.50228E+37 0.92614E+37 0.13758E+38 0.19364E+38 0.25181E+38 0.32637E+38 0.4
0260E+38 0.49020E+38 0.60276E+38 0.70453E+38 0.80072E+38 0.90770E+38 0.99309E+38 0.10902E+39 0.11575E+39 0
.12382E+39 0.12865E+39 0.13485E+39 0.17276E+39 0.19100E+39 0.21624E+39 0.13365E+39
0.579 0.000 0.54177E+21 0.14148E+25 0.59230E+32 0.20980E+35 0.84039E+35 0.15857E+36 0.27458E+36 0.518
03E+36 0.95901E+36 0.17624E+37 0.31044E+37 0.57241E+37 0.85034E+37 0.11968E+38 0.15563E+38 0.20172E+38 0.2
4883E+38 0.30297E+38 0.37254E+38 0.43544E+38 0.49489E+38 0.56101E+38 0.61379E+38 0.67381E+38 0.71543E+38 0
.76528E+38 0.79513E+38 0.83343E+38 0.10678E+39 0.11805E+39 0.13365E+39 0.82601E+38
# [End_of_File]

```

Fig. 130: Template of [specie].column.dat file

Acknowledgements

TCCON data were obtained from the TCCON Data Archive, operated by the California Institute of Technology, from the website at <http://tcccon.ipac.caltech.edu/>.

TANSO-FTS L2 data were obtained from the GOSAT User Interface Gateway GUIG, operated by the National Institute for Environmental Studies (NIES), from the website: <http://data.gosat.nies.go.jp/GosatUserInterfaceGateway/guig/GuigPage/open.do>.

IASI data are received through the EUMETSAT Unified Meteorological Archive and Retrieval Facility (UMARF). The UMARF archive can be accessed through a web interface at <http://archive.eumetsat.int/umarf>.

This work was performed under the project "Sensitivity Analysis and Application of KLIMA algorithms to GOSAT and OCO validation" (ESA-ESRIN contract N. 21612/08/I-OL).

The sensor IASI has been developed and built under the responsibility of the Centre National d'Etudes Spatiales (CNES, France). It is flown on-board the MetOp-A satellite as part of the EUMETSAT Polar System.

The authors wish to thank G-POD Team at ESA/ESRIN for their valuable effort and availability for the bulk processing of IASI data. The authors wish to thank the Japan Aerospace Exploration Agency (JAXA), the National Institute for Environmental Studies (NIES) and the Ministry of the Environment (MOE) for the important collaboration and information provided under the Greenhouse gases Observing SATellite (GOSAT) Project, which the project KLIMA is a part (PI: Ugo Cortesi).

Reference Documents

RD1:

ESA-ESRIN contract N. 21612/08/I-OL

RD2:

KLIMA-IASI Sensitivity Assessment Report

RD3:

Thomas Williams, Colin Kelley et al., Gnuplot 4.6: an interactive plotting program

RD4:

Guido van Rossum et al., The Python Language Reference, Python Software Foundation

RD5:

Travis E. Oliphant, Guide to NumPy, Trelgol Publishing, 2006

RD6:

John D. Hunter, Matplotlib: A 2D graphics environment, Computing In Science & Engineering

References

- [1] Bianchini, G.; Carli, B.; Cortesi, U.; Del Bianco, S.; Gai, M.; Palchetti, L.: Test of far-infrared atmospheric spectroscopy using wide-band balloon-borne measurements of the upwelling radiance J. Quant. Spectrosc. Radiat. Transf. 2008, 109, 6, 1030-1042.
- [2] Blumstein, D., Chalon, G., Carlier, T., Buil, C., Hebert, P., Maciaszek, T., Ponce, G., Phulpin, T., Tournier, B., Simeoni, D., Astruc, P., Clauss, A., Kayal, G., and Jegou, R.: IASI instrument: Technical overview and measured performances, in: Society of Photo-Optical Instrumentation Engineers (SPIE) Conference Series, 5543, 169-207, 2004.
- [3] Buchwitz, M., de Beek, R., Burrows, J. P., Bovensmann, H., Warneke, T., Notholt, J., Meirink, J.F., Goede, A. P. H., Bergamaschi, P., Korner, S., Heimann, M., and Schulz, A.: Atmospheric methane and carbon dioxide from SCIAMACHY satellite data: initial comparison with chemistry and transport models, Atmos. Chem. Phys., 5, 941962, 2005, 5 <http://www.atmos-chem-phys.net/5/941/2005/>.
- [4] Canadell J.G., LeQur C., Raupach M.R., Field C.B., Buitenhuis E.T., Ciais P., Conway T.J., Gillett N.P., Houghton R.A., Marland G.: Contributions to accelerating atmospheric CO₂ growth from economic activity, carbon intensity, and efficiency of natural sinks. Proc. Natl. Acad. Sci. U.S.A. 104, 1886618870, 2007.

- [5] Carli, B., Bazzini, G., Castelli, E., Cecchi-Pestellini, C., Del Bianco, S., Dinelli, B.M., Gai, M., Magnani, L., Ridolfi, M. and Santurri, L.: MARC: a code for the retrieval of atmospheric parameters from millimetre-wave limb measurements, *JQSRT* 105, 476-491 (2007).
- [6] Chédin, C., A., Scott, N. A., Crevoisier, C., and Armante, R.: First global measurement of mid-tropospheric CO₂ from NOAA polar satellites: the tropical zone, *J. Geophys. Res.*, 108, 4581, doi:10.1029/2003JD003439, 2003.
- [7] Chédin, A., Saunders, R., Hollingsworth, A., Scott, N. A., Matricardi, M., Etcheto, J., Clerbaux, C., Armante, R., and Crevoisier, C.: The feasibility of monitoring CO₂ from high-resolution infrared sounders, *J. Geophys. Res.*, 108(D2), 4064, doi:10.1029/2001JD001443, 2003.
- [8] Chédin A., Scott, N. A., Armante, R., Pierangelo, C., Crevoisier, C., Foss, O., and Ciais, P.: A quantitative link between CO₂ emissions from tropical vegetation fires and the daily tropospheric excess (DTE) of CO₂ seen by NOAA-10 (1987/1991), *J. Geophys. Res.*, 113, D05302, doi:10.1029/2007JD008576, 2008
- [9] Chevallier, F., Fisher, M., Peylin, P., Serrar, S., Bousquet, P., Breon, F.-M., Chédin, A., and Ciais, P.: Inferring CO₂ sources and sinks from satellite observations: method and application to TOVS data, *J. Geophys. Res.*, 110, D24309, doi:10.1029/2005JD006390, 2005.
- [10] Chevallier, F., Bron, F.-M., Rayner, P. J.: The contribution of the Orbiting Carbon Observatory to the estimation of CO₂ sources and sinks: Theoretical study in a variational data assimilation framework. *J. Geophys. Res.*, 112, D09307, doi:10.1029/2006JD007375, 2007.
- [11] Clerbaux, C., Boynard, A., Clarisse, L., George, M., Hadji-Lazaro, J., Herbin, H., Hurtmans, D., Pommier, M., Razavi, A., Turquety, S., Wespes, C., and Coheur, P.-F.: Monitoring of atmospheric composition using the thermal infrared IASI/ MetOp sounder, *Atmos. Chem. Phys.*, 9, 6041-6054. doi:10.5194/acp-9-6041-2009, 2009.
- [12] Clerbaux, C., Hadji-Lazaro, J., Turquety, S., George, M., Coheur, P. F., Hurtmans, D., Wespes, C., Herbin, H., Blumstein, D., Tournier, B., and Phulpin, T.: The IASI/MetOp I mission: First observations and highlights of its Potential Contribution to GMES, *COSPAR inf. Bul.*, vol. 2007, 1924, 2007.
- [13] Clerbaux, C., Boynard, A., Clarisse, L., George, M., Hadji-Lazaro, J., Herbin, H., Hurtmans, D., Pommier, M., Razavi, A., Turquety, S., Wespes, C., and Coheur, P.-F.: Monitoring of atmospheric composition using the thermal infrared IASI/MetOp sounder, *Atmos. Chem. Phys.*, 9, 6041-6054, doi:10.5194/acp-9-6041-2009, 2009.
- [14] Clough et al.: Line-by-Line Calculations of Atmospheric Fluxes and Cooling Rates. Application to Water Vapour. *J. Geo Research*, 97, No. D14, 15,761-15,785. 1992.
- [15] Cogan, A., Boesch, H., Parker, R., Feng, L., Palmer, P., Blavier, J., Deutscher, N. M., Macatangay, R., Notholt, J., Roehl, C. M., Warneke, T., Wunch, D.: Atmospheric carbon dioxide retrieved from the Greenhouse gases Observing SATellite (GOSAT): Comparison with ground-based TCCON observations and GEOS-Chem model calculations. *Journal of Geophysical Research D: Atmospheres*, 117 (21), D21301., 2012.
- [16] Cortesi, U., et al.: KLIMA-IASI Sensitivity Assessment Report, Final Report for Phase 1 of the project Sensitivity Analysis and Application of KLIMA algorithms to GOSAT and OCO validation ESA-ESRIN contract N. 21612/08/I-OL, 2009.
- [17] Cortesi U., et al.: Carbon dioxide retrieval from IASI measurements using the klima inversion algorithm. ESA Living Planet symposium, Bergen. 2010.
- [18] Coudert, L. H., Wagner, G., Birk, M., Baranov, Yu, I., Lafferty, W. J., and Flaud, J.-M. The H₂16O molecule: Line position and line intensity analyses up to the second triad, *J. Mol. Spectrosc.*, 251(12), doi:10.1016/j.jms.2008.03.021, 2008.
- [19] Crevoisier C., Chdin A., Scott N. A., Matsueda H., Machida T., and Armante R.: First year of upper tropospheric integrated content of CO₂ from IASI hyperspectral infrared observations, *Atmos. Chem. Phys.*, 9, 4797-4810, 2009.
- [20] Del Bianco, U. Cortesi, B. Carli.: Utilization of all spectral channels of IASI for the retrieval of the atmospheric state, ESA Living Planet symposium, Bergen. 2010.

- [21] Engelen, R. J., Serrar, S., and Chevallier, F.: Four-dimensional data assimilation of atmospheric CO₂ using AIRS observations, *J. Geophys. Res.*, 114, D03303, doi:10.1029/2008JD010739, 2009.
- [22] ESA-ESRIN contract N. 21612/08/I-OL.
- [23] Fiorenza C., Formisano, V.: A solar spectrum for PFS data analysis, *Planetary and Space Science* 53, 10091016, 2005.
- [24] Friedlingstein, P., Houghton, R.A., Marland, G., Hackler, J., Boden, T.A., Conway, T.J., Canadell, J.G., Raupach, M.R., Ciais, P., Le Qur, C.: Update on CO₂ emissions, *Nature Geoscience* 3, 811812, doi:10.1038/ngeo1022, Published online, 2010.
- [25] Geibel, M., Messerschmidt, J., Gerbig, C., Blumenstock, T., Chen, H., Hase, F., Kolle, O., Lavric, J. V., Notholt, J., Palm, M., Rettinger, M., Schmidt, M., Sussmann, R., Warneke, T., and Feist, D. G.: Calibration of column-averaged CH₄ over European TCCON FTS sites with airborne in-situ measurements, *Atmos. Chem. Phys.*, 12, 87638775, doi:10.5194/acp-12-8763-2012.
- [26] Gordon I.E., et al.: Current updates of the water-vapor line list in HITRAN: a new diet for air-broadened half-widths. *J. Quant. Spectrosc. Ra.* 108 (3):389-402, 2007.
- [27] Gurney, K. R., et al.: Towards robust regional estimates of CO₂ sources and sinks using atmospheric transport models, *Nature*, 415, 626630, 2002.
- [28] Houghton, R. A.: How well do we know the flux of CO₂ from land-use change? *Tellus, Series B: Chemical and Physical Meteorology*, 62, 337-351, 2010.
- [29] Hungershofer, K., Breon, F.-M., Peylin, P., Chevallier, F., Rayner, P., Klonecki, A., Houweling, S., and Marshall, J.: Evaluation of various observing systems for the global monitoring of CO₂ surface fluxes, *Atmos. Chem. Phys.*, 10, 1050310520, doi:10.5194/acp-10-10503-2010, 2010.
- [30] Kuze, A., Suto, H., Nakajima, M., and Hamazaki, T.: Thermal and near infrared sensor for carbon observation Fourier-transform spectrometer on the Greenhouse Gases Observing Satellite for greenhouse gases monitoring, *Appl. Optics*, 48, 67166733, 2009.
- [31] John D. Hunter, Matplotlib: A 2D graphics environment, *Computing In Science & Engineering*, 9(3), 90–95, 2007
- [32] IASI Level 2 Product Guide, EUM/OPS-EPS/MAN/04/0033 v2G, 19 July 2012
- [33] Imasu, R. et al.: Upper-atmospheric CO₂ concentration retrieved from thermal infrared spectra observed using GOSAT TANSO-FTS (TIR) sensor. *SPIE Vol. 7474 74740K-1*, 2009.
- [34] Ingmann, P.: A-SCOPE, Advanced Space Carbon and Climate Observation of Planet Earth, Report of Assessment, SP-1313/1, ESA Communication Product Office, Noordwijk, The Netherlands, 2009.
- [35] IPCC AR4 WG1, Solomon, S., Qin, D., Manning, M., Chen, Z., Marquis, M. Averyt, K.B., Tignor, M., and Miller, H.L.: ed. *Climate Change 2007: The Physical Science Basis, Contribution of Working Group I to the Fourth Assessment Report of the Intergovernmental Panel on Climate Change*, Cambridge University Press, 2007.
- [36] Canadell J.G., LeQuéré C., Raupach M.R., Field C.B., Buitenhuis E.T., Ciais P., Conway T.J., Gillett N.P., Houghton R.A., Marland G.: Contributions to accelerating atmospheric CO₂ growth from economic activity, carbon intensity, and efficiency of natural sinks. *Proc. Natl. Acad. Sci. U.S.A.* 104, 1886618870, 2007.
- [37] Masiello, G., Matricardi, M., and Serio, C.: The use of IASI data to identify systematic errors in the ECMWF forecasts of temperature in the upper stratosphere, *Atmos. Chem. Phys.*, 11, 1009-1021, doi:10.5194/acp-11-1009-2011, 2011
- [38] Messerschmidt, J., Geibel, M. C., Blumenstock, T., Chen, H., Deutscher, N. M., Engel, A., Feist, D. G., Gerbig, C., Gisi, M., Hase, F., Katrynski, K., Kolle, O., Lavri, J. V., Notholt, J., Palm, M., Ramonet, M., Rettinger, M., Schmidt, M., Sussmann, R., Toon, G. C., Truong, F., Warneke, T., Wennberg, P. O., Wunch, D., and Xueref-Remy, I.: Calibration of TCCON column-averaged CO₂: the first aircraft campaign over European TCCON sites, *Atmos. Chem. Phys.*, 11, 10765-10777, doi:10.5194/acp-11-10765-2011, 2011.

- [39] Miller, C. E., Crisp, D., DeCola, P.L., Olsen, S. C., Randerson, J. T., Michalak, A. M., Alkhaled, Rayner, P., Jacob, D. J., Suntharalingam, P., Jones, D. B. A., Denning, A. S., Nicholls, M. E., Doney, S. C., Pawson, S., Boesh, H., Connor, B. J., Fung, I. Y., O'Brien, D., Salawitch, R. J., Sander, S. P., Sen, B., Tans, P., Toon, G. C., Wennberg, P. O., Wofsy, S. C., Yung, Y. L., Law, R.M.: Precision requirements for space-based XCO₂ data, *J. Geophys. Res.*, 112, D10314, doi:10.1029/2006JD007659, 2007.
- [40] Morino, I., Uchino, O., Inoue, M., Yoshida, Y., Yokota, T., Wennberg, P. O., Toon, G. C., Wunch, D., Roehl, C. M., Notholt, J., Warneke, T., Messerschmidt, J., Griffith, D. W. T., Deutscher, N. M., Sherlock, V., Connor, B., Robinson, J., Sussmann, R., and Rettinger, M.: Preliminary validation of column-averaged volume mixing ratios of carbon dioxide and methane retrieved from GOSAT short-wavelength infrared spectra, *Atmos. Meas. Tech.*, 4, 1061-1076, doi:10.5194/amt-4-1061-2011, 2011.
- [41] Niro, F., et al.: Spectra calculations in central and wing regions of CO₂ IR bands. IV: software and database for the computation of atmospheric spectra. *J. Quant. Spectrosc. Ra.*, 95, 469–481. 2005a.
- [42] Niro, F., et al.: Spectra calculations in central and wing regions of CO₂ IR bands between 10 and 20 mm. III: atmospheric emission spectra. *J. Quant. Spectrosc. Ra.*, 90, 61–76. 2005b.
- [43] Perevalov, V. I. and Tashkun, S. A.: CDS-296 (Carbon Dioxide Spectroscopic Databank): Updated and Enlarged Version for Atmospheric Applications, Proceedings of the 10th HITRAN database conference, Cambridge, MA, USA, June 2008.
- [44] Travis E. Oliphant: Guide to NumPy, Trelgol Publishing, 2006, <http://www.tramy.us>
- [45] Rayner, P. J., and D. M. O'Brien: The utility of remotely sensed CO₂ concentration data in surface source inversions, *Geophys. Res. Lett.*, 28, 175–178, 2001.
- [46] Remedios JJ.: Extreme atmospheric constituent profiles for MIPAS. In: European symposium on atmospheric measurements from space. vol. 2. Noordwijk, Netherlands: ESTEC; 1999, p. 77983.
- [47] Remedios, J. J. et al.: MIPAS reference atmospheres and comparisons to V4.61/V4.62 MIPAS level 2 geophysical data sets, *Atmos. Chem. Phys. Discuss.*, 7, 9973-10017, 2007.
- [48] Reuter, M., et al.: Retrieval of atmospheric CO₂ with enhanced accuracy and precision from SCIAMACHY: Validation with FTS measurements and comparison with model results, *J. Geophys. Res.*, 116, D04301, doi:10.1029/2010JD015047.
- [49] Rothman LS, Jacquemart D, Barbe A, Chris Benner D, Birk M, Brown LR, et al. The HITRAN 2004 molecular spectroscopic database. *JQSRT*, 96:139-204, 2005.
- [50] Rothman, L. S. et al.: The HITRAN 2008 molecular spectroscopic database, *JQSRT* 110, 533572, 2009.
- [51] Rodgers, C. and Connor, B.: Intercomparison of remote sounding instruments, *J. Geophys. Res.*, 108, 41164229, 2003.
- [52] Roedenbeck, C., Houweling, S., Gloor, M., and Heimann, M.: CO₂ flux history 1982-2001 inferred from atmospheric data using a global inversion of atmospheric transport, *Atmos. Chem. Phys.*, 3, 1919-1964, 2003.
- [53] van Rossum Guido et al.: The Python Language Reference, Python Software Foundation, <http://docs.python.org/2/reference>.
- [54] Sabine C.L., Feely, R. A., Gruber, N., Key, R.M., Lee, K., Bullister, J.L., Wanninkhof, R., Wong, C.S., Wallace, D.W.R., Tilbrook, B., Millero, F.J., Peng, T.-H., Kozyr, A., Ono, T., Rios, A.F.: The Oceanic Sink for Anthropogenic CO₂, *Science*, 305, 367-371, 2004
- [55] Sarmiento, J. L., and Wofsy, S.C.: A U.S. Carbon Cycle science plan, 1999.
- [56] Shephard, M.W., et al.: Performance of the line-by-line radiative transfer model (LBLRTM) for temperature and species retrievals: IASI case studies from JAIVEx. *Atm. Chem. Phys.*, 9, 7397-7417. 2009.
- [57] Simeoni, D. Et al.: Design and Development of the IASI instrument, Infrared Spaceborne Remote Sensing XII. Edited by Strojnik, Marija. Proceedings of the SPIE, Volume 5543, 208-219, 2004.

- [58] Schneising, O., P. Bergamaschi, H. Bovensmann, M. Buchwitz, J. P. Burrows, N. M. Deutscher, D. W. T. Griffith, J. Heymann, R. Macatangay, J. Messerschmidt, J. Notholt, M. Rettinger, M. Reuter, R. Sussmann, V. A. Velasco, T. Warneke, P. O. Wennberg, and D. Wunch: Atmospheric greenhouse gases retrieved from SCIAMACHY: comparison to ground-based FTS measurements and model results, *Atmos. Chem. Phys.*, 12, 1527-1540, 2012.
- [59] Yoshida, Y., Ota, Y., Eguchi, N., Kikuchi, N., Nobuta, K., Tran, H., Morino, I., and Yokota, T.: Retrieval algorithm for CO₂ and CH₄ column abundances from short-wavelength infrared spectral observations by the Greenhouse gases observing satellite, *Atmos. Meas. Tech.*, 4, 717734, doi:10.5194/amt-4-717-2011, 2011.
- [60] Washenfelder, R. A., Toon, G. C., Blavier, J.F., Yang, Z., Allen, N. T., Wennberg, P. O., Vay, S. A., Matross, D. M., and Daube, B. C.: Carbon dioxide column abundances at the Wisconsin tall tower site, *J. Geophys. Res.*, 111, D22305, doi:10.1029/2006JD007154.
- [61] Williams, T., Kelley, C., et al.: Gnuplot 4.6: an interactive plotting program, <http://www.gnuplot.info/documentation.html>
- [62] Wunch, D., Toon, G. C., Wennberg, P. O., Wofsy, S. C., Stephens, B. B., Fischer, M. L., Uchino, O., Abshire, J. B., Bernath, P., Biraud, S. C., Blavier, J.-F. L., Boone, C., Bowman, K. P., Browell, E. V., Campos, T., Connor, B. J., Daube, B. C., Deutscher, N. M., Diao, M., Elkins, J. W., Gerbig, C., Gottlieb, E., Griffith, D. W. T., Hurst, D. F., Jimnez, R., Keppel-Aleks, G., Kort, E. A., Macatangay, R., Machida, T., Matsueda, H., Moore, F., Morino, I., Park, S., Robinson, J., Roehl, C. M., Sawa, Y., Sherlock, V., Sweeney, C., Tanaka, T., and Zondlo, M. A.: Calibration of the Total Carbon Column Observing Network using aircraft profile data, *Atmos. Meas. Tech.*, 3, 1351-1362, doi:10.5194/amt-3-1351-2010, 2010.
- [63] Wunch, D., Toon, G. C., Blavier, J.-F. L., Washenfelder, R. A., Notholt, J., Connor, B. J., Griffith, D. W. T., Sherlock, V., Wennberg, P. O.: The Total Carbon Column Observing Network. *Phil. Trans. R. Soc. A* (2011) 369, doi:10.1098/rsta.2010.0240.
- [64] Wunch, D., et al.: A method for evaluating bias in global measurements of CO₂ total columns from space, *Atmos. Chem. Phys.*, 11, 12, 31712, 337, doi:10.5194/acp-11-12317-2011.

Definitions and Acronyms

AF	Airborne Fraction
AFM/ARM	Accelerated Forward/Retrieval Model
AIRS	Atmospheric Infrared Sounder
AMSU	Advanced microwave Sounding Unit
ANN	Artificial Neural Network
A-SCOPE	Advanced Space Carbon and Climate Observation of Planet Earth
ATOVS	Advanced TIROS (Television and Infrared Observational Satellite) Operational Vertical Sounder
AVHRR	Advanced Very High Resolution Radiometer
BUFR	Binary Universal Form for the Representation of meteorological data
CNR	Consiglio Nazionale delle Ricerche
CNES	Centre National dEtudes Spatiales
CONTRAIL	Comprehensive Observation Network for Trace gases by Airliner
DHF	Data Handling Facility
DOAS	Differential optical Absorption Spectroscopy
DVB	Digital Video Broadcast
ECMWF	European Centre for Medium-Range Weather Forecasts
ENVISAT	ENVIronmental SATellite
EPS	EUMETSAT Polar System
ESA	European Space Agency
ESRL	Earth System Research Laboratory
EUMETCAST	EUMETSAT's Data Distribution System
EUMETSAT	European Organization for the Exploitation of Meteorological Satellites
FM	Forward Model
FOV	Field Of View
GOSAT	Greenhouse gases Observing SATellite
G-POD	Grid Processing On Demand
GTS	Global Telecommunication System
GUI	Graphical User Interfaces
GUIG	GOSAT User Interface Gateway
HDF	Hierarchical Data Format
HITRAN	HIgh-resolution TRANsmission molecular absorption database
IASI	Infrared Atmospheric Sounding Interferometer
IIS	Integrated Imaging Subsystem
IFAC	Institute for Applied Physics "Nello Carrara"
IFOV	Instantaneous Field Of View
IPP	Interferogram Processing Program
ISRF	Instrument Spectral Response Function
JAIVEx	Joint Airborne IASI Validation Experiment
JAXA	Japan Aerospace Exploration Agency
KLIMA	Kyoto protocoL Informed Management of the Adaptation
L0	Level 0
L1	Level 1
L1A	Level 1 A
L1B	Level 1 B
L1C	Level 1 C
L2	Level 2
LBLRTM	Line-by-line Radiative Transfer Model
LUC	Land Use Change
MARC	Millimetre-Wave Atmospheric Retrieval Code
MARSCHALS	Millimetre-wave Airborne Receiver for Spectroscopic CHaracterization of Atmospheric Limb-Sounding
METOP	METeorological SATellite
MHS	Microwave Humidity Sounder
MLP	Multi-Layer Perceptron
MOE	Ministry of the Environment

MSG	Meteosat Second Generation
MSS	Measurement Space Solution
MWIR	Mid Wave InfraRed
NASA	National Aeronautic and Space Administration
NLSF	Non-linear Least-Square Fit
NLTE	Non Local Thermodynamic Equilibrium
NSR	Null Space Regularization
NIES	National Institute for Environmental Studies
NIR	Near InfraRed
NESR	Noise Equivalent Spectral Radiance
NOAA	National Oceanic and Atmospheric Administration
NWP	Numerical Weather Prediction
OCO	Orbiting Carbon Observatory
OEM	Optimal Estimation Method
PCA	Principal Component Analysis
PI	Principal Investigator
QC	Quality Control
REFIR	Radiation Explorer in the Far InfraRed
RM	Retrieval Model
RMSS	Regularized Measurement Space Solution
RT	Radiative Transfer
RFM/RRM	Reference Forward/Retrieval Model
SCIAMACHY	Scanning Imaging Absorption Spectrometer for Atmospheric Chartography/Chemistry
SWIR	Short Wave InfraRed
TANSO-CAI	Thermal And Near-infrared Sensor for carbon Observation- Cloud and Aerosol Imager
TANSO-FTS	Thermal And Near-infrared Sensor for carbon Observation- Fourier Transform Spectrometer
TCCON	Total Carbon Column Observing Network
TIROS	Television and Infrared Observational Satellite
TIR	Thermal InfraRed
UMARF	Unified Meteorological Archive and Retrieval Facility
VCM	Variance Covariance Matrix
V1	Version 1
V2	Version 2
WFM-DOAS	Weighting Function Modified DOAS

Table of Contents

1	Introduction	2
2	Objectives and rationale of the project	3
3	Summary and conclusions of Phase 1 activities: sensitivity tests and performances of the KLIMA-IASI code	7
3.1	KLIMA-IASI forward model	7
3.1.1	Reference Forward Model	7
3.1.2	Accelerated Forward Model	9
3.2	KLIMA-IASI retrieval model	11
3.2.1	The Reference Retrieval Model and the ultimate IASI performances	12
3.2.2	The Accelerated Retrieval Model and the sensitivity tests	13
3.3	Application of WFM-DOAS CO ₂ and CH ₄ retrieval algorithm to the processing of SCIAMACHY L1 version 6 data	16
4	An overview of the observations: instruments and retrieval codes	17
4.1	IASI/MetOp-A: instrument description and CO ₂ operational retrieval code	17
4.2	TANSO-FTS/GOSAT: instrument description and CO ₂ operational retrieval code	17
4.3	TCCON and CO ₂ retrieval code	19
4.4	KLIMA CO ₂ retrieval code	19
4.4.1	Comparison between IASI L1B and L1C datasets	21
4.4.2	IASI spectral band selection	21
5	Identification and acquisition of IASI, TANSO-FTS and TCCON datasets	24
5.1	IASI data	24
5.1.1	IASI data dissemination means	24
5.1.2	IASI data products	24
5.1.3	IASI data formats	24
5.2	GOSAT data	25
5.2.1	GOSAT data products	25
5.2.2	Data processing and data products distribution	26
5.2.3	Validation of GOSAT data products	26
5.3	TCCON data	26
5.3.1	TCCON Database	26
5.3.2	TCCON Data Processing	27
5.3.3	TCCON Calibration	27
6	KLIMA-IASI software suite: integration on G-POD	28
6.1	The logic flow of the analysis	28
6.1.1	The input of the pre-processor	28
6.1.2	The Auxiliary data for pre-processor module	28
6.1.3	The output of the pre-processor: the KLIMA Input Dataset	28
6.1.4	The input of the retrieval module	30
6.1.5	The auxiliary data of the retrieval module	30
6.1.6	The output of the retrieval module	31
6.1.7	The retrieval diagnostics	32
6.2	The integration of the KLIMA code on ESA G-POD for Earth Observation Application system	33
7	IASI data processing using KLIMA retrieval code and inter-comparison strategies	35
7.1	Method to compare retrieval products with different AKs and a priori	36
8	Global distribution of KLIMA XCO₂ monthly averaged products	38
8.1	KLIMA products overview	38
8.2	Errors of KLIMA retrievals	52

9 Comparison between KLIMA-IASI and EUMETSAT-IASI operational products	57
9.1 EUMETSAT products overview	57
9.2 Objectives of comparison	57
9.3 Results of the comparison	58
10 Comparison between KLIMA and TANSO-FTS/GOSAT	67
10.1 TANSO-FTS/GOSAT XCO ₂ Product Overview	67
10.2 Objectives and strategy of the comparison	67
10.3 Results of the comparison	67
10.3.1 Co-located comparison	67
10.3.2 Comparison of XCO ₂ average values	71
10.3.3 Seasonal variations and mean values over macro areas comparison	71
11 Comparison between KLIMA-L2 and TCCON PRODUCTS	78
11.1 TCCON products overview	78
11.2 Objectives of the comparison	78
11.3 Results of the comparison	78
12 Conclusions	83
13 Open issues and possible future work	85
A The KLIMA-IASI Pre-Processor	88
B The Measurement Space Solution method	92
C Jacobian maps wrt IASI target parameters	95
D Comparison between KLIMA and TANSO-FTS/GOSAT V1	98
E INPUT and OUTPUT file templates	101
Acknowledgements	145
Reference Documents	145
Bibliography	145
Definitions and Acronyms	150